

Digital twin development for improved operation of batch process systems

Citation for published version (APA):

Méndez Blanco, C. S. (2023). *Digital twin development for improved operation of batch process systems*. [Phd Thesis 1 (Research TU/e / Graduation TU/e), Electrical Engineering]. Eindhoven University of Technology.

Document status and date:

Published: 21/09/2023

Document Version:

Publisher's PDF, also known as Version of Record (includes final page, issue and volume numbers)

Please check the document version of this publication:

- A submitted manuscript is the version of the article upon submission and before peer-review. There can be important differences between the submitted version and the official published version of record. People interested in the research are advised to contact the author for the final version of the publication, or visit the DOI to the publisher's website.
- The final author version and the galley proof are versions of the publication after peer review.
- The final published version features the final layout of the paper including the volume, issue and page numbers.

[Link to publication](#)

General rights

Copyright and moral rights for the publications made accessible in the public portal are retained by the authors and/or other copyright owners and it is a condition of accessing publications that users recognise and abide by the legal requirements associated with these rights.

- Users may download and print one copy of any publication from the public portal for the purpose of private study or research.
- You may not further distribute the material or use it for any profit-making activity or commercial gain
- You may freely distribute the URL identifying the publication in the public portal.

If the publication is distributed under the terms of Article 25fa of the Dutch Copyright Act, indicated by the "Taverne" license above, please follow below link for the End User Agreement:

www.tue.nl/taverne

Take down policy

If you believe that this document breaches copyright please contact us at:

openaccess@tue.nl

providing details and we will investigate your claim.

Digital twin development for improved operation of batch process systems

Thesis

ter verkrijging van de graad van doctor aan de Technische Universiteit Eindhoven,
op gezag van de rector magnificus prof. dr. S.K. Lenaerts, voor een commissie
aangewezen door het College voor Promoties, in het openbaar te verdedigen op
donderdag 21 september 2023 om 13:30 uur

door

Carlos Samuel Méndez Blanco

geboren te Puerto Ordaz, Venezuela.

Dit proefschrift is goedgekeurd door de promotoren en de samenstelling van de promotiecommissie is als volgt:

voorzitter: prof. dr. ir. H.J. Visser
promotor: prof. dr. ir. P.M.J. Van den Hof
promotor: dr. L. Özkan
leden: prof. dr. ir. J.A. van Oijen
prof. dr. A. Mitsos (RWTH Aachen University)
prof. dr. ir. J. Van Impe (KU Leuven)
adviseurs: dr. ir. J.D. Stigter (Wageningen University & Research)
ir. A.E.M. Huesman (Shell)

Het onderzoek of ontwerp dat in dit proefschrift wordt beschreven is uitgevoerd in overeenstemming met de TU/e Gedragscode Wetenschapsbeoefening.

Digital twin development for improved operation of batch process systems



Institute for
Sustainable
Process Technology



TKI ENERGIE & INDUSTRIE
Topsector Energie

This work is part of the INSPEC project with the support of ISPT and TKI Energie en Industrie.

disc

This dissertation has been completed in fulfilment of the requirements of the Dutch Institute of Systems and Control (DISC) for graduate study.

A catalogue record is available from the Eindhoven University of Technology Library
ISBN: 978-90-386-5822-3.

Copyright © 2023 by Carlos Samuel Méndez Blanco

All rights reserved. No part of the material protected by this copyright notice may be reproduced or utilized in any form or by any means, electronic or mechanical, including photocopying, recording or by any information storage and retrieval system, without written permission from the copyright owner.

Printed by Gildeprint | www.gildeprint.nl

Cover design by Isabella Becerra

*Science is a wonderful thing
if one does not have to earn one's living at it...
Only when we do not have to be accountable to anybody
can we find joy in scientific endeavor.*

Albert Einstein

Contents

Summary	xiii
1 Introduction	1
1.1 Motivation	1
1.1.1 The role of digital twins in process industry	2
1.1.2 The computational model: First-principle approach	4
1.2 Structural and operational identifiability	8
1.2.1 Structural identifiability	9
1.2.2 Operational identifiability	10
1.3 Offline and online parameter estimation.	13
1.4 Modeling approaches for reaction process systems	14
1.5 Research questions	15
1.6 Outline of the thesis	18
2 Mathematical preliminaries	21
2.1 General notation	22
2.2 Numbers, vectors and vector norms	22
2.3 Vector spaces and matrices.	23

2.4	Vector and matrix calculus.	26
2.5	Formal power series.	28
2.6	Subspaces	30
3	Structural identifiability of linear models in open and closed-loop	31
3.1	Introduction.	32
3.2	Structural properties	33
3.3	Structural Identifiability	35
3.3.1	The invariant vector	37
3.3.2	Types of structurally identifiable models and parameter redundancy	39
3.4	Structural identifiability in closed-loop	45
3.5	Structural identifiability: An output sensitivity controllability perspective	51
3.5.1	Relation between structural output sensitivity controllability and parameter identifiability	52
4	Operational identifiability and offline gradient-based parameter estimation	63
4.1	Introduction.	64
4.2	Sensitivity-based operational identifiability	65
4.3	The output parametric sensitivity matrix $\mathbf{S}(\mathbf{p})$ and its relation to operational identifiability.	67
4.3.1	The successive orthogonalization method (SOM)	70
4.3.2	Normalization of the output parametric sensitivities	75

4.4	Sensitivity measures	79
4.5	Single shooting gradient-based parameter estimation.	83
4.5.1	Enforcing a relative sensitivity matrix.	86
4.6	Multiple shooting parameter estimation.	91
4.6.1	Standard multiple shooting parameter estimation	91
4.6.2	Ranked interval multiple shooting parameter estimation (RIM-SPE).	93
5	Online parameter estimation: A control design perspective	103
5.1	Introduction.	104
5.2	Parameter estimation as a control problem	105
5.2.1	Integral action	107
5.2.2	Proportional + integral action	108
5.2.3	Exponential control law	110
5.2.4	Computation of the weighting matrix \mathbf{W}	112
5.3	Example: Fed-batch penicillin reactor	113
6	Extent-based sequential state and parameter estimation for process systems	119
6.1	Introduction.	120
6.2	Extents of Reaction.	121
6.3	Variant and Invariant Spaces of Reaction Systems	123
6.4	The inlet composition uncertainty matrix $\Delta \mathbf{X}_{\text{in}}$	128
6.4.1	Properties of \mathbf{X}_{in} and $\Delta \mathbf{X}_{\text{in}}$	129

6.4.2	Equivalence between the system and model representations	129
6.5	Estimating $\Delta\mathbf{X}_{in}$ from mole measurement in a semi-batch reactor	132
6.6	Estimating $\Delta\mathbf{X}_{in}$ from mole measurement in a continuous stirred-tank reactor	134
6.7	Estimation of moles, reaction rate, and chemical kinetic parameters	137
6.7.1	Asymptotic observer	140
6.7.2	Estimation of \mathbf{x}_r for uncertain \mathbf{X}_{in}	142
6.7.3	Reaction rate estimator	144
6.7.4	Chemical kinetic parameter estimation	145
6.8	Numerical example	146
7	Industrial Case Study: Resin production by reactive batch distillation	157
7.1	Introduction.	158
7.2	Polyesterification reaction	159
7.2.1	Polyesterification reaction mechanism	160
7.2.2	Chemical reactions	161
7.2.3	Rate equations and stoichiometry	164
7.3	Reactive distillation process	166
7.3.1	Thermodynamic relationships	176
7.3.2	Fluid dynamic relationships	182
7.4	Polymer viscosity	186
7.4.1	Modeling of viscosity	187

7.4.2	The logistic equation: population growth dynamics	190
7.5	Simulation of the reactive batch distillation column model.	191
7.5.1	Loading flow	191
7.5.2	Jacket oil inlet temperature	194
7.5.3	Pressure control valve and reflux flow	195
8	Model Calibration and Optimization of Reactive Batch Distillation Column	203
8.1	Introduction.	204
8.2	Model calibration	205
8.2.1	Sensitivity analysis	207
8.2.2	Ranking of parameters based on output parametric sensitivity per operational step	208
8.2.3	Ranked interval multiple shooting parameter estimation	211
8.3	Optimization of the RBD process	213
9	Conclusions and recommendations	225
9.1	Conclusions	226
9.1.1	Structural identifiability	226
9.1.2	Operational identifiability and offline gradient-based parameter estimation	227
9.1.3	Online parameter estimation.	228
9.1.4	Extent-based sequential estimation for process systems with unknown reaction dynamics	229
9.1.5	Reactive batch distillation column: modeling and calibration .	230

9.2 Recommendations	230
9.2.1 Identifiability and control design.	230
9.2.2 Closed-loop identifiability in the nonlinear case.	231
9.2.3 Process model update: Input-output pairing and measurement selection.	231
9.2.4 Inlet composition uncertainty	231
List of Acronyms	233
A Mathematical proofs and derivations	237
A.1 Mathematical proofs	238
A.1.1 Proof Theorem 3.4	238
A.1.2 Proof Theorem 6.1	242
A.1.3 Proof Theorem 6.2	244
A.1.4 Proof Theorem 6.3	245
A.2 Mathematical derivations.	247
A.2.1 Successive orthogonalization method matrix decomposition . .	247
A.2.2 Relationship between convolution integral and the extents of inlet	250
Acknowledgements	267
Curriculum Vitæ	269
List of Publications	271

Summary

The interest in opportunities to improve operation of industrial process is in high demand due to the current technological, environmental, and societal challenges. To this end, digital twins have emerged as a very valuable solution due to the flexibility and potential uses they have. In general, digital twins comprise a 3D representation of the system for visualization purposes, and an underlying simulation model that describes the dynamic behavior of the system, which receives real-time data from the real system. More specifically, the simulation model of a digital twin is arguably its main attribute as it allows multiple model-based designs, e.g. control, model parameter estimation, process optimization. However, these models tend to lose their fidelity over time with respect to the process they describe due to internal and external operational changes, e.g. new process set-points, fouling in the equipment, catalyst poisoning. These operational variations need to be taken into account to calibrate the simulation model and obtain a good description of the process. One way to approach this issue is to assume there is no undermodeling in the model, i.e. no relevant dynamics has been neglected. The calibration of the model can then be understood as re-estimating the model parameters to minimize the model-plant error.

Another important aspect of the simulation models is the operation mode of system, as industrial processes can be operated in two regimes: continuous and batch. The main difference between continuous and batch processes is that the former is operated continuously for an undetermined time in steady-state regime at a specific operating point. The latter is operated in batches with a predefined time window around a dynamic operating trajectory. In the context of model parameter estimation, the standard practice is to estimate a single parameter set that describe the process trajectories for either operation mode. However, batch processes usually do not reach a steady-state and dynamic transients are always present in the process trajectories. The dynamic trajectory generally exhibits distinct operational stages where different phenomena dominate the process behavior. This feature can be exploited to estimate multiple model parameter sets in different portions of the process trajectory, leading to potentially better match between plant and model output matching.

Given the importance of having high-fidelity models to describe process dynamics and ensuring good model-based operation performance, parameter estimation for model calibration is the main topic addressed in this thesis. This objective is

investigated considering two parts:

- a. What to update: Selection of parameters to be updated within the set of all model parameters.
- b. How to update: Methodologies to update parameters offline and online to ensure good performance of the simulation model.

The *what to update* part is studied from two perspectives: structural identifiability and operational identifiability, which correspond to Chapters 3 and 4, respectively. In the structural identifiability setting, the mathematical relationships between input, output, and parameters are explored to determine the set of parameters that can be estimated. Structural identifiability answers the yes or no question of whether the parameters in a model are identifiable. In this thesis, we extend these ideas to the closed-loop case because most processes in industry are in a closed-loop configuration, and control design techniques do not take model parameter identifiability into account. This limits the effectiveness of closed-loop parameter estimation. Therefore, we present an approach to determine the conditions under which a controller will not impoverish parameter identifiability. Additionally, the connection between identifiability and controllability of a linear model is established, relating these two concepts to system theoretic tools. On the other hand, operational identifiability is based on the numerical computation of the output parametric sensitivity, i.e. the sensitivity of the output around a nominal point to variations in the model parameters.

Furthermore, operational identifiability answers the more nuanced question "how identifiable is a parameter?" However, this approach is sensitive to scaling of physical units, while also relying heavily on user-defined criteria to perform the identifiability assessment. As a consequence, we also propose several algorithms to improve the selection of identifiable parameter sets for offline estimation and model calibration. We base our developments on the computation of parametric sensitivities around an operating point or a trajectory.

In Chapters 4 and 5, the part on *how to update* is studied. Here, offline and online parameter estimation methodologies are presented. In the offline setting, we developed two nonlinear least-squares algorithms based on the greedy random adaptive search procedure [48]. This procedure is modified to include an extra step of iterative re-selection of the identifiable parameter set. The idea is that every optimum defines a new operating point in the model, and different set of parameters might be identifiable as a consequence. Additionally, a more advanced approach is also explored, namely the multiple shooting method, which facilitates dealing with ill-conditioned parameter spaces by segmenting the output trajectory in shooting intervals. This method is also extended to include the re-selection procedure of the parameter set, and its application to each shooting interval independently. Adding

this modification to the multiple shooting method implies solving different optimization problems for each interval using the best parameter set in each of them. This improves the convergence of the estimated parameters significantly, even using initial parameter seeds locally away from the optimum.

We develop a control-based approach to estimate parameters in an online setting, where the model parameters are treated as artificial inputs to the system. Taking the parameter as inputs, we propose several control laws to make the model output track the measured output. These control laws are implemented only on the identifiable parameter set, related by an output controllability condition. Furthermore, the control laws are constructed assuming that the only source of model-plant mismatch is due to incorrect parameter values. The control design uses a Lyapunov function-based approach, where the control action should make the time derivative of the Lyapunov function negative definite.

In Chapter 6, we explore how process models are affected by uncertainty in the inlet composition as it compromises control design and process performance. The analysis and developments are performed using the extent representation as it allows to decouple the process dynamics into its different effects (reaction dynamics, transport dynamics, and invariant dynamics), and work in a reaction-independent setting. An extent-based method to estimate the uncertainty in the inlet composition under partial mole measurement and unknown reaction dynamics is presented. The estimation of the uncertainty is viewed as a parameter estimation problem, where the error between the true dynamics and the model dynamics are due to the effect of the uncertainty matrix. Additionally, the computation of the uncertainty matrix is performed under the assumption that the variation in the composition is not too abrupt, and that the residence time can be measured. The corrected inlet composition is computed based on the estimated uncertainty matrix. This also enables the estimation of the unmeasured number of moles, the unknown reaction dynamics (under some compactness assumption), and the chemical kinetic parameters using a standard least-squares approach.

Finally, in Chapters 7 and 8, we present the development of a detailed reactive batch distillation column simulator that can serve as a digital twin describing a real-life polymer-producing process. Key dynamics such as mole, temperature, pressure, and viscosity are modeled. A novel empirical viscosity model based on the logistic differential equation to predict the evolution of the polymer viscosity is proposed. The simulator model is calibrated using real plant data and utilizing the modified multiple shooting presented in Chapter 4. The calibrated model is subsequently used to optimize each batch step individually computing the optimal input profiles that minimize batch time and maximize the polymer viscosity.

1

Introduction

1.1. Motivation

Process industry is continuously experiencing technological and societal challenges. In the last couple of decades, environmental regulations and the market driven economy have forced chemical plants move towards more flexible plant operation. The current trends such as circular economy, the use of renewable energy sources in the production, and varying raw materials require a higher degree of flexibility, adaptability, and autonomy in the process operations. Industrial processes generated 2.90 Gt of CO₂ emissions in 2018, which accounts to 6% of all emissions across all economic sectors according to Climate Watch [199]. This number represents an almost three-fold increase in the emissions compared to 1990, which can be seen in the chart illustrated in Figure 1.1. Therefore, process industry needs to improve its operations to accommodate with the current environmental policies to slow climate change down. However, maximization of yields, reduction of batch times, etc. impose operating regimes that are usually beneficial for the production campaigns but that impact negatively the environment due to increased energy demands, higher raw material consumption, and/or more by-product waster generated during production [167]. In view of this, new tools are required to help operate processes at or close to the optimal trade-off between maximal throughput and minimal environmental impact.

In recent years, the emergence of new technologies, such as Internet of Things (IoT), and the increasing durability of computational power have allowed all sectors of industry to harness the potential of their operation by connecting physical systems

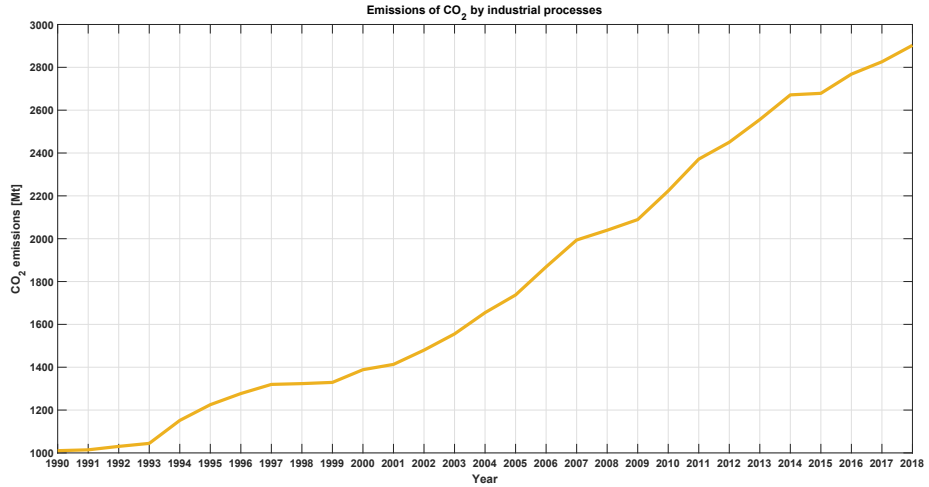


Figure 1.1: Increase of CO₂ emissions from 1990 to 2018 from industrial processes [199].

to the digital world within the context of Industry 4.0. The connectivity between these two parts enables a more cohesive operation, which can positively impact sustainability since it provides more accurate, high-quality management and real-time event management for the external environment [31]. Within IoT in industry, one particular element stands out, namely the Digital Twin (DT), which serves as a platform to run simulations, test, and scale processes before implementing them in reality. Additionally, digital twins can also benefit from sharing information for online tasks in the operation, which will be explored in detail in the next sections.

1.1.1. The role of digital twins in process industry

The development and exploitation of Digital Twin is a new trend in industry as well as in other sectors, which emerged with the development of the so-called Industry 4.0 [100]. There is no precise definition of what a DT is, but in general, it is the integration of an actual physical system with a virtual replica, which can be a computational model usually combined with an external user interface or a 3D representation of the system. Furthermore, the integration between the virtual replica and the system is achieved by the constant exchange of data captured via sensors, data acquisition cards, and software to monitor, analyze, and predict future process performance [121]. A representation of the digital twin paradigm is presented in Figure 1.2. The digital twin paradigm has become one of the main topics for research, implementation, and investment in today's industry because of its prospective capability to improve, innovate, design, and enable a more assimilated manufacturing of products and assets exploiting features of IoT. Moreover, it also provides (near)

real-time insights to continuously optimize and transform businesses, making use of novel technological applications such as predictive control, machine learning (ML), data analysis (Big Data), etc. On the other hand, a DT can be developed and implemented at different levels. These levels are [64]

- Micro or machine level: A digital twin for specific units or machines.
- Meso or factory level: A digital twin for assembly line, power plant, process plant.
- Macro or organizational level: A digital twin for supply chain, electricity delivery network, transport fleet, etc.

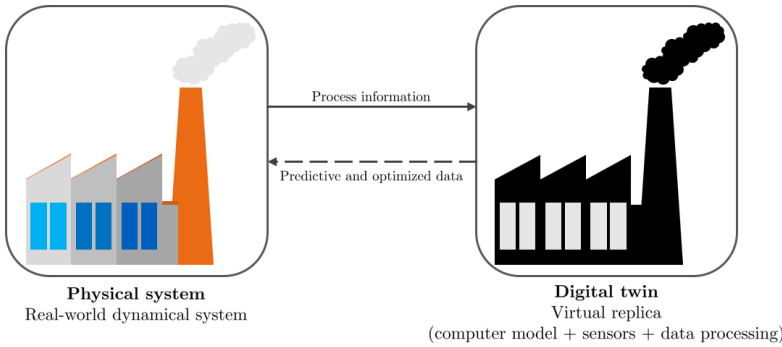


Figure 1.2: Schematic of the digital twin paradigm (based on [121]).

Given the flexibility offered by the application levels and the capability of carrying out simulations in controlled risk-free digital environments, it has received a great amount of attention in different industrial sectors such as smart manufacturing ([175], [58], [173]), oil and gas ([132], [20], [197]), transportation ([133]), food and beverage ([59]), agriculture ([89]), aerospace ([103], [57]), construction ([91]), and energy ([77]). Moreover, digital twins have several applications that can be condensed into three major domains: production campaigns, predictive maintenance, and after-sale support [121].

Production campaigns

Digital twins take the approach of virtual models one step further by fusing a simulation model with real-time data to continuously update current process states. This synergy between a model and data proves to be helpful to assess a multiplicity of production scenarios under different operating conditions, which allows to perform risk analysis on the system. This naturally provides an opportunity to improve and optimize the operation to maximize yield and/or comply with environmental

regulations. Not only can a specific production campaign be optimized but also monitored in real time by constantly comparing the predicted output of the DT and the data obtained from the plant. These two general characteristics have the potential to generate better business outcomes [66].

Predictive maintenance

The DT paradigm makes it possible for industry to replace reactive maintenance by predictive maintenance, improving efficiency, and extending the life cycle of units and processes, which ultimately reduce the overall operational costs. An important feature of the DT is its capability to combine plant data with information provided by the simulation model, which can be used as an analysis tool to predict future behavior and the impact of the operating conditions on the operation unit, and its remaining useful life. As a consequence downtime can be greatly reduced through dedicated model-and-data-based warnings [103],[176],[170].

After-sales support

The use of DT helps log final product characteristics while keeping track of the history of the operating conditions of a particular batch or production line. In general, it may serve to identify and trace abnormal features that might be present in sold final product more efficiently. Additionally, it also could help provide clients with more information about the final product [121].

1.1.2. The computational model: First-principle approach

For the digital twin to function properly and provide reliable information, a high-level computational model is required, which serves as the "brain" of the DT ensemble. Continuous adjustment and alignment of these models to changing operating conditions will keep the model-based operation up to date [11]. In the process industry, the development and use of process simulation models dates back to 1980's. The value of these models lie in the fact that they are quite versatile, and can be employed for several model-based tasks such as process design, plant revamping, process optimization, process monitoring, estimation of unmeasurable process variables, fault detection, and control [193].

The different domains of application presented in Figure 1.3 shows the wide range of capabilities a first-principles models can offer to on- and offline applications. These models can be used for one or more tasks to obtain the best performance in the operation. For instance, model-based control uses the set-points computed in the real-time optimization (RTO) layer. Likewise, the first-principle model can be used to perform also real-time monitoring and behavior prediction. Another

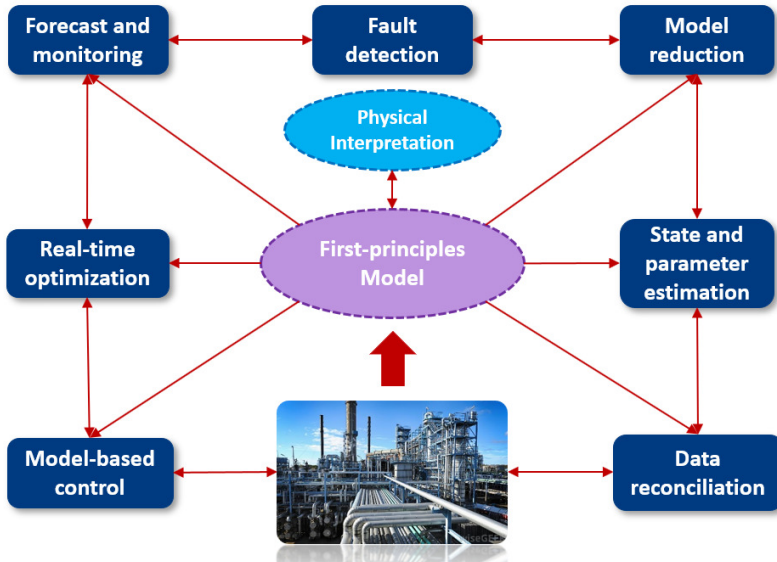


Figure 1.3: Domains of application of first-principle models.

example is the maintenance of the first-principles model using state and parameter estimation based on actual process data to keep the model-plant error below some error threshold. In general, the first-principle models offer a high degree of flexibility in operation than data driven models because they provide a description of the system based on physical laws.

Despite their advantages, first-principle model development usually requires a large amount of time and a high level of expertise in the particular application because these models describe the dynamic changes in a process with relatively high degree of detail. The description of these models can be as detailed as required at the expense of a higher structural complexity. Nevertheless, prior knowledge is frequently not sufficient to fully derive appropriate mathematical models and their constitutive equations require the inclusion of several unknown parameters, which become less accessible through measurement [205]. These are parameters that describe physical properties of the system and are used to fit model simulated outputs to the observed plant data. Nonetheless, such approximations can lead to significant inaccuracies in the final result, meaning all effects cannot be confidently captured to their full extent. The trade-off between high level of detail in a model and the accessibility to information through measurement is illustrated in Figure 1.4.

Since the development of process simulation models is expensive and time consuming, strategies enabling model adjustment is a necessity in protecting the effort and investment put in these models. Model adjustment is usually achieved re-estimating model parameters under the operation conditions of interest. Although, decades of

research have been devoted to analyzing models and building techniques to estimate model parameters, parametric uncertainty is still present in process operation. Therefore, there is still a need for more reliable model parameter identification methodologies to reduce the impact of plant-model mismatch on the performance of model-based operation systems.

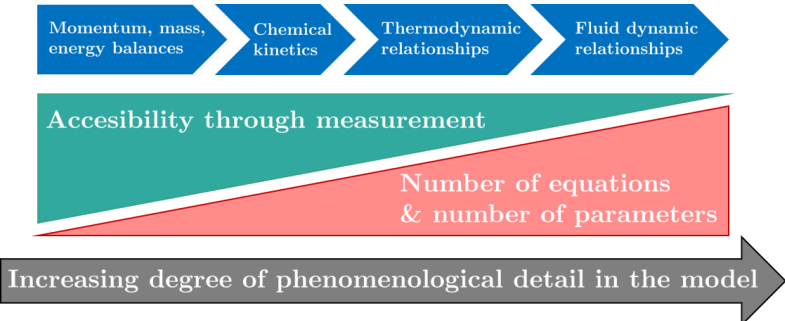


Figure 1.4: Complexity of first-principle models.

Another important aspect of the simulation models is the operation mode of system as industrial processes can be operated in two regimes: continuous and batch. The main difference between continuous and batch processes is that the former is operated continuously for an undetermined time in steady-state regime at a specific operating point. The latter is operated in batches with a predefined time window around a dynamic operating trajectory. In the context of model parameter estimation, the standard practice is to estimate a single parameter set that describe the process trajectories for either operation mode. However, batch processes usually do not reach a steady-state and dynamic transients are always present in the process trajectories. This feature can be exploited to estimate distinct parameter sets in different portions of the process trajectory, leading to potentially better match between plant and model output matching.

Additionally, most of batch processes are operated under a simple open-loop operating policy where the same input trajectory is applied to each batch [25]. This approach makes the assumption that a historically successful input trajectory (applied to previous batches) will result in the same desired product quality. Open-loop policies are beneficial in that they are easy to implement, do not require online measurement or process models, and can be easily adapted from laboratory-scale procedures. Nonetheless, due to the potential differences between laboratory and production scales, there will be a plant-model mismatch. Moreover, since open-loop policies lack the feedback mechanisms, there is no capability to reject such disturbances [129].

A common control approach for batch processes is dynamic trajectory tracking, where a particular process variables is measured and forced to follow a specific

trajectory in accordance with the production recipe. This aforementioned trajectory is assumed to be a consistently successful operating regime taken from previous batches, and thus, by tracking it the same product quality can be ensured. In practice, PI controllers are implemented to achieve this task, but also techniques such as gain scheduling may be applied to account for the time-varying nonlinear evolution of the process states [17], [18]. Despite its simplicity and widespread implementation, this approach might not deliver the desired product quality because the relationship between the controlled variable and the final quality target may differ significantly with feedstock variations and other uncertainties. Furthermore, this approach is inherently time-indexed, which may become a drawback when the duration of batches is inconsistent [129].

Another control approach widely used in batch processes is iterative learning control ILC, where the repetitive nature of batch process is exploited to improve the process performance in every subsequent batch based on the error from the previous batch runs (see [97] for a survey). However, the conventional applications of ILC are operated in open loop, making them unable to reject disturbances in real time. Therefore, several modifications have been performed to the standard ILC to make it more robust against dynamic changes in each batch such as feedforward iterative learning control [198], model predictive control iterative learning control [115], or batch-to-batch ILC with PI control using a maximum a posteriori iterative identification procedure [53] to improve the overall run-to-run performance of the batch process.

The simulation model is developed such that it uses the information of past and current observations in the control objective. A variety of modeling methodologies have been applied to obtain such models. One approach has been to train artificial neural networks on batch data [178]. The most commonly used modeling method, however, is projection to latent spaces PLSs [161],[52],[51],[9],[196],[37]. In these contributions, measured process variables are related to input via a linear static map. These approaches are useful if a large volume of data is available and the process is difficult to model using first-principle. However, data-based approaches, including the PLSs methodology, have major drawbacks such as the lack of a sufficient number or informative measurements, as well as the absence of physical intuition of the process at hand. Several other approaches have addressed this problem including the use of missing data algorithms [51]. Analogously, building first-principle dynamic models has also been used as an alternative given their prediction and extrapolation capabilities, while preserving the process physical meaning of the process variables (see e.g. [37], [114]). Nonetheless, due to the constant dynamic evolution of batch processes, model parameters are generally more difficult to estimate because parameter identifiability will change at different stages of the trajectory [105], [69].

Given these limitations and challenges of first-principle models, we investigate parameter identifiability and estimation addressing two aspects in this thesis: what to update, and how to update. Following these ideas, the global research objective is

stated next

Global objective

Develop effective tools for the online maintenance of first-principle models of batch reaction processes

In addressing the different aspects of parameter identifiability and estimation, we assume that the model is given by a nonlinear differential algebraic equation (DAE) of the form

$$\mathcal{M}(\mathbf{p}) = \begin{cases} \dot{\mathbf{x}}(t, \mathbf{p}) &= \mathbf{f}(\mathbf{x}(t), \mathbf{u}(t), \mathbf{z}(t), \mathbf{p}) & \mathbf{x}(t_0) = \mathbf{x}_0 \\ \mathbf{0} &= \mathbf{h}(\mathbf{x}(t), \mathbf{u}(t), \mathbf{z}(t), \mathbf{p}) \\ \mathbf{y}(t, \mathbf{p}) &= \mathbf{g}(\mathbf{x}(t), \mathbf{z}(t), \mathbf{p}) \end{cases} \quad (1.1)$$

where $\mathbf{x}(t, \mathbf{p}) \in \mathbb{R}^{n_x}$ is the vector of differential states, $\mathbf{u}(t) \in \mathbb{R}^{n_u}$ is the known input vector, $\mathbf{y}(t, \mathbf{p}) \in \mathbb{R}^{n_y}$ is the measurement or the output vector, $\mathbf{z}(t, \mathbf{p}) \in \mathbb{R}^{n_z}$ is the algebraic state, and $\mathbf{p} \in \mathbb{P} \subseteq \mathbb{R}^{n_p}$ the parameter vector. The vector functions \mathbf{f} , \mathbf{g} , and \mathbf{h} are assumed to be analytic functions, the Jacobian $\partial_{\mathbf{z}} \mathbf{h}$ is invertible at all points $(\mathbf{x}, \mathbf{z}, \mathbf{u})$, and the differentiation index of the model is assumed to be 1.

1.2. Structural and operational identifiability

Parameter identifiability is the model property that encompasses the issue of what to update. Identifiability allows to determine which model parameters can be estimated uniquely, i.e. with a low level of uncertainty. This property can be analyzed from two complementary perspectives: structural and operational. The former is an analytic setting where the mathematical relationship between variables and parameters in the model equations are studied without the explicit use of data. The latter uses collected input and output data to quantify identifiability in a numerical context. The structural identifiability analysis is necessary because it serves to determine which parameters can be estimated a priori from the model structure. Analogously, operational identifiability is also relevant since it provides the numerical data to determine whether a model parameter set can be uniquely estimated under the current operating conditions. These two properties play a major role in the development of tools for online model maintenance as they allow to pinpoint the set (or subset) of parameters that should be targeted during the re-estimation procedure.

1.2.1. Structural identifiability

Structural identifiability analysis verifies the parameter identifiability of models exploring their structure. It essentially answers the yes/no question whether the set of model parameters are identifiable. The first techniques developed date back to the 70's for linear systems with the seminal paper of [16]. In this publication, special attention was given to biological linear compartmental models. For this type of models, the Laplace transform approach [16] and the similarity transformation approach [191] were developed to perform such an analysis. Another method was explored in [32],[36] where the coefficients of the transfer functions that define the input-output map of linear or linearized models were used to assess the identifiability of a particular model structure. On the other hand, [142] proposed a power series expansion to test for identifiability of nonlinear ODE models, using the Taylor expansion coefficients at $t^+ = 0$. A related but more complex approach was proposed in [96], in which the nonlinear model is decomposed into an infinite generating Volterra series to test parametric identifiability. Moreover, the similarity transformation approach laid out in [191] was extended to nonlinear systems in [183],[182],[33]. They proposed the computation of a local state isomorphism under the assumption that the nonlinear model is locally accessible and locally observable at \mathbf{x}_0 to assess its global or local identifiability. Finally, [41] proposed a direct comparison test for uncontrolled autonomous systems to test identifiability, where drift vector field dependent on any parameter vector \mathbf{p} is equated to another one with the same structure but dependent on another parameter vector \mathbf{p}^* . The direct test is reduced to verifying whether a unique equality $\mathbf{p} = \mathbf{p}^*$ could be obtained.

Another important aspect of structural identifiability is the notion of identifiability given an initial state \mathbf{x}_0 . Initial conditions might provide extra information, apart from the standard input-output map, when performing identifiability analysis. This is known as *locally strongly identifiable* [179] or \mathbf{x}_0 -*identifiable* [81]. Additionally, a general definition of structural identifiability for ODE models called geometric identifiability was proposed in ([203],[82],[179]), and it implies that the parameters in the parameter vector can be determined extracting the information from the input signal, the measured output, and the initial states [82]. This notion is closely related to the nonlinear observability at the initial condition of the system and the rank of the observability matrix under different parameter combinations. More recently, [188] developed a technique to assess structural identifiability using the concept of extended observability based on [179]. They integrated a matrix decomposition algorithm using genetic optimization to circumvent dimensionality issues in the computation of the observability matrix and its rank.

An alternative definition based on differential algebra was introduced in[60],[104]. In the differential algebra-based identifiability, parameters are determined using information from the input-output map [82]. The notion of algebraic identifiability serves as the basis of a handful of methods (see for example [82],[104],[203]). In this

setting, a system structure is said to be algebraically identifiable if a meromorphic function can be constructed in a finite number of steps of algebraic calculations or differentiation, such that this function equals zero but its Jacobian with respect to the parameters is not singular. This analysis, however, considers the input-output map under generic initial conditions, i.e. equal to zero [149]. The problem arises when the initial conditions are not generic. Thus, the notion of algebraic identifiability was extended to incorporate the influence of known nonzero initial condition \mathbf{x}_0 on parameter identifiability [203]. In [151] it is shown that the concept of accessibility from the initial conditions plays a major role when assessing identifiability. If a model structure is locally accessible from the initial conditions, then knowledge of it will not add information for the identifiability of the parameter vector \mathbf{p} . Conversely, if we assume that the structure is algebraically observable, and the initial conditions belong to a set from which the system is not locally accessible, it is necessary to take them into consideration in the identifiability analysis. In fact, [202] showed that the knowledge of the initial conditions is equivalent to having more observations of the output such that the parameter identifiability (or estimation) reliability is enhanced. Finally, Stigter and Peeters [171] approached the identifiability problem from a state sensitivity perspective for input-affine nonlinear models. The particular structure of this model class allowed the computation of their accessibility algebra to verify structural identifiability for one parameter at a time. However, this method is limited to a particular form of nonlinear models of low-dimension due to the computational power required to calculate symbolic Lie brackets.

1.2.2. Operational identifiability

Structural identifiability provides methods to evaluate whether a particular model structure, i.e. its parametrization, is identifiable without the need of computing any numerical value. However, identifiability in practice depends on the experimental conditions and whether the recorded data is informative enough. The structural identifiability approach assumes that it is possible to recover all the information about the model structure from the output measurement data. This is in general not true in practice, since the input might not excite the system appropriately. As a consequence, some parameters might be indistinguishable from each other in the collected output data, even if these parameters are structurally identifiable [150]. This is where operational identifiability plays a major role. This analysis will help determine numerically which parameters are indeed identifiable under the prescribed experiment conditions. Analogously, operational identifiability has been largely explored in literature, and can be also subdivided into two classes of methodologies: local sensitivity analysis (gradient-based analysis) and global (gradient-free) sensitivity analysis.

In local operational identifiability analysis (gradient-based sensitivity analysis), a

performance index is examined. This performance index is usually the square of the error between the data and the model prediction. The analysis accounts to determine if this function has an optimum for a unique set of parameters. The optimality condition depends on a mathematical object called the parameter sensitivity matrix \mathbf{S} , which determines the gradient vector and Hessian matrix of the performance index [187]. The sensitivity matrix \mathbf{S} is central in the local approaches because it contains the partial derivatives of the outputs with respect to the model parameter vector, i.e. the parametric sensitivities.

One of the first approaches was to perform an eigenvalue decomposition to the Hessian matrix (approximated as $\mathbf{S}^\top \mathbf{S}$), proposed by [182] and then extended in [143], [157],[144]. Other approaches to address the parametric sensitivity analysis of a dynamic model are tuning importance (TI) [39],[160],[180] and principal component analysis (PCA) [39],[84],[99]. The TI method uses a criterion called overall sensitivity measure, which takes into consideration scaling factors of different physical units. PCA differs from TI because it analyzes sensitivity matrices constructed for each output independently, and then establishes identifiability of each parameter per output. Moreover, these two methods use a normalized version of the sensitivity matrix. The normalization is done to avoid scaling errors that might affect the analysis, in case that the nominal operating values of each parameter differ in several orders of magnitude. A similar approach was proposed in [200] through the use of the Hessian matrix condition number; the method selects subsets of $\mathbf{S}^\top \mathbf{S}$ by removing one column at a time to assess the condition numbers of each of the submatrices. A large condition number indicates either weak individual sensitivity or high degree of correlation (linear dependence) within \mathbf{S} . Moreover, [75] proposed to compute the singular value decomposition (SVD) of the Hessian matrix, and label as unidentifiable the linear combination of parameters whose singular direction magnitudes are smaller than a certain cut-off value. Finally, the orthogonal method was introduced in [204], and improved using an efficient computation algorithm [106],[107]. The orthogonal decomposition method is advantageous over others because most of the gradient-based approaches require linear transformations of the sensitivity matrix \mathbf{S} , which results in linear combinations of the original eigenvectors. This makes difficult to spot which parameter needs to be removed. The orthogonal decomposition method computes the perpendicular distance of one column to the vector space spanned by other columns to directly measure the degree of linear dependency between them. The column with the largest degree of collinearity is removed and the extraction order is stored in a permutation matrix. The method provides a parameter rank based on the order of extraction and the magnitude of the orthogonal sensitivity directions.

A different approach to local (gradient-based) analysis is global analysis. Local analysis is characterized by perturbing one model parameter at a time by a small amount to compute the parameter sensitivities. Global sensitivity analysis tests for the individual influence of parameters in the model's output as well as the interaction between these parameters. There are also multiple approaches to global sensitivity

analysis such as correlation and regression coefficient-based analysis [76],[45],[34] and variance-based methods [80],[166],[153],[154]. The global sensitivity analysis methods differ from the local ones in that they inspect the whole range of parameter, sampling the parameter space, and computing normalized global correlation or variance indexes. However, these methods require high computational power as they scale with a factorial rate with the size of the outputs and the parameter set.

Operational identifiability establishes the setting and methods to assess the influence of model parameters in the model's outputs. However, it has not been discussed how it can be discerned whether a subset of a parameter vector can be decided as identifiable or unidentifiable. Thus, an important aspect of operational identifiability is the establishment of criteria that serve as a measure to set a decision threshold. In general, the criterion will depend on the experimental or operating conditions and the relevant model parameters. Typically, the approximate Hessian matrix of the prediction error cost function with respect to the model parameters is the mathematical object used to construct such criteria [195].

The Hessian matrix is used because its inverse provides an approximation of the Fisher information matrix, which contains information about the total variance in the model. One of the most common criteria is D-optimality, which seeks to keep the inverse of the Hessian matrix's determinant below a cut-off value. This methodology is popular due to the fact that the volume of the ellipsoidal confidence regions of the parameter estimates $\hat{\mathbf{p}}$ is minimized [27]. Another criterion is the L-optimality (linear) that comprises some subcriteria such as A-optimality, T-optimality, and C-optimality. The first one verifies whether the inverse of the Hessian matrix's trace is bounded by some predefined cut-off value. In other words, A-optimality checks if the sum averaged variance of the estimated parameters is bounded [28]. The second criterion is T-optimality, which establishes whether the trace of the Hessian is above a threshold. The third criterion is C-optimality, which corresponds to a scaled version of the A-criterion. This last linear criterion is preferred because the scaling removes all the scale dependencies on the sensitivities. E-optimality (eigenvalue) is another widely used criterion that checks whether the 2-norm of the inverse Hessian matrix is below a user-defined cut-off value. Likewise, a very similar method to E-optimality is Turing's measure of conditioning, which verifies whether the diameter of spherical confidence regions is below some specified threshold [174]. In [164] the G-optimality criterion is proposed, which is used to monitor and keep the total maximum variance of the prediction. The V-criterion [1] is a very similar measure to that of G-optimality, but instead of using the maximum variance, the V-optimality criterion verifies that the average variance remains bounded by a user-defined value. Despite providing a nice intuition on the amount of variance in the model, all of these methods rely on an arbitrary cut-off value that requires tuning and/or experience with the process or model at hand.

1.3. Offline and online parameter estimation

Parameter estimation is the discipline that uses theory and tools for the efficient use of data to estimate parameters in mathematical models. Parameter estimation is a key element in the development of models that accurately represent physical phenomena. Many methods have been developed over the years to address parameter estimation in physical models under different conditions. In this respect, models can be divided into linear or nonlinear in the parameter or with static or time-varying parameters. Recursive methods are widely used in parameter estimation because model parameters are continuously updated every time a new measurement is available. Therefore, it has the potential to correct initial guesses over time, while also capturing the possible time-varying nature of the system. Among the most popular methods for static linear-in-the-parameter models is recursive linear least-squares, which minimizes the quadratic prediction error. This approach is attractive due to its asymptotic statistical properties such as unbiasedness and minimum variance if the system is in the model set, including the parameter model description [8]. Recursive least-squares can also be modified to ensure an excitation condition using Tikhonov regularization or ridge regularization [8]. Nevertheless, these two modifications require to provide an estimate of the parameter covariance to initialize the recursion. Moreover, there are other additional variations of the linear recursive least square method such as weighted recursive least-squares and generalized least-squares. These variations address the issue of heteroskedastic noise in the data, i.e. noise whose variance is not constant over time [19].

For linear-in-the-parameter models with time-varying models, two cases can be covered: abrupt but infrequent changes in the parameters, and slow but continuous changes. For the first case, [8] proposed a reset of the covariance matrix periodically to enforce large step changes in the estimator. For the second case, in the same reference, the authors proposed an exponential forgetting factor between 0 and 1 that gives a smaller weight to old data. Another approach is the use of a Kalman filter to estimate model parameters [86] [87]. However, it is necessary to impose a model to describe the parameter behavior over time. The Kalman filter comprises a two-step procedure, namely the time and measurement updates, where a prediction is performed with past data (time update) and then refined (filtered) with the covariance matrix (measurement update).

In the case of nonlinear-in-the-parameters models, nonlinear least-squares can be used with efficient algorithms such as Gauss-Newton or Levenberg-Marquardt [56]. However, given the nonlinear nature of the models, the estimation can get stuck in local minima. To circumvent this issue, gradient-free optimization can be implemented at the expense of consuming more computational power. Another solution is to use multistart methods with dedicated sampling schemes such as latin hypercube sampling LHS or orthogonal sampling to explore several initial points that might converge to better optima [56]. An even more state-of-the-art solution is to lift the

parameter space adjoining the model states using a multiple shooting parameter estimation method [145]. This method segments the time-based trajectory data into shooting nodes to solve smaller optimization problems jointly coupled with a compatibility constraint. The multiple shooting parameter estimation method is more efficient at dealing with multiple local minima but increases largely the dimension of the optimization search space and computational load. On the other hand, the Kalman filter can be modified in several ways to accommodate to nonlinear models. The most popular one is the extended Kalman filter, which linearizes the model at each operating point using a truncated Taylor expansion to apply the same linear tools of the classical Kalman filter. One of the main problems of the extended Kalman filter is that it requires the computation of the Jacobian matrices with respect to the parameters, which is computationally expensive [141]. An alternative that does not require the explicit computation of the Jacobian matrices is the unscented Kalman filter, which performs a nonlinear transformation to the data to approximate its mean and covariance matrix to a Gaussian distribution with a cloud of sigma points [85]. It ultimately avoids the necessity to compute Jacobian matrices and it is more computationally efficient than the extended Kalman filter. If a model is not well known or is inaccurate, then Monte Carlo methods, especially particle filters, are employed for parameter estimation. These techniques predict the posterior probability distribution based on past data but are more computationally expensive even at moderately-dimensioned state space representations [40].

1.4. Modeling approaches for reaction process systems

The use of first-principle models of reaction systems for online applications, such as model-based control and process real-time monitoring, remains limited in the daily operation of chemical processes/plants. These models are generally not utilized in online model-based applications due to their nonlinear nature and usually large state space dimension. Despite these disadvantages, there are some ways to use rigorous models if the models are represented in a suitable way that is easier to work with. To this end, an analysis on the response modes of a continuous stirred tank reactor (CSTR) employing a state-space decomposition and reduction using linear transformations is introduced in [7]. The proposed method separates independently the different dynamics that govern the evolution of the reaction within the reactor. The (asymptotic) stability of the system is also checked by considering the eigenvalues of the reaction matrix of the system. This decomposition allows for easier sensitivity and stability analyses of reaction systems. Later, in [6] the reaction invariants in the control of continuous chemical reactors using general equilibrium reactions is studied. Two cases are explored: isothermal and adiabatic reactors, and implemented basic proportional feedback controllers to manipulate the inlet flow. The true invariant dynamics in the system are neglected. For isothermal operation, the enthalpy balance in the reactor is a true invariant, whilst for the adiabatic operation, the enthalpy becomes an asymptotic invariant. The sensitivity and sta-

bility analyses are simplified as these invariant sets represent both the controllable modes, that can be made asymptotically stable with the correct manipulated variable, and the uncontrollable modes of the system. In [50] the relevance of reaction invariants in the analysis of several elements and properties of the system is explored, such as its eigenvectors, controllability and observability. It is found that the CSTR is uncontrollable if it is operated at steady-state with a flow rate control with constant feed composition. Moreover, they observed that the reaction invariant imposes restrictions over the observability matrix and may render some dynamics unobservable.

An extension of the work on reaction variants and invariants is introduced in [5]. Reactions variants and invariants sometimes lack physical meaning when initial conditions are different from zero, thus they do not represent a true extent of reaction. The authors studied reaction systems with inlets and outlets. Each dynamics (reaction, inlet flow and outlet flow) could be decoupled into their own spanned mathematical space applying appropriate linear transformations and manipulations while discounting the initial conditions to generate real extents of reaction, extents of inlet streams and outlet streams. They applied this theory in three isothermal reactive system examples: batch, semibatch and continuous-stirred tank reactors. The extension of the theory proved to be very useful in decoupling the dynamics, simplifying the model and helping perform tests on sensitivity of the system more easily. Additionally, [22] extended the concept of extents to multiphase reaction system, and [73] treated the case of non-isothermal reaction system. Likewise, [116], [114], [113] also analyzed non-isothermal reaction systems, including a batch reactive distillation process, to obtain a suitable extent-based representation for control, state estimation, and parameter identification.

1.5. Research questions

As it was explained in the previous sections, first-principle simulation models are important components of a digital twin, and thus, the analysis of their properties is a relevant aspect of their development and maintenance. Therefore, it is natural to ask how both structural and operational identifiability can be improved for the purpose of model update and parameter estimation. Following this line, this thesis addresses the following questions related to parametric identifiability and parameter estimation techniques to keep first-principle models up to date.

Parametric sensitivity provides information about infinitesimal changes of a variable with respect to the parameters. It is useful because it is a quantity that has an easily translatable physical meaning. Since identifiability is a property of the input-output map of a model representation, the interest lies on the output parametric sensitivity. This variable generally depends directly on the internal states and state

parametric sensitivities, and indirectly on the input. Therefore, output controllability analysis potentially provides a mathematical setting where the identifiability can be examined using system theoretic tools. Hence, we propose the following question to further explore this connection between these two important concept, namely structural identifiability and structural output controllability.

1. Research subquestion

How is state and output parametric sensitivity controllability related to identifiability of a parametric plant model?

Structural identifiability analysis is performed in an open-loop setting where the system belongs to the model set of interest. However, most of the processes operate in closed-loop, especially in cases where the process is unstable or requires to be kept within tight operation boundaries. This implies that some parameters structurally identifiable in an open-loop analysis, may not be identifiable in a closed-loop analysis. Therefore, in order to establish a framework that connects controllability, controller design, and structural identifiability analysis, we formulate the following research subquestion.

2. Research subquestion

What is the effect of feedback and controllers on the structural identifiability?

On the other hand, we have mentioned that operational identifiability and parameter estimation depend on the plant's operating point or trajectory. However, since the data only contain some information due to a limited number of measurements, not every parameter in the model can be estimated. Furthermore, the particular mathematical structure of the model can make the cost function used to estimate the parameter vector to stall in certain regions of the search space. Additionally, most parameter estimation approaches try to find only one set of parameter values for the whole data set. This neglects the fact that at different points of an operating trajectory, parameters and their respective sensitivities can vary. This particular effect is especially noticeable in batch processes that follow a specific operating trajectory, which is usually segmented in different operation modes. Hence, it is desired to improve on the current standard parameter estimation solutions for such cases. The following subquestion addresses this issue:

3. Research subquestion

How can parameters be estimated accurately in models exploiting the variations of the parametric sensitivities along the output trajectories?

Usually these approaches work well in an offline setting, where all the data has been collected. However, parameters could be viewed as an extra (artificial) input to the model, and thus, parameter estimation could be addressed from an online optimal control perspective. This is summarized in the next question:

4. Research subquestion

How to design a parameter estimation methodology in an online setting to address potential parameter variations in a first-principle model?

Moreover, modeling approaches for reaction process systems are important for efficient model-based operations. Specifically, the extent decomposition offers a nice method to simplify model representations to estimate kinetic and other process parameters. Nevertheless, this approach requires full knowledge of the process matrices, which most of the time are only partially known. Therefore, it is relevant to find ways to estimate them to obtain some approximation of the missing information. This is explored in the following research questions.

5. Research subquestion

What is the effect of inlet composition uncertainty on the extent transformation and parameter estimation in reaction systems models?

Analogously, first-principle models of processes are great tools that provide a large amount of information and detail necessary for its understanding, control, and/or optimization. One of the more common yet complex industrial processes is the (batch) reactive distillation, in which two process systems are combined in one. This process intensification results in more efficiency at the expense of the introduction of interacting phenomena. Therefore, the development of rigorous first-principle models is relevant for improved operation of such processes. However, not only is the development of rigorous process system models important but also their accuracy with respect to the current process operating behavior. While parameter estimation is the standard way to obtain the desired accuracy, it also presents becomes impractical for models of large scale systems like the reactive distillation process.

The following question addresses the aforementioned issues

6. Research subquestion

How to develop both rigorous and accurate models of a reactive batch distillation process?

1.6. Outline of the thesis

In this thesis, the problems outlined in the previous section will be investigated. For the sake of clarity, a flowchart with the thesis outline is provided in Figure 1.5.

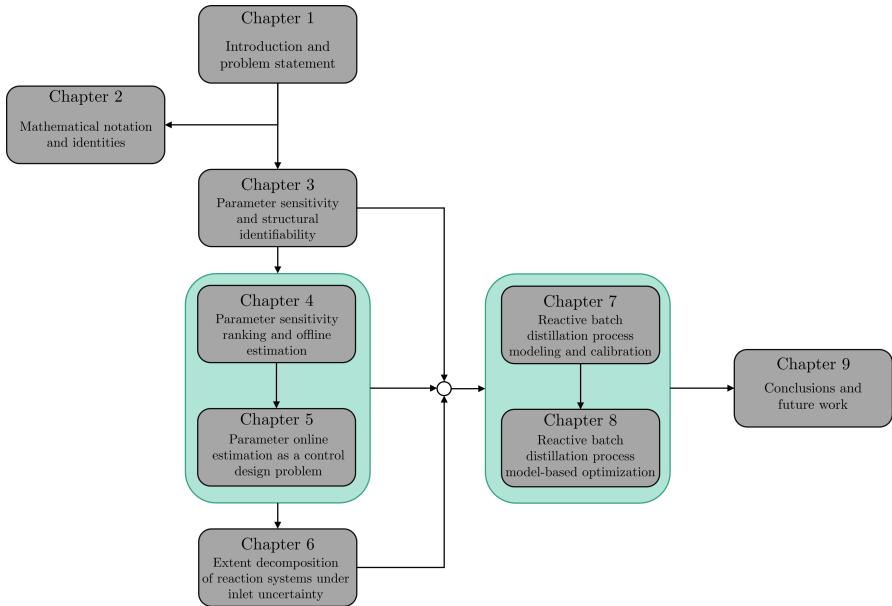


Figure 1.5: Thesis outline

Furthermore, an overview of the chapters is presented next:

Chapter 2 introduces the mathematical notation, properties , and identities used throughout the body of work. This chapter can be treated as a reference, and therefore, it is not required to read it fully before proceeding with the subsequent chapters.

Chapter 3 treats structural identifiability providing definitions and the theoretical

foundations to understand the concept. In this chapter, we present the connection between structural identifiability and output controllability, as well as methods to test whether a controller structure hampers structural identifiability in a closed-loop configuration. This chapter addresses the research subquestions 1 and 2.

Chapter 4 is concerned with assessment of parameter identifiability in an operational sense and estimation in an offline setting. Several multi-start parameter estimation methodologies are introduced to circumvent the difficulties of ill-conditioned search spaces. Additionally, a data segmentation approach is used along with a multiple shooting method to improve on the conditioning of the parameter estimation problem. This proves to be especially useful in batch processes with very differentiated operating regimes. This chapter addresses the research subquestion 3.

Chapter 5 deals with parameter estimation in an online setting using the tools developed in Chapter 4. Here, online parameter estimation is treated as a control design problem with an additional layer of recursive parameter selection to account for parameter time variations. This chapter addresses the research subquestion 4.

Chapter 6 addresses the issue of the extent decomposition when modeling reaction systems under inlet uncertainty. The extent decomposition requires perfect knowledge process matrices but in some cases, the inlet composition matrix is not perfectly known due to recycles or upstream variations. This chapter is centered around estimating this uncertainty to obtain a reliable decomposition for control and estimation purposes. This chapter addresses the research subquestion 5.

Chapters 7–8 focus on the development, calibration, and optimization of a simulation model of a real reactive batch distillation process that acts as a case study. This chapter allows to test some of the theoretical developments proposed through the thesis, while providing an operation solution to the inherent challenges of the reactive batch distillation process. Furthermore, this chapter also includes a dynamic gray box model for the viscosity of the polymer being produced. This is important because the viscosity is the critical variable in this process, and it is needed to assess the quality of the yield.

Chapter 9 contains the conclusions and future work that could follow from this piece of work. The chapter reflects on the developed techniques and its implications for their end use.

Appendix A provides all the proofs of theorems and mathematical derivations of the developments presented in the thesis.

A list of the publications related to this thesis can be found at the end of this thesis

2

Mathematical preliminaries

In this chapter we present the notation and mathematical conventions used throughout the thesis. In general, a lowercase boldfaced character represents a vector, an uppercase boldfaced character represents a matrix, and a light typeface represents a scalar value.

2.1. General notation

- \mathbb{N} The set of natural numbers (with zero included).
- \mathbb{Z} The set of integer numbers.
- \mathbb{Z}_+ The set of strictly positive integer numbers.
- \mathbb{R} The set of real numbers.
- \mathbb{C} The set of complex numbers.
- \mathbf{I}_k The identity matrix of dimension $k \times k$.
- $\mathbf{0}_{k \times \ell}$ The zero matrix of dimension $k \times \ell$.
- \mathbf{d} Total derivative.
- ∂ Partial derivative.
- $\|\cdot\|$ Any norm of a vector, matrix, function, or system.
- $\text{vec}(\cdot)$ Vectorization operator.
- $\mathbf{e}_k(i)$ The k -dimensional unit vector whose i -th entry is 1 and 0 elsewhere.
- $\mathbf{1}_k$ The k -dimensional column vector of ones.
- $\mathbf{0}_k$ The k -dimensional column vector of zeros.
- $\delta_{i,j}$ Kronecker delta.
- $\mathbb{E}[\cdot]$ Expectation operator.
- \odot Element-wise product.
- \odot^{-1} Element-wise division.

2.2. Numbers, vectors and vector norms

Consider the following definitions for column vectors $z \in \mathbb{C}$ of the form $z = a + bj$, with $a, b \in \mathbb{R}$, and $j = \sqrt{-1}$ the imaginary unit.

- $\text{Re}(z)$ The real part of z defined as $\text{Re}(z) := a$.
- $\text{Im}(z)$ The imaginary part of z defined as $\text{Im}(z) := b$.
- z^* The conjugate of z defined as $z^* = a - bj$.
- $|z|$ The modulus of z defined as $|z| := \sqrt{[\text{Re}(z)]^2 + [\text{Im}(z)]^2} = \sqrt{a^2 + b^2}$.

Consider the following definitions for column vectors $\mathbf{x}, \mathbf{y} \in \mathbb{R}^n$ with n rows

- x_i The element of \mathbf{x} in row i .
- \mathbf{x}^\top Transpose of \mathbf{x} .
- $\langle \mathbf{x}, \mathbf{y} \rangle$ The inner product between \mathbf{x} and \mathbf{y} defined as $\mathbf{x}^\top \mathbf{y}$.

- $\|\mathbf{x}\|_k$ The k -th norm of \mathbf{x} is defined as

$$\|\mathbf{x}\|_k := \begin{cases} \left(\sum_{i=1}^n |x_i|^k \right)^{\frac{1}{k}} & \text{for } k \in \mathbb{Z}_+ \\ \max_{i \in \{1, 2, \dots, n\}} |x_i| & \text{for } k = \infty \end{cases}$$

Any pair of real-valued vectors \mathbf{x}, \mathbf{y} that satisfy $\mathbf{x}^\top \mathbf{y} \equiv 0$ are said to be orthogonal. If they satisfy the orthogonality property, and additionally, their 2-norms are the unit, i.e. $\|\mathbf{x}\|_2 = \|\mathbf{y}\|_2 \equiv 1$, they are called orthonormal.

2.3. Vector spaces and matrices

Every matrix $\mathbf{A} \in \mathbb{R}^{m \times n}$ defines a linear transformation $T(\mathbf{A}) : \mathbb{R}^n \mapsto \mathbb{R}^m$ that maps a vector $\mathbf{x} \in \mathbb{R}^n$ to the matrix product $\mathbf{y} = \mathbf{Ax}$, which is a vector of \mathbb{R}^m .

Matrices

- $a_{i,j}$ The element of \mathbf{A} in the i -th row and the j -th column.
- \mathbf{A}^\top The transpose of \mathbf{A} .

- $\ker(\mathbf{A})$ The kernel (or null space) of \mathbf{A} . It is defined as

$$\ker(\mathbf{A}) := \{\mathbf{x} \in \mathbb{R}^n \mid \mathbf{Ax} = 0\}$$

- $\text{col}(\mathbf{A})$ or $\mathcal{R}(\mathbf{A})$ The column space (or range space) of \mathbf{A} . It is defined as

$$\text{col}(\mathbf{A}) := \{\mathbf{y} \in \mathbb{R}^m \mid \mathbf{y} = \mathbf{Ax} \text{ for some } \mathbf{x} \in \mathbb{R}^n\}$$

- $\text{rank}(\mathbf{A})$ The rank of \mathbf{A} . It describes the number of independent rows or columns. The rank satisfies the inequality

$$\text{rank}(\mathbf{A}) \leq \min(m, n)$$

We say a matrix is full (row or column) rank when the previous equation holds with equality.

- \mathbf{A}^+

The Moore-Penrose pseudo-inverse of \mathbf{A} . The pseudo-inverse $\mathbf{A}\mathbf{A}^+ \in \mathbb{R}^{n \times m}$ exists for every matrix \mathbf{A} . However, whenever \mathbf{A} is full (row or column) rank, it is defined as

$$\begin{aligned}\mathbf{A}^+ &= (\mathbf{A}^\top \mathbf{A})^{-1} \mathbf{A}^\top \Leftrightarrow \mathbf{A}^+ \mathbf{A} = \mathbf{I}_n \text{ left inverse if } \text{rank}(\mathbf{A}) = n \\ \mathbf{A}^+ &= \mathbf{A}^\top (\mathbf{A} \mathbf{A}^\top)^{-1} \Leftrightarrow \mathbf{A} \mathbf{A}^+ = \mathbf{I}_m \text{ right inverse if } \text{rank}(\mathbf{A}) = m\end{aligned}$$

- $\|\mathbf{A}\|_{k,l}$

The (k,l) -induced norm of \mathbf{A} . It is defined as

$$\|\mathbf{A}\|_{k,l} := \sup_{x \neq 0} \frac{\|\mathbf{A}\mathbf{x}\|_k}{\|\mathbf{x}\|_l}$$

- $\|\text{vec}(\mathbf{A})\|_{k,l}$

The (k,l) element-wise norm of \mathbf{A} . It is defined as

$$\|\text{vec}(\mathbf{A})\|_{k,l} = \left(\sum_{j=1}^n \left(\sum_{i=1}^m |a_{i,j}|^k \right)^{\frac{l}{k}} \right)^{\frac{1}{l}}$$

Square matrices

Consider the following definitions for square matrices $\mathbf{A} \in \mathbb{R}^{n \times n}$

- $\lambda \in \mathbb{C}$

Eigenvalue of \mathbf{A} and satisfy $\mathbf{A}\mathbf{v} = \lambda\mathbf{v}$ for some $\mathbf{v} \neq \mathbf{0} \in \mathbb{C}^n$.

- $\mathbf{v} \in \mathbb{C}^n$

Right eigenvector of \mathbf{A} associated with the eigenvalue $\lambda \in \mathbb{C} \Rightarrow \mathbf{A}\mathbf{v} = \lambda\mathbf{v}$.

- $\mathbf{w} \in \mathbb{C}^n$

Left eigenvector of \mathbf{A} associated with the eigenvalue $\lambda \in \mathbb{C} \Rightarrow \mathbf{w}^* \mathbf{A} = \lambda \mathbf{w}^*$.

-

The matrix \mathbf{A} is called symmetric if $\mathbf{A} = \mathbf{A}^\top$.

-

The real square matrix \mathbf{A} is called orthogonal if its rows and columns are orthonormal vectors. Any orthogonal matrix \mathbf{A} satisfies $\mathbf{A}\mathbf{A}^\top = \mathbf{A}^\top \mathbf{A} = \mathbf{I}_n$

- $\text{tr}(\mathbf{A})$

The trace of \mathbf{A} . It is defined as

$$\text{tr}(\mathbf{A}) := \sum_{i=1}^n a_{i,i}$$

- $\det(\mathbf{A})$

The determinant of \mathbf{A} . The determinant is nonzero if the matrix is full rank.

- \mathbf{A}^{-1}

The inverse of \mathbf{A} . For square matrices, the inverse matrix satisfies $\mathbf{A}\mathbf{A}^{-1} = \mathbf{A}^{-1}\mathbf{A} = \mathbf{I}_n$

- $\lambda(\mathbf{A})$ The spectrum or eigenspace of \mathbf{A} . It is defined as

$$\lambda(\mathbf{A}) := \{\lambda \in \mathbb{C} \mid \mathbf{A}\mathbf{v} = \lambda\mathbf{v} \text{ for some } \mathbf{v} \neq \mathbf{0} \in \mathbb{C}^n\}$$

Matrix norms

The (k, l) -induced norm of \mathbf{A} is called the k -induced norm if $k = l$, i.e. $\|\mathbf{A}\|_k := \|\mathbf{A}\|_{k,l}$.

For a matrix $\mathbf{A} \in \mathbb{R}^{m \times n}$, the special cases when $k = 1, 2, \infty$ are typically considered

$$\|\mathbf{A}\|_1 = \max_{1 \leq j \leq n} \sum_{i=1}^m |a_{i,j}|$$

$$\|\mathbf{A}\|_2 = \max(\lambda(\mathbf{A}^\top \mathbf{A}))$$

$$\|\mathbf{A}\|_\infty = \max_{1 \leq j \leq m} \sum_{i=1}^n |a_{i,j}|$$

The (k, l) element-wise norm of \mathbf{A} is called the k element-wise norm if $k = l$, i.e. $\|\text{vec}(\mathbf{A})\|_k := \|\text{vec}(\mathbf{A})\|_{k,l}$.

For a matrix $\mathbf{A} \in \mathbb{R}^{m \times n}$, the special cases when $k = 2, \infty$ are typically considered

$$\|\text{vec}(\mathbf{A})\|_2 = \|\mathbf{A}\|_{\text{F}} = \sqrt{\text{tr}(\mathbf{A}^\top \mathbf{A})} = \sqrt{\sum_{i=1}^m \sum_{j=1}^n |a_{i,j}|^2} \quad (\text{Frobenius norm})$$

$$\|\text{vec}(\mathbf{A})\|_\infty = \|\mathbf{A}\|_{\text{max}} = \max_{i,j} |a_{i,j}| \quad (\text{max norm})$$

Equivalence of norms

For all matrices $\mathbf{A} \in \mathbb{R}^{m \times n}$, any two matrix norms $\|\cdot\|_\alpha$ $\|\cdot\|_\beta$ satisfy

$$p\|\cdot\|_\alpha \leq \|\cdot\|_\beta \leq q\|\cdot\|_\alpha$$

for positive numbers p and q . Since $\mathbb{R}^{m \times n}$ has finite dimension $m \times n$, all norms on $\mathbb{R}^{m \times n}$ are *equivalent*. We list some typical norm equivalences for a matrix $\mathbf{A} \in \mathbb{R}^{m \times n}$ with rank r [61]:

- $\frac{1}{\sqrt{n}}\|\mathbf{A}\|_\infty \leq \|\mathbf{A}\|_2 \leq \sqrt{m}\|\mathbf{A}\|_\infty$

- $\frac{1}{\sqrt{m}}\|\mathbf{A}\|_1 \leq \|\mathbf{A}\|_2 \leq \sqrt{n}\|\mathbf{A}\|_1$

- $\|\mathbf{A}\|_{\max} \leq \|\mathbf{A}\|_2 \leq \sqrt{mn}\|\mathbf{A}\|_{\max}$

- $\|\mathbf{A}\|_2 \leq \|\mathbf{A}\|_{\text{F}} \leq \sqrt{r}\|\mathbf{A}\|_2$

2

2.4. Vector and matrix calculus

In this section, we provide some definitions and identities of matrix calculus using the convention followed by Brewer [29].

For matrices $\mathbf{A} \in \mathbb{R}^{m \times n}$, $\mathbf{B} \in \mathbb{R}^{p \times q}$, $\mathbf{C} \in \mathbb{R}^{r \times s}$, $\mathbf{D} \in \mathbb{R}^{n \times p}$, and column vectors $\mathbf{x} \in \mathbb{R}^k$ and $\mathbf{y} \in \mathbb{R}^\ell$.

- $\mathbf{E}_{ij}^{m \times n}$ The elementary matrix with dimensions $m \times n$ whose (i, j) entry is 1 and is zeros everywhere else. It is defined as

$$\mathbf{E}_{ij}^{m \times n} := \mathbf{e}_m(i)\mathbf{e}_n^\top(j)$$

- $\mathbf{A} \otimes \mathbf{B}$ The Kronecker product of matrices \mathbf{A} and \mathbf{B} defined as

$$\mathbf{A} \otimes \mathbf{B} := \begin{bmatrix} a_{11}\mathbf{B} & a_{12}\mathbf{B} & \cdots & a_{1n}\mathbf{B} \\ a_{21}\mathbf{B} & a_{22}\mathbf{B} & \cdots & a_{2n}\mathbf{B} \\ \vdots & \vdots & \ddots & \vdots \\ a_{m1}\mathbf{B} & a_{m2}\mathbf{B} & \cdots & a_{mn}\mathbf{B} \end{bmatrix} \in \mathbb{R}^{mp \times nq}$$

- $\mathbf{K}_{m \times n}$ The square commutation matrix with dimensions $mn \times mn$ that has precisely a single 1 in each row and in each column. The commutation matrix is a special type of permutation matrix (orthogonal). It is defined as

$$\mathbf{K}_{m \times n} := \sum_i^m \sum_j^n \mathbf{E}_{ij}^{(m \times n)} \mathbf{E}_{ij}^{(n \times m)}$$

- $\bar{\mathbf{K}}_{m \times n}$ The rectangular commutation matrix $\mathbf{K}_{m \times n}$ with dimensions $m^2 \times n^2$. This matrix is not orthogonal and defined as

$$\bar{\mathbf{K}}_{m \times n} := \sum_i^m \sum_j^n \mathbf{E}_{ij}^{(m \times n)} \mathbf{E}_{ij}^{(m \times n)}$$

- $\text{vec}(\mathbf{A})$ The vectorization of \mathbf{A} defined as

$$\text{vec}(\mathbf{A}) := [a_{11} \quad \cdots \quad a_{m1} \quad a_{12} \quad \cdots \quad a_{m2} \quad \cdots \quad a_{mn}]^\top \in \mathbb{R}^{mn}$$

The Kronecker product and the vectorization operation are related by the following identity:

$$\begin{aligned}\text{vec}(\mathbf{ADB}) &= (\mathbf{B}^\top \mathbf{D}^\top \otimes \mathbf{I}_m) \text{vec}(\mathbf{A}) \\ &= (\mathbf{B}^\top \otimes \mathbf{A}) \text{vec}(\mathbf{D}) \\ &= (\mathbf{I}_q \otimes \mathbf{AD}) \text{vec}(\mathbf{B})\end{aligned}$$

- $\text{vec}_{m,n}^{-1}(\mathbf{a})$ The inverse of $\mathbf{a} = \text{vec}(\mathbf{A})$. For known positive integers m and n , the inverse of the vectorization is defined as:

$$\text{vec}_{m,n}^{-1}(\mathbf{a}) = \left(\text{vec}^\top(\mathbf{I}_n) \otimes \mathbf{I}_m \right) (\mathbf{I}_n \otimes \mathbf{a}) = \mathbf{A}$$

- $\frac{\partial \mathbf{x}}{\partial \mathbf{y}^\top}$ Vector derivative with respect to another vector (Jacobian matrix). The vector derivative with respect to another vector has the following properties:

$$\begin{aligned}&\bullet \frac{\partial \mathbf{x}}{\partial \mathbf{x}^\top} = \mathbf{I}_k \\ &\bullet \frac{\partial \mathbf{x}}{\partial \mathbf{y}} = \text{vec} \left(\frac{\partial \mathbf{x}}{\partial \mathbf{y}^\top} \right) \\ &\bullet \left(\frac{\partial \mathbf{x}}{\partial \mathbf{y}^\top} \right)^\top = \frac{\partial \mathbf{x}^\top}{\partial \mathbf{y}}\end{aligned}$$

- $\frac{\partial \mathbf{A}}{\partial \mathbf{B}}$ Matrix derivative with respect to a matrix. It is defined as

$$\frac{\partial \mathbf{A}}{\partial \mathbf{B}} = \sum_{i,j} \mathbf{E}_{ij}^{p \times q} \otimes \frac{\partial \mathbf{A}}{\partial b_{ij}} = \begin{bmatrix} \partial_{b_{1,1}} \mathbf{A} & \partial_{b_{1,2}} \mathbf{A} & \cdots & \partial_{b_{1,q}} \mathbf{A} \\ \partial_{b_{2,1}} \mathbf{A} & \partial_{b_{2,2}} \mathbf{A} & \cdots & \partial_{b_{2,q}} \mathbf{A} \\ \vdots & \vdots & \ddots & \vdots \\ \partial_{b_{p,1}} \mathbf{A} & \partial_{b_{p,2}} \mathbf{A} & \cdots & \partial_{b_{p,q}} \mathbf{A} \end{bmatrix} \in \mathbb{R}^{mp \times nq}$$

where $b_{i,j}$ corresponds to the (i,j) element of \mathbf{B}

The matrix derivative with respect to another matrix satisfy the following identities:

$$\bullet \frac{\partial \mathbf{A}}{\partial \mathbf{A}^\top} = \mathbf{K}_{m \times n}$$

- $\frac{\partial \mathbf{A}}{\partial \mathbf{A}} = \bar{\mathbf{K}}_{m \times n}$

Matrix derivative: the product rule

2

- $\frac{\partial(\mathbf{AD})}{\partial \mathbf{B}} = \frac{\partial \mathbf{A}}{\partial \mathbf{B}} (\mathbf{I}_q \otimes \mathbf{D}) + (\mathbf{I}_p \otimes \mathbf{A}) \frac{\partial \mathbf{D}}{\partial \mathbf{B}}$

Matrix derivative: the chain rule

- $$\begin{aligned} \frac{\partial \mathbf{A}(\mathbf{C}(\mathbf{B}))}{\partial \mathbf{B}} &= \left(\mathbf{I}_p \otimes \frac{\partial \mathbf{A}}{\partial \text{vec}(\mathbf{C})} \right) \left(\frac{\partial [\text{vec}(\mathbf{C}^\top)]^\top}{\partial \mathbf{B}} \otimes \mathbf{I}_n \right) \\ &= \left(\frac{\partial [\text{vec}(\mathbf{C})]^\top}{\partial \mathbf{B}} \otimes \mathbf{I}_m \right) \left(\mathbf{I}_q \otimes \frac{\partial \mathbf{A}}{\partial \text{vec}(\mathbf{C})} \right) \end{aligned}$$

Although it was defined for matrices, this chain rule obviously also applies to vectors.

2.5. Formal power series

Formal power series are a generalization of polynomials, where the number of terms is allowed (but not required) to be infinite. In this section, we introduce the use of formal power series to treat polynomials as their properties and operators are useful when dealing with transfer functions.

Let $f(s)$ and $g(s)$ be formal power series given by $f(s) = \sum_{k=0}^{\infty} f_k s^k$, and $g(s) = \sum_{k=0}^{\infty} g_k s^k$. We list some important operations that can be used within the context of formal power series [136]

- Addition: $\sum_{k \in \mathbb{N}} f_k s^k + \sum_{k \in \mathbb{N}} g_k s^k = \sum_{k \in \mathbb{N}} (f_k + g_k) s^k$
- Multiplication: $\sum_{k \in \mathbb{N}} f_k s^k \times \sum_{k \in \mathbb{N}} g_k s^k = \sum_{n \in \mathbb{N}} \left(\sum_{k=0}^n f_k g_{n-k} s^n \right)$
- Division: $\frac{\sum_{k \in \mathbb{N}} g_k s^k}{\sum_{k \in \mathbb{N}} f_k s^k} = \sum_{k \in \mathbb{N}} h_k s^k$. The division is defined if and only if the constant term f_0 is not zero.

A recursive formula can be used to compute the n -th term of $h(s)$:

$$h_0 = \frac{1}{f_0}$$

$$h_n = \frac{1}{f_0} \left(g_n - \sum_{k=1}^n f_k h_{n-k} \right)$$

A special case of the division operation is the multiplicative inverse of $f(s)$. The series $g(s)$ is assumed to have the constant term $g_0 = 1$, and $g_k = 0$, $\forall k \in \mathbb{N}$. Thus, the coefficients of the inverse are defined as:

$$h_0 = \frac{1}{f_0}$$

$$h_n = -\frac{1}{f_0} \sum_{k=1}^n f_k h_{n-k}$$

The coefficient extraction operator denoted by $[s^n]f(s) = f_n$ is a functional $[s^n] : \mathcal{F} \mapsto \mathbb{R}$, where \mathcal{F} is the set of formal power series over a field (in the context of this thesis, the field is \mathbb{R}), defined by the rule $[s^n][s^k] = \delta_{n,k}$ [128]. The coefficient extraction operator satisfy the following properties

- Linearity: $[s^n](\alpha f(s) + \beta g(s)) = \alpha[s^n]f(s) + \beta[s^n]g(s)$
- Shifting: $[s^n]sf(s) = [s^{n-1}]f(s)$
- Differentiation: $[s^n]f'(s) = (n+1)[s^{n+1}]f(s)$
- Convolution: $[s^n]f(s)g(s) = \sum_{k=0}^{\infty} ([s^k]f(s))([s^{n-k}]g(s))$
- Composition: $[s^n]f(g(s)) = \sum_{k=0}^{\infty} ([s^k]f(s))[s^n]g(s)^k$

We also introduce the notation $[\mathbf{s}]f(s)$ to denote the extraction of **all** coefficients of a series $f(s)$ to collect them in a vector.

$$[\mathbf{s}]f(s) = \begin{bmatrix} f_n \\ f_{n-1} \\ \vdots \\ f_0 \end{bmatrix}$$

2.6. Subspaces

Let \mathcal{U} and \mathcal{V} be finite-dimensional vector spaces, and let \mathcal{W} be a subspace of \mathcal{V} .

2

- $\dim(\mathcal{V})$ The dimension of \mathcal{V}
- $\mathcal{W} \subseteq \mathcal{V}$ \mathcal{W} is a subspace of \mathcal{V} . This means that any vector $\mathbf{w} \in \mathcal{W}$ is also $\mathbf{w} \in \mathcal{V}$. A strict inclusion $\mathcal{W} \subset \mathcal{V}$ is used if there exists at least one vector $\mathbf{v} \in \mathcal{V}$ but $\mathbf{v} \notin \mathcal{W}$
- $\mathcal{U} \cap \mathcal{V}$ The intersection of \mathcal{U} and \mathcal{V} . It is defined as

$$\mathcal{U} \cap \mathcal{V} := \{\mathbf{x} \in \mathcal{U}, \mathbf{x} \in \mathcal{V}\}$$

- \mathcal{W}^\perp The orthogonal complement of \mathcal{W} . It is defined as

$$\mathcal{W}^\perp := \{\mathbf{w} \in \mathcal{W} \mid \langle \mathbf{w}, \mathbf{v} \rangle = 0, \forall \mathbf{v} \in \mathcal{V}\}$$

The orthogonal complement allows us to characterize the relationship between the four main subspaces of a linear transformation $T(\mathbf{A})$ defined by a matrix \mathbf{A} .

- $(\text{col}(\mathbf{A}))^\perp = \ker(\mathbf{A}^\top)$
- $(\text{col}(\mathbf{A}^\top))^\perp = \ker(\mathbf{A})$

Grassmann Dimension Formula

$$\dim(\mathcal{U} + \mathcal{V}) = \dim(\mathcal{U}) + \dim(\mathcal{V}) - \dim(\mathcal{U} \cap \mathcal{V})$$

3

Structural identifiability of linear models in open and closed-loop

In this chapter, structural identifiability of linear models is considered. The concept of structural identifiability is introduced and analyzed in open and closed-loop settings. In the former, the model is tested to verify that the parameters are identifiable from the model's input-output map. In the latter, the influence of controllers on structural identifiability is studied in detail. Guidelines for identifiability-aware control design are also proposed. Additionally, the relationship between the output sensitivity controllability matrix and identifiability is analyzed from a controllability perspective.

Publications of this chapter:

Structural Identifiability of Linear State Space Model: A State and Output Sensitivity Controllability Approach, Méndez-Blanco, C., Özkan, L. 2020 59th IEEE Conference on Decision and Control (CDC) ([124])

3.1. Introduction

First-principle models are generally a collection of differential and algebraic equations describing constitutive relationships between different phenomena in a system. These models are comprised by internal variables and parameters. The former describe the physical quantities of a system's dynamics, while the latter scale and relate the internal variables with each other. First-principle models are costly to develop, thus it is important to keep them up to date, i.e. calibrate, to avoid model-plant mismatch, while extending the model's uselife. The classical way to calibrate a model is through the estimation of its parameters. The previous approach works on the basis that parameters scale the model dynamics to match that of the real system. However, before performing parameter estimation, one must assess which set of parameters can be confidently estimated, namely parameter identifiability. This aforementioned notion can be addressed from two perspectives: structural identifiability and operational identifiability. The former is related to the structure of the model, i.e. the way how the model has been parametrized in the differential and algebraic equations. The latter deals with signal properties and richness of the data to obtain reliable parameter estimates. Structural analysis should in principle be carried out before operational analysis to evaluate the parameter set that the model itself allows to estimate. Structural identifiability has been extensively studied in literature (see e.g. [16], [149], [36], [193]) for different types of parametrized models, especially in the mathematical biology domain. Most of these techniques resort to a certain type of transformation to obtain a suitable input-output representation of the model. Another approach to address the identifiability problem is to use system sensitivity theory ([55]). Sensitivity analysis for structural identifiability has been explored mainly for both linear and nonlinear ordinary differential equation (ODE) models. In the case of nonlinearly parametrized linear state space models, [44] proposed a method based on the symmetric positive definite solution of the matrix Lyapunov equation, with the assumption that the system under inspection is stabilizable. Along the same lines of [44], [184] applied a similar analysis for large-scale linear ODE models analyzing the sensitivity representation of the Markov parameters to assess identifiability using the singular value decomposition (SVD) of the sensitivity matrix. Furthermore, [171] has dealt with nonlinear ODE models using observability and accessibility algebras to draw conclusions on parameter identifiability.

Another important aspect is identifiability in closed-loop because controllers can potentially hamper identifiability. Likewise, this topic has received great attention in literature throughout the years (see for example [74],[54],[72],[15]), but the main focus has been on operational identifiability, i.e. the properties of the controller to guarantee that the signals fed to the plant provide maximum information. Nonetheless, little attention has been given to the controller parametric structure to ensure that the identifiability of the structure remains the same with respect to the true physical parameters.

In this chapter, we consider the structural identifiability of linear or linearized non-linear DAE models around an operating point or trajectory. We introduce tools existing in literature to perform the analysis in open-loop. We also propose a new perspective on structural identifiability for transfer functions and linear state space representations based on the output controllability matrix. Finally, we also develop and provide novel results on the closed-loop structural identifiability case along with controller design constraints to avoid the impoverishment of structural identifiability.

3.2. Structural properties

Let $\mathcal{M}(\cdot)$ be the structure chosen for the model, which defines the class of possible models, let $\mathbf{p} \in \mathbb{P} \subseteq \mathbb{R}^{n_p}$ be a vector of parameters, where \mathbb{P} is the feasible parameter space, and let $\mathcal{M}(\mathbf{p})$ be the specific model obtained when the parameters take the values \mathbf{p} . A property is structural if it holds for almost $\mathbf{p} \in \mathbb{P}$ except on a subspace of zero measure. Although there are several structural properties, we shall focus on *structural identifiability*. Additionally, we will also restrict our analysis to general nonlinear systems that can be written as a system of differential algebraic equations (DAE) as:

$$\mathcal{M}(\mathbf{p}) = \begin{cases} \dot{\mathbf{x}}(t, \mathbf{p}) &= \mathbf{f}(\mathbf{x}(t), \mathbf{u}(t), \mathbf{z}(t), \mathbf{p}) & \mathbf{x}(t_0) = \mathbf{x}_0 \\ \mathbf{0} &= \mathbf{h}(\mathbf{x}(t), \mathbf{u}(t), \mathbf{z}(t), \mathbf{p}) \\ \mathbf{y}(t, \mathbf{p}) &= \mathbf{g}(\mathbf{x}(t), \mathbf{z}(t), \mathbf{p}) \end{cases} \quad (3.1)$$

where $\mathbf{x}(t, \mathbf{p}) \in \mathbb{R}^{n_x}$ is the vector of differential states, $\mathbf{u}(t) \in \mathbb{R}^{n_u}$ is the known input vector, $\mathbf{y}(t, \mathbf{p}) \in \mathbb{R}^{n_y}$ is the measurement or the output vector, $\mathbf{z}(t, \mathbf{p}) \in \mathbb{R}^{n_z}$ is the algebraic state, and $\mathbf{p} \in \mathbb{P} \subseteq \mathbb{R}^{n_p}$ the parameter vector. The vector functions \mathbf{f} , \mathbf{g} , and \mathbf{h} are assumed to be analytic functions, the Jacobian $\partial_{\mathbf{z}} \mathbf{h}$ is invertible at all points $(\mathbf{x}, \mathbf{z}, \mathbf{u})$, and the differentiation index of the model is assumed to be 1.

Since the differentiation index is 1, (3.1) can be converted to

$$\mathcal{M}(\mathbf{p}) = \begin{cases} \dot{\mathbf{x}}(t, \mathbf{p}) &= \mathbf{f}(\mathbf{x}(t), \mathbf{z}(t), \mathbf{u}(t), \mathbf{p}), & \mathbf{x}(t_0) = \mathbf{x}_0 \\ \dot{\mathbf{z}}(t, \mathbf{p}) &= -\left(\partial_{\mathbf{z}} \mathbf{h}\right)^{-1} \partial_{\mathbf{x}} \mathbf{f}(\mathbf{x}(t), \mathbf{z}(t), \mathbf{u}(t), \mathbf{p}), & \mathbf{z}(t_0) = \mathbf{z}_0 \\ \mathbf{y}(t, \mathbf{p}) &= \mathbf{g}(\mathbf{x}(t), \mathbf{z}(t), \mathbf{p}) \end{cases} \quad (3.2)$$

where the algebraic state \mathbf{z} is now a differential state, and both \mathbf{x}_0 and \mathbf{z}_0 must

satisfy $\mathbf{h}(\mathbf{x}_0, \mathbf{z}_0) = 0$.

However, most of the systems function at a particular operating point or trajectory. Therefore, their dynamics of interest are described by the linearized versions of their respective nonlinear models. In view of this, given its use and practicality, it is worthwhile to analyze identifiability of linear models.

Let the linearized model structure $\bar{\mathcal{M}}(\mathbf{p})$ be a minimal state space model obtained from linearizing (3.2) about an operating trajectory $(\bar{\mathbf{x}}^*, \mathbf{u}^*, \mathbf{y}^*)$ such that

$$\bar{\mathcal{M}}(\mathbf{p}) = \begin{cases} \delta \dot{\bar{\mathbf{x}}}(t, \mathbf{p}) = \mathbf{A}(\mathbf{p})\delta \bar{\mathbf{x}}(t, \mathbf{p}) + \mathbf{B}(\mathbf{p})\delta \mathbf{u}(t), & \delta \bar{\mathbf{x}}(0) = \delta \bar{\mathbf{x}}_0 \\ \delta \mathbf{y}(t, \mathbf{p}) = \mathbf{C}(\mathbf{p})\delta \bar{\mathbf{x}}(t, \mathbf{p}) \\ \dot{\mathbf{p}} = \mathbf{0} \end{cases} \quad (3.3)$$

where $\delta \bar{\mathbf{x}} = \bar{\mathbf{x}} - \bar{\mathbf{x}}^*$, $\delta \mathbf{u} = \mathbf{u} - \mathbf{u}^*$, $\delta \mathbf{y} = \mathbf{y} - \mathbf{y}^*$, $\mathbf{A}(\mathbf{p}) = \partial_{\bar{\mathbf{x}}} \bar{\mathbf{f}}|_{\bar{\mathbf{x}}^*, \mathbf{u}^*}$, $\mathbf{B}(\mathbf{p}) = \partial_{\mathbf{u}} \bar{\mathbf{f}}|_{\bar{\mathbf{x}}^*, \mathbf{u}^*}$, $\mathbf{C}(\mathbf{p}) = \partial_{\bar{\mathbf{x}}} \mathbf{g}|_{\bar{\mathbf{x}}^*, \mathbf{u}^*}$, $\bar{\mathbf{f}} = \begin{bmatrix} \mathbf{f}^\top & -\partial_{\mathbf{x}} \mathbf{f}^\top (\partial_{\mathbf{z}} \mathbf{h})^{-\top} \end{bmatrix}^\top$, and $\bar{\mathbf{x}} = [\mathbf{x}^\top \quad \mathbf{z}^\top]^\top$

In general, there are three common scenarios when addressing the identifiability of the parameter vector \mathbf{p} [130].

- (i) Constant parameter only $\dot{\mathbf{p}} = \mathbf{0}$
- (ii) Time-varying parameters only $\dot{\mathbf{p}} \neq \mathbf{0}$
- (iii) A combination of both constant and time-varying parameters

In most cases, the methodologies developed in literature consider only time-invariant parameters, although the definitions of identifiability will also hold for time-varying parameters. Ljung and Glad [104] make a clear distinction between parameters and states. They understand parameters as static values in a model structure, while states are regarded as everything else that may evolve in time. Generally, identifiability of time-varying parameters is more difficult to assess given their evolution in time. A frequent approach is to assume that time-varying parameters can be regarded as extra states whose dynamics are known and parametrized in terms of unknown static parameters. Throughout this thesis, we shall adhere to the interpretation that parameters are time-invariant, i.e. $\dot{\mathbf{p}} = \mathbf{0}$.

3.3. Structural Identifiability

Structural identifiability tests if the functional or structural form of a particular model allows for the determination of a unique admissible parameter set from noise-free measurements [62]. A general representation of the structural identifiability setting is shown in Figure 3.1. It is worth noting that the structural identifiability is carried within an idealized framework with the following assumptions [193]:

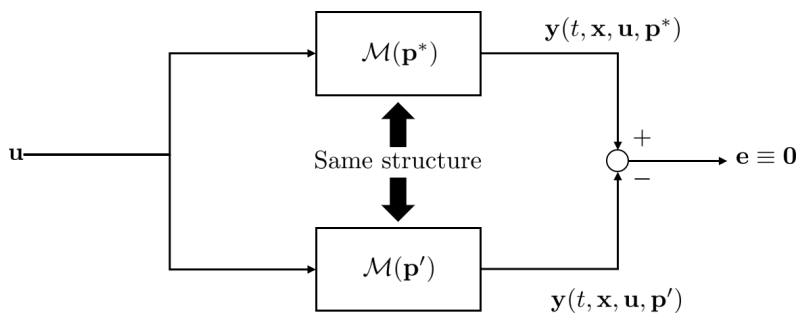


Figure 3.1: Structural identification setting [193]

- (i) The process and its model have the same structure \mathcal{M} (no plant-model mismatch).
- (ii) The data is noise-free.
- (iii) The input signal is persistently exciting the system and it is computed independently from the output. Thus the lack of identifiability is not due to lack of excitation but determined by the model structure.

Making use of these aforementioned assumptions we can check if the parameter set is globally or locally identifiable, or neither. Let us introduce the following definitions and denote \mathbf{p}' and \mathbf{p}^* the parameters that specify the models and the process, respectively.

Definition 3.1 (Global structural identifiability of a model structure [193]):
A model structure is structurally globally identifiable (SGI) if

$$\mathcal{M}(\mathbf{p}') = \mathcal{M}(\mathbf{p}^*) \Rightarrow \mathbf{p}'_i = \mathbf{p}^*_i \quad \forall \mathbf{p}^* \in \mathbb{P} \quad (3.4)$$

Definition 3.2 (Local structural identifiability of a model structure [193]):
A model structure is structurally locally identifiable (SLI) if

$$\mathcal{M}(\mathbf{p}') = \mathcal{M}(\mathbf{p}^*) \Rightarrow \mathbf{p}'_i = \mathbf{p}_i^* \quad \forall \mathbf{p} \in v(\mathbf{p}^*) \quad (3.5)$$

where $v(\mathbf{p}^*)$ is an open neighborhood of \mathbf{p}^* .

These definitions introduced by [193] are general for any model structure. We can, however, particularize them for systems described by (3.2). Before introducing the notion of structural identifiability in DAE models, let us first define global and local identifiability for DAE models

3

Definition 3.3 (Global identifiability of DAE models [104]): A model given by (3.1) is globally identifiable if for any admissible input $u(t)$

$$\begin{aligned} \mathbf{y}(t, \mathbf{x}'(t), \mathbf{u}(t), \mathbf{p}') &= \mathbf{y}(t, \mathbf{x}^*(t), \mathbf{u}(t), \mathbf{p}^*) \Rightarrow \mathbf{p}' = \mathbf{p}^* \\ &\quad \forall \mathbf{p}^* \in \mathbb{P} \end{aligned} \quad (3.6)$$

holds

Definition 3.4 (Local identifiability of DAE models [104]): A model given by (3.1) is locally identifiable at \mathbf{p}^*

$$\begin{aligned} \mathbf{y}(t, \mathbf{x}'(t), \mathbf{u}(t), \mathbf{p}') &= \mathbf{y}(t, \mathbf{x}^*(t), \mathbf{u}(t), \mathbf{p}^*) \Rightarrow \mathbf{p}' = \mathbf{p}^* \\ &\quad \forall \mathbf{p} \in v(\mathbf{p}^*) \end{aligned} \quad (3.7)$$

where $v(\mathbf{p}^*)$ is an open neighborhood of \mathbf{p}^* .

Furthermore, the notion of identifiability given an initial state \mathbf{x}_0 is also important because it shows that initial conditions might provide extra information when performing identifiability analyses. This is known as *locally strongly identifiable* [179] or \mathbf{x}_0 -*identifiable* [81]

Definition 3.5 (Local strong identifiability [179]/[82]): For an admissible input signal $\mathbf{u}(t)$ in a time interval $t \in [t_0, t_f]$, and a given initial state $\mathbf{x}_0 = \mathbf{x}(t_0)$, which is not dependent on \mathbf{p} and is not an equilibrium point of (3.1), if there exists a subset \mathbb{P}' within the parameter space \mathbb{P} such that for $\mathbf{p}^*, \mathbf{p}' \in \mathbb{P}'$, and $\mathbf{p}^* \neq \mathbf{p}'$, the solutions $\mathbf{x}(t, \mathbf{x}_0, \mathbf{u}(t), \mathbf{p}')$, and $\mathbf{y}(t, \mathbf{x}_0, \mathbf{u}(t), \mathbf{p}') \neq \mathbf{y}(t, \mathbf{x}_0, \mathbf{u}(t), \mathbf{p}^*)$ exist for $[t_0, t_0 + \varepsilon]$, the system structure is said to be locally strongly identifiable (or \mathbf{x}_0 -identifiable).

Based on the definitions 3.3, 3.4, and 3.5, we provide a general definition of structural identifiability for DAE models

Definition 3.6 (Local strong identifiability [203]): Let $\mathcal{C}_{\mathbf{u}}^n[t_0, t_f]$ denote the function space spanned by all input functions \mathbf{u} on the interval $t \in [t_0, t_f]$ which are differentiable up to order n , and let $\mathbb{X}_0 \subseteq \mathbb{R}^{n_x}$ denote an open subset of initial system states. The system is said to be structurally identifiable if there exists open and dense subsets $\mathbb{X}'_0 \subset \mathbb{X}_0$, $\mathbb{P}' \subset \mathbb{P}$, and $\mathbb{U}' \subset \mathcal{C}_{\mathbf{u}}^N[t_0, t_f]$ such that the system is locally strongly identifiable at \mathbf{p}^* given \mathbf{u} for any $\mathbf{x}_0 \in \mathbb{X}'_0$, $\mathbf{p}^* \in \mathbb{P}'$, and $\mathbf{u} \in \mathbb{U}'$

The previous definition is also called geometric identifiability ([82],[179]), and it implies that the parameters in the parameter vector \mathbf{p} can be determined extracting the information from the input signal \mathbf{u} , the measured output \mathbf{y} , and the initial states \mathbf{x}_0 [82]. It is worth noting that, based on definitions 3.5 and 3.6, structural identifiability is a property of the input-output map of the model.

3.3.1. The invariant vector

One issue with the definitions of structural identifiability presented previously, is that testing for identifiability of model structures is often not very practical, as it would require the analytic solution of the outputs in terms of the states \mathbf{x} , the parameters \mathbf{p} , the input signal \mathbf{u} , and possibly time t [192]. The model structure can be transformed in order to eliminate the explicit dependency on the input signal and time, while keeping the essential information necessary to test for these structural properties. This notion is collected in the "invariant vector" [181] or "exhaustive summary" [36], [35], [190].

Definition 3.7 (Invariant vector [181]): The mapping $\kappa : \mathbb{P} \mapsto \mathbb{R}^{n_k}$ is an invariant vector of the model $\mathcal{M}(\mathbf{p})$ if and only if

$$\begin{aligned} & \{\mathbf{y}(t, \mathbf{x}'(t), \mathbf{u}(t), \mathbf{p}') = \mathbf{y}(t, \mathbf{x}^*(t), \mathbf{u}(t), \mathbf{p}^*), \\ & \forall (\mathbf{x}_0, \mathbf{u}) \in \mathbb{X}_0 \times \mathcal{C}_{\mathbf{u}}^N[t_0, t_f]\} \Leftrightarrow \kappa(\mathbf{p}') = \kappa(\mathbf{p}^*) \end{aligned} \quad (3.8)$$

The invariant vector κ is useful to assess structural identifiability in an easier way. Furthermore, it can be helpful when finding a suitable reparametrization that might simplify the model structure. In the following, we shall present the relation between the concept of invariant vector and the structural identifiability.

Theorem 3.1 (Structural identifiability [181]): Consider the model $\mathcal{M}(\mathbf{p})$ where $\mathbf{p} \in \mathbb{P}$. Let $\kappa(\mathbf{p})$ be an invariant vector of the model and assume that κ is analytic over \mathbb{P} . Define the Jacobian matrix $\mathbf{J}(\mathbf{p}) \in \mathbb{R}^{n_k \times n_p}$ as

$$\mathbf{J}(\mathbf{p}) = [(\kappa)_1 \quad (\kappa)_2 \quad \cdots \quad (\kappa)_{n_p}] \quad (3.9)$$

where

$$(\boldsymbol{\kappa})_i = \frac{\partial \boldsymbol{\kappa}(\mathbf{p})}{\partial p_i}, \quad i = 1, 2, \dots, n_p \quad (3.10)$$

and let

3

$$\rho[\mathbf{J}(\mathbf{p})] = \text{rank}(\mathbf{J}(\mathbf{p})). \quad (3.11)$$

The model is structurally identifiable if and only if $\rho[\mathbf{J}(\mathbf{p})] = n_p$ for some $\mathbf{p} \in \mathbb{P}$ regardless of the choice of invariant vector $\boldsymbol{\kappa}$. ■

The proof of this theorem can be found in [181].

Remark 3.1: Naturally, if the number of elements in the invariant vector $\boldsymbol{\kappa}$ is strictly less than the number of parameters, i.e. $n_k < n_p$, the structure is trivially structurally unidentifiable. The rank will be smaller or equal to the number of elements in $\boldsymbol{\kappa}$ because $\text{rank}(\mathbf{J}(\mathbf{p})) \leq \min(n_k, n_p)$.

The invariant vector is a mathematical object that contains all the relevant information of the model. In the case of linear ODE models, the moments of the corresponding transfer function completely determines the structure of a model, and thus, can be used to assess structural identifiability [185]. More specifically, for single-input single-output (SISO) models $2n$ Markov parameters uniquely determine a linear system with n the McMillan degree, whereas in the multiple-input multiple-output (MIMO) the model is determined by $\lambda + \mu$, with λ and μ are the controllability and observability degrees, respectively [185]. In the case of nonlinear ODE models, the coefficients of the invariant vector are given by the infinite Taylor expansion with respect to time and evaluated at t_0 [193]. These coefficients would provide the \mathbf{x}_0 -identifiability as stated in Definition 3.6. However, the Taylor expansion approach has several drawbacks. First, the number of coefficients required is not precisely known and one would have to differentiate a great number of times to construct the Jacobian matrix. This brings forward its impracticality for large state space dimensions with complex model structures because the more states there are, the more convoluted the differentiation and coefficients become, making the operations intractable.

In the specific case of a model represented by a transfer function $G(s)$, the invariant vector $\boldsymbol{\kappa}$ is given by the parameter-dependent coefficients of the numerator and

denominator of the transfer function $G(s) = N(s)/D(s)$. The invariant vector can be defined using the coefficient extraction operator as follows:

$$\kappa(\mathbf{p}) = [[s^{m_g}]N(s) \quad \cdots \quad [s^0]N(s) \quad [s^{m_g}]D(s) \quad \cdots \quad [s^0]D(s)]^\top \quad (3.12)$$

where $m_g = \max(\deg(N(s)), \deg(D(s)))$.

3.3.2. Types of structurally identifiable models and parameter redundancy

The models that are structurally identifiable will have Jacobian matrices whose ranks equal the number of parameters in their respective models. In this case, the Jacobian dimensions satisfy $n_k \geq n_p$. However, since the analysis is based on a generalized rank, one can distinguish between different rank types, namely *essentially full rank* or *conditionally full rank* [36]. These two types of rank are defined next

Definition 3.8 (Essentially full rank model [36]): A structurally identifiable model is essentially full rank if its corresponding Jacobian matrix $\mathbf{J}(\mathbf{p})$ is full (column) rank for all $\mathbf{p} \in \mathbb{P}$ or $\mathbf{p} \in v(\mathbf{p})$.

Definition 3.9 (Conditionally full rank model [36]): A structurally identifiable model is conditionally full rank if its corresponding Jacobian matrix $\mathbf{J}(\mathbf{p})$ is full (column) rank almost everywhere except at a measurable set $\bar{\mathbb{P}} \subset \mathbb{P}$ of possibly infinite but countably many points, i.e. the measure of $\bar{\mathbb{P}}$ is zero.

We can determine the type of model considering the permuted LU decomposition of the Jacobian matrix $\mathbf{J}(\mathbf{p}) = \boldsymbol{\Pi}^\top \mathbf{L}(\mathbf{p}) \mathbf{U}(\mathbf{p})$. The matrix $\boldsymbol{\Pi}$ is a permutation matrix, while the matrices $\mathbf{L}(\mathbf{p})$ and $\mathbf{U}(\mathbf{p})$ satisfy the following properties

- $\mathbf{L}(\mathbf{p}) \in \mathbb{R}^{n_k \times n_k}$ is square lower triangular and invertible, whose diagonal elements are exactly 1.
- $\mathbf{U}(\mathbf{p}) = \begin{bmatrix} \mathbf{U}_1(\mathbf{p}) \\ \mathbf{0} \end{bmatrix}$ where $\mathbf{U}_1(\mathbf{p}) \in \mathbb{R}^{r \times n_p}$ whose rows are linearly independent. The number of rows r corresponds to the rank of $\mathbf{J}(\mathbf{p})$ and span its row space. Since we are dealing with structurally identifiable models it follows that $r = n_p$, i.e. $\mathbf{U}(\mathbf{p}) = \mathbf{U}_1(\mathbf{p})$ is also square and invertible.
- Let $\tilde{\mathbf{L}}(\mathbf{p}) = \boldsymbol{\Pi}^\top \mathbf{L}(\mathbf{p})$, and partition $\tilde{\mathbf{L}}(\mathbf{p}) = [\tilde{\mathbf{L}}_1(\mathbf{p}) \quad \tilde{\mathbf{L}}_2(\mathbf{p})]$ compatibly, then $\tilde{\mathbf{L}}_1(\mathbf{p}) \in \mathbb{R}^{n_k \times r}$ spans the column space of $\mathbf{J}(\mathbf{p})$.

Notice that $\mathbf{U}_1(\mathbf{p})$ is square and its rows provide the rank of $\mathbf{J}(\mathbf{p})$, therefore, a structurally identifiable model is essentially full rank if and only if $\det(\mathbf{U}_1) \neq 0 \quad \forall \mathbf{p} \in \mathbb{P}$, i.e. the determinant is not a function of \mathbf{p} . Conversely, a structurally identifiable model is conditionally full rank if $\det(\mathbf{U}_1) = 0$ for some $\mathbf{p} \in \bar{\mathbb{P}} \subset \mathbb{P}$, i.e. the determinant is a function of the parameters, and becomes zero for some combination of them. Analogously, when $\rho[\mathbf{J}(\mathbf{p})] = n_q < n_p$ the model is said to be *parameter redundant*, and therefore, there are only q estimable parameters. This allows us to establish a measure of "how far" we are from having perfect identifiability called *deficiency*. It is defined as $n_d = n_p - n_q$ [36]. Furthermore, Catchpole *et al.* [32] showed that if $\mathbf{J}(\mathbf{p})$ has deficiency n_d , then there exists a maximal set of non-zero linearly independent vector functions $\boldsymbol{\nu}_1(\mathbf{p}), \dots, \boldsymbol{\nu}_{n_d}(\mathbf{p}), \quad \forall \mathbf{p}$ such that

$$\mathbf{J}(\mathbf{p})\boldsymbol{\nu}_j(\mathbf{p}) = 0, \quad j = 1, \dots, n_d. \quad (3.13)$$

Clearly, in (3.13) we are trying to find the vectors that span the null space of the Jacobian matrix. Let $\nu_{ij}(\mathbf{p}), \quad i = 1, \dots, n_p \quad j = 1, \dots, n_d$ be an element of $\boldsymbol{\nu}_j(\mathbf{p})$, then any $\nu_{ij}(\mathbf{p})$ which is zero for all j then it corresponds to a parameter \mathbf{p}_i that is identifiable. The rest of parameters cannot be uniquely determined but rather a combination of them can be identified. To obtain the possible identifiable parameter combination, a set of linear first-order partial differential equations (PDE) must be solved given by

$$\sum_{i=1}^p \nu_{ij} \frac{\partial \varphi_j}{\partial p_i} = 0, \quad j = 1, \dots, n_d \quad (3.14)$$

The proof of how (3.14) provides the set of identifiable parameters in a structurally unidentifiable model can be found in [32]. However, notice that the first step in the determination of the identifiability of a model $\mathcal{M}(\mathbf{p})$ is the determination of the symbolic rank of $\mathbf{J}(\mathbf{p})$. This can be a very difficult task, especially if we are dealing with a high-dimensional and structurally complex model, with a large number of parameters. Therefore, the concepts of reduced-form invariant vector and reparametrization were introduced in [36], which are given next

Definition 3.10 (Reduced-form invariant vector [36]): A reduced-form invariant vector $\mathbf{q}(\mathbf{p})$ is a reparametrization such that

$$\rho[\mathbf{J}(\mathbf{q}(\mathbf{p}))] = \text{rank}([\kappa_1 \quad \kappa_2 \quad \dots \quad \kappa_q]) = n_q \quad (3.15)$$

where

$$(\kappa)_i = \frac{\partial \kappa(\mathbf{q})}{\partial q_i}, \quad i = 1, 2, \dots, n_q \quad (3.16)$$

Based on this definition, it is clear that the reduced-form invariant vector is not unique. However, the reduced-form invariant vector is structurally simpler than the original invariant vector, and the symbolic rank of $\mathbf{J}(\mathbf{q})$ is easier to compute, while providing the sufficient information about the parameter redundancy in the original model $\mathcal{M}(\mathbf{p})$. Furthermore, \mathbf{q} can be used to formulate the conditions to find a reduced-form invariant vector [36].

The reparametrization holds under the following conditions [36]:

- (a) If $\rho[\mathbf{J}(\mathbf{q})] = \dim(\mathbf{q})$ then \mathbf{q} is a reduced-form invariant vector. The original invariant vector $\kappa(\mathbf{p})$ can be rewritten as $\kappa(\mathbf{q})$ and it can be used to examine the structural properties of the original model.
- (b) If $\rho[\mathbf{J}(\mathbf{q})] < \dim(\mathbf{q})$, then \mathbf{q} is not a reduced-form invariant vector. A reduced-form invariant vector can be found by solving (3.13) and (3.14) using $\mathbf{J}(\mathbf{q})$.
- (c) If $\rho[\partial \mathbf{q} / \partial \mathbf{p}] = \dim(\mathbf{q})$, then the number of identifiable parameters is equal to $\rho[\mathbf{J}(\mathbf{q})]$. It follows that if $\rho[\mathbf{J}(\mathbf{q})] = n_p$ then the model in terms of \mathbf{p} does not have parametric redundancy. Conversely, if $\rho[\mathbf{J}(\mathbf{q})] < n_p$, then the model in terms of \mathbf{p} presents parameter redundancy.

A reparametrized model should be structurally equivalent to the original one. Moreover, a possible advantage of reparametrization is finding a minimal structure of a particular model, which could be convenient for example for control purposes due to its simpler structure. However, an issue with this is the non-uniqueness of the reparametrization. One could choose a "smart" reparametrization such that this minimal structure is simpler than the original one, which is not sometimes easy, and often requires knowledge on the particular model to find such reparametrization. Another caveat to be considered is the fact that solving (3.14) may hint possible candidates for reparametrization, but as the model dimension grows, finding the integral surfaces of these partial differential equations can become an intractable problem.

The concepts introduced previously in the chapter will be illustrated in the following example:

Example 3.1 (Simple biological compartmental model [16]): Assume the model structure is given by a linear state space representation

$$\begin{aligned} \begin{bmatrix} \dot{\mathbf{x}}_1 \\ \dot{\mathbf{x}}_2 \end{bmatrix} &= \begin{bmatrix} -(p_1 + p_2) & p_3 \\ p_2 & -(p_3 + p_4) \end{bmatrix} \begin{bmatrix} \mathbf{x}_1 \\ \mathbf{x}_2 \end{bmatrix} + \begin{bmatrix} 1 \\ 0 \end{bmatrix} u, & \mathbf{x}(0) = \mathbf{0} \\ y &= [0 \quad 1] \begin{bmatrix} \mathbf{x}_1 \\ \mathbf{x}_2 \end{bmatrix} \end{aligned} \quad (3.17)$$

with $\mathbf{p} = [p_1 \quad p_2 \quad p_3 \quad p_4]^\top$. Computing its transfer function $G(s)$

3

$$\begin{aligned} Y(s) &= \underbrace{C(sI - A)^{-1} \mathbf{X}_0(s)}_0 + C(sI - A)^{-1} BU(s) \\ &= \frac{p_2}{s^2 + (p_1 + p_2 + p_3 + p_4)s + p_1p_3 + p_1p_4 + p_2p_4} U(s) \\ \Rightarrow G(s) &= \frac{Y(s)}{U(s)} = \frac{p_2}{s^2 + (p_1 + p_2 + p_3 + p_4)s + p_1p_3 + p_1p_4 + p_2p_4} \end{aligned} \quad (3.18)$$

The invariant vector $\boldsymbol{\kappa}$ is generated from the transfer function $G(s)$ using (3.12) and has the form

$$\boldsymbol{\kappa}(\mathbf{p}) = \begin{bmatrix} 0 \\ 0 \\ p_2 \\ 1 \\ p_1 + p_2 + p_3 + p_4 \\ p_1p_3 + p_1p_4 + p_2p_4 \end{bmatrix} \quad (3.19)$$

Notice that $n_k = 6$ but only three rows of $\boldsymbol{\kappa}$ have parameter-dependent elements. It is easy to observe that the Jacobian matrix $\mathbf{J}(\mathbf{p})$ will have three row of zeros and three non-zero rows but the number of parameters is $n_p = 4$. This implies that the Jacobian matrix $\mathbf{J}(\mathbf{p})$ will have at most rank equal to three, thus, the model structure is not structurally identifiable. However, the identifiable combinations can be retrieved solving (3.14). Let us compute the Jacobian matrix of the structure

$$\mathbf{J}(\mathbf{p}) = \frac{\partial \boldsymbol{\kappa}(\mathbf{p})}{\partial \mathbf{p}^\top} = \begin{bmatrix} 0 & 0 & 0 & 0 \\ 0 & 0 & 0 & 0 \\ 0 & 1 & 0 & 0 \\ 0 & 0 & 0 & 0 \\ 1 & 1 & 1 & 1 \\ p_3 + p_4 & p_4 & p_1 & p_1 + p_2 \end{bmatrix} \quad (3.20)$$

whose null space is spanned by

$$\boldsymbol{\nu} = \begin{bmatrix} -p_2 \\ 0 \\ p_1 + p_2 - p_3 - p_4 \\ p_3 - p_1 + p_4 \end{bmatrix} \quad (3.21)$$

From (3.21), we see that p_2 is uniquely identifiable because the component of the null space in its direction is zero. Nevertheless, the directions of p_1, p_3, p_4 cannot be uniquely determined, and thus, only a combination of these three parameters can be structurally estimated. Since $\rho[\mathbf{J}(\mathbf{p})] = 3$ and the number of parameter is $n_p = 4$, the deficiency $n_d = 1$. As mentioned previously, the null space vector $\boldsymbol{\nu}$ can be used to solve n_d partial differential equations of the form (3.14) to find the corresponding parameter combinations. These combinations correspond to the level curves or characteristic curves of the integral surface of the PDE. For this example, (3.14) is

$$-p_2 \frac{\partial \varphi}{\partial p_1} + (p_1 + p_2 - p_3 - p_4) \frac{\partial \varphi}{\partial p_3} + (p_3 - p_1 + p_4) \frac{\partial \varphi}{\partial p_4} = 0 \quad (3.22)$$

Solving (3.22) up to the constants (level curves), we have that the identifiable set \mathbf{q} is

$$\mathbf{q} = \begin{bmatrix} q_1 \\ q_2 \\ q_3 \end{bmatrix} = \begin{bmatrix} p_2 \\ p_1 + p_3 + p_4 \\ p_1 p_3 + p_1 p_4 + p_2 p_4 \end{bmatrix} \quad (3.23)$$

The reduced set \mathbf{q} is a candidate to generate a reparametrization of the model structure. Notice that the transfer function $G(s)$ can be written in terms of the reduced set as

$$\tilde{G}(s) = \frac{q_1}{s + (q_1 + q_2)s + q_3} \quad (3.24)$$

Computing the corresponding invariant vector $\tilde{\mathbf{k}}(\mathbf{q})$ and Jacobian matrix, we have

$$\tilde{\kappa}(\mathbf{q}) = \begin{bmatrix} q_1 \\ q_1 + q_2 \\ q_3 \end{bmatrix} \Rightarrow \tilde{\mathbf{J}}(\mathbf{q}) = \begin{bmatrix} 1 & 0 & 0 \\ 1 & 1 & 0 \\ 0 & 0 & 1 \end{bmatrix} \quad (3.25)$$

The reparametrization generates a reduced model Jacobian matrix whose rank matches the number of identifiable parameters. Therefore, the reparametrized model is structurally identifiable in \mathbf{q} . Nevertheless, the reduced model Jacobian matrix $\tilde{\mathbf{J}}(\mathbf{q})$ may be essentially or conditionally full rank depending on the particular structure of the model.

3

The model structure in this simple example assumes that the initial conditions are zero. Recall that identifiability is a property of the input-output map, thus, any other signal that acts as an input and/or output will help in the conditioning of the identifiability. In this sense, the initial conditions will act as an extra input signal. To illustrate this, let $\mathbf{x}_0 \neq \mathbf{0}$. Thus, $G(s)$ is now a transfer matrix:

$$\begin{aligned} G(s) &= [C(sI - A)^{-1} \quad C(sI - A)^{-1}B] \\ &= \frac{[p_2 \quad s + p_1 + p_2 \quad p_2]}{s^2 + (p_1 + p_2 + p_3 + p_4)s + p_1p_3 + p_1p_4 + p_2p_4} \end{aligned} \quad (3.26)$$

Since \mathbf{B} is not a function of \mathbf{p} , the third element of $G(s)$ is the same as the first component. Therefore, the analysis can be performed taking in the invariant vector either the numerators of first and second components or the second and third components of $G(s)$. Furthermore, notice that since all transfer functions share the same denominator, we only need to include it once in the invariant vector $\boldsymbol{\kappa}$. The Jacobian matrix for this structure is

$$\boldsymbol{\kappa} = \begin{bmatrix} 0 \\ 0 \\ p_2 \\ 0 \\ 1 \\ p_1 + p_2 \\ 0 \\ 0 \\ p_2 \\ 1 \\ p_1 + p_2 + p_3 + p_4 \\ p_1p_3 + p_1p_4 + p_2p_4 \end{bmatrix} \Rightarrow \mathbf{J}(\mathbf{p}) = \begin{bmatrix} 0 & 0 & 0 & 0 \\ 0 & 0 & 0 & 0 \\ 0 & 1 & 0 & 0 \\ 0 & 0 & 0 & 0 \\ 0 & 0 & 0 & 0 \\ 0 & 1 & 1 & 0 \\ 0 & 0 & 0 & 0 \\ 0 & 0 & 0 & 0 \\ 0 & 1 & 0 & 0 \\ 0 & 0 & 0 & 0 \\ 1 & 1 & 1 & 1 \\ p_3 + p_4 & p_4 & p_1 & p_1 + p_2 \end{bmatrix} \quad (3.27)$$

whose rank $\rho[\mathbf{J}(\mathbf{p})] = n_p = 4$, i.e. structurally identifiable. As a consequence, the structure is also strongly locally accessible from initial points of the first state $x_{01} \neq 0$. Moreover, performing LU decomposition, the determinant of the upper triangular matrix $\mathbf{U}_1(\mathbf{p})$ is

$$\det(\mathbf{U}_1(\mathbf{p})) = \begin{vmatrix} 1 & 1 & 0 & 0 \\ 0 & 1 & 0 & 0 \\ 0 & 0 & 1 & 1 \\ 0 & 0 & 0 & p_2 \end{vmatrix} = p_2 \quad (3.28)$$

3

Therefore, the structure is conditionally full rank, and structurally identifiable away from $p_2 = 0$. This is sensible because p_2 defines the gain of one of the transfer functions. A value of $p_2 = 0$ would imply that one of the input-output maps is also zero, and no information could be extracted from it.

■

3.4. Structural identifiability in closed-loop

The previous definitions apply in principle for model structures regardless if the model is open loop or closed loop. However, it is well-known that in closed loop, the controllers induce a linearizing effect in the model structure. As a consequence, it leads to a loss of identifiability of the parameter set. Usually, this is avoided by choosing a sufficiently *complex* controller. The idea of complexity in the controller structure might lead to the misleading argument that a controller could potentially improve identifiability of a model structure. However, this is not possible, as a controller structure can only reduce or preserve identifiability but not increase it from a structural sense¹. We formalize this problem in this section.

Let us define the open-loop transfer function (matrix) $G_{\text{ol}}(s, \mathbf{p})$ of the structure $\bar{\mathcal{M}}(\mathbf{p})$ in (3.3) and the linear controller structure $K(s, \mathbf{p})$. The controller structure can only be designed in terms of the identifiable parameter combinations, i.e. the reparametrization vector $\mathbf{q}(\mathbf{p})$. This is logical, since \mathbf{q} is the only information that can be extracted from the open-loop input-output map. These two structures are interconnected as shown in Figure 3.2

¹In this context, reduction or preservation of structural identifiability is understood as keeping or decreasing the generalized rank of the closed-loop structure Jacobian matrix \mathbf{J}_{cl}

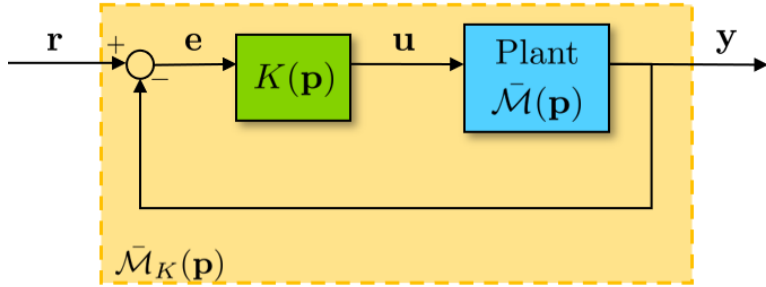


Figure 3.2: Closed-loop interconnection between the model and controller structures

$G_{\text{ol}}(s, \mathbf{p})$ and $K(s, \mathbf{p})$ are matrices if there are multiple inputs \mathbf{u} , outputs \mathbf{y} , and reference signals \mathbf{r} . Without loss of generality, it will be assumed that $n_u = n_y = n_r = 1$. Let us represent both $G_{\text{ol}}(s, \mathbf{p})$ and $K(s, \mathbf{p})$ in terms of their numerators and denominators as follows

$$G_{\text{ol}}(s, \mathbf{p}) = \frac{N(s, \mathbf{p})}{D(s, \mathbf{p})} \quad \text{and} \quad K(s, \mathbf{p}) = \frac{N_c(s, \mathbf{p})}{D_c(s, \mathbf{p})}$$

with the $G_{\text{ol}}(s, \mathbf{p})$ and $K(s, \mathbf{p})$ are proper rational functions whose denominators are monic polynomials. The closed-loop transfer function $F(s, \mathbf{p})$ of the closed-loop of the linearized model structure $\bar{\mathcal{M}}_K(\mathbf{p})$, i.e. the input-output map from $\mathbf{r} \mapsto \mathbf{y}$ can be written as

$$F(s, \mathbf{p}) = \frac{G_{\text{ol}}(s, \mathbf{p})K(s, \mathbf{p})}{1 + G_{\text{ol}}(s, \mathbf{p})K(s, \mathbf{p})} = \frac{N(s, \mathbf{p})N_c(s, \mathbf{p})}{N(s, \mathbf{p})N_c(s, \mathbf{p}) + D(s, \mathbf{p})D_c(s, \mathbf{p})} \quad (3.29)$$

Applying the coefficient extraction operator as defined in 2.5, the numerator and denominator of the closed-loop structure can be written as a matrix product

$$\boldsymbol{\kappa}_{\text{cl,num}} = [\mathbf{s}] \left(N(s, \mathbf{p})N_c(s, \mathbf{p}) \right) = \mathbf{N}_c \boldsymbol{\kappa}_{\text{ol,num}} \quad (3.30)$$

$$\boldsymbol{\kappa}_{\text{cl,den}} = [\mathbf{s}] \left(N(s, \mathbf{p})N_c(s, \mathbf{p}) + D(s, \mathbf{p})D_c(s, \mathbf{p}) \right) = [\mathbf{N}_c \quad \mathbf{D}_c] \begin{bmatrix} \boldsymbol{\kappa}_{\text{ol,num}} \\ \boldsymbol{\kappa}_{\text{ol,den}} \end{bmatrix} \quad (3.31)$$

where

$$\mathbf{N}_c = \begin{bmatrix} [s^0]N_c & [s^1]N_c & \cdots & [s^{m_d}]N_c \\ 0 & [s^0]N_c & \cdots & [s^{m_d}]N_c \\ \vdots & \vdots & \ddots & \vdots \\ 0 & 0 & \cdots & [s^0]N_c \end{bmatrix}, \quad \mathbf{D}_c = \begin{bmatrix} [s^0]D_c & [s^1]D_c & \cdots & [s^{m_d}]D_c \\ 0 & [s^0]D_c & \cdots & [s^{m_d}]D_c \\ \vdots & \vdots & \ddots & \vdots \\ 0 & 0 & \cdots & [s^0]D_c \end{bmatrix},$$

$$\boldsymbol{\kappa}_{\text{ol,num}} = \begin{bmatrix} [s^0]N \\ [s^1]N \\ \vdots \\ [s^{m_d}]N \end{bmatrix}, \text{ and } \boldsymbol{\kappa}_{\text{ol,den}} = \begin{bmatrix} [s^0]D \\ [s^1]D \\ \vdots \\ [s^{m_d}]D \end{bmatrix}$$

with $[s^i]$ denotes the extraction of the i -th degree coefficient in a (finite) series of s . The number $m_d = \deg(DD_c)$

Note that the vector $\begin{bmatrix} \boldsymbol{\kappa}_{\text{ol,num}} \\ \boldsymbol{\kappa}_{\text{ol,den}} \end{bmatrix}$ is the open-loop invariant vector $\boldsymbol{\kappa}_{\text{ol}}$ introduced in definition 3.7 padded with extra zeros to account for the extra terms in the closed-loop polynomials. Stacking (3.30) and (3.31) together, we arrive at the full closed-loop invariant vector $\boldsymbol{\kappa}_{\text{cl}}$

$$\boldsymbol{\kappa}_{\text{cl}} = \begin{bmatrix} \mathbf{N}_c & \mathbf{0} \\ \mathbf{N}_c & \mathbf{D}_c \end{bmatrix} \begin{bmatrix} \boldsymbol{\kappa}_{\text{ol,num}} \\ \boldsymbol{\kappa}_{\text{ol,den}} \end{bmatrix} = \boldsymbol{\Gamma} \boldsymbol{\kappa}_{\text{ol}} \quad (3.32)$$

From Theorem 3.1, the closed-loop model structure is identifiable if the Jacobian matrix is full column rank. Differentiating (3.32) with respect to the parameters, we obtain the closed-loop Jacobian matrix \mathbf{J}_{ol} in terms of the open-loop Jacobian matrix \mathbf{J}_{cl}

$$\mathbf{J}_{\text{cl}} = \frac{\partial \boldsymbol{\kappa}_{\text{cl}}}{\partial \mathbf{p}^\top} = \frac{\partial \boldsymbol{\Gamma}}{\partial \mathbf{p}^\top} (\mathbf{I}_{n_p} \otimes \boldsymbol{\kappa}_{\text{ol}}) + \underbrace{\boldsymbol{\Gamma} \frac{\partial \boldsymbol{\kappa}_{\text{ol}}}{\partial \mathbf{p}^\top}}_{\mathbf{J}_{\text{ol}}} \quad (3.33)$$

In the following theorem, we propose that the number of closed-loop identifiable parameters is at most the same as in open-loop.

Theorem 3.2: If the open-loop structure $\bar{\mathcal{M}}(\mathbf{p})$ is structurally unidentifiable from the available input-output map, then the closed-loop structure $\bar{\mathcal{M}}_K(\mathbf{p})$ is also structurally unidentifiable irrespective of the order of the controller.

Proof:

Let the model structure $\bar{\mathcal{M}}(\mathbf{p})$ be structurally unidentifiable. Then there exists a set of non-zero vector function $\boldsymbol{\nu}(\mathbf{p}) = \{\boldsymbol{\nu}(\mathbf{p})_1, \dots, \boldsymbol{\nu}(\mathbf{p})_{n_d}\}$ such that the Jacobian matrix $\mathbf{J}_{\text{ol}}(\mathbf{p})\boldsymbol{\nu}_j = \mathbf{0}$ for $j = 1, \dots, n_d$, i.e. $\boldsymbol{\nu}(\mathbf{p}) = \ker(\mathbf{J}_{\text{ol}})$. Multiplying the closed-loop Jacobian matrix \mathbf{J}_{cl} with any of the vectors $\boldsymbol{\nu}_j$ we have

$$\begin{aligned} \mathbf{J}_{\text{cl}}\boldsymbol{\nu}_j &= \frac{\partial \boldsymbol{\Gamma}}{\partial \mathbf{p}^\top} (\mathbf{I}_{n_p} \otimes \boldsymbol{\kappa}_{\text{ol}}) \boldsymbol{\nu}_j + \boldsymbol{\Gamma} \mathbf{J}_{\text{ol}} \boldsymbol{\nu}_j \\ &= \frac{\partial \boldsymbol{\Gamma}}{\partial \mathbf{p}^\top} (\mathbf{I}_{n_p} \otimes \boldsymbol{\kappa}_{\text{ol}}) \boldsymbol{\nu}_j \\ &= \frac{\partial \boldsymbol{\Gamma}}{\partial \mathbf{p}^\top} (\boldsymbol{\nu}_j \otimes \boldsymbol{\kappa}_{\text{ol}}) \end{aligned} \quad (3.34)$$

Following the implicit differentiation rule using the matrix calculus convention described in [29], and recalling the controller is a function of the identifiable parameter combinations \mathbf{q} , we have that

$$\frac{\partial \boldsymbol{\Gamma}}{\partial \mathbf{p}^\top} = \left(\mathbf{1} \otimes \frac{\partial \boldsymbol{\Gamma}}{\partial \mathbf{q}^\top} \right) \left(\frac{\partial \mathbf{q}}{\partial \mathbf{p}^\top} \otimes \mathbf{I}_{2m_d+2} \right) \quad (3.35)$$

Replacing (3.35) in (3.34)

$$\begin{aligned} \mathbf{J}_{\text{cl}}\boldsymbol{\nu}_j &= \left(\mathbf{1} \otimes \frac{\partial \boldsymbol{\Gamma}}{\partial \mathbf{q}^\top} \right) \left(\frac{\partial \mathbf{q}}{\partial \mathbf{p}^\top} \otimes \mathbf{I}_{2m_d+2} \right) (\boldsymbol{\nu}_j \otimes \boldsymbol{\kappa}_{\text{ol}}) \\ &= \frac{\partial \boldsymbol{\Gamma}}{\partial \mathbf{q}^\top} \left(\frac{\partial \mathbf{q}}{\partial \mathbf{p}^\top} \boldsymbol{\nu}_j \otimes \boldsymbol{\kappa}_{\text{ol}} \right) \end{aligned} \quad (3.36)$$

The term $\frac{\partial \mathbf{q}}{\partial \mathbf{p}^\top} \boldsymbol{\nu}_j$ is equivalent to (3.14), where each element of \mathbf{q} satisfies the aforementioned equation, and so $\frac{\partial \mathbf{q}}{\partial \mathbf{p}^\top} \boldsymbol{\nu}_j = \mathbf{0}$. This implies that the closed-loop structure has at least the same null space of the open-loop structure, and therefore, the controller cannot improve the model structure $\bar{\mathcal{M}}(\mathbf{p})$ identifiability regardless of its complexity.

Since \mathbf{J}_{cl} is composed as the sum of two matrices, we have the following well-known result in algebra

Fact 1 (Kernel inclusion [79]): Let \mathbf{X} and \mathbf{Y} be any two matrices of the same dimension whose null spaces are not zero. The following inclusion holds

$$\ker(\mathbf{X}) \cap \ker(\mathbf{Y}) \subset \ker(\mathbf{X} + \mathbf{Y})$$

Let $\boldsymbol{\nu}_{\text{ol}} \in \ker(\mathbf{J}_{\text{ol}})$, and $\dim(\ker(\mathbf{J}_{\text{ol}})) = n_{\nu_{\text{ol}}}$. Clearly by Fact 1 and Theorem 3.2, the inclusion

$$\boldsymbol{\nu}_{\text{ol}} \in \left(\ker(\partial_{\mathbf{P}^\top} \boldsymbol{\Gamma} (\mathbf{I}_{n_p} \otimes \boldsymbol{\kappa}_{\text{ol}})) \cap \ker(\mathbf{T}\mathbf{J}_{\text{ol}}) \right) \subset \ker \left(\partial_{\mathbf{P}^\top} \boldsymbol{\Gamma} (\mathbf{I}_{n_p} \otimes \boldsymbol{\kappa}_{\text{ol}}) + \mathbf{T}\mathbf{J}_{\text{ol}} \right)$$

holds.

The conclusion that can be derived from Theorem 3.2 is that the parametric information contained in the open-loop structure remains in the closed-loop interconnection. Since structural identifiability is a property of the model structure input-output map, the only way to improve the identifiability is by incorporating extra inputs (actuators), extra outputs (sensors), or both, such that these add independent information on the parametric structure. Moreover, controllers could potentially affect structural identifiability if they are not designed with care. This is straightforward from the rank condition of \mathbf{J}_{cl}

$$\begin{aligned} \text{rank}(\mathbf{J}_{\text{cl}}) &= \text{rank} \left(\begin{bmatrix} \frac{\partial \boldsymbol{\Gamma}}{\partial \mathbf{P}^\top} & \boldsymbol{\Gamma} \end{bmatrix} \begin{bmatrix} (\mathbf{I}_{n_p} \otimes \boldsymbol{\kappa}_{\text{ol}}) \\ \mathbf{J}_{\text{ol}} \end{bmatrix} \right) \\ &= \text{rank} \left(\begin{bmatrix} (\mathbf{I}_{n_p} \otimes \boldsymbol{\kappa}_{\text{ol}}) \\ \mathbf{J}_{\text{ol}} \end{bmatrix} \right) \\ &\quad - \dim \left(\mathcal{R} \left(\begin{bmatrix} (\mathbf{I}_{n_p} \otimes \boldsymbol{\kappa}_{\text{ol}}) \\ \mathbf{J}_{\text{ol}} \end{bmatrix} \right) \cap \ker \left(\begin{bmatrix} \frac{\partial \boldsymbol{\Gamma}}{\partial \mathbf{P}^\top} & \boldsymbol{\Gamma} \end{bmatrix} \right) \right) \end{aligned} \tag{3.37}$$

Notice that if the null space of the controller structure contains vectors that are also contained in the column space of the open-loop structure, the controller will impoverish the structural identifiability. In the following theorem, we provide a practical approach to verify whether a particular controller structure affects parameter identifiability in closed-loop.

Theorem 3.3: Let the LU decomposition of $\begin{bmatrix} (\mathbf{I}_{n_p} \otimes \boldsymbol{\kappa}_{\text{ol}}) \\ \mathbf{J}_{\text{ol}} \end{bmatrix}$ be given as in Section 3.3.2, then the controller does not impoverish structural identifiability if and only if $\ker([\partial_{\mathbf{P}^\top} \boldsymbol{\Gamma} \quad \boldsymbol{\Gamma}]) \not\subset \mathcal{R}(\tilde{\mathbf{L}}_1)$

■

Proof:

Notice that the rank of $\begin{bmatrix} (\mathbf{I}_{n_p} \otimes \boldsymbol{\kappa}_{\text{ol}}) \\ \mathbf{J}_{\text{ol}} \end{bmatrix}$ is always n_p . This follows from the fact that \mathbf{J}_{ol} is the result of applying differentiation (a linear operator) over $\boldsymbol{\kappa}_{\text{ol}}$, and so $\mathcal{R}(\mathbf{J}_{\text{ol}}) \subset \mathcal{R}(\boldsymbol{\kappa}_{\text{ol}})$

3

Necessity

Suppose that $\ker([\partial_{\mathbf{p}^\top} \boldsymbol{\Gamma} \quad \boldsymbol{\Gamma}]) \subset \mathcal{R}(\tilde{\mathbf{L}}_1)$. It follows that:

$$\begin{aligned} \mathbf{J}_{\text{cl}} &= \begin{bmatrix} \frac{\partial \boldsymbol{\Gamma}}{\partial \mathbf{p}^\top} & \boldsymbol{\Gamma} \end{bmatrix} \begin{bmatrix} (\mathbf{I}_{n_p} \otimes \boldsymbol{\kappa}_{\text{ol}}) \\ \mathbf{J}_{\text{ol}} \end{bmatrix} \\ &= \begin{bmatrix} \frac{\partial \boldsymbol{\Gamma}}{\partial \mathbf{p}^\top} & \boldsymbol{\Gamma} \end{bmatrix} [\tilde{\mathbf{L}}_1 \quad \tilde{\mathbf{L}}_2] \begin{bmatrix} \mathbf{U}_1 \\ \mathbf{0} \end{bmatrix} \\ &= \begin{bmatrix} \frac{\partial \boldsymbol{\Gamma}}{\partial \mathbf{p}^\top} & \boldsymbol{\Gamma} \end{bmatrix} \tilde{\mathbf{L}}_1 \mathbf{U}_1 = \mathbf{0} \end{aligned} \tag{3.38}$$

Sufficiency

Suppose that $\ker([\partial_{\mathbf{p}^\top} \boldsymbol{\Gamma} \quad \boldsymbol{\Gamma}]) \not\subset \mathcal{R}(\tilde{\mathbf{L}}_1)$ and that the rank $([\partial_{\mathbf{p}^\top} \boldsymbol{\Gamma} \quad \boldsymbol{\Gamma}] \tilde{\mathbf{L}}_1 \mathbf{U}_1) < n_p$. The product $[\partial_{\mathbf{p}^\top} \boldsymbol{\Gamma} \quad \boldsymbol{\Gamma}] \tilde{\mathbf{L}}_1 \mathbf{U}_1 \neq \mathbf{0}$ but because the rank is less than n_p , there exists a vector $\boldsymbol{\nu} \neq \mathbf{0}$ such that $\tilde{\mathbf{L}}_1 \mathbf{U}_1 \boldsymbol{\nu} = \begin{bmatrix} (\mathbf{I}_{n_p} \otimes \boldsymbol{\kappa}_{\text{ol}}) \\ \mathbf{J}_{\text{ol}} \end{bmatrix} \boldsymbol{\nu} = \mathbf{0}$.

Since $\ker\left(\begin{bmatrix} (\mathbf{I}_{n_p} \otimes \boldsymbol{\kappa}_{\text{ol}}) \\ \mathbf{J}_{\text{ol}} \end{bmatrix}\right) = \ker(\mathbf{I}_{n_p} \otimes \boldsymbol{\kappa}_{\text{ol}}) \cap \ker(\mathbf{J}_{\text{ol}})$, we analyze the null space of each matrix. Recall that $\text{rank}(\mathbf{I}_{n_p} \otimes \boldsymbol{\kappa}_{\text{ol}}) = n_p \Leftrightarrow \ker(\mathbf{I}_{n_p} \otimes \boldsymbol{\kappa}_{\text{ol}}) = \emptyset$ and that $\ker(\mathbf{J}_{\text{ol}}) = \boldsymbol{\nu}_{\text{ol}}$, thus, $\ker(\mathbf{I}_{n_p} \otimes \boldsymbol{\kappa}_{\text{ol}}) \cap \ker(\mathbf{J}_{\text{ol}}) = \emptyset$. Hence, the only vector in the null space is $\boldsymbol{\nu} = \boldsymbol{\nu}_{\text{ol}}$, and the controller does not impact structural identifiability in closed-loop.

■

The meaning of Theorem 3.3 is that the controller structure should not eliminate the available information contained in the open-loop structure. In practice, this is not easy to achieve because controllers flatten out the system dynamics to ensure a prescribed performance specification.

3.5. Structural identifiability: An output sensitivity controllability perspective

In the previous sections we have investigated the structural identifiability problem from an input-output perspective described by the transfer function representation. However, it is also possible to perform this analysis for state space models. One issue with state space models is that they are a latent variable representation and the input-output map of the model structure is not explicit. Nonetheless, the sensitivity model can be exploited to analyze structural identifiability using system theoretic concepts. In this section, we establish the connection between identifiability and output controllability of parameter sensitivities.

Assume that the model is given by (3.3), the state \mathbf{x} and output \mathbf{y} are smooth functions of t and \mathbf{p} . The state and output parameter sensitivity dynamics are given by the total derivative of the model with respect to parameters². Using matrix calculus from [29], the sensitivity model is

$$\begin{aligned}\delta\dot{\bar{\mathbf{x}}}_{\mathbf{p}^\top} &= \frac{\partial \mathbf{A}}{\partial \mathbf{p}^\top} (\mathbf{I}_{n_p} \otimes \delta\bar{\mathbf{x}}) + \mathbf{A}\delta\bar{\mathbf{x}}_{\mathbf{p}^\top} + \frac{\partial \mathbf{B}}{\partial \mathbf{p}^\top} (\mathbf{I}_{n_p} \otimes \delta\mathbf{u}) + \mathbf{B}\delta\mathbf{u}_{\mathbf{p}^\top} \\ \delta\mathbf{y}_{\mathbf{p}^\top} &= \frac{\partial \mathbf{C}}{\partial \mathbf{p}^\top} (\mathbf{I}_{n_p} \otimes \delta\bar{\mathbf{x}}) + \mathbf{C}\delta\bar{\mathbf{x}}_{\mathbf{p}^\top}\end{aligned}\tag{3.39}$$

where $\delta\bar{\mathbf{x}}_{\mathbf{p}^\top} = \frac{\partial \delta\bar{\mathbf{x}}}{\partial \mathbf{p}^\top} \in \mathbb{R}^{n_x \times n_p}$, $\delta\mathbf{u}_{\mathbf{p}^\top} = \frac{\partial \delta\mathbf{u}}{\partial \mathbf{p}^\top} \in \mathbb{R}^{n_u \times n_p}$, and $\delta\mathbf{y}_{\mathbf{p}^\top} = \frac{\partial \delta\mathbf{y}}{\partial \mathbf{p}^\top} \in \mathbb{R}^{n_y \times n_p}$.

In the open-loop case, the input function \mathbf{u} does not depend on the model parameter vector \mathbf{p} . Hence, without loss of generality $\delta\mathbf{u}_{\mathbf{p}^\top} = \frac{\partial \delta\mathbf{u}}{\partial \mathbf{p}^\top} \equiv 0$. The model has an equivalent vectorized representation in terms of $\frac{\partial \delta\bar{\mathbf{x}}}{\partial \mathbf{p}^\top} = \text{vec}\left(\frac{\partial \delta\bar{\mathbf{x}}}{\partial \mathbf{p}^\top}\right)$

$$\begin{aligned}\begin{bmatrix} \delta\dot{\bar{\mathbf{x}}} \\ \delta\dot{\bar{\mathbf{x}}}_{\mathbf{p}} \end{bmatrix} &= \begin{bmatrix} \mathbf{A} & \mathbf{0}_{n_x \times n_x n_p} \\ \mathcal{A} & \mathfrak{A} \end{bmatrix} \begin{bmatrix} \delta\bar{\mathbf{x}} \\ \delta\bar{\mathbf{x}}_{\mathbf{p}} \end{bmatrix} + \begin{bmatrix} \mathbf{B} \\ \mathcal{B} \end{bmatrix} \delta\mathbf{u}, \quad \begin{bmatrix} \delta\bar{\mathbf{x}}(0) \\ \delta\bar{\mathbf{x}}_{\mathbf{p}}(0) \end{bmatrix} = \begin{bmatrix} \delta\bar{\mathbf{x}}_0 \\ \mathbf{0} \end{bmatrix} \\ \begin{bmatrix} \delta\dot{\bar{\mathbf{y}}} \\ \delta\dot{\bar{\mathbf{y}}}_{\mathbf{p}} \end{bmatrix} &= \begin{bmatrix} \mathbf{C} & \mathbf{0}_{n_y \times n_x n_p} \\ \mathcal{C} & \mathfrak{C} \end{bmatrix} \begin{bmatrix} \delta\bar{\mathbf{x}} \\ \delta\bar{\mathbf{x}}_{\mathbf{p}} \end{bmatrix}\end{aligned}\tag{3.40}$$

²For the sake of ease of notation, we shall not write explicitly the dependency of \mathbf{A} , \mathbf{B} , \mathbf{C} , $\delta\mathbf{x}$, $\delta\mathbf{u}$ and $\delta\mathbf{y}$ with respect to \mathbf{p} , but it is worth noting that these matrices and vectors are all functions of the parameter vector \mathbf{p} .

where the matrices of the representation are given by

- $\mathcal{A} = \frac{\partial \mathbf{A}}{\partial \mathbf{p}} = \left(\mathbf{I}_{n_p} \otimes \frac{\partial \mathbf{A}}{\partial \mathbf{p}^\top} \right) (\text{vec}(\mathbf{I}_{n_p}) \otimes \mathbf{I}_{n_x})$
- $\mathcal{B} = \frac{\partial \mathbf{B}}{\partial \mathbf{p}} = \left(\mathbf{I}_{n_p} \otimes \frac{\partial \mathbf{B}}{\partial \mathbf{p}^\top} \right) (\text{vec}(\mathbf{I}_{n_p}) \otimes \mathbf{I}_{n_u})$
- $\mathcal{C} = \frac{\partial \mathbf{C}}{\partial \mathbf{p}} = \left(\mathbf{I}_{n_p} \otimes \frac{\partial \mathbf{C}}{\partial \mathbf{p}^\top} \right) (\text{vec}(\mathbf{I}_{n_p}) \otimes \mathbf{I}_{n_x})$
- $\mathfrak{A} = \mathbf{I}_{n_p} \otimes \mathbf{A}$
- $\mathfrak{C} = \mathbf{I}_{n_p} \otimes \mathbf{C}$

3

with \otimes the Kronecker product.

The representation in (3.40) is advantageous as it allows for a more flexible structural identifiability analysis for MIMO systems. Furthermore, this analysis can be done using tools of system theory, so a connection between structural identifiability and other structural properties can be established. This connection is explored in the following.

3.5.1. Relation between structural output sensitivity controllability and parameter identifiability

The representation developed in (3.40) has the structure of a linear time-invariant (LTI) model. These models structures have well-established properties that can be computed explicitly, such as controllability, observability, stability, etc. Given the input-output nature of structural identifiability, it is related to both controllability and observability of the representation (3.39). In particular, we can say that the structural identifiability establishes how current inputs influence the outputs and output sensitivities in the future. This feature is characterized by the output controllability matrix of the extended system (3.40). In the context of sensitivity analysis, structural identifiability can be interpreted as an output sensitivity controllability problem ([171]). We answer whether each output sensitivity vector trajectory can be steered from an initial condition to any point in the state-sensitivity space with an admissible input signal and how it is mapped to the output-sensitivity space.

Let us define the matrix $\mathbf{\Lambda}_e$ as

$$\mathbf{\Lambda}_e = \begin{bmatrix} (\mathbf{\Lambda}_e)_0 & (\mathbf{\Lambda}_e)_1 & \cdots & (\mathbf{\Lambda}_e)_{n_x(n_p+1)-1} \end{bmatrix} = \begin{bmatrix} \mathbf{\Lambda}^x \\ \mathbf{\Lambda}^{x_p} \end{bmatrix} \quad (3.41)$$

where

$$(\Lambda_e)_0 = \begin{bmatrix} \mathbf{I}_{n_x} & \\ & \mathbf{I}_{n_x n_p} \end{bmatrix} \text{ and } (\Lambda_e)_i = \begin{bmatrix} \mathbf{A}^i & \mathbf{0} \\ \sum_{j=0}^{i-1} \mathfrak{A}^j \mathcal{A} \mathbf{A}^{i-j-1} & \mathfrak{A}^i \end{bmatrix}$$

and the matrix \mathbf{O}_e as

3

$$\mathbf{O}_e = \begin{bmatrix} \mathbf{C} & \mathbf{0} \\ \mathcal{C} & \mathfrak{C} \end{bmatrix} \begin{bmatrix} \Lambda^x \\ \Lambda^{x_p} \end{bmatrix} = \begin{bmatrix} \mathbf{C} \Lambda^x \\ \mathcal{C} \Lambda^x + \Lambda^{x_p} \mathfrak{C} \end{bmatrix} \quad (3.42)$$

The extended state controllability matrix can be written in terms of Λ_e

$$\mathbf{K}_e = \Lambda_e \left(\mathbf{I}_{n_x(n_p+1)} \otimes \begin{bmatrix} \mathbf{B} \\ \mathcal{B} \end{bmatrix} \right) = [(\mathbf{K}_e)_0 \quad (\mathbf{K}_e)_1 \quad \cdots \quad (\mathbf{K}_e)_{n_x(n_p+1)-1}] \quad (3.43)$$

The first n_x rows of the extended controllability matrix \mathbf{K}_e correspond to the usual state controllability matrix \mathbf{K}^x , whereas the remaining $n_x n_p$ rows define the state sensitivity controllability matrix \mathbf{K}^{x_p} .

Using the extended state controllability matrix and the output matrix of (3.40), we can compute the extended output controllability matrix \mathbf{W}_e [137].

$$\mathbf{W}_e = \underbrace{\begin{bmatrix} \mathbf{C} & \mathbf{0} \\ \mathcal{C} & \mathfrak{C} \end{bmatrix} \begin{bmatrix} \Lambda^x \\ \Lambda^{x_p} \end{bmatrix}}_{\mathbf{K}_e} \left(\mathbf{I}_{n_x(n_p+1)} \otimes \begin{bmatrix} \mathbf{B} \\ \mathcal{B} \end{bmatrix} \right) \quad (3.44)$$

The definition of matrix differentiation used in (3.39) induces a specific ordering of the input and output parametric sensitivities. We can find suitable transformation matrices \mathbf{T}^y , and \mathbf{T}^u such that \mathbf{W}_e has a specific structure to analyze each input/output sensitivity separately.

Choosing the transformation matrices as

$$\mathbf{T}^y = \begin{bmatrix} \mathbf{I}_{n_y} & \\ & \Pi^y \end{bmatrix}, \quad \mathbf{T}^u = \begin{bmatrix} \mathbf{I}_{n_u} & \\ & \Pi^u \end{bmatrix} \quad (3.45)$$

where $\mathbf{\Pi}^y$ and $\mathbf{\Pi}^u$ are permutation matrices of compatible size. We can now construct the permuted extended output controllability $\bar{\mathbf{W}} = \mathbf{T}^y \mathbf{W} \mathbf{T}^u$ of the extended system given by

$$\begin{aligned} \bar{\mathbf{W}} &= \begin{bmatrix} \mathbf{C} & \mathbf{0} \\ \mathcal{C}_1 & \mathfrak{C}_1 \\ \vdots & \vdots \\ \mathcal{C}_{n_y} & \mathfrak{C}_{n_y} \end{bmatrix} \begin{bmatrix} \mathbf{K}_1^x & | & \cdots & | & \mathbf{K}_{n_u}^x \\ \mathbf{K}_1^{x_p} & | & \cdots & | & \mathbf{K}_{n_u}^{x_p} \end{bmatrix} \\ &= \begin{bmatrix} \bar{\mathbf{W}}_1^x & \cdots & \bar{\mathbf{W}}_{n_u}^x \\ \bar{\mathbf{W}}_{11}^{x_p} & \cdots & \bar{\mathbf{W}}_{1n_u}^{x_p} \\ \vdots & \ddots & \vdots \\ \bar{\mathbf{W}}_{n_y 1}^{x_p} & \cdots & \bar{\mathbf{W}}_{n_y n_u}^{x_p} \end{bmatrix} = \begin{bmatrix} \bar{\mathbf{W}}^x \\ \bar{\mathbf{W}}^{x_p} \end{bmatrix} \end{aligned} \quad (3.46)$$

The first n_y rows of $\bar{\mathbf{W}}$ correspond to the output controllability matrix with its column permuted. The other $n_y n_p$ rows characterize the output sensitivity controllability.

Definition 3.11 (Output controllability [137]): A linear time invariant state space system is said to be completely output controllable if and only if the matrix

$$[\mathbf{CB} \quad \mathbf{CAB} \quad \mathbf{CA}^2\mathbf{B} \quad \cdots \quad \mathbf{CA}^{n_x-1}\mathbf{B}]$$

has rank equal to the number of outputs.

Based on the permuted extended output controllability matrix $\bar{\mathbf{W}}$ and Definition 3.11, it is now possible to analyze the controllability of the output sensitivity and structural identifiability of the model. In the following, we assume that the measurement matrix \mathbf{C} is full row rank. This assumption is not too stringent as in most state space models the number of internal states is much larger than the number of measured variables.

Proposition 3.1: Let the number of states be larger than or at least the same as the number of outputs, i.e. $n_x \geq n_y$. Then, the maximal number of output sensitivities that can be controlled with input signals u_1, \dots, u_{n_u} is given by

$$\text{rank}(\bar{\mathbf{W}}^{x_p}) \leq n_y n_p \quad (3.47)$$

Proof: From Definition 3.11 the number of controllable outputs equals the rank of $\bar{\mathbf{W}}$.

$$\begin{aligned}\text{rank}(\bar{\mathbf{W}}) &= \text{rank} \left(\begin{bmatrix} \bar{\mathbf{W}}^x \\ \bar{\mathbf{W}}^{x_p} \end{bmatrix} \right) \\ &= \text{rank}(\bar{\mathbf{W}}^x) + \text{rank}(\bar{\mathbf{W}}^{x_p} \mathbf{Q}^x)\end{aligned}\quad (3.48)$$

with $\mathbf{Q}^x = \mathbf{I}_{(n_p+1)n_u} - \bar{\mathbf{W}}^{x^+} \bar{\mathbf{W}}^x$ is the orthogonal projector onto the kernel of $\bar{\mathbf{W}}^x$, where $+$ indicates the Moore-Penrose pseudoinverse.

The first term on the right-hand side equals:

$$\begin{aligned}\text{rank}(\bar{\mathbf{W}}^x) &= \text{rank}(\mathbf{C}\mathbf{K}^x) \\ &= \text{rank}(\mathbf{C}) - \dim(\mathcal{R}(\mathbf{C}^\top) \cap \mathcal{R}(\mathbf{K}^x)^\perp) \\ &= \text{rank}(\mathbf{C}) - \dim(\mathcal{R}(\mathbf{C}^\top) \cap \emptyset) \\ &= \text{rank}(\mathbf{C}) = n_y\end{aligned}\quad (3.49)$$

Hence, the output of the system is controllable. The remaining rows of $\bar{\mathbf{W}}$ correspond to the output parametric sensitivities.

The second term on the right-hand side

$$\begin{aligned}\text{rank}(\bar{\mathbf{W}}^{x_p} \mathbf{Q}^x) &= \\ &= \text{rank}(\bar{\mathbf{W}}^{x_p}) - \dim(\mathcal{R}(\bar{\mathbf{W}}^{x_p^\top}) \cap \mathcal{R}(\mathbf{Q}^x)^\perp) \\ &= \text{rank}(\bar{\mathbf{W}}^{x_p}) - \dim(\mathcal{R}(\bar{\mathbf{W}}^{x_p^\top}) \cap \mathcal{R}(\bar{\mathbf{W}}^x)) \\ &\Rightarrow \text{rank}(\bar{\mathbf{W}}^{x_p} \mathbf{Q}^x) \leq \text{rank}(\bar{\mathbf{W}}^{x_p})\end{aligned}\quad (3.50)$$

Moreover from the properties of the rank

$$\text{rank}(\bar{\mathbf{W}}^{x_p}) \leq \min(n_y n_p, n_x(n_p + 1)) \quad (3.51)$$

From the assumption that $n_x \geq n_y$

$$\text{rank}(\bar{\mathbf{W}}^{x_p}) \leq n_y n_p \quad (3.52)$$

The aforementioned rank provides information of the maximal number of output sensitivities that can be controlled at the same time during an experiment. It is worth noting that this analysis is the output controllability analogous to that presented in [138]. However, the goal here is not insensitive/robust control design but developing a representation suitable for identifiability analysis and parameter identification.

Therefore, we can use $\bar{\mathbf{W}}^{x_p}$ to characterize the structural identifiability condition. We introduce the following theorem:

3

Theorem 3.4: Let

$$\mathfrak{O} = \begin{bmatrix} \bar{\mathbf{O}}_{11}^{x_p} & \cdots & \bar{\mathbf{O}}_{n_y 1}^{x_p} & \cdots & \bar{\mathbf{O}}_{1 n_u}^{x_p} & \cdots & \bar{\mathbf{O}}_{n_y n_u}^{x_p} \end{bmatrix}$$

and

$$\mathfrak{W} = \begin{bmatrix} \bar{\mathbf{W}}_{11}^{x_p} & \cdots & \bar{\mathbf{W}}_{n_y 1}^{x_p} & \cdots & \bar{\mathbf{W}}_{1 n_u}^{x_p} & \cdots & \bar{\mathbf{W}}_{n_y n_u}^{x_p} \end{bmatrix}$$

The model structure (3.3) is locally structurally identifiable for $\delta \bar{\mathbf{x}}_0 \neq \mathbf{0}$ if

$$\text{rank}([\mathfrak{O} \quad \mathfrak{W}]) = n_p \quad (3.53)$$

■

The proof of Theorem 3.4 can be found in Appendix A.

In the previous theorem, the initial conditions are non-trivial, and thus, could potentially provide extra information on the identifiability of the linearized structure through the free response. Assuming that the input \mathbf{u} is persistently exciting, the free response provides extra information whenever $\delta \bar{\mathbf{x}}_0 \neq \mathbf{0}$ and $\mathbf{I}_{n_x(n_p+1)} \otimes \begin{bmatrix} \mathbf{B} \\ \mathcal{B} \end{bmatrix}$ does not have full row rank blocks. This follows from the fact that $\mathbf{W}^{x_p} = \mathbf{O}^{x_p} \left(\mathbf{I}_{n_x(n_p+1)} \otimes \begin{bmatrix} \mathbf{B} \\ \mathcal{B} \end{bmatrix} \right)$, and thus

$$\mathcal{R}(\mathbf{W}^{x_p}) = \mathcal{R} \left(\mathbf{O}^{x_p} \left(\mathbf{I}_{n_x(n_p+1)} \otimes \begin{bmatrix} \mathbf{B} \\ \mathcal{B} \end{bmatrix} \right) \right) \subseteq \mathcal{R}(\mathbf{O}^{x_p})$$

The inclusion holds with equality, i.e. $\mathcal{R}(\mathbf{W}^{x_p}) = \mathcal{R}(\mathbf{O}^{x_p})$ if and only if $\begin{bmatrix} \mathbf{B} \\ \mathcal{B} \end{bmatrix}$ is full row rank. This means that if the input excites all states, the set of output free response trajectories generate the same vector space of the output forced response, and no additional information can be obtained. Therefore, it suffices to perform the analysis on \mathfrak{W} .

In case the structure has trivial initial conditions, i.e. initial conditions are exactly zero, the information is solely contained in the output controllability matrix. Hence, structural identifiability in this case is laid out in the following corollary:

Corollary 3.1: If $\delta\bar{\mathbf{x}}_0 = \mathbf{0}$, then the system is identifiable if

$$\text{rank}(\mathfrak{W}) = n_p \quad (3.54)$$

3

The proof of Corollary 3.1 follows trivially from the proof of Theorem 3.4 by setting $\delta\bar{\mathbf{x}}_0 = \mathbf{0}$ ■

The rank condition in Theorem 3.4 provides a way to check if the model structure is identifiable from the mapping between the different inputs and output sensitivities. This representation is advantageous when the input \mathbf{u} , the measurement \mathbf{y} , and the parameter vector \mathbf{p} has physical meaning. Notice that the matrix \mathfrak{W} is a linear map between the input and the output sensitivities; where the latter also preserve their physical meaning. Additionally, if the rank condition is not satisfied, then the unidentifiable space is the span of the left null space of \mathfrak{W} . The identifiable parameter combinations can be retrieved solving the set of partial differential equations (see [32],[46]).

We now revisit the simple biological compartment model described previously to illustrate the results in the state space case. Recall that the state space representation of this model was given in (3.17) with parameter vector $\mathbf{p} = [p_1 \ p_2 \ p_3 \ p_4]^\top$, $\mathbf{x}_0 = \mathbf{0}$, and $y = x_2$. From the assumption of zero initial conditions, due to Corollary 3.1 the identifiability information is only contained in the output controllability matrix \mathcal{W} . Computing the rank of this matrix, we see that $\text{rank}(\mathcal{W}) = 3$. Due to the fact that the model is SISO, the computed rank not only provides the number of structurally identifiable parameters but also the maximal number of controllable sensitivities.

The output controllability matrix approach has the advantage of providing information on the number of maximally controllable sensitivities, which is relevant during experiment design, i.e. we can determine how many independent inputs and outputs

are needed to excite all or a determined subgroup of model parameter sensitivities. Moreover, it can deal with the analysis of structural identifiability of linear MIMO model structures in a simpler way with the construction of a single mathematical object (the output controllability matrix), rather than computing explicit transfer functions for each of the input-output pair in the state space model and analyzing them one at a time.

Chapter summary

Structural identifiability

- Structural identifiability is one of the structural properties of ODE models. It is an idealized setting in which there is no model-plant mismatch, and establishes which parameters can be uniquely estimated from the model input-output map structure. A core assumption of this approach is that the system is persistently excited by the input.
- Structural identifiability is a analysis tool that answers whether a structure is identifiable or not. In this context, structural identifiability is considered if all parameters in the structure are uniquely estimable from the input-output information. Model structures that are identifiable can be divided into globally or locally identifiable.
- This structural identifiability is a general setting that can be applied to both linear and nonlinear models. The analysis for nonlinear models is substantially more difficult due to the nonlinear structure, which makes the analysis quickly intractable. Attention has been given to linear models because models are utilized around a particular operating point or trajectory in most of engineering applications. Therefore, the interest lies on whether parameters can be identified on such particular operating region of the state space.
- In linear models, structural identifiability can be tested using a mathematical object called invariant vector, which encapsulates all the input-output map information. It can be used to generate a Jacobian matrix, and check its generic rank condition. If the associated Jacobian matrix to the input-output map is full column rank, then the linear (resp. linearized) model structure is identifiable, otherwise it is unidentifiable.
- Two types of rank conditions on the Jacobian can be distinguished when the model structure is identifiable. The first one is essentially full rank, which corresponds to the case where the rank of the Jacobian is independent of the parameters; naturally essentially full rank implies that the structure is globally identifiable. The second one is conditionally full rank, which corresponds to a rank that does depend on the model parameters, and thus, the model is locally identifiable. Conditional full rank implies that for possibly infinite but countably many points in the parameter space, the model structure is not identifiable, and thus, it is necessary to stay (locally) away from those points to ensure identifiability.

Chapter summary

- For a model structure, structural identifiability is a property of the input-output map, and as such, the initial conditions can provide extra parametric information because they act as another source of excitation in the model. Therefore, a model can be unidentifiable from some initial conditions (typically zero) but identifiable from another set of initial conditions.

3

Structural identifiability in closed-loop

- Controllers cannot improve structural identifiability. Since this structural property depends on the input-output map of the model structure, the interconnection with a controller cannot excite the model structure null space. This is due to the fact that the closed-loop structure contains the null space of the open-loop structure.
- Controllers might impoverish structural identifiability if the controller structure is not chosen with care. If the null space of the controller only contains the zero vector or if it does not lie within the column space of the open-loop structure, then the controller will not impoverish structural identifiability in the reference-to-output map.

Structural identifiability from an output controllability perspective

- Structural identifiability can also be treated from an output controllability perspective of the output sensitivity trajectories. This approach allows us to deal with MIMO models in a simpler way than using the invariant vector approach.
- The rank of output sensitivity controllability matrix provides the number of maximal controllable output sensitivities with the input signal. This is beneficial if experiment design has to be carried out to condition the model for parameter estimation.
- The maximal number of controllable output sensitivities agrees with the rank of Jacobian matrix in the invariant vector approach when the model structure is SISO. In the MIMO case, the ranks of both matrices do not need to agree. The output sensitivity controllability matrix needs to be block permuted to test identifiability of the whole MIMO structure.

Chapter summary

- The output sensitivity controllability matrix provides more information about the linear (linearized) model structure because it ultimately allows to assess (un)controllability of sensitivities and at the same time structural parameter identifiability. However, it might require more computation power because it is constructed using up to $n_x(n_p + 1) - 1$ power of the system matrix. Depending on the number of state and parameters, the computation of the extended output controllability matrix and its rank can become intractable.

4

Operational identifiability and offline gradient-based parameter estimation

In this chapter, we present the operational aspects of parameter identifiability and its effect on the parameter estimation problem. Advantages and pitfalls of sensitivity-based and gradient-based approaches are presented, as well as some possible solutions to address these shortcomings. Dedicated focus is given to the sensitivity matrix, its construction, the information extraction, sensitivity measures, and cut-off values. The chapter explores implementation aspects of parameter estimation, as well as the differences between single shooting and multiple shooting parameter estimation. A new parameter estimation method that combines sensitivity analysis and multiple shooting parameter estimation is introduced. This method improves the convergence and accuracy of the parameter estimates compared to the classical approaches in the literature.

Publications of this chapter:

Local parameter identifiability of large-scale nonlinear models based on the output sensitivity covariance matrix, Méndez-Blanco, C., Özkan, L. 16th IFAC Symposium on Advanced Control of Chemical Processes (ADCHEM) 2021 ([126])

Parameter Estimation for Multi-Stage Processes: A multiple shooting approach integrated with sensitivity analysis (in preparation), Méndez-Blanco, C., Özkan, L. To be submitted to Industrial & Engineering Chemistry Research ([127])

4.1. Introduction

Processes usually have a limited number of measured inputs and outputs, which constrains the amount of information that can be extracted from them. Moreover, identifiability in practice heavily depends on the experimental conditions, and whether the recorded data is informative enough. More specifically, a model structure depends on the admissible input signal set \mathcal{U} that is used to run the identification experiment [150], and as a consequence, not all parameters might be identifiable from the available inputs and outputs. The vector of input signals \mathbf{u} might as well not excite the system appropriately, making it difficult or impossible to detect the influence of some parameters in the collected output data, even if these parameters are structurally identifiable. Additionally, if the model is structurally complex, using analytic approaches like structural identifiability may become intractable. To deal with these shortcomings, numerical approaches to assess parameter identifiability can be employed. In particular, sensitivity-based operational identifiability is an attractive approach because not only does it allow to assess parameter identifiability, but also the design of insensitive control ([138]), input design for parameter identification ([171]), model parameter reduction ([172]), etc. The sensitivity matrix is the main object of analysis in gradient-based operational identifiability, as relevant information can be extracted from it, e.g. the magnitudes of the sensitivity vector, the collinearity indexes, etc. The information can be extracted by implementing various matrix decomposition methods such as singular value decomposition (SVD) [75], tuning importance ([160],[180],[39]), principal component analysis ([84],[99],[39]), eigenvalue decomposition ([182],[143],[144]), successive orthogonalization method (SOM) ([204],[106],[107]). These methods allow to recognize subset of parameters that are identifiable based on a specific metric and cut-off value. The selection of both the method and the cut-off value play a crucial role in the selection of the identifiable parameter subset, which are the parameter that can be most reliably estimated. Moreover, not only is the correct parameter selection important for parameter estimation but also for the conditioning of the optimization problem. Gradient-based operational identifiability is a local analysis performed at or in the neighborhood of an operating point. Different parameter values define different operating points, which implies that the search manifold can have problematic regions such as flat regions where the sensitivity function is zero or ill-defined regions where the sensitivity function is not smooth. For such problems different approaches have been developed such as multi-start optimization [48],[117], incremental single shooting parameter estimation [131], and multiple shooting parameter estimation [10] [145]. These methods provide alternative ways to bypass or be robust against problematic regions in the search manifold to obtain more reliable parameter estimates.

In this chapter, we recall the concept of operational identifiability and important aspects of it, such as the (relative) sensitivity matrix, sensitivity measures selection, and cut-off value computation, etc. We also develop new methods exploiting the operational identifiability in different operating points to obtain better parameter

estimates and lower cost function values. The concepts and new developments are tested in a simple illustrative example of the roll motion of a ship.

4.2. Sensitivity-based operational identifiability

Sensitivity analysis is used to evaluate the variation of a system's output due to changes in the inputs signals as well as to changes in parameters in the model, i.e. parametric sensitivity analysis. The analysis of such a variation can give important information about parameter identifiability if output data is collected [130]. A parameter whose change induces a large variation in the output of the plant will be more likely to be observed, and its contribution can be more easily identified and estimated.

Sensitivity-based operational identifiability analysis does not use the model structure to test for identifiability. Instead, it requires pre-specified parameter values in the parameter space (either nominal or available estimates), as well as the number and time stamps of the measurements to test for identifiability around the given value of the parameter vector. Sensitivity-based identifiability is a local test because it tests the behavior of changes due to variations in the parameters around the vicinity of the trajectory. Furthermore, it is also a data based-approach, and as such, it requires a criterion that allows us to quantify "how identifiable" a parameter is.

Consider the model described in (3.1), let \mathbf{y}_m be the available vector of output measurement of N elements, and consider the minimization with respect to \mathbf{p} of the following quadratic cost

$$V(\mathbf{p}) := \frac{1}{2} \sum_{k=0}^{N-1} \|\mathbf{y}_m(t_k) - \mathbf{y}(t_k, \mathbf{p})\|_2^2 = \frac{1}{2} \boldsymbol{\varepsilon}(\mathbf{p})^\top \boldsymbol{\varepsilon}(\mathbf{p}) \quad (4.1)$$

The quadratic cost function (4.1) is a natural choice, as it minimizes the quadratic error between the observed data \mathbf{y}_m and the predicted output $\mathbf{y}(\mathbf{p})$. Furthermore, the error $\boldsymbol{\varepsilon}$ is assumed to have zero mean and a probability density function (PDF) f that satisfies the maximum likelihood estimator (MLE) regularity conditions. Parameter estimation now consists of finding a parameter vector \mathbf{p}^* as a minimizing argument of the cost function (4.1), i.e.

$$\mathbf{p}^* = \arg \min_{\mathbf{p}} V(\mathbf{p}) \quad (4.2)$$

The solution (4.2) is found by approximating the cost function $V(\mathbf{p})$ in (4.1) around a point \mathbf{p}_0 in the parameter space as

$$V(\mathbf{p}) \approx V(\mathbf{p}_0) + \mathbf{J}^\top(\mathbf{p}_0)(\mathbf{p} - \mathbf{p}_0) + \frac{1}{2}(\mathbf{p} - \mathbf{p}_0)^\top \mathbf{H}(\mathbf{p}_0)(\mathbf{p} - \mathbf{p}_0) \quad (4.3)$$

where $\mathbf{J}(\mathbf{p}_0)$ and $\mathbf{H}(\mathbf{p}_0)$ are the Jacobian and Hessian matrices, respectively evaluated at the point \mathbf{p}_0 .

The necessary condition to minimize (4.3) is

4

$$\mathbf{J}(\mathbf{p}_0) + \mathbf{H}(\mathbf{p}_0)(\mathbf{p} - \mathbf{p}_0) = 0 \quad (4.4)$$

Hence, if the Hessian is invertible, the parameter vector \mathbf{p}^* that minimizes the cost function is given by

$$\mathbf{p}^* = \mathbf{p}_0 - \mathbf{H}^{-1}(\mathbf{p}_0)\mathbf{J}(\mathbf{p}_0) \quad (4.5)$$

Using the matrix calculus outlined in [29], and let the matrix $\mathbf{S} = \frac{\partial \mathbf{y}(\mathbf{p})}{\partial \mathbf{p}^\top} \in \mathbb{R}^{Nn_y \times n_p}$, we can find explicit expressions for the Jacobian and the Hessian of $V(\mathbf{p})$ with respect to the parameters:

$$\begin{aligned} \mathbf{J}(\mathbf{p}) &= \frac{1}{2} \frac{\partial V(\mathbf{p})}{\partial \mathbf{p}} = \frac{1}{2} \frac{\partial \boldsymbol{\varepsilon}(\mathbf{p})^\top}{\partial \mathbf{p}} \boldsymbol{\varepsilon}(\mathbf{p}) + \frac{1}{2} (\mathbf{I}_{n_p} \otimes \boldsymbol{\varepsilon}(\mathbf{p})^\top) \frac{\partial \boldsymbol{\varepsilon}(\mathbf{p})}{\partial \mathbf{p}} \\ &= \left(\frac{\partial \boldsymbol{\varepsilon}(\mathbf{p})}{\partial \mathbf{p}^\top} \right)^\top \boldsymbol{\varepsilon}(\mathbf{p}) \\ &= - \left(\frac{\partial \mathbf{y}(\mathbf{p})}{\partial \mathbf{p}^\top} \right)^\top (\mathbf{y}_m - \mathbf{y}(\mathbf{p})) \\ &= -\mathbf{S}^\top (\mathbf{y}_m - \mathbf{y}(\mathbf{p})) \end{aligned} \quad (4.6)$$

$$\begin{aligned} \mathbf{H}(\mathbf{p}) &= \frac{\partial^2 V(\mathbf{p})}{\partial \mathbf{p}^\top \partial \mathbf{p}} = \frac{\partial^2 \boldsymbol{\varepsilon}(\mathbf{p})^\top}{\partial \mathbf{p}^\top \partial \mathbf{p}} (\mathbf{I}_{n_p} \otimes \boldsymbol{\varepsilon}(\mathbf{p})) + \frac{\partial \boldsymbol{\varepsilon}(\mathbf{p})^\top}{\partial \mathbf{p}} \frac{\partial \boldsymbol{\varepsilon}(\mathbf{p})}{\partial \mathbf{p}^\top} \\ &= \frac{\partial^2 \boldsymbol{\varepsilon}(\mathbf{p})^\top}{\partial \mathbf{p}^\top \partial \mathbf{p}} (\mathbf{I}_{n_p} \otimes \boldsymbol{\varepsilon}(\mathbf{p})) + \frac{\partial \mathbf{y}(\mathbf{p})^\top}{\partial \mathbf{p}} \frac{\partial \mathbf{y}(\mathbf{p})}{\partial \mathbf{p}^\top} \\ &= \frac{\partial \mathbf{S}^\top}{\partial \mathbf{p}^\top} (\mathbf{I}_{n_p} \otimes \boldsymbol{\varepsilon}(\mathbf{p})) + \mathbf{S}^\top \mathbf{S} \end{aligned} \quad (4.7)$$

The matrix \mathbf{S} is the absolute sensitivity matrix, which contains the variations of the output vector $\mathbf{y}(\mathbf{p})$ with respect to variations in the parameter vector \mathbf{p} . The Hessian is usually expensive to compute due to the extra differentiation term $\partial_{\mathbf{p}^\top} \mathbf{S}^\top$. However, around the vicinity of the optimum \mathbf{p}^* , the second derivative and the error itself are weakly correlated [187], and thus, the Hessian can be approximated by

$$\mathbf{H}(\mathbf{p}) \approx \mathbf{S}^\top(\mathbf{p})\mathbf{S}(\mathbf{p}) \quad (4.8)$$

Using (4.8), the solution to the optimization problem (4.5) is simplified to

4

$$\mathbf{p}^* = \mathbf{p}_0 - (\mathbf{S}^\top(\mathbf{p}_0)\mathbf{S}(\mathbf{p}_0))^{-1}\mathbf{S}^\top(\mathbf{p}_0)(\mathbf{y}_m - \mathbf{y}(\mathbf{p}_0)) \quad (4.9)$$

Local operational identifiability at \mathbf{p}^* is generally assessed checking whether $V(\mathbf{p})$ has locally a unique minimum [150]. Uniqueness of the estimate \mathbf{p}^* is guaranteed if the Hessian matrix $\mathbf{H}(\mathbf{p}^*)$ is positive definite, which provides a sufficient condition for local operational identifiability at \mathbf{p}^* [75]. If the approximation (4.8) holds, then it suffices to determine the rank of the absolute sensitivity matrix \mathbf{S} since

$$\text{rank}(\mathbf{S}(\mathbf{p}^*)) = n_p \Leftrightarrow \text{rank}(\mathbf{S}^\top(\mathbf{p}^*)\mathbf{S}(\mathbf{p}^*)) = n_p \Leftrightarrow \mathbf{S}^\top(\mathbf{p}^*)\mathbf{S}(\mathbf{p}^*) \succ 0 \quad (4.10)$$

Given that the uniqueness of the parameter vector \mathbf{p} is determined by the Hessian $\mathbf{H}(\mathbf{p})$, and that the Hessian is usually approximated by the product $\mathbf{S}^\top(\mathbf{p})\mathbf{S}(\mathbf{p})$, the analysis of the sensitivity matrix $\mathbf{S}(\mathbf{p})$ is crucial to assess local operational identifiability of \mathbf{p} .

4.3. The output parametric sensitivity matrix $\mathbf{S}(\mathbf{p})$ and its relation to operational identifiability

The sensitivity matrix¹ \mathbf{S} can be constructed easily from the sensitivity time trajectories if a dynamic parametric model is available. However, this is not always possible in practice because models can be large-dimensional with an even larger number of parameters, making the analytic computation of parametric sensitivities impractical. Therefore, it is necessary to resort to numerical approximations to construct the output parametric sensitivity matrix \mathbf{S} . Despite the fact that newer and

¹For ease of notation, we shall drop the explicit dependency of \mathbf{S} with respect to \mathbf{p} .

robust methods for analytic differentiation such as automatic and symbolic differentiation exist, avoiding the truncation error of numerical differentiation, they might fail if the model is too large or structurally complex as noted by Boudjemaa et al.[26] The standard way of calculating sensitivities numerically is to approximate $\frac{\partial \mathbf{y}_i}{\partial \mathbf{p}_j}(t_k)$ as a total variation $\frac{\Delta \mathbf{y}_i(t_k)}{\Delta \mathbf{p}_j}$. The total variation will approximate the true partial derivative if $\Delta \mathbf{p}$ is made small. The output variation $\Delta \mathbf{y}_i$ is calculated varying one parameter at a time, while keeping the rest fixed at their nominal value, and then collecting the corresponding perturbed model output. Moreover, there are many methods to estimate the total variation $\frac{\Delta \mathbf{y}_i(t_k)}{\Delta \mathbf{p}_j}$; however, we shall use central (symmetric) differences to make this computation because it tends to be more precise than forward or backward differences.

4

The central differences scheme requires to simulate the model $\mathcal{M}(\mathbf{p})$ twice per parameter ($2n_p$ simulations with n_p the number of parameter) from initial time t_0 to final time t_f : one time using a parameter vector \mathbf{p}^- perturbed in the negative direction, and a second time with another parameter vector \mathbf{p}^+ perturbed in the positive direction.

Let h_{p_j} be a small perturbation affecting only the the j -th element of \mathbf{p} , then we have that

$$\begin{aligned}\mathbf{p}_j^+ &= [p_1 \quad \cdots \quad p_j + h_{p_j} \quad p_{j+1} \quad \cdots \quad p_{n_p}]^\top \\ \mathbf{p}_j^- &= [p_1 \quad \cdots \quad p_j - h_{p_j} \quad p_{j+1} \quad \cdots \quad p_{n_p}]^\top\end{aligned}\tag{4.11}$$

where \mathbf{p}_j^+ and \mathbf{p}_j^- are the vectors of positive and negative perturbations on j -th parameter.

Furthermore, let $\mathbf{y}(t, \mathbf{p}) \in \mathbb{R}^{n_y}$ be the model output with N points in the interval $t \in [t_0, t_f]$. We can approximate the absolute output parametric sensitivity (AOPS) as

$$\frac{\partial \mathbf{y}_i(t, \mathbf{p})}{\partial \mathbf{p}_j} \approx s_{i,j}(t) = \frac{1}{2h_{p_j}}(\mathbf{y}_{i,j}^+ - \mathbf{y}_{i,j}^-), \quad \forall i = 1, \dots, n_y, \quad \forall j = 1, \dots, n_p \tag{4.12}$$

where

$$\mathbf{y}_{i,j}^- = \begin{bmatrix} y_i(t_0, \mathbf{p}_j^-) \\ y_i(t_1, \mathbf{p}_j^-) \\ \vdots \\ y_i(t_f, \mathbf{p}_j^-) \end{bmatrix}, \quad \mathbf{y}_{i,j}^+ = \begin{bmatrix} y_i(t_0, \mathbf{p}_j^+) \\ y_i(t_1, \mathbf{p}_j^+) \\ \vdots \\ y_i(t_f, \mathbf{p}_j^+) \end{bmatrix} \quad (4.13)$$

We collect each sensitivity \mathbf{s} in the matrix $\mathbf{S} \in \mathbb{R}^{Nn_y \times n_p}$ as follows

$$\mathbf{S} = \begin{bmatrix} \mathbf{s}(t_0) \\ \mathbf{s}(t_1) \\ \vdots \\ \mathbf{s}(t_{N-1}) \end{bmatrix} \quad (4.14)$$

where

$$\mathbf{s}(t_k) = \begin{bmatrix} s_{11}(t_k) & s_{12}(t_k) & \cdots & s_{1n_p}(t_k) \\ \vdots & \vdots & \ddots & \vdots \\ s_{n_y 1}(t_k) & s_{n_y 2}(t_k) & \cdots & s_{n_y n_p}(t_k) \end{bmatrix}$$

Once constructed, the sensitivity matrix \mathbf{S} can be exploited to analyze the identifiability of parameters. Recall that if the prediction error terms in $\boldsymbol{\varepsilon}(\mathbf{p})$ is normally distributed (which satisfies the regularity conditions), then function $V(\mathbf{p})$ is the likelihood function of the experiment [150]. This implies that the estimated \mathbf{p}^* is the best asymptotically ($k \rightarrow \infty$) unbiased estimate of \mathbf{p} , whose lower bound on the parameter covariance matrix is given by the Cramer-Rao inequality

$$\text{cov}(\mathbf{p}^*) \geq \mathbf{F}^{-1}(\mathbf{p}^*) \quad (4.15)$$

where $\mathbf{F}(\mathbf{p}^*)$ is the Fisher information matrix (FIM) defined as

$$\mathbf{F}(\mathbf{p}^*) = \mathbb{E} \left[\frac{\partial^2 V(\mathbf{p})}{\partial \mathbf{p}^\top \partial \mathbf{p}} \right] \Big|_{\mathbf{p}=\mathbf{p}^*} = \mathbb{E} [\mathbf{H}(\mathbf{p})] \Big|_{\mathbf{p}=\mathbf{p}^*} \quad (4.16)$$

This is relevant because some of the singular values of the Hessian may be very small, whose associated directions in the parameter space have a rather limited influence over the cost function $V(\mathbf{p})$. In other words, in these particular directions the parameter estimates exhibit very large variance. The lower limit establishes a bound on how "close" the estimate is to the "true" parameter present in the output data.

Despite the existence of several methods to extract and analyze the information contained in the sensitivity matrix \mathbf{S} and the Hessian matrix \mathbf{H} , we shall focus on the successive orthogonalization method (SOM) proposed by [204] using the efficient implementation developed in [106] and [107]. The advantages of the SOM lies in the fact that it makes it possible to retrieve the parameters that generate specific sensitivity directions. Other methods, on the contrary, introduce linear transformations that make it difficult to precisely pinpoint parameters that might lead to operational unidentifiability.

4.3.1. The successive orthogonalization method (SOM)

4

The SOM computes the perpendicular distance of one column to the vector space spanned by other columns to directly measure the degree of linear dependency between them. Additionally, this information is stored in a permutation matrix that allows to obtain a ranking of the most and least operationally identifiable parameters using the Euclidean norm as the selection metric. The SOM exploits the fact that the QR factorization of the sensitivity matrix can be written as:

$$\mathbf{S}\boldsymbol{\Pi} = \mathbf{Q}\boldsymbol{\Sigma}\tilde{\mathbf{R}} \quad (4.17)$$

where $\boldsymbol{\Pi}$ is a permutation matrix, \mathbf{Q} is an orthogonal matrix, $\boldsymbol{\Sigma}$ is a diagonal matrix whose non-zero are the magnitudes of the orthogonal fractions of the original sensitivity vectors, and $\tilde{\mathbf{R}}$ is an upper triangular matrix whose non-zero elements are the ratio between each vector and their projections onto the other normalized vectors. A detailed explanation of the structure of each of these matrices can be found in Appendix A.

The SOM is an iterative process. At iteration i the column \mathbf{s}_j of \mathbf{S} with the highest 2-norm is selected, labeled $\bar{\mathbf{s}}_i$, and normalized to make it a unit vector \mathbf{u}_i . The unit vector \mathbf{u}_i is stored as the i -th column of a matrix \mathbf{Q} , while the column \mathbf{s}_j is removed from \mathbf{S} . The order of selection is stored in the permutation matrix $\boldsymbol{\Pi}$ placing a 1 in the j -th row in the i -th column. Subsequently, the rest of the non-selected columns of \mathbf{S} are made orthogonal to \mathbf{u}_i . Finally, the procedure is repeated with the remaining $n_p - i$ vectors in \mathbf{S} until all the n_p columns of \mathbf{S} are made orthogonal to each other. A pseudocode of the SOM is given in Algorithm 1.

Based on the structure of the decomposition generated by the SOM, the locally most identifiable parameters are those that correspond to the larger magnitudes of the elements of $\boldsymbol{\Sigma}$. Each of this magnitudes can be directly link to its particular parameter through the permutation matrix $\boldsymbol{\Pi}$.

Algorithm 1 Successive orthogonalization method [106]

Require: $\mathbf{S} = [\mathbf{s}_1 \ \cdots \ \mathbf{s}_{n_p}]$

- 1: Construct the sets $\mathbb{S} = \{\mathbf{s}_1, \dots, \mathbf{s}_{n_p}\}$, $\mathbb{S}^\Pi = \emptyset$, and $j = \{1, 2, \dots, n_p\}$
 - 2: Initialize $i \leftarrow 1$
 - 3: Initialize $k \leftarrow 1$
 - 4: Initialize $\mathbf{R} = \mathbf{0}_{n_p \times n_p}$
 - 5: Initialize $\boldsymbol{\Pi} = \mathbf{0}_{n_p \times n_p}$
 - 6: **while** $\text{card}(\mathbb{S})$ is larger than zero **do**
 - 7: Select the element $\mathbf{s}_i \in \mathbb{S}$ such that $\|\mathbf{s}_i\|_2 = \max(\|\mathbf{s}_j\|_2)$
 - 8: $k \leftarrow [j]$ such that $\mathbf{s}_k = \mathbf{s}_i$ ▷ The symbol $[.]$ means 'element of.'
 - 9: $\mathbb{S} \leftarrow \mathbb{S} \setminus \{\mathbf{s}_i\}$
 - 10: $\mathbf{v}_i \leftarrow \frac{\mathbf{s}_i}{\|\mathbf{s}_i\|_2}$
 - 11: $\mathbf{s}_{j \neq i} \leftarrow \mathbf{s}_{j \neq i} - \mathbf{v}_i \langle \mathbf{v}_i, \mathbf{s}_{j \neq i} \rangle$
 - 12: $\mathbb{S} \leftarrow \{\mathbf{s}_{j \neq i}\}$
 - 13: $\mathbb{S}^\Pi \leftarrow \mathbb{S}^\Pi \cup \{\mathbf{v}_i\}$
 - 14: $\boldsymbol{\Pi}_{(k,i)} \leftarrow 1$
 - 15: $\mathbf{R}_{i,j} \leftarrow \langle \mathbf{v}_i, \mathbf{s}_j \rangle$
 - 16: $i \leftarrow i + 1$
 - 17: $j \leftarrow j \setminus i$
 - 18: **end while**
 - 19: $\mathbf{Q} = [\mathbb{S}^\Pi]$
 - 20: Decompose \mathbf{R} into a diagonal matrix $\boldsymbol{\Sigma}$ and $\tilde{\mathbf{R}}$ such that $\mathbf{R} = \boldsymbol{\Sigma} \tilde{\mathbf{R}}$
 - 21: **return** $\mathbf{Q}, \boldsymbol{\Sigma}, \tilde{\mathbf{R}}, \boldsymbol{\Pi}$
-

In the following example, we present a simplified model of a ship roll motion. This model will allow us to illustrate how parametric sensitivities and the SOM can be used to assess operational identifiability.

Example 4.1 (Simple ship roll motion model [140]): Let the model describing the roll motion of a ship be given by:

$$\begin{aligned} \begin{bmatrix} \dot{\theta} \\ \ddot{\theta} \end{bmatrix} &= \frac{1}{I_b} \begin{bmatrix} 0 & I_b \\ -G & -D \end{bmatrix} \begin{bmatrix} \theta \\ \dot{\theta} \end{bmatrix} + \frac{1}{I_b} \begin{bmatrix} 0 \\ \tau_c \end{bmatrix} \\ \theta &= [1 \quad 0] \begin{bmatrix} \theta \\ \dot{\theta} \end{bmatrix} \end{aligned} \quad (4.18)$$

where θ is the roll angle, $\dot{\theta}$ is the roll rate (angular velocity), $\ddot{\theta}$ is the roll acceleration, τ_c is the control torque. $I_b > 0 \in \mathbb{R}$ is the vessel total moment of inertia about the origin, $D > 0 \in \mathbb{R}$ is the (linear) damping factor, and $G > 0 \in \mathbb{R}$ is the (linear) restoring coefficient.

4

The roll torque generated by the fins neglecting drag effects can be computed as:

$$\tau_c = \mathbf{a}^\top \boldsymbol{\alpha} \rho_s r V_f^2 A_f \quad (4.19)$$

$$\text{with } \mathbf{a} = \begin{bmatrix} a_3 \\ a_2 \\ a_1 \\ a_0 \end{bmatrix} \text{ and } \boldsymbol{\alpha} = \begin{bmatrix} (-\alpha_{\dot{\theta}-V_b} - \alpha_m)^3 \\ (-\alpha_{\dot{\theta}-V_b} - \alpha_m)^2 \\ -\alpha_{\dot{\theta}-V_b} - \alpha_m \\ 1 \end{bmatrix}$$

where ρ is the seawater density, r is the fin arm length to the center of rotation, V_f is the relative speed between the fins and the flow, A_f is the area of the fin, $\alpha_{\dot{\theta}-V_b}$ is the induced flow angle, α_m is the mechanical angle of the fins, and a_3, a_2, a_1 , and a_0 are the polynomial coefficients of the lift coefficient. The induced flow angle can be computed as:

$$\alpha_{\dot{\theta}-V_b} = \arctan \left(\frac{r \dot{\theta}}{V_f} \right) \quad (4.20)$$

The measured output is the roll angle θ while input is α_m . The values of the nominal parameters for the simple ship roll motion model are displayed in 4.1.

We analyze the sensitivity of θ to the parameter vector

$$\mathbf{p} = [D \quad G \quad I \quad r \quad a_3 \quad a_2 \quad a_1 \quad a_0]^\top$$

under the action of a sinusoidal input $\alpha_m = \sin(\frac{\pi}{15}t)$. Since the model has low

Table 4.1: Ship roll model nominal parameters (above dash line: parameter to estimate. Below dash line: fixed known parameters).

Parameter	Description	Value	Bounds	Unit
D	Linear damping factor	3.5×10^6	$[1, 4.2] \times 10^6$	N s rad^{-1}
G	Linear restoring coefficient	2×10^5	$[1, 3.5] \times 10^5$	N rad^{-1}
I	Moment of inertia of the vessel	9.5625×10^8	$[1, 8.5] \times 10^8$	kg m^{-2}
r	Fin arm length to the center of mass	20.8	$[0, 25]$	m
a_3	Lift coefficient polynomial coefficient	19.68	$[12, 22]$	rad^{-3}
a_2	Lift coefficient polynomial coefficient	-2.69	$[-5, -1]$	rad^{-2}
a_1	Lift coefficient polynomial coefficient	6.53	$[2, 10]$	rad^{-1}
a_0	Lift coefficient polynomial coefficient	0.48	$[0, 2]$	—
<hr/>				
V_f	Relative speed of the vessel	6	—	m s^{-1}
A_f	Area of the fin	21.1	—	m^2
ρ_s	Seawater density	1.025	—	kg m^{-3}

complexity, an explicit dynamic parameter sensitivity model can be derived. The model output and input are shown in Figure 4.1. Likewise, the parameter output sensitivities for the ship roll model are displayed in Figure 4.2

The decomposition generates the ranking

$$\mathbf{p}_{\text{ranked}} = \boldsymbol{\Pi}^\top \mathbf{p} = [a_0 \quad r \quad a_2 \quad G \quad a_1 \quad a_3 \quad D \quad I]^\top \quad (4.21)$$

where the diagonal elements of $\boldsymbol{\Sigma}$ are plotted in Figure 4.3

Note that the orthogonal fraction of the moment of inertia sensitivity under the applied input profile is in the order of 10^{-25} , which is practically zero. This implies, that the moment of inertia does not generate a unique variation on the the roll

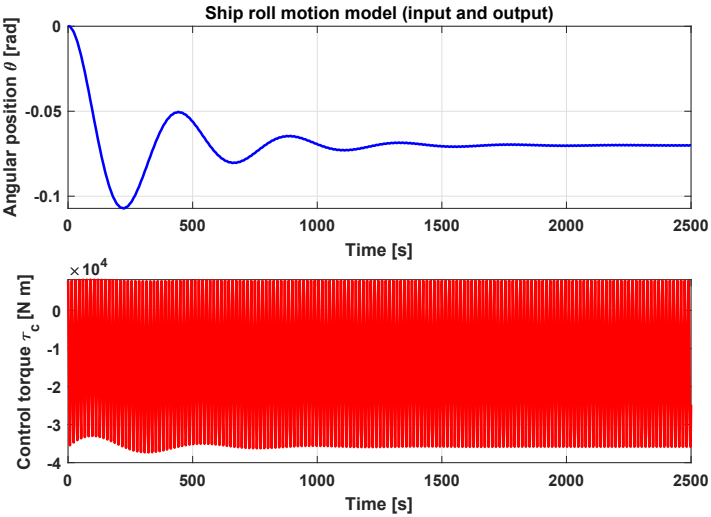


Figure 4.1: Input and output of the ship roll motion model

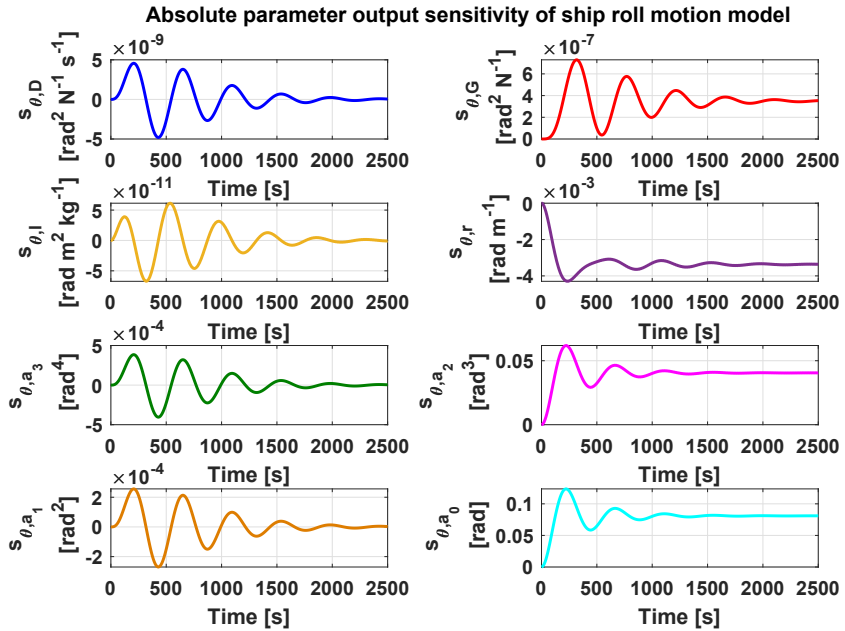


Figure 4.2: Absolute output parametric sensitivities

angle θ . However, it is not obvious whether the rest of parameters is operationally identifiable. Therefore, it is necessary to establish a sensitivity measure to assert whether a parameter or a subset thereof is identifiable. This shall be discussed in

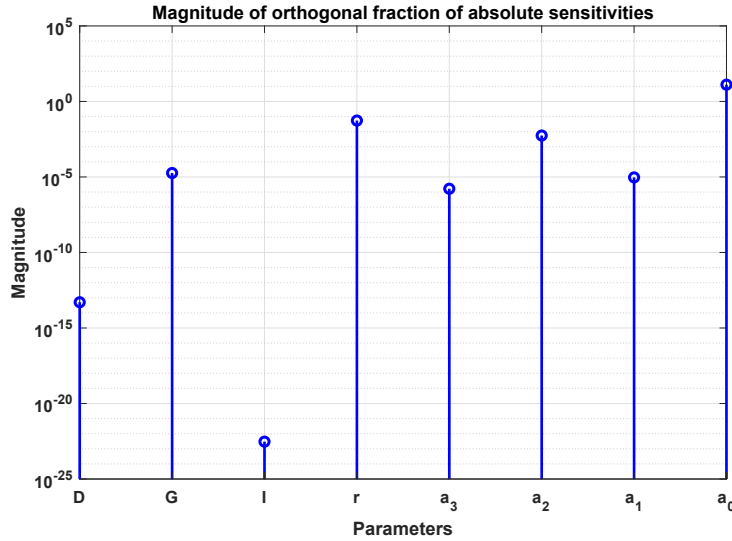


Figure 4.3: Magnitudes of the orthogonal fractions of the absolute output parametric sensitivity vectors

detail in Section 4.4. On the other hand, it is evident from Figure 4.2 that the parameter output sensitivities have natural units, which make the analysis with SOM scaling dependent. This is especially important in models where parameters might differ in magnitudes by several orders of magnitude, e.g. the moment of inertia I ($\sim 10^6$) vs. fin arm length to the center of mass r (~ 10). This scaling issue can be addressed by normalizing the sensitivity trajectories to construct a relative sensitivity matrix.

4.3.2. Normalization of the output parametric sensitivities

Recall that the AOPS of the i -th output with respect to the j -th parameter is approximated (for sufficiently small h_{pj}) in (4.12). The output variations $\mathbf{y}_i(t, \mathbf{p}_j^+)$ and $\mathbf{y}_i(t, \mathbf{p}_j^-)$ can be written in terms of an arbitrary nominal trajectory $\mathbf{y}_i(t, \mathbf{p}_{\text{nom}})$ determined by \mathbf{p}_{nom} , which is the vector of parameter fixed at a nominal value as follows

$$\begin{aligned}\mathbf{y}_i(t, \mathbf{p}_j^+) &= \mathbf{y}_i(t, \mathbf{p}_{\text{nom}})(1 + \delta_{+}y_i) \\ \mathbf{y}_i(t, \mathbf{p}_j^-) &= \mathbf{y}_i(t, \mathbf{p}_{\text{nom}})(1 + \delta_{-}y_i)\end{aligned}\tag{4.22}$$

It is worth noting that (4.22) represents the deviation that the perturbed trajectories

have from the nominal trajectory. Additionally, $\delta_+ y_i$ and $\delta_- y_i$ are time-varying and, in general, $\delta_+ y_i \neq \delta_- y_i$ because the output might not be perturbed in the same proportion in the positive and negative directions due to nonlinear effects of the model. Analogously, let \mathbf{p}_j^+ and \mathbf{p}_j^- be variations on the j -th element of \mathbf{p} in both the positive and negative directions. We define these two quantities in terms of the j -th element p_{nom_j} of \mathbf{p}_{nom}

$$\begin{aligned}\mathbf{p}_j^+ &= p_{\text{nom}_j} + h_{p_j} = \mathbf{p}_{\text{nom}_j}(1 + \delta p_j) \\ \mathbf{p}_j^- &= p_{\text{nom}_j} - h_{p_j} = \mathbf{p}_{\text{nom}_j}(1 - \delta p_j)\end{aligned}\quad (4.23)$$

4

where δp_j is the percent variation of \mathbf{p}_j^+ and \mathbf{p}_j^- with respect to \mathbf{p}_{nom} . The assumption here is that the percentage variation δp_j is the same in both the increasing and decreasing directions. We note again that the each of the perturbed parameters in (4.23) are elements of \mathbf{p}_j^+ and \mathbf{p}_j^- , respectively. Let us replace (4.22) and (4.23) in (4.12), thus

$$s_{i,j}(t) = \frac{\mathbf{y}_i(t, \mathbf{p}_{\text{nom}})(\delta_+ y_i - \delta_- y_i)}{2\mathbf{p}_{\text{nom}_j} \delta p_j} \quad (4.24)$$

Notice that the expression in (4.24) depends on the i -th nominal output trajectory $\mathbf{y}_i(t, \mathbf{p}_{\text{nom}})$ and the j -th nominal parameter value $\mathbf{p}_{\text{nom}_j}$. These two variables can be used to normalize the absolute sensitivities and eliminate the physical units

$$\frac{\partial \ln(\mathbf{y}_i(t, \mathbf{p}))}{\partial \ln(\mathbf{p}_j)} \approx \bar{s}_{i,j}(t) = \frac{\mathbf{p}_{\text{nom}_j}}{\mathbf{y}_i(t, \mathbf{p}_{\text{nom}})} \frac{\mathbf{y}_i(t, \mathbf{p}_{\text{nom}})(\delta_+ y_i - \delta_- y_i)}{2\mathbf{p}_{\text{nom}_j} \delta p_j} = \frac{\delta_+ y_i - \delta_- y_i}{2\delta p_j} \quad (4.25)$$

where $\bar{s}_{i,j}(t)$ is the relative output parametric sensitivity (ROPS). The ROPS only depends on dimensionless quantities, i.e. the percentage unit of variation in both the output and parameter.

The scaling used in (4.25) uses the ratio between $\mathbf{p}_{\text{nom}_j}$ and $\mathbf{y}_i(t, \mathbf{p}_{\text{nom}})$. However, other choices of scaling based on $y_i(t, \mathbf{p}_{\text{nom}})$ are also possible [71],[70], such as the arithmetic average, the median, the maximum value, or the steady-state value. If measured output data $\mathbf{y}_m(t)$ of a system is available, it can also be used as a scaling factor.

Furthermore, the relative sensitivity $\bar{s}_{i,j}$ might not be defined at points where $\mathbf{y}_i(t, \mathbf{p}_{\text{nom}}) = 0$ or not be smooth due to sign changes. Nevertheless, this can be

solved by shifting each output trajectory with a vector of constants \mathbf{c}_i to make every element in $\tilde{\mathbf{y}}_i(t, \mathbf{p}_{\text{nom}}) = \mathbf{y}_i(t, \mathbf{p}_{\text{nom}}) + \mathbf{c}_i > 0$. The shifting constant \mathbf{c}_i must satisfy

$$\mathbf{c}_i \geq |\min(\mathbf{y}_i(t, \mathbf{p}_{\text{nom}}))|$$

The addition of such a constant vector does not affect the analysis since the AOPS of $\tilde{\mathbf{y}}_i(t, \mathbf{p})$ and $\mathbf{y}_i(t, \mathbf{p})$ remain the same

$$\frac{\partial \tilde{\mathbf{y}}_i(t, \mathbf{p})}{\partial \mathbf{p}_j} = \frac{\partial (\mathbf{y}_i(t, \mathbf{p}) + \mathbf{c}_i)}{\partial \mathbf{p}_j} = \frac{\partial \mathbf{y}_i(t, \mathbf{p})}{\partial \mathbf{p}_j} = s_{i,j}(t) \quad (4.26)$$

Thus, $\tilde{\mathbf{y}}_i(t, \mathbf{p}_{\text{nom}})$ can be used in (4.25) as a scaling vector to obtain the ROPS. Finally, the relative sensitivity matrix $\bar{\mathbf{S}}$ has the form

$$\bar{\mathbf{S}} = \begin{bmatrix} \bar{\mathbf{s}}(t_0) \\ \bar{\mathbf{s}}(t_1) \\ \vdots \\ \bar{\mathbf{s}}(t_{N-1}) \end{bmatrix} \quad (4.27)$$

where

$$\bar{\mathbf{s}}(t_k) = \begin{bmatrix} \frac{p_{\text{nom}1}}{y_1(t_k)} s_{11}(t_k) & \frac{p_{\text{nom}2}}{y_1(t_k)} s_{12}(t_k) & \cdots & \frac{p_{\text{nom}n_p}}{y_1(t_k)} s_{1n_p}(t_k) \\ \vdots & \vdots & \ddots & \vdots \\ \frac{p_{\text{nom}1}}{y_{n_y}(t_k)} s_{n_y 1}(t_k) & \frac{p_{\text{nom}2}}{y_{n_y}(t_k)} s_{n_y 2}(t_k) & \cdots & \frac{p_{\text{nom}n_p}}{y_{n_y}(t_k)} s_{n_y n_p}(t_k) \end{bmatrix}$$

Using the relative sensitivity matrix $\bar{\mathbf{S}}$ with the SOM in the ship roll motion example, we obtain the relative output parametric sensitivity trajectories shown in Figure 4.4

These trajectories result in the ranking

$$\mathbf{p}_{\text{ranked}} = \boldsymbol{\Pi}^\top \mathbf{p} = [a_2 \quad G \quad I \quad a_0 \quad r \quad a_3 \quad D \quad a_1]^\top \quad (4.28)$$

The orthogonal fractions are plotted in Figure 4.5.

Notice that the ROPS lack units, therefore, they can be compared sensibly because they represent the ratio of the variations in the model as explained in (4.25). In this case, the ROPS provide a different ranking, where the moment of inertia ranks third as opposed to the last position when the analysis was performed using AOPS.

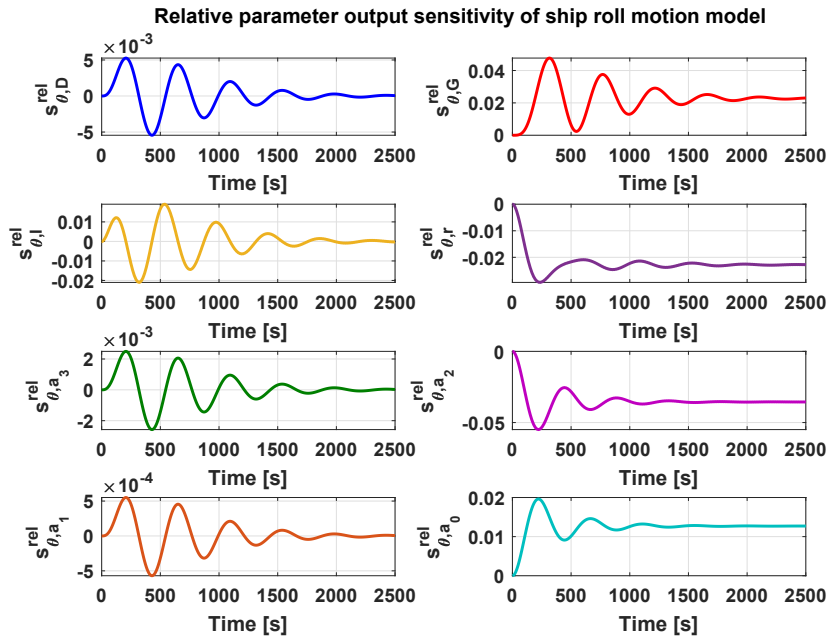


Figure 4.4: Relative output parametric sensitivities

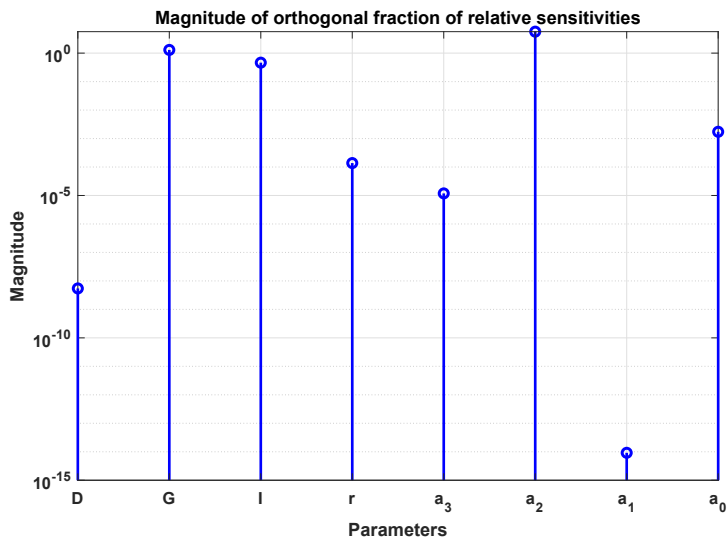


Figure 4.5: Magnitudes of the orthogonal fractions of the original output parametric sensitivity vectors

Likewise, the use of ROPS does not exempt us from the need of metrics to establish which parameters or a subset of them is identifiable. Since the matrix Σ from the SOM provides the magnitudes of the orthogonal fractions of the sensitivities, it is the mathematical object that can be used to establish cut-off values to decide on identifiability. The different measures that can be applied to Σ and their rationales will be explained in more detail in the following section.

4

4.4. Sensitivity measures

In the previous section, we adopted the use of the SOM to establish a ranking of parameters using an operating trajectory. The matrices Σ and Π are the key objects in the analysis, as they provide the magnitude of the independent sensitivity directions and a decreasing parameter ranking, respectively. However, since SOM is a numerical decomposition, the information in Σ is valuable but incomplete when assessing identifiability of parameters. Orthogonal directions of parameters that have a small value (in this context small means a value equal or less than the epsilon of the machine) are easily labeled as unidentifiable. On the other hand, parameter ranked in the first positions are clearly operational identifiable. Nonetheless, parameters that are located between the extremes tend to be more difficult to assess, and it is not clear which are identifiable or unidentifiable. In order to address this issue from quantitative perspective, several indexes have been proposed in the literature to assess the identifiability of set of parameters \mathbf{p} .

Let $\mathbf{p}^{\text{red}} = [p_1 \ p_2 \ \cdots \ p_{n_r}] \subseteq \mathbf{p} \subseteq \mathbb{P}$ for $n_r \leq n_p$, and the associated matrix Σ_{n_r} such that

$$\Sigma = \left[\begin{array}{c|c} \Sigma_{n_r} & \\ \hline & \Sigma_{n_p - n_r} \end{array} \right]$$

We now introduce the criteria \mathcal{J} to assess operational identifiability

D-criterion (determinant)

This criterion is defined by

$$\mathcal{J}_D = \det(\Sigma_{n_r}^2) = \det(\Pi_{n_r}^\top \mathbf{S}^\top \mathbf{S} \Pi_{n_r}) \quad (4.29)$$

and so the number of identifiable parameters corresponds to the n_r first elements of the diagonal of Σ such that

$$n_r = \{\min(\dim(\mathbb{P})) \quad | \quad \mathcal{J}_D \geq \gamma_D\} \quad (4.30)$$

where γ_D is a user-defined cut-off value. This criterion establishes the number of parameters in the ranking that generates the largest determinant. This methodology is one of the most common implemented in practice because the determinant of the inverse FIM is related to volume of the ellipsoidal uncertainty regions of the parameter [27]. By choosing the maximum of $\det(\boldsymbol{\Sigma}_r^2)$, we ensure that the determinant of the inverse of the FIM is small, and so are the volume of the uncertainty regions.

4

A-criterion (average or trace ratio)

This criterion is given by

$$\mathcal{J}_A = \frac{\text{tr}(\boldsymbol{\Sigma}_{n_r}^2)}{\text{tr}(\boldsymbol{\Sigma}^2)} \quad (4.31)$$

Thus, the number of identifiable parameters corresponds to the n_r first elements of the diagonal of $\boldsymbol{\Sigma}$ such that

$$n_r = \{\min(\dim(\mathbb{P})) \quad | \quad \mathcal{J}_A \geq \gamma_A\} \quad (4.32)$$

where γ_A is a user-defined cut-off value. Notice that the trace of a positive definite matrix is monotonous increasing. Therefore, it will attain its maximum if all the parameters are chosen. However, if the ratio between the traces of $\boldsymbol{\Sigma}_r$ and $\boldsymbol{\Sigma}$ explains more than γ_A of the total trace, then the $n_p - n_r$ parameters are unnecessary and labeled unidentifiable. This criterion takes into account the total contribution of parameters to the sensitivity through the trace operator. The trace of the inverse of the FIM is related to the total variance generated by the parameters in the estimation [28].

E-criterion (2-norm)

Let $\boldsymbol{\sigma} = \text{diag}(\boldsymbol{\Sigma})$, the E-criterion is then given by

$$\mathcal{J}_E = \frac{\|\boldsymbol{\sigma}_{n_r}\|_2}{\|\boldsymbol{\sigma}\|_2} \quad (4.33)$$

In this case, the number of identifiable parameters corresponds to the first n_r elements of the diagonal of Σ such that

$$n_r = \{\min(\dim(\mathbb{P})) \quad | \quad \mathcal{J}_E \geq \gamma_E\} \quad (4.34)$$

The criterion \mathcal{J}_E describes the ratio of the 2-norms of the vector of diagonal elements of Σ . This criterion provides a ratio of the 2-norms, and thus, it is constrained in the range $(0, 1]$. The 2-norm of the diagonal represents the confidence regions of the parameters. The diameter (two times the longest semi-axis) of these ellipsoidal confidence regions is proportional to $\|F^{-1}(\mathbf{p})\|_2^{\frac{1}{2}}$. Therefore, choosing a sufficiently large γ_E can be understood geometrically as making the diameter of the confidence ellipsoid small [28].

Inverse condition number criterion

This criterion is defined as:

$$\mathcal{J}_K = \frac{1}{\text{cond}(\Sigma_{n_r})} \quad (4.35)$$

The number of identifiable parameters corresponds to the n_r first elements of the diagonal of Σ such that

$$n_r = \{\min(\dim(\mathbb{P})) \quad | \quad \mathcal{J}_K \geq \gamma_K\} \quad (4.36)$$

The condition number criterion provides information about the posedness of the matrix. On the one hand, a large condition number implies that the matrix is ill-conditioned, thus, some directions of sensitivities are small or linearly dependent. On the other hand, a small condition number means that the matrix is well-conditioned, and that all sensitivity directions have similar magnitudes and are independent. In this case, the inverse is chosen because it constrains the criterion to be between $(0, 1]$. Clearly, a value of \mathcal{J}_K close to zero indicates that some parameters create a degeneracy in the sensitivity matrix. This index plays an important role in numerical approaches for gradient-based parameter estimation in selecting the parameters that make the problem well-posed [155].

Determinant-to-trace ratio criterion

This criterion consists of a ratio between the average variation (trace) and the generalized variation (determinant) to assess identifiability. This ratio allows us to have a range of values in $[0, 1]$. By the Arithmetic mean–Geometric mean (AM-GM) inequality, the criterion is defined as

$$\mathcal{J}_R = n_r \frac{\sqrt[n_r]{\det(\Sigma_{n_r}^2)}}{\text{tr}(\Sigma_{n_r}^2)} \quad (4.37)$$

4

Therefore, the number of identifiable parameters is the first n_r nonzero elements of Σ such that

$$n_r = \{\min(\dim(\mathbb{P})) \mid \mathcal{J}_R \geq \gamma_R\} \quad (4.38)$$

This value represents the ratio between the generalized variation to the average variation. A number close to 1 corresponds with high parametric sensitivity with low correlation between outputs, whereas a number close to 0 implies that the output is not sensitive to parameter variations or that induces high correlation between outputs.

Considerations on the cut-off value

It is important to point out that there is no criterion that answers the question of the number of unidentifiable parameters uniquely. Each criterion focuses on a particular metric that favors a particular choice of parameters. Furthermore, also notice that all of the criteria require a user-defined cut-off γ value that will affect final number of identifiable parameters n_r . These criteria are numerical and will depend on the specific precision of the computer being used to carry out the analysis. One possible way to characterize the cut-off values γ_i is defining the number $\delta_s = n_p \times \delta_\epsilon(\|\Sigma\|_2)$, n_p is the number of parameter is the original parameter set, and $\delta_\epsilon(\|\Sigma\|_2)$ is the distance from $\|\Sigma\|_2$ to the next larger floating-point number of the same precision as $\|\Sigma\|_2$. The quantity δ_s takes into account the smallest number the computer can represent before the matrix Σ drops in rank due to floating-point errors. A caveat on δ_s is that this quantity is in general a very small positive number close to the epsilon of the machine. This choice, despite being less conservative, might also select parameters that are close to be operationally unidentifiable. Thus, more conservative choice can be made in order to limit the maximum allowable total variance in the parameters.

To show the effect of the cut-off value on the number of identifiable parameters, we revisit Example 4.1. Using the matrix $\bar{\Sigma}$, i.e. the matrix of orthogonal fraction of the relative parametric sensitivities in \bar{S} , we compute the cut-off values γ_i as well as the number of identifiable parameters n_r . The results are shown in Table 4.2.

Table 4.2: Cut-off values for the different sensitivity measures based on Example 4.1.

Criterion	Cut-off (γ_i)	Value	n_r
\mathcal{J}_D	$\gamma_D = \delta_s$	7.105427×10^{-15}	6
\mathcal{J}_A	$\gamma_A = 1 - \delta_s$	0.999993	6
\mathcal{J}_E	$\gamma_E = 1 - \delta_s$	0.999993	6
\mathcal{J}_K	$\gamma_K = \delta_s$	7.105427×10^{-15}	6
\mathcal{J}_R	$\gamma_R = \frac{\sqrt[n]{\delta_s \times \max(\det(\Sigma_i))}}{\text{tr}(\Sigma)}$	1.560860×10^{-5}	6

All the criteria provide the same number of identifiable parameters. The numerical rank of \bar{S} is 7, which can be confirmed by visual inspection of Figure 4.5. However, the rank of $\bar{S}^\top \bar{S}$ is 6, which corresponds to the results obtained using the different sensitivity measures. Since the selection relies heavily on the cut-off value, the cut-off values tried to be as small as the computer precision allows to avoid an excess of conservatism. Finally, the reduced parameter set \mathbf{p}^{red} for the simple model of a ship roll motion is

$$\mathbf{p}^{\text{red}} = [a_2 \quad G \quad I \quad a_0 \quad r \quad a_3]^\top \quad (4.39)$$

4.5. Single shooting gradient-based parameter estimation

In gradient-based parameter estimation, an optimization problem is set up to minimize a performance criterion, e.g. the error between the measured variable and the model prediction. This optimization problem is solved computing the gradient of a cost function to find a point that maximizes or minimizes the performance criterion. In general, one would want to obtain a global optimal point as a solution to the optimization problem, i.e an optimal point such that no other point provides a smaller minimum. However, this is not always possible due to the existence of regions in the cost function manifold where the functional or its gradient is ill defined. Therefore, the optimization algorithms will likely converge to a local optimal solution within the constraints of the optimization variables. Although finding a global optimum cannot be guaranteed, it is possible to find better local optima by implementing some modifications to the standard parameter estimation problem. One of such modifications segments the data into various intervals, called shooting intervals (ShI). The method solves the parameter estimation problem providing independent initial guesses to each interval, and implementing a compatibility constraint [10]. This

approach receives the name of multiple-shooting parameter estimation (MSPE), as opposed to approaches where the whole data is not segmented into several intervals. The latter class of methods are the classical methods used to perform parameter estimation, and are known as single-shooting parameter estimation (SSPE). The MSPE will be explained in detail in Section 4.6.

In the case of SSPE, a way to address the issue of several local minima is through the use of multiple initial points in the optimization algorithm. This is known as multi-start optimization. A large variety of multi-start methods is available in literature (see [117]). Among the available methods, one especially popular strategy is the greedy random adaptive search procedure (GRASP) introduced in [48]. This algorithm will be used as a benchmark, given its widespread and ease of implementation.

4

The GRASP starts selecting an initial vector \mathbf{p}_0 of parameters and determining a parameter ranking based on it. Subsequently, n_s random vectors $\mathbf{p}_{0_i}^{\text{red}}$ of identifiable parameters are generated, while the unidentifiable parameters are kept fixed. The cost function (4.1) is minimized for each of these n_s initial parameter vectors. Finally, the parameter vector $\mathbf{p}_i^{\text{red}*}$ that yields the lowest value of the cost function from the set of solutions is selected as the best one to the nonlinear least-square problem. The original GRASP selects parameters from a random uniform distribution. However, we modify this sampling method using Latin Hypercube Sampling (LHS). This sampling method creates a more even distribution of parameter values over a set range than a simple random number generator, avoiding clusters or gaps in the samples taken [67]. The GRASP is illustrated in Algorithm 2:

Algorithm 2 Greedy random adaptive search procedure [48]

- 1: Initialize $\mathbf{p}_0 \in [\mathbf{p}_{\min}, \mathbf{p}_{\max}]$
 - 2: Run SOM to determine ranking
 - 3: Select $\mathbf{p}^{\text{red}} \subseteq \mathbf{p}$
 - 4: Generate the set $\mathbb{P}_0^{\text{red}}$ of n_s vectors $\mathbf{p}_{0_i}^{\text{red}}$ using LHS sampling in $[\mathbf{p}_{\min}^{\text{red}}, \mathbf{p}_{\max}^{\text{red}}]$
 - 5: Construct the sets $\mathbb{P}^* = \emptyset$ and $\mathbb{V} = \emptyset$
 - 6: **for** $i = 1$ to n_s **do**
 - 7: Solve $\min_{\mathbf{p}_i^{\text{red}}} V_i(\mathbf{p})$ using $\mathbf{p}_{0_i}^{\text{red}}$ as initial condition
 - 8: $\mathbf{p}_i^{\text{red}*} \leftarrow \arg \min \left(V(\mathbf{p}) \right)$
 - 9: $\mathbb{P}_i^* \leftarrow \{\mathbf{p}_i^{\text{red}*}\} \cup \{\mathbf{p}^{\text{unident}}\}$
 - 10: $\mathbb{P}^* \leftarrow \mathbb{P}^* \cup \{\mathbf{p}_i^*\}$
 - 11: $\mathbb{V} \leftarrow \mathbb{V} \cup \{V_i(\mathbf{p}_i^*)\}$
 - 12: **end for**
 - 13: **return** $\mathbf{p}^{\text{best}} \in \mathbb{P}^* = \min\{\mathbb{V}\}$
-

The GRASP chooses a set of parameters to optimize based on the parametric output sensitivity employing the SOM. In this case, both the identifiability ranking and

the identifiable parameter selection are assumed to remain the same throughout the optimization process. This assumption is beneficial because it enables us to reduce the number of parameters to be optimized, thus, reducing the computational effort. However, given that most dynamic physical models are nonlinear, the solution manifold might change its shape depending on the operating point. As a consequence, a new parametric ranking will be obtained at that point, potentially improving the overall solution of \mathbf{p}^* . In order to address the condition-dependent variability in parameter sensitivities, we propose two methods to take into account this effect, and use them to our benefit in finding a better local minimum.

The first proposed method is the modified GRASP (mGRASP). This approach incorporates the SOM-based parameter identifiability ranking into the GRASP. First, the mGRASP provides a vector of parameter values \mathbf{p}_{0_s} as a seed. Then, it proceeds to generate n_s vectors of initial guesses \mathbf{p}_0 within their upper and lower bounds based on \mathbf{p}_{0_s} implementing LHS. Subsequently, the parameter identifiability ranking and parameter subset selection is performed for every generated initial vector of parameters \mathbf{p}_0 . The inclusion of a ranking and subset selection steps ensure that we get the most identifiable parameters seeds \mathbf{p}_{0_s} . This translates in initial operating points of the state space where the cost function is well-defined to obtain better parameter estimates. The remainder of the optimization procedure is identical to that of the GRASP. The mGRASP is shown in Algorithm 3

Algorithm 3 Modified greedy random adaptive search procedure

- 1: Initialize $\mathbf{p}_{0_s} \in [\mathbf{p}_{\min}, \mathbf{p}_{\max}]$
 - 2: Generate the set \mathbb{P}_0 of n_s vectors \mathbf{p}_{0_i} from \mathbf{p}_{0_s} using LHS sampling in $[\mathbf{p}_{\min}, \mathbf{p}_{\max}]$
 - 3: Construct the sets $\mathbb{P}^* = \emptyset$ and $\mathbb{V} = \emptyset$
 - 4: **for** $i = 1$ to n_s **do**
 - 5: Run SOM to determine ranking
 - 6: Select $\mathbf{p}_i^{\text{red}} \in (\mathbb{P}_0, \preceq)$
 - 7: Solve $\min_{\mathbf{p}_i^{\text{red}}} V_i(\mathbf{p})$ using $\mathbf{p}_{0_i}^{\text{red}}$ as initial condition
 - 8: $\mathbf{p}_i^{\text{red}*} \leftarrow \arg \min \left(V(\mathbf{p}) \right)$
 - 9: $\mathbf{p}_i^* \leftarrow \{\mathbf{p}_i^{\text{red}*}\} \cup \{\mathbf{p}^{\text{unident}}\}$
 - 10: $\mathbb{P}^* \leftarrow \mathbb{P}^* \cup \{\mathbf{p}_i^*\}$
 - 11: $\mathbb{V} \leftarrow \mathbb{V} \cup \{V_i(\mathbf{p}_i^*)\}$
 - 12: **end for**
 - 13: **return** $\mathbf{p}^{\text{best}} \in \mathbb{P}^* = \min\{\mathbb{V}\}$
-

The second proposed method is the cascade identifiable adaptive optimization (CIAO), which provides a way to potentially find a better local optimum after one optimization run has finished. It is an iterative method that treats the optimum of the prior optimization run as the initial set of parameters of the subsequent optimization. A ranking procedure is performed with the new initial set using SOM. If the parame-

ter ranking has changed with respect to the previous optimization iteration, CIAO selects the new set of the most identifiable parameters to optimize. For the parameter selection of the reduced set, any of the proposed criteria in Section 4.4 can be implemented, keeping the cut-off value constant over all iterations. The re-ranking, selecting, and optimizing parameters steps continue until the partial order induced by the ranking in the previous iteration equals the current one. By optimizing over different sets of parameters when the identifiability ranking changes, new search directions in the cost function are exploited during the minimization of the cost function. The CIAO is illustrated in Algorithm 4

Algorithm 4 Cascaded identifiable adaptive optimization

4

```

1: Initialize  $\mathbf{p}_0 \in [\mathbf{p}_{\min}, \mathbf{p}_{\max}]$ 
2: Run SOM with  $\mathbf{p}_0$  to determine ranking
3: Select  $\mathbf{p}_0^{\text{red}} \in (\mathbb{P}_0, \preceq)$ 
4: Initialize  $i \leftarrow 0$ 
5: Initialize  $\mathbf{p}_{i-1} = \mathbf{0}$ 
6: while  $\mathbf{p}_{i-1} \neq \mathbf{p}_i^{\text{red}}$  do
7:   Solve  $\min_{\mathbf{p}_i^{\text{red}}} V_i(\mathbf{p})$  using  $\mathbf{p}_{0_i}^{\text{red}}$  as initial condition
8:    $\mathbf{p}_i^{\text{red}*} \leftarrow \arg \min \left( V(\mathbf{p}) \right)$ 
9:    $\mathbf{p}_i^* \leftarrow \{\mathbf{p}_i^{\text{red}*}\} \cup \{\mathbf{p}^{\text{unident}}\}$ 
10:  Run SOM with  $\mathbf{p}_i^*$  to determine ranking
11:   $\mathbf{p}_{i+1}^{\text{red}} \leftarrow \mathbf{p}_i^{\text{red}*}$ 
12:   $i \leftarrow i + 1$ 
13: end while
14: return  $\mathbf{p}_i^*$ 
```

4.5.1. Enforcing a relative sensitivity matrix

In the implementation of gradient-based parameter estimation routines, sensitivity analysis and parameter ranking are performed on the basis of the approximate relative sensitivity matrix $\bar{\mathbf{S}}$. However, the standard output error minimization problem in (4.1) uses the approximate absolute sensitivity matrix \mathbf{S} to compute the gradient of the cost function shown in (4.6). This poses a problem as the absolute sensitivity directions might differ from the relative ones as observed in Figures 4.3 and 4.5. To circumvent this, we perform the following transformation:

- a. Define bounds $[\mathbf{p}_{\max}^{\text{red}}, \mathbf{p}_{\min}^{\text{red}}]$ for the parameter set.
- b. Normalize and recenter the parameters such that $\underline{\mathbf{p}}^{\text{red}} \in [0, 1]$.
- c. Transform the normalized parameter set to the logarithmic parameter set $\ln(\underline{\mathbf{p}}^{\text{red}}) = \bar{\mathbf{p}}^{\text{red}}$. This also transforms the bounds to $\bar{\mathbf{p}}_{\min}^{\text{red}} = -\infty$ and $\bar{\mathbf{p}}_{\max}^{\text{red}} = 0$

- d. Write the original parameters $\mathbf{p}^{\text{red}} = \phi(\bar{\mathbf{p}}^{\text{red}}) = (\mathbf{p}_{\max}^{\text{red}} - \mathbf{p}_{\min}^{\text{red}}) \exp(\bar{\mathbf{p}}^{\text{red}}) + \mathbf{p}_{\min}^{\text{red}}$ to preserve the input-output map. The optimization is then performed over $\bar{\mathbf{p}}^{\text{red}}$, which then ensures that an approximate semi-relative sensitivity matrix is used in the parameter estimation procedure.

- e. Normalize the cost function $V(\mathbf{p})$ letting

$$\bar{V}(\mathbf{p}) = \sum_{k=0}^{N-1} \|\mathbf{y}_m(t_k) \odot^{-1} \tilde{\mathbf{y}}_m(t_k) - \mathbf{y}(t_k, \mathbf{p}) \odot^{-1} \tilde{\mathbf{y}}_m(t_k)\|_2^2 \quad (4.40)$$

where \odot^{-1} is element-wise division, $\tilde{\mathbf{y}}_m(t_k) = \mathbf{y}_m(t_k) + \mathbf{c}$ with \mathbf{c} defined as in Section 4.3.2. The addition of the constant vector \mathbf{c} might not be needed if $\mathbf{y}_m(t_k)$ and $\mathbf{y}(t_k, \mathbf{p})$ represent physical quantities that are strictly positive or in an absolute scale, e.g. mass, entropy, absolute temperature, absolute temperature, etc.

4

Following the steps to normalize the parameters and the cost function, the GRASP and mGRASP are studied to compare their performance making use of the simple roll motion model of a ship. The performance is evaluated running the three methods to 100 different initial sets of parameters. Additionally, the performance is assessed using the best initial set of parameters as benchmark. The A-criterion with a cut-off value of $\gamma_A = 1 - 0.99999$ is used to rank the parameters with SOM. Additionally, we also limit the number of function evaluations to 3000. The true parameter values as well as the maximum and minimum values are listed in Table 4.1. The value of the cost functions and the elapsed time taken to compute the optimal values for both GRASP and mGRASP, respectively are reported in Table 4.3.

Table 4.3: Comparison of methods GRASP and mGRASP of best initial guess based on 100 realizations of initial conditions

Method	Ranking	Est. value	Elapsed time (seconds)
GRASP	a_0 (-)	0.336	361.64
	G (N rad^{-1})	182520	
	I (kg m^{-2})	872693290	
mGRASP	r (m)	22.685	365.02
	G (N rad^{-1})	196219	
	D (N s rad^{-1})	3274069	

The GRASP uses a single ranking computed from the first initial set of parameters, while mGRASP ranks each of the 100 initial sets. Both methods have comparable performance in terms of computation time. Additionally, in both cases the cost function is minimized within the tolerance at a magnitude of $\sim 10^{-7}$. The GRASP method provides a total error of 3.097×10^{-7} , while mGRASP 1.84×10^{-7} , which corresponds to a 40% decrease with respect to GRASP. The variations of cost

function values per realization of both methods are shown in Figure 4.6. Likewise, the trajectories generated by the best realizations in each method are shown in Figure 4.7, which shows that both methods achieve extremely good agreement with the data.

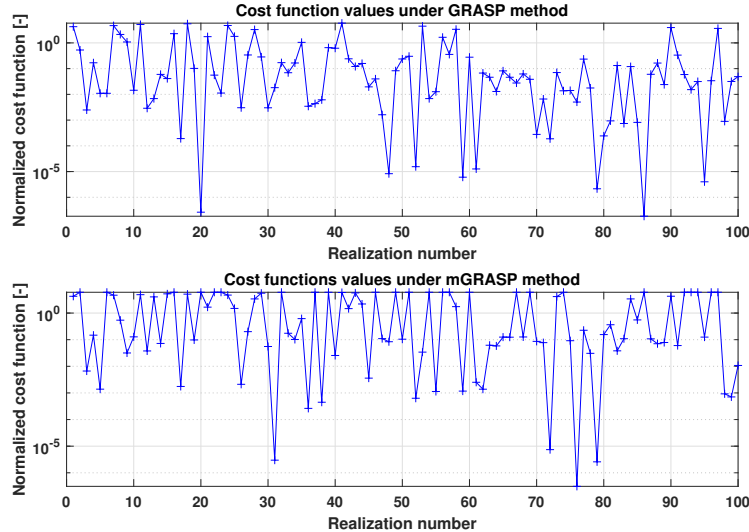


Figure 4.6: Cost function values for 100 realizations of the initial point for GRASP and mGRASP

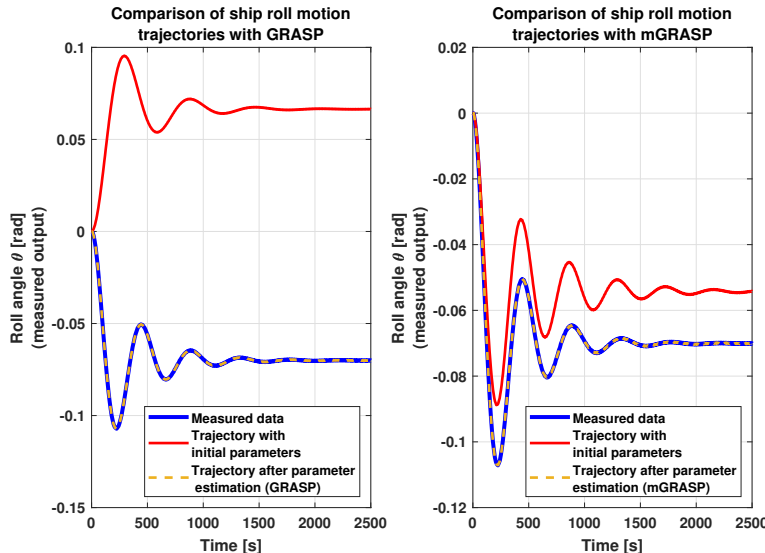


Figure 4.7: Trajectories after parameter estimation using GRASP and mGRASP based on the best realizations.

Despite the advantages offered by GRASP and mGRASP to find better local optima, these two methods might converge to points where the cost function is not sufficiently minimized, i.e. the optimization stalls. In such a case, CIAO shows a better performance than the other two because it is capable of exploring different directions in the search space to make the cost function smaller. This is illustrated using the worst initial set of parameters of GRASP and mGRASP. These are initial parameter values that make both GRASP and mGRASP to converge to points where the model prediction error is still large as shown in Figure 4.8. The results of CIAO are shown in Table 4.4.

Table 4.4: Comparison of methods GRASP, mGRASP, and CIAO based on worst realization of the initial guesses

Method	Ranking	Est. value	Elapsed time (seconds)
GRASP	a_0 (-)	1.684	
	G (N rad $^{-1}$)	182900	333.297
	I (kg m $^{-2}$)	9.99×10^8	
mGRASP	G (N rad $^{-1}$)	100000	
	a_0 (-)	1.062	255.089
	I (kg m $^{-2}$)	8.50×10^8	
CIAO	G (N rad $^{-1}$)	163995	
	a_2 (rad $^{-2}$)	-4.999	917.117
	I (kg m $^{-2}$)	8.50×10^8	

The worst initial sets correspond to realizations 18 for GRASP and 16 for mGRASP out of the 100 generated. These initial sets generate model output trajectories that have fundamental frequency and magnitudes different to the one represented in the data as observed in Figure 4.8. The cost function values are 4.1519 and 2.2833 for GRASP and mGRASP after 3000 iterations, respectively. It can be inferred that the set of parameters defines a point difficult to minimize for both methods. The CIAO solves this problem by performing a new ranking at the optimal point, as it defines a new operating point. The value of the cost function after the last iteration using CIAO is 0.1076, which corresponds to a reduction of 97.40% and 95.29% with respect to GRASP and mGRASP, respectively. The improvement in optimality comes at the expense of higher computation power and time. The trajectory with the estimated parameters using CIAO is considerably more similar to the one generated in the data compared to the ones generated by GRASP and mGRASP as shown in Figure 4.8. The CIAO method manages to bring the model trajectory to a similar magnitude level, while matching the fundamental frequency of the response.

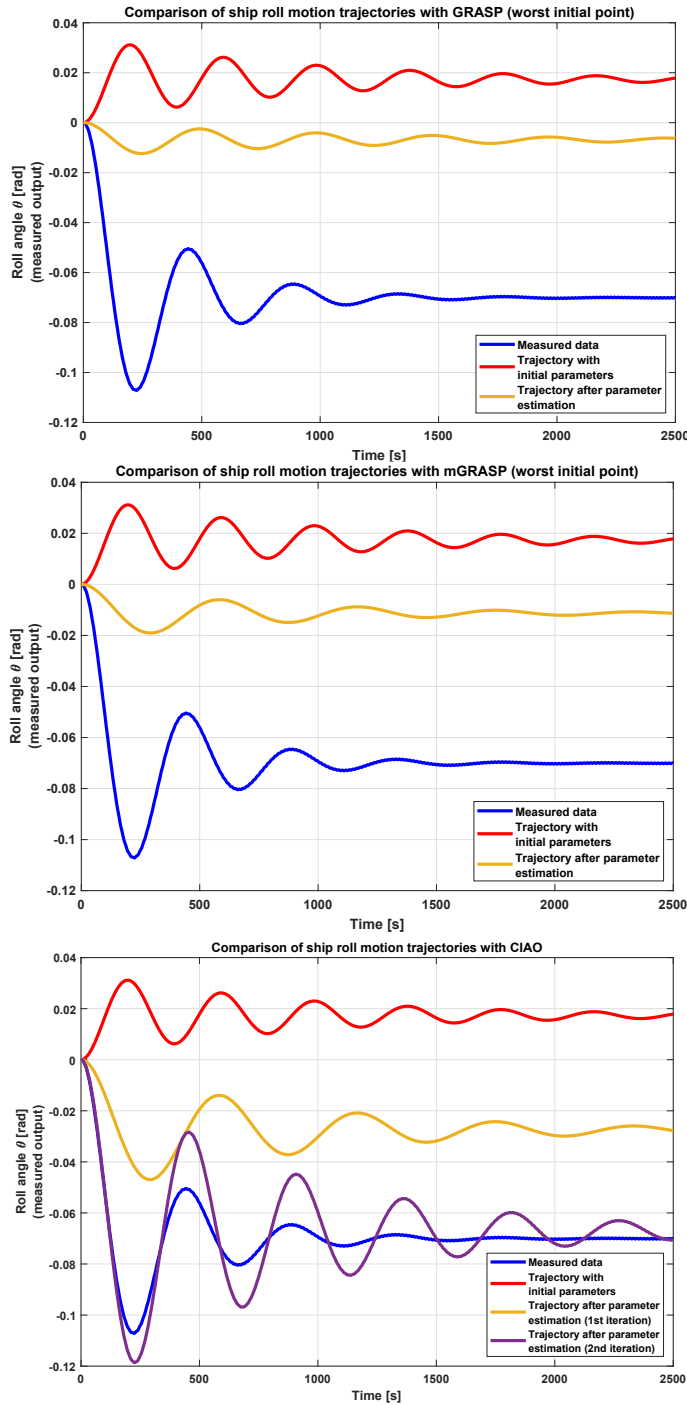


Figure 4.8: Trajectories after parameter estimation using GRASP, mGRASP, and CIAO based on the worst realization

4.6. Multiple shooting parameter estimation

It was mentioned that the GRASP, mGRASP, and CIAO are SSPE methods, which minimize the performance criterion using the entirety of the measured trajectory data. Despite the advantages provided by these methods, they might still converge to local minima due to the lack of smoothness or flatness in the vector fields of the underlying model that describe the system behavior. The first and second order derivatives with respect to the model parameters are ill-defined in certain regions of the parameter space [145]. To circumvent the shortcomings of SSPE, multiple shooting parameter estimation (MSPE) is considered as an alternative. The MSPE segments the measured trajectory data in shooting intervals (ShI), and assigns an initial parameter set to each interval along the trajectory to solve the parameter estimation problem. The parameter space is extended with discontinuous state trajectories based on the number of ShI. We explain the standard MSPE for parameter estimation as presented in [10] in the following section:

4.6.1. Standard multiple shooting parameter estimation

Let $t \in I = [t_0, t_f]$ and let the model with assumed known initial condition \mathbf{x}_0 be given by

$$\begin{aligned}\dot{\mathbf{x}}(t, \mathbf{p}) &= \mathbf{f}(\mathbf{x}(t), \mathbf{u}(t), \mathbf{p}), & \mathbf{x}(t_0) &= \mathbf{x}_0 \\ \mathbf{y}(t, \mathbf{p}) &= \mathbf{g}(\mathbf{x}(t), \mathbf{u}(t), \mathbf{p})\end{aligned}\tag{4.41}$$

Furthermore, let us subdivide the time interval in multiple shooting nodes as

$$t_0 = \tau_0 < \tau_1 < \cdots < \tau_\ell = t_f$$

The splitting of the time interval generates the set of $\ell + 1$ shooting nodes

$$L = \{\mathbf{x}_l := \mathbf{x}(\tau_l) \mid l = 0, 1, \dots, \ell\}$$

Since \mathbf{x}_0 is assumed to be known, the set of the last ℓ nodes is adjoined to the vector of parameters \mathbf{p} in a vector \mathbf{z} . As a consequence, the parameter space includes also the values of the states at the shooting nodes. The structure of extended parameter vector is $\mathbf{z} = [\mathbf{x}_1^\top \quad \mathbf{x}_2^\top \quad \cdots \quad \mathbf{x}_\ell^\top \quad \mathbf{p}^\top]^\top$. Hence, in each shooting interval $I_\lambda = [\tau_l, \tau_{l+1}]$ for $\lambda = 1, \dots, \ell$, there is an independent initial value problem given by

$$\begin{aligned}\dot{\mathbf{x}}_{l+1}(t, \mathbf{p}) &= \mathbf{f}(\mathbf{x}_{l+1}(t), \mathbf{u}_{l+1}(t), \mathbf{p}), \quad \mathbf{x}_l = \mathbf{x}(\tau_l), \quad t \in [\tau_l, \tau_{l+1}] \\ \mathbf{y}_{l+1}(t, \mathbf{p}) &= \mathbf{g}(\mathbf{x}_{l+1}(t), \mathbf{u}_{l+1}(t), \mathbf{p})\end{aligned}\quad (4.42)$$

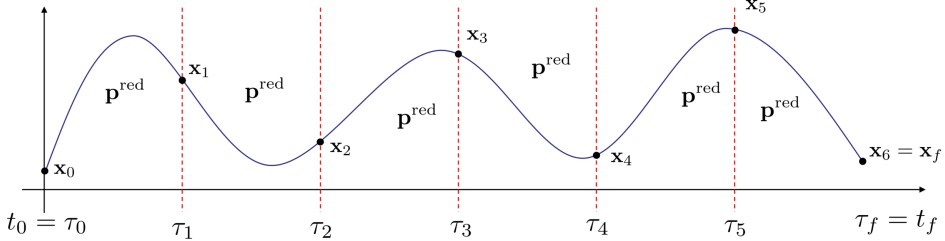
The cost function for the MSPE based on (4.1) is given by

$$V^{\text{MSM}}(\mathbf{z}) = \sum_{k=0}^{N-1} \sum_{l=0}^{\ell} \|\mathbf{y}_{m_l}(t_k) - \mathbf{y}_l(t_k, \mathbf{p})\|_2^2 \quad (4.43)$$

Notice also that since each of the ℓ initial value problems are independent, they will generate discontinuous trajectories. Furthermore, the final value of the state in the interval $[\tau_l, \tau_{l+1}]$ is the initial condition in the interval $[\tau_l, \tau_{l+1}]$. Hence, it is necessary to include a constraint that ensures the compatibility between the final state of a ShI and the initial state of the subsequent one. Therefore, the MSPE constrained minimization problem is

$$\begin{aligned}\min_{\mathbf{z}} \quad & V^{\text{MSM}}(\mathbf{z}) \\ \text{subject to} \quad & G_l(\mathbf{z}) = \mathbf{x}_l - \mathbf{x}(\tau_l) = 0 \\ & \mathbf{p}_{\min} \leq \mathbf{p} \leq \mathbf{p}_{\max}\end{aligned}\quad (4.44)$$

The optimization in (4.44) is performed over the reduced parameter set of identifiable parameters, i.e. $\mathbf{z}^{\text{red}} = [\mathbf{x}_1^\top \dots \mathbf{x}_\ell^\top \mathbf{p}^{\text{red}\top}]^\top$. The standard MSPE minimizes the error between the predicted output and the observed values. However, rather than using the entire data set to optimize the predicted response, the method splits the data into smaller subsets and runs the model over each subset. This makes the simulation length a design parameter, which avoids error accumulation in the cost function within ill-defined regions of the parameter space, and allows to solve problems that would be infeasible using a single shooting method. Additionally, the parameter ranking is assumed to remain constant throughout the standard MSPE parameter estimation, i.e. the ranking is kept fixed in every discrete trajectory. A schematic of the MSPE is illustrated in Figure 4.9



$$\begin{aligned} \min_{\mathbf{z}^{\text{red}}} \quad & V^{\text{MSM}}(\mathbf{z}^{\text{red}}) \\ \text{s.t.} \quad & G_l(\mathbf{z}^{\text{red}}) = 0 \end{aligned}$$

Figure 4.9: Schematic of multiple shooting parameter estimation for parameter estimation. In this case, six shooting nodes are chosen.

4

The optimization problem (4.44) is equivalent to the standard formulation in (4.1), which is provided in the following theorem

Theorem 4.1 (Ribeiro et al. [145]): If $\mathbf{x}_l = \mathbf{x}(\tau_l)$ for $l = 0, \dots, \ell$, and $\mathbf{x}_0 = \mathbf{x}(\tau_0)$, then $V(\mathbf{p}) = V^{\text{MSM}}(\mathbf{z})$

Proof: See Theorem 2 in [145] ■

However, since parametric sensitivities may be dynamic, especially in the case of batch processes, the ranking of identifiable parameters might change on different portions of the trajectory. Therefore, we propose a multiple shooting parameter estimation with an interval-based parameter ranking approach to estimate the model parameters that takes into account the parametric sensitivity variation. This method will help reduce the parameter estimation complexity to find more accurate parameter estimates.

4.6.2. Ranked interval multiple shooting parameter estimation (RIM-SPE)

Parameters are usually ranked based on the AOPS or ROPS magnitudes using the whole model output trajectory data. However, since the AOPS and ROPS may vary with time, the effect of some parameters might dominate or vanish in different portions of the model output trajectory. This is especially evident in systems with very different time-scale dynamics or systems with various operating modes such as batch processes. In order to exploit the time-varying nature of the parametric sensitivities, we developed the ranked interval multiple shooting parameter estima-

tion (RIMSPE). The RIMSPE splits the output trajectory in rank intervals (RI) of sufficient length. The SOM is applied in each of the RI, and a different vector \mathbf{z} to be optimized is obtained based on these parameter rankings. Finally, the RI are further subdivided into a number ShI, where the each optimization problem is solved using the standard MSPE. The RIMSPE is explained in detailed below

Let $t \in I = [t_0, t_f]$ and let the model be given by (4.41)

The time interval is split in different ranking nodes:

$$t_0 = \pi_0 < \pi_1 < \cdots < \pi_\rho = t_f$$

4

Each rank interval $I_\varrho = [\pi_r, \pi_{r+1}]$, $\forall \varrho = 1, \dots, \rho$ $\forall r = 0, 1, \dots, \rho$ is subdivided with multiple shooting nodes:

$$\pi_r = \tau_0 < \tau_1 < \cdots < \tau_\ell = \pi_{r+1}$$

In this case each rank interval I_ϱ generates a set of $\ell + 1$ shooting nodes

$$L^\varrho = \{\mathbf{x}_l := \mathbf{x}(\tau_l) \mid l = 0, 1, \dots, \ell\}$$

Since \mathbf{x}_0 in each I_ϱ is assumed to be known, only the set of the last ℓ nodes is adjoined to the vector of parameters \mathbf{p} in a vector $\mathbf{z}_\varrho = [\mathbf{x}_1^\top \quad \mathbf{x}_2^\top \quad \cdots \quad \mathbf{x}_\ell^\top \quad \mathbf{p}_\varrho^\top]^\top$. Additionally, there are in total ℓ independent initial value problems per rank interval of the form

$$\begin{aligned} \dot{\mathbf{x}}_{l+1}(t, \mathbf{p}_\varrho) &= \mathbf{f}(\mathbf{x}_{l+1}(t), \mathbf{u}_{l+1}(t), \mathbf{p}_\varrho), & \mathbf{x}_l &= \mathbf{x}(\tau_l), & t &\in [\tau_l, \tau_{l+1}] \\ \mathbf{y}_{l+1}(t, \mathbf{p}_\varrho) &= \mathbf{g}(\mathbf{x}_{l+1}(t), \mathbf{u}_{l+1}(t), \mathbf{p}_\varrho) \end{aligned} \quad (4.45)$$

The cost function (4.43) is minimized in every rank interval I_ϱ according to the following optimization problem

$$\begin{aligned} \min_{\mathbf{z}_\varrho} \quad & V_\varrho^{\text{MSM}}(\mathbf{z}_\varrho) \\ \text{subject to} \quad & G_l(\mathbf{z}_\varrho) = \mathbf{x}_l - \mathbf{x}(\tau_l) = 0 \\ & \mathbf{p}_{\min} \leq \mathbf{p} \leq \mathbf{p}_{\max} \end{aligned} \quad (4.46)$$

where solution of the optimization in the previous RI is implemented as the initial condition of the current one, i.e. $\mathbf{z}_{0,\varrho} = \mathbf{z}_{\varrho-1}^*$.

Finally, only a reduced set of identifiable parameters is optimized in (4.46), and so $\mathbf{z}_\varrho^{\text{red}} = \begin{bmatrix} \mathbf{x}_1^\top & \mathbf{x}_2^\top & \cdots & \mathbf{x}_\ell^\top & \mathbf{p}_\varrho^{\text{red}\top} \end{bmatrix}^\top$. A schematic of the algorithm is depicted in Figure 4.10

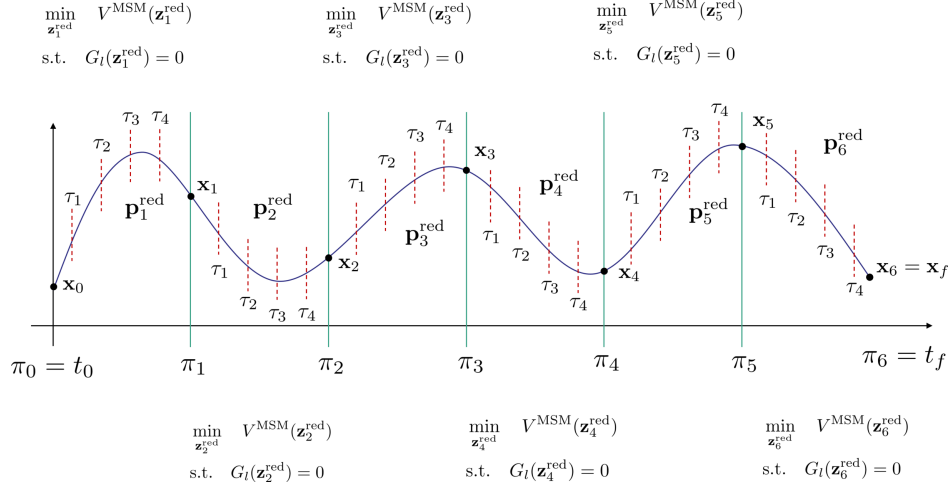


Figure 4.10: Schematic of the ranked interval multiple shooting parameter estimation. In this case, six rank intervals are chosen with five shooting intervals per rank interval

The advantage of RIMSPE over MSPE is that the former takes into account the varying sensitivities of parameters in different points of the output trajectory. RIMSPE naturally provides more flexibility to minimize the prediction error in (4.43) by letting different identifiable parameter sets explain the data in every RI, rather than trying to find a single parameter set that explains all the data at once. Furthermore, the parameters in each RI do not need to have the same values because independent optimization problems are solved, which results in different parameter vectors \mathbf{p}_ϱ . However, in some cases, it might be necessary to report a single value per parameter. In that case, we can select the parameters using a weighted average calculated from the associated parameter variance of each optimization problem.

We compute the weighted average of the estimated parameter vector $\hat{\mathbf{p}}$ over ρ optimizations

$$\bar{\hat{\mathbf{p}}} = \sum_{\varrho=1}^{\rho} \mathbf{W}_\varrho \hat{\mathbf{p}}_\varrho \quad (4.47)$$

where ρ is the number of RI, and $\mathbf{W}_\varrho = \text{diag}([w_{1,\varrho} \ \cdots \ w_{n_\rho,\varrho}])$ is the matrix of normalized weights in the ϱ -th optimization. Each element $w_{i,\varrho}$ of \mathbf{w}_ϱ is calculated using the harmonic mean

$$w_{i,\varrho} = \frac{1}{\sum_{\varrho=1}^{\rho} \frac{1}{\text{var}(\hat{p}_{i,\varrho})}} \quad (4.48)$$

where $\text{var}(p_{i,\varrho})$ is the variance of the i -th parameter in $\hat{\mathbf{p}}_\varrho$.

Both approaches are compared working with the Example 4.1 using the worst initial parameter set used for the SSPE methods. The optimization algorithm is constrained to 3000 function evaluations, 9 ShI are selected. The results of the standard MSPE is presented in Table 4.5. Additionally, the model output trajectory with the estimated parameters using the standard MSPE is displayed in Figure 4.11.

4

Table 4.5: Results of standard multiple shooting parameter estimation methods

Standard multiple shooting parameter estimation			
Ranking	Est. value	Cost function	Elapsed time (seconds)
G (N rad $^{-1}$)	232642		
a_0 (-)	0.229		
I (kg m $^{-2}$)	908712534	9.1018×10^{-5}	121.688
a_2 (rad $^{-2}$)	-2.646		
r (m)	18.441		

For the RIMSPE method, 4 RI of the output trajectory are chosen. Parameter estimation is performed applying MSPE with 9 ShI based on the ranking in each of the RI. The results of RIMSPE are summarized in Table 4.6 and the trajectory generated using RIMSPE is shown in Figure 4.12.

Table 4.6: Results of ranked interval multiple shooting parameter estimation methods

Ranked interval multiple shooting parameter estimation			
Parameter	Est. value (mean)	Cost function	Elapsed time (seconds)
G (N rad $^{-1}$)	232642		
a_0 (-)	0.640		
I (kg m $^{-2}$)	908712534	7.3755×10^{-5}	81.84245
a_2 (rad $^{-2}$)	-2.687		
r (m)	17.376		

In Figures 4.11 and 4.12, it is observed that both multiple shooting methods minimize the error between the data and the predicted output from an initial point where classical SSPE methods stall in local minima and fail to converge. The convergence issues are observed when GRASP and mGRASP are implemented as shown

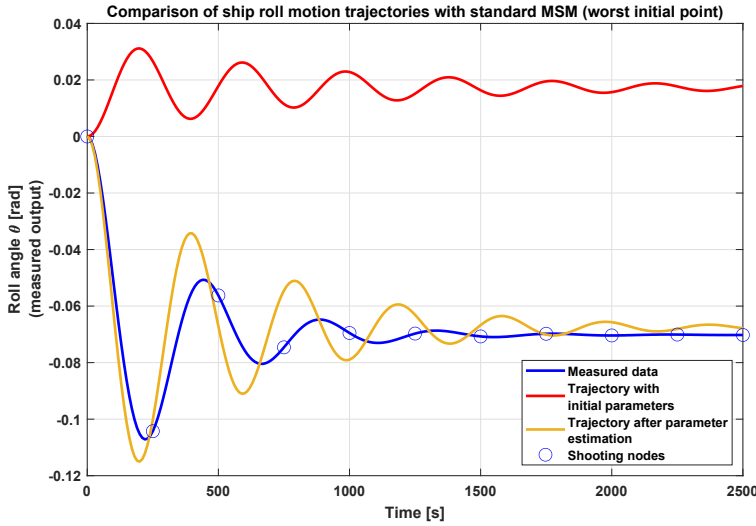


Figure 4.11: Trajectories after parameter estimation using the standard MSPE based on the worst realization

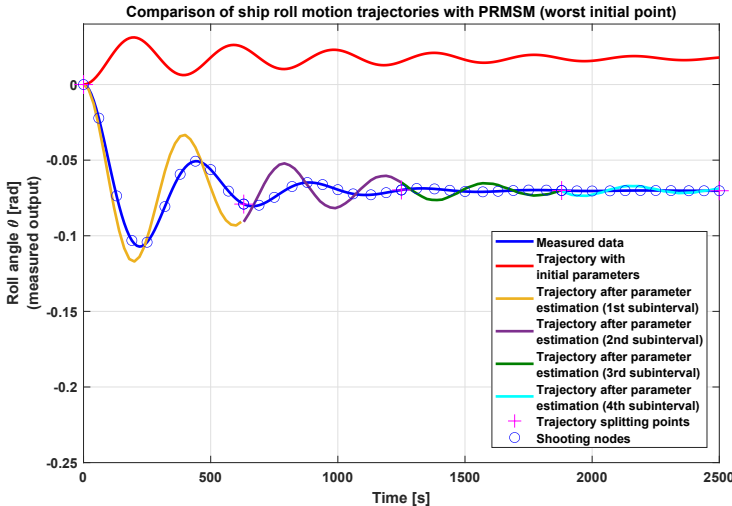


Figure 4.12: Trajectories after parameter estimation using the RIMSPE based on the worst realization

in Figure 4.8. However, for the same optimization conditions, the RIMSPE achieves a smaller accumulated error than the standard MSPE. This is more noticeable at steady state, where the standard MSPE has some offset, while the RIMSPE does not. Additionally, since each portion being optimized with RIMSPE has a shorter length

of data using its specific ranking, each optimization is much faster than the standard MSPE, even when the accumulated time is taken into account. The RIMSPE functions as a cascade optimization where each cost function runs independently using the information of the previous optimization. This is advantageous because the search directions in the parameter space do not remain constant, allowing for an extra degree of freedom when estimating parameters.

Chapter summary

Sensitivity-based operational identifiability

- Sensitivity-based operational parameter identifiability depends on the operating point at which the model is analyzed, and therefore, it is a local analysis.
- Operational identifiability makes use of numerical computations of the variations of the outputs to variations in the parameters. It allows to determine the set of parameters that induce a large variation in the measured outputs.
- Operational parameter identifiability allows not only to determine whether a parameter is identifiable or not, but also ranks parameters according to their overall sensitivity contribution. This ranking can be performed using several decomposition methods of the so-called sensitivity matrix.
- The ranking allows to perform a selection of a reduced subset of parameters that can be reliable estimated using the available, i.e. parameter estimates with low variance.

4

Parametric ranking

- The parametric ranking is performed by checking the most dominant sensitivity directions to ascertain the subset of parameter that is the most identifiable. This information is embedded in the sensitivity matrix, i.e. the matrix with output parametric sensitivity trajectories.
- The sensitivity directions and magnitudes can be revealed using the successive orthogonalization method. The SOM allows to associate specific sensitivity directions with their corresponding parameters because the order of parameter selection is stored in a permutation matrix.
- The parametric ranking is scale dependent. This means that different inherent units of outputs and parameters play a role in the analysis. Therefore, it is necessary to analyze operational identifiability in a dimensionless setting that allows the comparison of each output parametric sensitivity vector.

Chapter summary

- The removal of unit dimensions of the sensitivity matrix can be achieved by normalizing the output parametric sensitivity trajectories with the nominal output trajectories and nominal parameter values. The resulting matrix is the relative sensitivity matrix, which provides the variations of the output with respect to the parameter in a logarithmic scale.
- The ranking of parameter provides a more nuanced information about the identifiability of parameters because it is based on the numerical magnitude and collinearity index of the sensitivity trajectories. However, the choice of an identifiable subset also becomes more critical as it depends on the specific sensitivity selection criterion and cut-off values.
- Selection criteria for parameter identifiability play a crucial role in the construction of a reduced identifiable parameter set. A user-defined cut-off value is chosen based on the selection criterion to assess the identifiability of the parameter set. This value will have an important impact on the number of parameters in the reduced parameter set.

Gradient-based parameter estimation

- Gradient-based parameter estimation is performed minimizing a cost function and explicitly computing the gradient of the cost function to find the direction of steepest descent towards a minimum.
- Gradient-based parameter estimation provide local optimal solution to parameters because the gradients update the parameters in the vicinity of their initial points. Thus, it does not explore the entire manifold of the cost function.
- Gradient-based approaches are computationally efficient but they might fail to find an global optimal solution if the cost function manifold has multiple minima and maxima. As a consequence, the algorithms tend to get stuck at points where the cost function is not fully minimized within the set tolerance.
- The inherent issues of gradient-based optimization can be addressed using methods such as GRASP, mGRASP, and CIAO. The first two methods (GRASP and mGRASP) use multiple initial points to explore more of search space, while CIAO sequentially solves different optimization problems using different parameter ranking based on the previous optimal point.

Chapter summary

- Methods like GRASP, mGRASP, and CIAO are single shooting parameter estimation. These type of methods attempt to estimate a set of parameters using all the data points at once, which might lead to failure of the algorithms.
- The standard MSPE and the proposed RIMSPE are multiple shooting alternatives to single shooting parameter estimation, as they split the data in several sections to solve each of them individually. These individual optimization problems bypass possible intricate regions on the manifold where single shooting parameter estimation might get stuck. The main difference between these two methods is that the standard MSPE use one ranking for all the optimization problems, while RIMSPE solves each section of the data using a possible different set of parameters based on the parametric sensitivity corresponding to a specific section of the data.

5

Online parameter estimation: A control design perspective

In this chapter, we present parameter estimation as a control problem, where the control law is designed such that the model parameters are updated. This is done under the assumption that there is no undermodeling of the system's dynamics and that the mismatch error between the system and the model outputs is a function of the parameters only. The approach considers the parameters as an artificial input to the model and different control laws are used to perform estimate possibly time-varying parameters in an online fashion. Two control laws for parameter update are provided obtained from the basis of an error-based Lyapunov function: a proportional-integral PI design and an exponential control law to enforce an exponential convergence to the parameter estimates. The two methods are explored in detail and their applicability is demonstrated in a nonlinear fed-batch bio-reactor example.

5.1. Introduction

Plant-model mismatch is a recurrent problem in model-based operation. Models may lose their fidelity over time due to dynamical changes in the process, making the prediction generated by the model not reliable. This mismatch has to be eliminated or minimized to guarantee a good process performance. In general, there are two paradigms to address model-plant mismatch, structural and parametric. On the one hand, the structural mismatch arises from the fact that there are unmodeled dynamics in the model, e.g. an unknown reaction in a chemical process, or a damping effect due to internal parts in mechanical systems. This makes the model-plant reconciliation more difficult because the plant dynamics does not belong to the chosen model set, and the structure of the missing dynamics is not known. Approaches such as modifier adaptation (MA), output modifier adaption (MAy), and internal modifier adaptation (IMA) have been successfully implemented in real-time optimization (RTO) to take into account the structural model-plant mismatch minimizing the difference between the predicted and real outputs (see [109], [111], [110], [139]). Likewise, [118] proposed combining different models of the same process with different structures, such that the optimal combination minimizes the amount of modification introduced by the MAy. However, one of the main issues with MA, MAy, and IMA is that the plant gradients, i.e. gradients of the outputs with respect to the inputs, are required. These quantities are usually difficult to obtain in real time due to lack of excitation in the process or due to noise amplification introduced by differentiation. To address this issue, [119] also proposed to estimate these gradients using a neural network of radial basis functions. On the other hand, parametric mismatch is related to deviations in the model and process trajectories due to the uncertainty in the model parameters. This mismatch can be reduced recalculating the model parameters within some bounds such that the error between the prediction and process measurement is minimized. Within this approach, the model is assumed to belong to the parameter set, i.e. no undermodeling is present.

Both online and offline parameter estimation are the classical approach used in every field of science and engineering, with an extensive literature to support its application (see e.g. [68], [69], [75], [90], [194]). In most engineering domains, mathematical models of systems often have the structure of a DAE according to (3.1). Under some regularity conditions, the DAE model in (3.1) can expressed as the ODE model in (3.2). The focus in this case is placed on estimating the unmeasurable parameter vector \mathbf{p} . In [47] a distinction is made between two classes of parameter estimation: explicit methods and implicit methods. Explicit methods, such as least squares estimators mainly deal with constant or slowly varying parameters. However, this assumption might not hold in general for nonlinear models, where parameters can vary at different rates. Conversely, implicit methods tend to be more useful in this context, as they make use of recursion to ensure convergence to a solution. This is done through a self-correcting procedure that converges to a local optimum solution.

One of the most recognized implicit method is the Kalman filter [86], [87], which is used extensively to solve state and parameter estimation problems. Due to its flexibility and robustness, it can be used for state and parameter estimation in both linear and nonlinear models. The Kalman filter was originally designed for linear models, but can be used in the nonlinear case in its extended form, where a local linearization with respect to the states and parameters (sensitivity model) of the nonlinear model is computed at every time step and used to perform local estimation. Nevertheless, the Kalman filter solves the parameter estimation problem from an observability point of view, where the parameter vector \mathbf{p} is appended to the state vector and assumed to be constant throughout the prediction step. The state and parameter predictions are corrected when new output measurements are available.

Another way of approaching online parameter estimation is viewing parameters as extra inputs to the system, and casting the parameter estimation task as a control problem. The parameters do not need to be assumed constant and they are updated following a specific control law, i.e. a parameter update rule. For instance, [102] proposed a design based on a PI controller structure. The PI controller structure is simple to design because it does not require the use of a sensitivity matrix at each iteration unlike the case of the Kalman filter. Nonetheless, the proportional and integral gains require some user-based knowledge in order to have a good design. Additionally, [208] also approached the parameter estimation problem from a control point of view using the least-square minimization as a starting point to develop a parameter update law. However, it is not explicit how to design the controller gains to converge to the parameter values.

In this chapter, we introduce an online parameter estimation method using an error-based Lyapunov function as a starting point to design parameter update laws. These update laws are derived such that the time derivative of the Lyapunov function is negative for all time. Moreover, two methodologies are developed: one based on proportional and integral (PI) actions, and another one imposing an exponential convergence rate to the estimated parameter vector. The method assumes that the chosen parameter set is identifiable to guarantee that the plant-model error is minimized by a unique set of parameters. It is also considered that a parameter sensitivity model is available. Finally, an example is provided to illustrate the use of these two methods, as well as testing them under noisy conditions.

5.2. Parameter estimation as a control problem

The behavior of a model can change mainly due to the action of the exogenous input signals or due to internal variations in the parameter vector values. The model parameter vector can be regarded as an extra input vector that acts directly on the model. Since the parameters are viewed as inputs, it can be used to steer

the model states and/or output trajectories designing specific control laws to track the system's output \mathbf{y} as the reference signal. The control law will allow to estimate the value of the model parameter vector.

Let the model be given as in (3.2), and define the error between the output of the system and the model as $\boldsymbol{\varepsilon}(\mathbf{p}) = \mathbf{y}_m - \mathbf{y}(\mathbf{p}) \in \mathbb{R}^{n_y}$. A sensitivity-based representation \mathcal{M}_S of the corresponding model is assumed to be available and of the form

$$\mathcal{M}_S(\mathbf{p}) = \begin{cases} \dot{\bar{\mathbf{x}}}_{\mathbf{p}^\top} &= \partial_{\bar{\mathbf{x}}^\top} \bar{\mathbf{f}} \bar{\mathbf{x}}_{\mathbf{p}^\top} + \partial_{\mathbf{p}^\top} \bar{\mathbf{f}}, \\ \mathbf{y}_{\mathbf{p}^\top} &= \partial_{\bar{\mathbf{x}}^\top} \mathbf{g} \bar{\mathbf{x}}_{\mathbf{p}^\top} + \partial_{\mathbf{p}^\top} \mathbf{g} \end{cases} \quad \mathbf{x}_{\mathbf{p}^\top}(t_0) = \mathbf{0} \quad (5.1)$$

Let us define the following Lyapunov function

5

$$V(\boldsymbol{\varepsilon}) = \frac{1}{2} \boldsymbol{\varepsilon}^\top \mathbf{W} \boldsymbol{\varepsilon} \quad (5.2)$$

where \mathbf{W} is a positive definite matrix that weighs the individual components of the error in a suitable manner, and V is a positive definite scalar function. The error $\boldsymbol{\varepsilon}$ will approach the origin (or its minimum) asymptotically if the time derivative \dot{V} of the Lyapunov function V is negative definite for all time.

Let us write the time derivative of V as

$$\dot{V} = \frac{1}{2} \frac{\partial V}{\partial \boldsymbol{\varepsilon}^\top} \dot{\boldsymbol{\varepsilon}} = \boldsymbol{\varepsilon}^\top \mathbf{W} \dot{\boldsymbol{\varepsilon}} \quad (5.3)$$

From the chain rule, the time derivative of the error $\dot{\boldsymbol{\varepsilon}}$ can be written as

$$\dot{\boldsymbol{\varepsilon}} = \frac{\partial \boldsymbol{\varepsilon}}{\partial \mathbf{p}^\top} \dot{\mathbf{p}} \quad (5.4)$$

Replacing (5.4) in (5.3)

$$\dot{V} = \boldsymbol{\varepsilon}^\top \mathbf{W} \left(\frac{\partial \boldsymbol{\varepsilon}}{\partial \mathbf{p}^\top} \right) \dot{\mathbf{p}} = -\boldsymbol{\varepsilon}^\top \mathbf{W} \mathbf{S} \dot{\mathbf{p}} \quad (5.5)$$

where $\frac{\partial \boldsymbol{\varepsilon}}{\partial \mathbf{p}^\top} = -\frac{\partial \mathbf{y}(\mathbf{p})}{\partial \mathbf{p}^\top} = -\mathbf{S}$ with \mathbf{S} is the matrix of output sensitivities.

Notice that $\dot{\mathbf{p}}$ determines the evolution of \mathbf{p} over time, and it can be viewed as the control law we want to construct to take the error to zero. The advantage of considering the parameter vector as an artificial input rather than as an artificial state is that it provides the flexibility to impose the structure of the dynamic evolution of the parameters. The structure of $\dot{\mathbf{p}}$ must be chosen such that the derivative of the Lyapunov function is negative definite. In the following sections, we show different structures for the time derivative of the parameter vector (control law).

5.2.1. Integral action

Let us choose the parameter adaptation law $\dot{\mathbf{p}}$ as

$$\dot{\mathbf{p}} = \mathbf{KS}^\top \mathbf{W}\boldsymbol{\varepsilon} \Rightarrow \mathbf{p} = \int_0^t \mathbf{KS}^\top \mathbf{W}\boldsymbol{\varepsilon} \, d\tau \quad (5.6)$$

where \mathbf{K} is a diagonal matrix that weighs the control action of each parameter. Substituting (5.6) in (5.5), the following expression is obtained

$$\dot{V} = -\boldsymbol{\varepsilon}^\top \mathbf{WSKS}^\top \mathbf{W}\boldsymbol{\varepsilon} < 0, \quad \forall \boldsymbol{\varepsilon} \neq \mathbf{0} \quad (5.7)$$

The configuration of the integral action control law derived in (5.6) is illustrated in Figure 5.1. However, this approach can induce large oscillations in the tracking due to error accumulation. Hence, variations to the Lyapunov function can be made in order to include proportional action that counteracts the error accumulation of the integral action [55]. Two different approaches are proposed to include a proportional action to mitigate the oscillations.

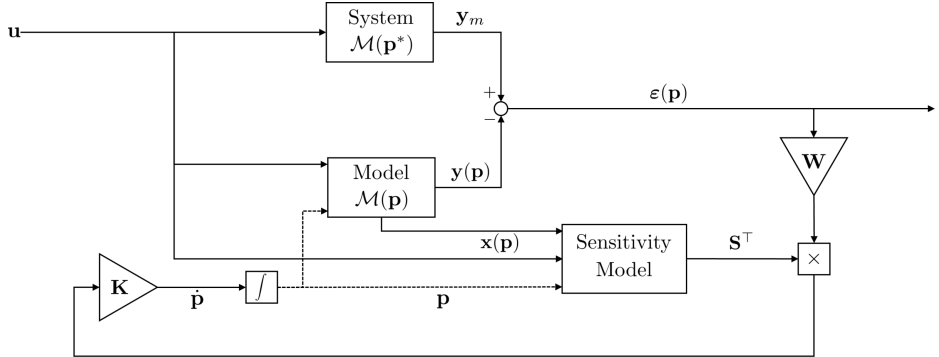


Figure 5.1: Parameter estimation using an integral action parameter adaption scheme.

5.2.2. Proportional + integral action

5

Let us introduce the following control law

$$\mathbf{p} = \mathbf{K}_1 \mathbf{W} \boldsymbol{\varepsilon} + \int_0^t \mathbf{K}_2 \mathbf{S}^\top \mathbf{W} \boldsymbol{\varepsilon} \, d\tau \quad (5.8)$$

Differentiating (5.8) with respect to time, and substituting (5.4) in the expression

$$\begin{aligned} \dot{\mathbf{p}} &= \mathbf{K}_1 \mathbf{W} \dot{\boldsymbol{\varepsilon}} + \mathbf{K}_2 \mathbf{S}^\top \mathbf{W} \boldsymbol{\varepsilon} \\ \Rightarrow \dot{\mathbf{p}} &= -\mathbf{K}_1 \mathbf{W} \mathbf{S} \dot{\mathbf{p}} + \mathbf{K}_2 \mathbf{S}^\top \mathbf{W} \boldsymbol{\varepsilon} \\ \Rightarrow \dot{\mathbf{p}} &= (\mathbf{I}_{n_p} + \mathbf{K}_1 \mathbf{W} \mathbf{S})^{-1} \mathbf{K}_2 \mathbf{S}^\top \mathbf{W} \boldsymbol{\varepsilon} \end{aligned} \quad (5.9)$$

where $\mathbf{K}_1 \in \mathbb{R}^{n_p \times n_y}$ and $\mathbf{K}_2 \in \mathbb{R}^{n_p \times n_p}$.

The proportional + integral action approach is shown in the block diagram in Figure 5.2

Replacing (5.9) in (5.5), we have

$$\dot{V} = -\boldsymbol{\varepsilon}^\top \mathbf{W} \mathbf{S} (\mathbf{I}_{n_p} + \mathbf{K}_1 \mathbf{W} \mathbf{S})^{-1} \mathbf{K}_2 \mathbf{S}^\top \mathbf{W} \boldsymbol{\varepsilon} \quad (5.10)$$

Since it is desired that the time derivative of the Lyapunov function is negative

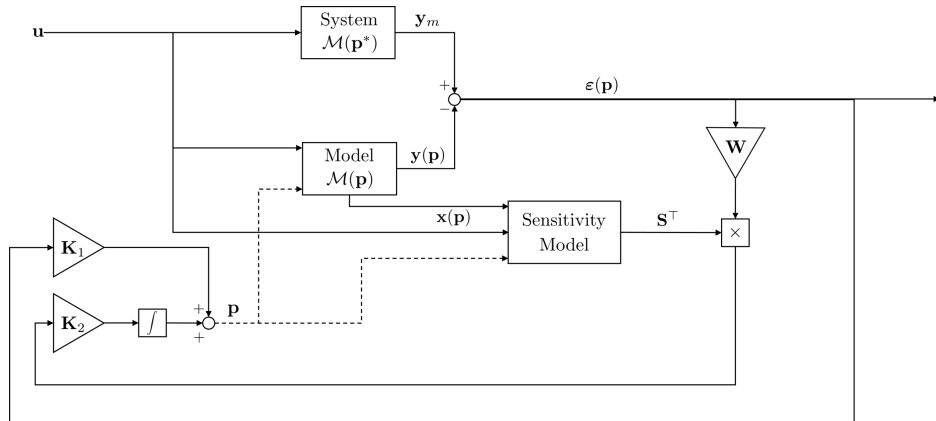


Figure 5.2: Scheme for parameter estimation using a self-adaptive model including a sensitivity model with integral action.

5

definite, (5.10) is equivalent to

$$\dot{V} < 0 \Leftrightarrow \mathbf{WS} (\mathbf{I}_{n_p} + \mathbf{K}_1 \mathbf{WS})^{-1} \mathbf{K}_2 \mathbf{S}^\top \mathbf{W} \succ \mathbf{0} \quad (5.11)$$

The equation (5.11) is satisfied if the following two conditions hold

$$\mathbf{K}_2 = (\mathbf{I}_{n_p} + \mathbf{K}_1 \mathbf{WS})^{-\top} \quad (5.12a)$$

$$\mathbf{K}_1 \neq -(\mathbf{WS})^+ \quad (5.12b)$$

Since $\mathbf{K}_1 \in \mathbb{R}^{n_p \times n_y}$ can be any matrix, an optimization is performed to select the proportional gain matrix \mathbf{K}_1 minimizing its Frobenius norm

$$\begin{aligned} \min_{\mathbf{K}_1} & \|\mathbf{K}_1\|_F^2 \\ \text{s.t. } & (\mathbf{I}_{n_p} + \mathbf{K}_1 \mathbf{WS})^{-1} (\mathbf{I}_{n_p} + \mathbf{K}_1 \mathbf{WS})^{-\top} \succeq \gamma \mathbf{I}_{n_p} \end{aligned} \quad (5.13)$$

where γ is a positive user-defined number to ensure sufficiently fast convergence of the error to zero.

5.2.3. Exponential control law

In the previous section, we introduced a parameter update law that behaves as a controller with proportional and integral action. However, the parameter adaptation solely depends on the error dynamics, which can make the convergence to the true parameters slower. This can be resolved by adding an extra term to the Lyapunov equation to enforce an exponential convergence rate of the parameter update. This configuration is displayed in Figure 5.3

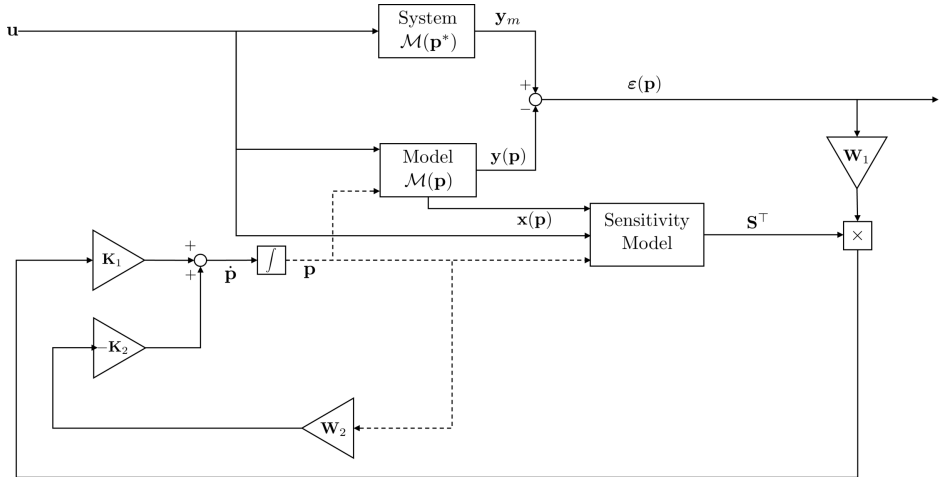


Figure 5.3: Scheme for parameter estimation using a self-adaptive model including a sensitivity model with explicit dependence on the parameter.

Let the Lypunov function (5.2) be modified with an extra term as follows

$$V = \frac{1}{2} \boldsymbol{\varepsilon}^\top \mathbf{W}_1 \boldsymbol{\varepsilon} + \frac{1}{2} \mathbf{p}^\top \mathbf{W}_2 \mathbf{p} \quad (5.14)$$

Differentiating (5.15) with respect to time

$$\begin{aligned} \dot{V} &= \boldsymbol{\varepsilon}^\top \mathbf{W}_1 \dot{\boldsymbol{\varepsilon}} + \mathbf{p}^\top \mathbf{W}_2 \dot{\mathbf{p}} \\ &= -\boldsymbol{\varepsilon}^\top \mathbf{W}_1 \mathbf{S} \dot{\mathbf{p}} + \mathbf{p}^\top \mathbf{W}_2 \dot{\mathbf{p}} \end{aligned} \quad (5.15)$$

Choosing a parameter control law of the form

$$\dot{\mathbf{p}} = \mathbf{K}_1 \mathbf{S}^\top \mathbf{W}_1 \boldsymbol{\varepsilon} - \mathbf{K}_2 \mathbf{W}_2 \mathbf{p} \quad (5.16)$$

Using the parameter control law, we have the time derivative of the Lyapunov function as

$$\dot{V} = - \begin{bmatrix} \boldsymbol{\varepsilon} \\ \mathbf{p} \end{bmatrix}^\top \begin{bmatrix} \mathbf{W}_1 \mathbf{S} \mathbf{K}_1 \mathbf{S}^\top \mathbf{W}_1 & -\mathbf{W}_1 \mathbf{S} \mathbf{K}_2 \mathbf{W}_2 \\ -\mathbf{W}_2 \mathbf{K}_1 \mathbf{S}^\top \mathbf{W}_1 & \mathbf{W}_2 \mathbf{K}_2 \mathbf{W}_2 \end{bmatrix} \begin{bmatrix} \boldsymbol{\varepsilon} \\ \mathbf{p} \end{bmatrix} \quad (5.17)$$

Similarly, we can impose negative definiteness on \dot{V} choosing invertible $\mathbf{K}_1 = \mathbf{K}_2 = \mathbf{K}$ such that the following LMI is satisfied

$$\dot{V} < 0 \Leftrightarrow \mathbf{\Gamma} = \begin{bmatrix} \mathbf{W}_1 \mathbf{S} \mathbf{K} \mathbf{S}^\top \mathbf{W}_1 & \mathbf{W}_1 \mathbf{S} \mathbf{K} \mathbf{W}_2 \\ \mathbf{W}_2 \mathbf{K} \mathbf{S}^\top \mathbf{W}_1 & \mathbf{W}_2 \mathbf{K} \mathbf{W}_2 \end{bmatrix} \succ 0 \quad (5.18)$$

Performing block LDU decomposition on (5.18), it is clear to see that

$$\mathbf{\Gamma} = \begin{bmatrix} \mathbf{I}_{n_y} & -\mathbf{W}_1 \mathbf{S} \mathbf{W}_2^{-1} \\ \mathbf{0} & \mathbf{I}_{n_p} \end{bmatrix} \begin{bmatrix} \mathbf{0} & \mathbf{0} \\ \mathbf{0} & \mathbf{W}_2 \mathbf{K} \mathbf{W}_2 \end{bmatrix} \begin{bmatrix} \mathbf{I}_{n_y} & \mathbf{0} \\ -\mathbf{W}_2^{-1} \mathbf{S}^\top \mathbf{W}_1 & \mathbf{I}_{n_p} \end{bmatrix} \quad (5.19)$$

This implies that $\mathbf{\Gamma} \succeq 0$, and that \dot{V} can only be made negative if and only if $\mathbf{W}_2 \mathbf{K} \mathbf{W}_2 \succ 0$. As in the integral action case, there are an infinite number of matrices that satisfy the positive-definiteness condition. Therefore, some constraints are needed to reduce the dimension of the solution space. In view of these limitations, in this work we will solve the following optimization to obtain the value of the controller gain \mathbf{K}

$$\begin{aligned} \min_{\mathbf{K}} & \|\mathbf{K}\|_F^2 \\ \text{s.t. } & \mathbf{W}_2 \mathbf{K} \mathbf{W}_2 \succeq \gamma \mathbf{I}_{n_p} \end{aligned} \quad (5.20)$$

where γ is a positive user-defined number to ensure sufficiently fast convergence of the error to zero.

The two methods proposed here work well when the assumptions on $\boldsymbol{\varepsilon}$ are satisfied, as well as a sensitivity model is available. However, we need to test whether these assumptions hold checking the controllability of the output error with respect to the parameters. This is equivalent to assessing identifiability of the parameter vector (see section 3.5.1).

Remark 5.1: The selection of parameter control actions are guaranteed to converge to the true parameter set \mathbf{p}^* if the parameter set to be estimated is fully

identifiable along the operating point or trajectory. Convergence can be guaranteed whenever the following two conditions are satisfied:

- $\varepsilon = \varepsilon(t, \mathbf{p})$ is a injective function of \mathbf{p}
- $\varepsilon = \varepsilon_{\min}$ when $\mathbf{p} = \mathbf{p}^*$.

On the one hand, the first condition states that the error $\varepsilon(\mathbf{p})$ is fully controllable by the artificial input \mathbf{p} . This is analogous to the rank condition of the extended output controllability developed in Theorem 3.4 of Chapter 3. On the other hand, the second condition establishes that the error is at least locally convex in the vicinity of the true parameter value \mathbf{p}^* , and thus, the error reaches its minimum exactly at \mathbf{p}^* . Convexity is guaranteed by the analyticity of the functions in model (3.2). The convexity condition implies that the gradient of the error with respect to each parameter is linearly independent from each other, the rank condition described in (4.10) within Chapter 4 is also satisfied.

5

5.2.4. Computation of the weighting matrix \mathbf{W}

In the previous section, we have discussed how to choose the controller gains \mathbf{K} for online parameter estimation. However, another important variable to tune is the weight matrix \mathbf{W} . In the first case of proportional + integral action, a way to choose \mathbf{W} is as the inverse of the covariance of ε such that we take into account a possible non-constant variance in the prediction error. In the second case, the weight matrices \mathbf{W}_1 and \mathbf{W}_2 are chosen based on the inverse covariance of ε and the inverse covariance of the previous estimation of \mathbf{p} , respectively. The second weight matrix \mathbf{W}_2 regularizes possible ill-conditioned directions in the sensitivity matrix \mathbf{S} to obtain parameter estimates at the expense of introducing some bias in the estimation. These approaches use all the data points to compute the weight matrices, and quantify the uncertainty given experimental data.

Throughout this work, we shall use another methodology developed in [83]. It accounts to construct these matrices dynamically based on the importance of one data points given other data points. The method relies on the fact that the uncertainty of $\hat{\mathbf{p}}$ given the output data \mathbf{y} is

$$\text{var}(\hat{\mathbf{p}}|\mathbf{y}) = \frac{1}{N} \text{tr}(\mathbf{F}^{-1}(\hat{\mathbf{p}})) \quad (5.21)$$

where N is the number of data points and $\mathbf{F}(\mathbf{p})$ is the FIM defined as in (4.16).

Similarly, the uncertainty of one set of data points \mathbb{S}_1 given another set of data points \mathbb{S}_2 using the Fisher Information is

$$\text{var}(\mathbb{S}_1|\mathbb{S}_2) = \frac{1}{N} \text{tr} (\mathbf{F}_{\mathbb{S}_1} \mathbf{F}_{\mathbb{S}_2}^{-1}) \quad (5.22)$$

where $\mathbf{F}_{\mathbb{S}_j}$ is the FIM computed using data set \mathbb{S}_j .

To quantify the importance of a data point the uncertainty of the i -th data point given all the other data points is calculated [83]. This is achieved defining $\mathbb{S}_1 = \{i\}$ and $\mathbb{S}_2 = \{1, 2, \dots, N \cdot n_y\} \setminus \mathbb{S}_1$. The FIM $\mathbf{F}_{\mathbb{S}_1}$ and $\mathbf{F}_{\mathbb{S}_2}$ are computed using the corresponding i -th row and all the other $N \cdot n_y - 1$ rows of the sensitivity matrix \mathbf{S} , respectively. The advantage of this approach is that the data uncertainty reflects whether one data point can be accurately predicted based on all other data points, producing a weight matrix that strategically emphasizes the most important data points in the online estimation procedure.

The use of the parameter control laws as well as the quantification of the importance of a data point based on partitioned covariance matrices will be illustrated in an example.

5.3. Example: Fed-batch penicillin reactor

Consider the fed-batch penicillin reactor described by the following set of equations [177]:

$$\mathcal{S} = \begin{cases} \dot{X} = X \left(\mu - \frac{F}{V} - c_L \right) \\ \dot{S} = -\sigma X + (S_f - S) \frac{F}{V} \\ \dot{P} = q_P X - P \left(\frac{F}{V} + K \right) \\ \dot{V} = F \end{cases} \quad (5.23)$$

where X is cell biomass concentration, S is the substrate concentration, P is the product concentration, K is the product decay constant, and V the reactor volume.

The time-varying parameters can be further parametrized in terms of constant parameters given by the following correlations:

Table 5.1: Fed-batch reactor growth correlations

Specific growth correlations	Equation
Specific growth rate	$\mu = \mu_m \frac{S}{K_X X + 10}$
Specific cell lysis rate	$c_L = c_{Lm} \frac{X e^{-\frac{S}{100}}}{K_L + X + 1}$
Specific substrate consumption rate	$\sigma = \frac{\mu}{Y_{X/S}} + \frac{q_P}{Y_{P/S}} + m_X$
Specific product formation rate	$q_P = 1.5 q_{Pm} \frac{S X}{4 K_P + S X (1 + \frac{S}{3 K_I})}$
Maintenance energy	$m_X = m_X m \frac{X}{X + 10}$

It is assumed that the model \mathcal{M} of the fed-batch reactor is given only by the balance equations of cell biomass concentration X and product concentration P . Furthermore, both of these states are measured along with feed flow F and reactor volume V . Thus

$$\mathcal{M} = \begin{cases} \dot{X} = X \left(\mu - \frac{F}{V} - c_L \right) \\ \dot{P} = q_P X - P \left(\frac{F}{V} + K \right) \\ \mathbf{y} = \begin{bmatrix} X \\ P \end{bmatrix} \end{cases} \quad (5.24)$$

In general, a parameter vector of constant parameters is desired because parameters are generally understood as static scaling quantities. However, the model \mathcal{M} depends on the functions μ , q_P , c_L , and the constant parameter K . These variables depend on the substrate concentration S , which correspond to unmodeled dynamics. Therefore, the proposed parameter vector is

$$\mathbf{p} = [\mu \ c_L \ q_P \ K]$$

The first three elements of the parameter vector will be time varying, and thus, they need to be estimated online to obtain the correct values over time. Nevertheless, before setting the control-based parameter estimation it is necessary to test if the proposed parameter set is identifiable.

After performing identifiability analysis, we see that only two parameters are identifiable, and therefore, the parameter vector \mathbf{p} must be reduced. In this case, we chose $\mathbf{p}^{\text{red}} = [\alpha \ \beta]^T = [\mu - c_L \ q_P X - PK]^T$

We compare the PI adaptation law shown in (5.8) and the exponential control law (5.16). For the the PI method, we chose a diagonal matrix $\mathbf{K}_1 = \text{diag}([20 \ 45])$ for

the proportional gain, while the algorithm computed the integral gain matrix \mathbf{K}_2 dynamically. Analogously, for the exponential control law approach, \mathbf{K} was computed solving the optimization problem (5.20) using a bound $\gamma = 30$. Additionally, noise was added to both the input and the measured outputs. The noise power values are given in Table 5.2.

Table 5.2: Noise power for inputs and measured outputs

Signal	Noise power
Inlet flow F	0.000025
Measured cell concentration X	0.04
Measured product concentration P	0.01

However, in the same way that the performance of a controller can be severely impacted by the noise in the loop, the reliability of the control-based approach for parameter estimation is hampered by the noise, and therefore, the noisy measured outputs need to be filtered before they can be fed to the online parameter estimation algorithm. In view of this, simple low-pass filters are designed to filter out the high frequency components of the measured output signals X and P . The results of the online parameter estimation methods are shown in Figure 5.4

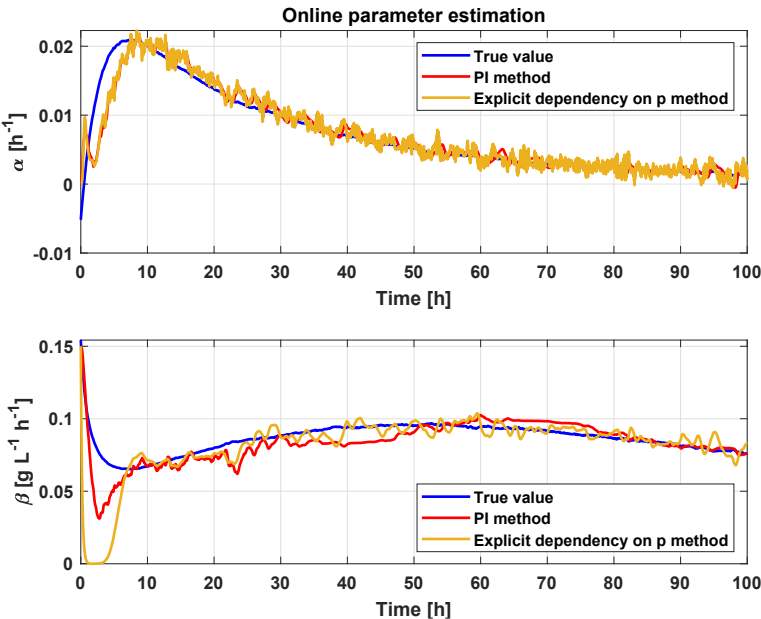


Figure 5.4: Comparison of estimated parameters between PI method and exponential control law methods.

Both methods estimate parameters that converge to the true value of the parameters. This is in agreement with the expected behavior, since both parameter α and β are

identifiable from the measured outputs. The estimation is clearly sensitive to noise, which was suppressed using a set of low-pass filters. As a consequence, the parameter estimates contain noise with a lower power content at the expense of the introduction of lag in the estimation, which can be seen especially at the start of the estimation. Likewise, the predicted outputs of the model using the estimated parameters are compared to the true outputs of the plant as well as the filtered outputs. The results are shown in Figure 5.5. The parameters using both methods make the predicted output X to converge to its true value, however, the predicted output P only converges to the filtered valued. This happens because the filter lag effect propagates from X to P in the model obtaining a slower response. Additionally, the model outputs X and P are, under the operating conditions of the fed-batch reactor, less sensitive to β . This implies that a more aggressive tuning must be put in place to ensure faster convergence at the risk of amplifying the noise power level again. The parameter estimation and output prediction RMSE¹ is shown in Table 5.3

5

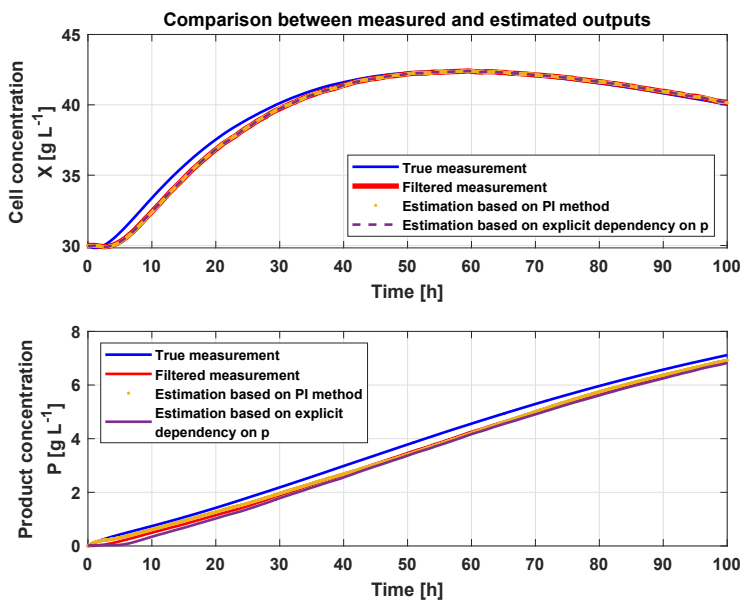


Figure 5.5: Comparison of predicted outputs between PI method and exponential control law methods.

¹The estimated output is compared to the filtered output

Table 5.3: Estimated outputs and parameters RMSE

Root-mean-square error		
	Predicted outputs	Estimated parameters
PI method	$\text{rmse}(X) = 0.407793 \text{ g/L}$ $\text{rmse}(P) = 0.250169 \text{ g/(L h)}$	$\text{rmse}(\alpha) = 0.002033 \text{ 1/h}$ $\text{rmse}(\beta) = 0.009766 \text{ g/(L h)}$
Exponential law	$\text{rmse}(X) = 0.358636 \text{ g/L}$ $\text{rmse}(P) = 0.379893 \text{ g/L}$	$\text{rmse}(\alpha) = 0.001386 \text{ 1/h}$ $\text{rmse}(\beta) = 0.013152 \text{ g/(L h)}$

Chapter summary

Online parameter estimation as a control design problem

- The parameter estimation problem can also be seen from a control perspective, where the parameter is updated based on a control law that makes the model output track the systems output (reference to the model).
- The convergence of the error to zero implies convergence to the "true" parameter value as long as the sensitivity matrix is full column rank at every point of the output trajectory.
- Parameters that are operationally identifiable according to a particular measure but have a smaller sensitivity magnitude are much difficult to estimate than others with larger sensitivity magnitudes. This means that the error will converge to zero more slowly. The controller gain should be tuned such that the error is made zero at a reasonable speed.
- The PI approach utilizes the classic construction of a proportional gain and an integral gain. This approach is similar to the one explored in [102], however, in our case the design is done to ensure that the time derivative of the Lyapunov equation is negative definite. This leads to the design of time-varying gains that depend on the parameter sensitivities.
- The design of the proportional and integral gains can be solved analytically enforcing a positive definiteness condition of a matrix. However, imposing positive definiteness is not necessary and the controller gains can be computed solving a norm maximization problem. The latter is computationally more expensive but is provides a faster convergence.
- The exponential control law is an approach akin to the ridge regularization, in which the current parameter value is used to establish a trade-off between the the variance (precision of the estimation) and the bias of the estimation (the accuracy of the estimation).
- Process and measurement noise are key issues in the control-based parameter estimation. Noise corrupts the signals that need to be fed back in the control law to estimate the parameters. Therefore, filtering noisy signals is important to ensure good performance.

6

Extent-based sequential state and parameter estimation for process systems

In this chapter, we present the design of a sequential estimator based on the extent representation to estimate the extents of reaction, chemical kinetic rates, and chemical kinetic parameters using only a limited number measured species. The sequential nature of the estimation allows to address each estimation problem separately. The estimator provides a tool to compute unknown concentration of species that can be difficult to measure, while providing insights on the behavior of the chemical kinetics. Furthermore, the inlet concentration may vary over time or not be completely known in some processes, e.g. process systems with recycle. In this case, the inlet composition matrix exhibits uncertainty, thus, we propose an optimization problem to reconstruct the uncertainty. The knowledge of this matrix is crucial to appropriately reconstruct the states of the system.

Publications of this chapter:

State and parameter estimation based on extent transformations, Márquez-Ruiz, A., Méndez-Blanco, C., Porru, M., Özkan, L. Computer Aided Chemical Engineering, 2018 ([116])

Constrained Control and Estimation of Homogeneous Reaction Systems Using Extent-Based Linear Parameter-Varying Models, Márquez-Ruiz, A., Méndez-Blanco, C., Özkan, L. Industrial & Engineering Chemistry Research, 2019 ([113])

Extent-based reconstruction of the inlet composition matrix in process systems with feed variability, Méndez-Blanco, C., Özkan, L. 13th IFAC Symposium on Dynamics and Control of Process Systems (DYCOPS), 2022 ([125])

6.1. Introduction

Reaction systems are usually modeled using conservation laws described by mass and energy balance equations. These equations represent different phenomena acting on the system, namely reaction, and transport dynamics [163]. The particular structure in the balance equations has been exploited to decouple the process dynamics in variants and invariants of reaction by means of a diffeomorphic linear transformation. The resulting dynamics is described in terms of extents [6]. This decomposition approach has been extended to include a more general representation of the reaction systems, such as systems with multiple phases, mass transfer, and non-isothermal dynamics ([5],[22],[114],[73]). There has also been substantial effort in using this decomposition for control, and state and parameter estimation purposes. In particular, the estimation of kinetic parameters has been addressed via the extent representation using incremental estimation or graph-based techniques ([116],[189]). Extent-based incremental parameter estimation refers to a two-step estimation procedure. First, the concentration/mole measurement is transformed into extent-based variables to decouple the effects. Secondly, the parameters affecting the dynamics are computed separately, which can lead to better parameter identifiability conditions. Additionally, a frequent problem in batch, semi-batch, and continuous process operations is the variability of the feedstock or raw material used. This poses a problem when applying the linear transformations to compute the extents for these two cases. Furthermore, the subsequent kinetic parameter estimation is not reliable due to the incorrect extent calculation as a consequence of the uncertainty in the inlet composition.

6

On the other hand, the need of real-time information on the evolution of chemical reactions in process systems is critical for process control and fault detection. Additionally, the unavailability of specialized instruments, such as online composition analyzers, motivates the development of state and parameter estimators for chemical processes. Estimators based on the extent representation are the suited for such purposes because it contains information on the process states, parameters, and possible disturbances. For estimation purposes, the most important advantage lies in the identification of reaction systems from measured data.

There are basically two approaches for online parameter-and-state estimation: simultaneous and sequential. In the simultaneous approach (sometimes called adaptive approach), a set of differential equations are included in the original model of the system to determine the time evolution of the parameters (parameter modeling). The parameters are assumed as a new set of extra states and the parameter-and-state estimation problem is transformed to a single state estimation problem [42]. However, this approach has some important drawbacks such as the selection of the models for the parameters (typically the parameters are considered as extra states with no dynamics), and the observability conditions of the system with the extended set of states. To address this issue, the sequential approach in a cascade

structure has been proposed [42]. The main idea of sequential estimation is to solve two estimation problems: one for the states and one for the parameters. Typically, observer-based estimators [14] and least squares formulations have been suggested for parameter estimation.

In this chapter, we consider the sequential identification approach for semi batch and continuous operations, where an optimization problem is proposed to reconstruct the uncertainty inlet concentration matrix based on a limited number of species. Using the estimated uncertainty, the true extents are computed using an asymptotic observer (AO) to estimate the chemical kinetic rates with a Luenberger observer, and ultimately to estimate the kinetic parameters solving a least-square problem. Finally, the approach is illustrated in a CSTR with a recycle stream.

6.2. Extents of Reaction

The extent of reaction, denoted with the Greek letter ξ , is a measure of the degree of completion of any reaction. In other words, it quantifies the progress of a reaction while it consumes the reactants [186]. It is more precisely defined as:

6

$$\xi_r = \frac{\text{mol of component } s \text{ generated or consumed in reaction } r}{\text{stoichiometric coefficient for component } s \text{ in reaction } r} \quad (6.1)$$

Consider a reactive system with S species and N_r independent reactions, the extents of reaction are defined mathematically by, as presented in [5]:

$$d\xi_r := \frac{dn_{s,r}}{\nu_{s,r}}, \quad \forall s = 1, \dots, S, \quad \forall r = 1, \dots, N_r \quad \xi_r(0) = 0 \quad (6.2)$$

Hence:

$$\nu_{s,r} \int d\xi_r = \int dn_{s,r} \implies \nu_{s,r} \xi_r = n_{s,r} \quad (6.3)$$

where $dn_{s,r}$ is the variation of the number of moles of the s -th species involved in the r -th reaction and $\nu_{s,r}$ is the corresponding stoichiometric coefficient. Note that $\nu_{s,r} < 0$ for reactants and $\nu_{s,r} > 0$ for products.

This setting can be exploited to achieve more suitable representation to more com-

plex reaction systems such as equilibrium reaction, reactions in series or in parallel, etc. In particular, models based on material balance can benefit from this representation, e.g batch or semi-batch stirred-tank reactors. This application is briefly explain

Batch reactors

Consider a batch reactor where S species react in N_r independent reactions. The volume of the liquid mixture is V_{ol}^l , which is a function of time due to the varying densities of the reactants and product. We also note that in a batch reactor there is neither inlet nor outlet streams ($\mathbf{F}_{\text{in}} = F_{\text{out}} = 0$), and the material accumulation is only driven by the reaction. The balance for the s -th species in the r -th reaction is

$$\dot{n}_{s,r} = \nu_{s,r} V_{\text{ol}}^l r_r \quad n_{s,r}(0) = n_{s,r_0} \quad (6.4)$$

Making use of equation (6.2) and remembering that $\xi_{r_0} = 0$, we transform (6.4)

6

$$\begin{aligned} \nu_{s,r} \dot{\xi}_r &= \nu_{s,r} V_{\text{ol}}^l r_r \\ \implies \dot{\xi}_r &= V_{\text{ol}}^l r_r \quad \xi_r(0) = 0 \end{aligned} \quad (6.5)$$

Semi-batch reactors

Now consider a semi-batch reactor where S species react in N_r independent reactions. In this case, there inlet stream remains equal to zero ($\mathbf{F}_{\text{in}} = \mathbf{0}_{N_r}$). However, the outlet stream is different from zero ($F_{\text{out}} \neq 0$). The material accumulation is driven by both the outlet flow and the reaction. Likewise, the volume of the liquid mixture is V_{ol}^l , is now a function of time due to the varying densities of the reactants and product as well as the outlet flow F_{out} . The balance for the s -th species in the r -th reaction is

$$\dot{n}_{s,r} = \nu_{s,r} V_{\text{ol}}^l r_r - \frac{F_{\text{out}}}{n_L} n_{s,r} \quad n_{s,r}(0) = n_{s,r_0} \quad (6.6)$$

where n_L is the total amount of moles in the liquid reacting mixture.

Substituting (6.2) in (6.6), we obtain:

$$\begin{aligned} \nu_{s,r}\dot{\xi}_r &= \nu_{s,r}V_{\text{ol}}^l r_r - \frac{F_{\text{out}}}{n_L} \nu_{s,r} \xi_r & n_{s,r}(0) &= n_{s,r_0} \\ \implies \dot{\xi}_r &= V_{\text{ol}}^l r_r - \frac{F_{\text{out}}}{n_L} \xi_r, & \xi_r(0) &= 0 \end{aligned} \quad (6.7)$$

In (6.5) and (6.7), it was shown how the extent of reaction can be directly applied where the evolution of moles in the system is reaction-dependent for a batch and a semi-batch reactors, respectively. In the case of a batch reactor, only chemical reactions occur in the process, making it straightforward to apply the extent transformation. For a semi-batch reactor with outlet stream and no inlet stream, the accumulation of material in the process depends on the reaction but also on the fraction of reacting mixture leaving the reactor through the outlet stream. The leaving fraction can be written in terms of the moles in the reactor, which allows to apply extent of reaction directly.

The continuous stirred-tank reactor (CSTR) case was not considered, because the inlet stream is independent of the reaction, thus, the representation in terms of extents of reaction cannot be directly applied. The resulting variable from the transformation would lack physical meaning.

6.3. Variant and Invariant Spaces of Reaction Systems

As mentioned in the previous section, the extent of reaction can be applied directly to chemical reaction processes where the evolution of moles in time is solely related to the reaction and the amount of reacting mixture. Under this circumstances, system is uniquely driven by the chemical reaction. Hence, the dynamic space can be split in two subspaces, namely the reaction variant and reaction invariant. These subspaces are defined next:

Definition 6.1 (Reaction variant space [5]): Any set \mathcal{P} of N_r linearly independent variables that evolve in the reaction space constitutes a reaction variant space.

Definition 6.2 (Reaction invariant space [5]): Any set \mathcal{I} of $S - N_r$ linearly independent variables that evolve in the space orthogonal to the reaction space constitutes a reaction invariant space.

The reaction variants coincide with the extent of reaction if and only if the initial conditions of the former are strictly zero. Moreover, if the process contains an inlet stream, then the change in time of moles is affected by two independent dynamics,

reaction and inlet flow. Under this situation, the reactor dynamics cannot be expressed in terms of the extent of reaction directly. To circumvent this situation, the concept of extent is extended to extents of reaction and inlet flows.

Consider the mole balance equation for CSTR with a well-stirred mixture of S species, N_r independent reactions, N_t independent inlet flows and **one** outlet flow¹, given by:

$$\dot{\mathbf{n}} = \mathbf{N}^\top \mathbf{r} + \mathbf{X}_{\text{in}} \mathbf{F}_{\text{in}} - \frac{F_{\text{out}}}{n_L} \mathbf{n}, \quad \mathbf{n}(0) = \mathbf{n}_0 \quad (6.8)$$

where $\mathbf{n} \in \mathbb{R}^S$ is the vector of moles, $\mathbf{r} \in \mathbb{R}^{N_r}$ is the vector of chemical independent reactions, $\mathbf{F}_{\text{in}} \in \mathbb{R}_{\geq 0}^{N_t}$ is the molar inlet flow vector, $\mathbf{N} \in \mathbb{R}^{N_r \times S}$ is the stoichiometric matrix, $\mathbf{X}_{\text{in}} \in \mathbb{R}_{[0,1]}^{S \times N_t}$ is the inlet molar fraction matrix, $F_{\text{out}} \in \mathbb{R}$ the molar outlet flow, and n_L is the total number of moles in the liquid reacting mixture.

The vector of chemical reactions plays a natural important role in reaction system. Therefore, throughout this work, we shall take the following assumption as valid.

6

Assumption 6.1: The vector of chemical reactions \mathbf{r} is, without loss of generality, a square-integrable uniformly continuous function in a convex domain $\mathbb{D}_r \forall t \in [0, \infty)$.

Assumption 6.1 implies that $\dot{\mathbf{r}}$ is bounded by uniform continuity. This is true in general because the rate of reactions directly depends on the number of moles in the system, which is physically bounded (mass is conserved). Furthermore, square-integrability of \mathbf{r} guarantees that the integral of \mathbf{r} is bounded. As a consequence of uniform continuity in \mathbb{D}_r and square-integrability, the vector of chemical rates (or reactions) \mathbf{r} converges to zero asymptotically [158] provided that the number of reactants decays to zero.

The mole balance in a CSTR shown in (6.8) is, in general nonlinear due to the reaction kinetics contained in the vector \mathbf{r} . It is possible to find a linear diffeomorphism \mathbf{T} such that the system can be re-expressed in terms of new states that each of them only evolves with respect to the reaction and the inlet flow as follows:

$$\mathbf{n} \longmapsto \begin{bmatrix} \mathbf{z}_r \\ \mathbf{z}_{\text{in}} \\ \mathbf{z}_{\text{inv}} \end{bmatrix} = \underbrace{\begin{bmatrix} \mathbf{T}_1^\top \\ \mathbf{T}_2^\top \\ \mathbf{T}_3^\top \end{bmatrix}}_{\mathbf{T}} \mathbf{n} \quad (6.9)$$

¹Notice that this is without loss of generality because if the liquid phase is well mixed, every outlet flow will have the same composition. The outlets of the process can be treated as one, which is equal to the sum of all of the individual outlet flows.

This transformation leads to the reaction and inlet flow variants \mathbf{z}_r and \mathbf{z}_{in} , respectively, and invariants \mathbf{z}_{inv} as:

$$\dot{\mathbf{z}}_r = \underbrace{\mathbf{T}_1^\top \mathbf{N}^\top \mathbf{r}}_{\mathbf{I}_{N_r}} + \underbrace{\mathbf{T}_1^\top \mathbf{X}_{\text{in}}}_{0_{N_r \times N_L}} \mathbf{F}_{\text{in}} - \frac{F_{\text{out}}}{n_L} \mathbf{z}_r, \quad \mathbf{z}_r(0) = \mathbf{T}_1^\top \mathbf{n}_0 \quad (6.10)$$

$$\dot{\mathbf{z}}_{\text{in}} = \underbrace{\mathbf{T}_2^\top \mathbf{N}^\top \mathbf{r}}_{0_{N_L \times N_r}} + \underbrace{\mathbf{T}_2^\top \mathbf{X}_{\text{in}}}_{\mathbf{I}_{N_L}} \mathbf{F}_{\text{in}} - \frac{F_{\text{out}}}{n_L} \mathbf{z}_{\text{in}}, \quad \mathbf{z}_{\text{in}}(0) = \mathbf{T}_2^\top \mathbf{n}_0 \quad (6.11)$$

$$\dot{\mathbf{z}}_{\text{inv}} = \underbrace{\mathbf{T}_3^\top \mathbf{N}^\top \mathbf{r}}_{0_{N_\varepsilon \times N_r}} + \underbrace{\mathbf{T}_3^\top \mathbf{X}_{\text{in}}}_{0_{N_\varepsilon \times N_L}} \mathbf{F}_{\text{in}} - \frac{F_{\text{out}}}{n_L} \mathbf{z}_{\text{inv}}, \quad \mathbf{z}_{\text{inv}}(0) = \mathbf{T}_3^\top \mathbf{n}_0 \quad (6.12)$$

where \mathbf{T}_1 transformation matrix of the reaction space, \mathbf{T}_2 is the transformation matrix of the inlet space, \mathbf{T}_3 transformation matrix of the reaction and the inlet invariant space, and $N_\varepsilon = S - N_r - N_L$.

However, the physical interpretation of these transformed variables is subject to the initial conditions \mathbf{n}_0 . If the initial conditions in the reactor are not zero, then the reaction and inlet flow variants cannot be interpreted as the true extents. The variants of reaction and inlets would have initial conditions different from zero, even when there is no reaction or material flowing into the reactor because both $\mathbf{T}_1 \mathbf{n}_0 \neq 0_{N_r}$ and $\mathbf{T}_2 \mathbf{n}_0 \neq 0_{N_L}$. Hence, these initial conditions must be discounted to obtain the true extents [5]. A new transformation matrix \mathbf{T}_0 can be computed to factor out the initial conditions and obtain a representation whose meaning can be identified with the concept of extents.

$$\begin{bmatrix} \mathbf{z}_r \\ \mathbf{z}_{\text{in}} \\ \mathbf{z}_{\text{inv}} \end{bmatrix} \longmapsto \begin{bmatrix} \mathbf{x}_r \\ \mathbf{x}_{\text{in}} \\ \mathbf{x}_{\text{inv}} \end{bmatrix} = \begin{bmatrix} \mathbf{z}_r \\ \mathbf{z}_{\text{in}} \\ \mathbf{z}_{\text{inv}} \end{bmatrix} - x_\lambda \begin{bmatrix} \mathbf{z}_{r0} \\ \mathbf{z}_{\text{in}0} \\ \mathbf{z}_{\text{inv}0} \end{bmatrix} \quad (6.13)$$

where \mathbf{x}_r is the extent of reaction, \mathbf{x}_{in} is the extent of inlet flow, \mathbf{x}_{inv} is the extent of reaction and inlet flow invariants and x_λ is the initial conditions discounting factor.

Finally, the true extents of reaction and inlet flow are calculated as:

$$\mathbf{n} \longmapsto \begin{bmatrix} \mathbf{x}_r \\ \mathbf{x}_{\text{in}} \\ \mathbf{x}_{\text{inv}} \\ x_\lambda \end{bmatrix} = \underbrace{\begin{bmatrix} \mathbf{T}_{10}^\top \\ \mathbf{T}_{20}^\top \\ \mathbf{T}_{30}^\top \\ \mathbf{T}_{40}^\top \end{bmatrix}}_{\mathbf{T}_0} \mathbf{n} \quad (6.14)$$

where \mathbf{T}_{10} is the transformation matrix of the reaction space, \mathbf{T}_{20} is the transformation matrix of the inlet space, \mathbf{T}_{30} is the transformation matrix of the reaction and inlet flow invariant space, all with discounted initial conditions \mathbf{n}_0 and \mathbf{T}_{40} portion of the reaction and inlet invariant spaces occupied by the initial conditions \mathbf{n}_0 .

The existence of the aforementioned linear diffeomorphism \mathbf{T}_0 is guaranteed if the following conditions hold:

6

1. The stoichiometric matrix \mathbf{N}^\top is full column rank, i.e. $\text{rank}(\mathbf{N}^\top) = N_r$
2. The inlet molar fraction matrix \mathbf{X}_{in} is full column rank, i.e. $\text{rank}(\mathbf{X}_{\text{in}}) = N_t$
3. $\text{rank}([\mathbf{N}^\top \quad \mathbf{X}_{\text{in}}]) = N_r + N_t \leq S$ for $\mathbf{n}_0 = 0$
4. $\text{rank}([\mathbf{N}^\top \quad \mathbf{X}_{\text{in}} \quad \mathbf{n}_0]) = N_r + N_t + 1 \leq S$ for $\mathbf{n}_0 \neq 0$

As noted in [113], the existence of the linear map \mathbf{T}_0 can be viewed as an input-to-state decoupling problem such that $\text{col}(\mathbf{N}^\top) \oplus \text{col}(\mathbf{X}_{\text{in}}) \oplus \text{col}(\mathbf{n}_0) \subseteq \mathbb{R}^S$, guarantees uniqueness of the decomposition, where \oplus is the direct sum. Additionally, $\ker(\mathbf{N}) \cap \ker(\mathbf{X}_{\text{in}}^\top) = \mathcal{I}$, which guarantees the existence of trajectories in the moles space that are reaction and inlet invariant. Finally, $\text{col}(\mathbf{n}_0) \subseteq \mathcal{I}$, which implies that the initial conditions must lie in the reaction and inlet invariant subspace, providing independent information about the trajectories in the mole space. If these conditions are satisfied, then the reaction, inlet, and invariant subspaces can be generated performing an orthogonal decomposition of the moles space. The subspace decomposition is illustrated in Figure 6.1

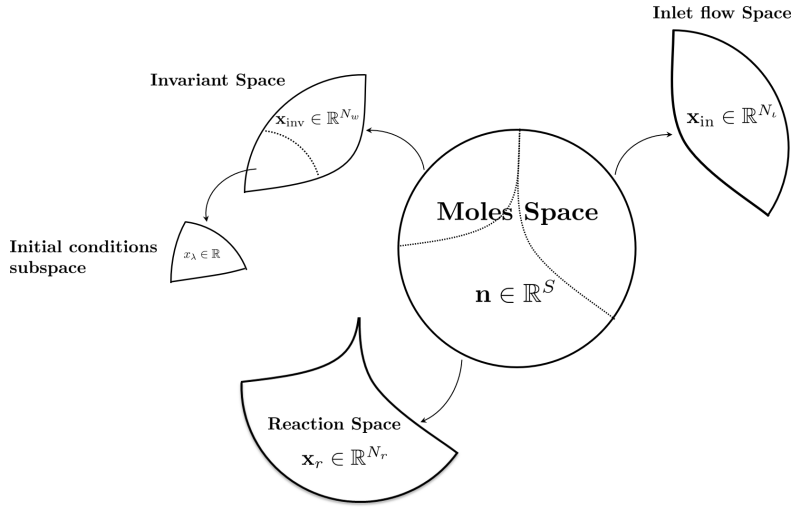


Figure 6.1: Mole-extent subspace decomposition (based on [5]).

The conditions that the linear diffeomorphism \mathbf{T}_0 must satisfy are detailed in Table 6.1

6

Table 6.1: Conditions on the linear diffeomorphism \mathbf{T}_0

Reaction space	Inlet space	Invariant space	Init. cond. subspace
$\mathbf{T}_{1_0}^\top \mathbf{N}^\top = \mathbf{I}_{N_r}$	$\mathbf{T}_{2_0}^\top \mathbf{N}^\top = \mathbf{0}_{N_t \times N_r}$	$\mathbf{T}_{3_0}^\top \mathbf{N}^\top = \mathbf{0}_{N_\varepsilon \times N_r}$	$\mathbf{T}_{4_0}^\top \mathbf{N}^\top = \mathbf{0}_{1 \times N_r}$
$\mathbf{T}_{1_0}^\top \mathbf{X}_{\text{in}} = \mathbf{0}_{N_r \times N_t}$	$\mathbf{T}_{2_0}^\top \mathbf{X}_{\text{in}} = \mathbf{I}_{N_t}$	$\mathbf{T}_{3_0}^\top \mathbf{X}_{\text{in}} = \mathbf{0}_{N_\varepsilon \times N_t}$	$\mathbf{T}_{4_0}^\top \mathbf{X}_{\text{in}} = \mathbf{0}_{1 \times N_t}$
$\mathbf{T}_{1_0}^\top \mathbf{n}_0 = \mathbf{0}_{N_r \times 1}$	$\mathbf{T}_{2_0}^\top \mathbf{n}_0 = \mathbf{0}_{N_t \times 1}$	$\mathbf{T}_{3_0}^\top \mathbf{n}_0 = \mathbf{0}_{N_\varepsilon \times 1}$	$\mathbf{T}_{4_0}^\top \mathbf{n}_0 = 1$

The nonlinear differential equation for the mole balance is transformed to:

$$\dot{\mathbf{x}}_r = \underbrace{\mathbf{T}_{1_0}^\top \mathbf{N}^\top}_{\mathbf{I}_{N_r}} \mathbf{r} + \underbrace{\mathbf{T}_{1_0}^\top \mathbf{X}_{\text{in}}}_{0_{N_r \times N_t}} \mathbf{F}_{\text{in}} - \frac{F_{\text{out}}}{n_L} \mathbf{x}_r, \quad \mathbf{x}_r(0) = \mathbf{T}_{1_0}^\top \mathbf{n}_0 = \mathbf{0}_{N_r} \quad (6.15)$$

$$\dot{\mathbf{x}}_{\text{in}} = \underbrace{\mathbf{T}_{2_0}^\top \mathbf{N}^\top}_{0_{N_t \times N_r}} \mathbf{r} + \underbrace{\mathbf{T}_{2_0}^\top \mathbf{X}_{\text{in}}}_{\mathbf{I}_{N_t}} \mathbf{F}_{\text{in}} - \frac{F_{\text{out}}}{n_L} \mathbf{x}_{\text{in}}, \quad \mathbf{x}_{\text{in}}(0) = \mathbf{T}_{2_0}^\top \mathbf{n}_0 = \mathbf{0}_{N_t} \quad (6.16)$$

$$\dot{\mathbf{x}}_{\text{inv}} = \underbrace{\mathbf{T}_{3_0}^\top \mathbf{N}^\top}_{0_{N_\varepsilon \times N_r}} \mathbf{r} + \underbrace{\mathbf{T}_{3_0}^\top \mathbf{X}_{\text{in}}}_{0_{N_\varepsilon \times N_t}} \mathbf{F}_{\text{in}} - \frac{F_{\text{out}}}{n_L} \mathbf{x}_{\text{inv}}, \quad \mathbf{x}_{\text{inv}}(0) = \mathbf{T}_{3_0}^\top \mathbf{n}_0 = \mathbf{0}_{N_\varepsilon} \quad (6.17)$$

$$\dot{x}_\lambda = \underbrace{\mathbf{T}_{4_0}^\top \mathbf{N}^\top}_{0_{1 \times N_r}} \mathbf{r} + \underbrace{\mathbf{T}_{4_0}^\top \mathbf{X}_{\text{in}}}_{0_{1 \times N_t}} \mathbf{F}_{\text{in}} - \frac{F_{\text{out}}}{n_L} x_\lambda, \quad x_\lambda(0) = \mathbf{T}_{4_0}^\top \mathbf{n}_0 = 1 \quad (6.18)$$

Since $\mathbf{x}_{\text{inv}}(0) = \mathbf{0} \implies \mathbf{x}_{\text{inv}}(t) = \mathbf{0} \ \forall t \geq 0$, it can be left out. The model of the CSTR in terms of extents is:

$$\dot{\mathbf{x}}_r = \mathbf{r} - \frac{F_{\text{out}}}{n_L} \mathbf{x}_r, \quad \mathbf{x}_r(0) = \mathbf{0}_{N_r} \quad (6.19)$$

$$\dot{\mathbf{x}}_{\text{in}} = \mathbf{F}_{\text{in}} - \frac{F_{\text{out}}}{n_L} \mathbf{x}_{\text{in}}, \quad \mathbf{x}_{\text{in}}(0) = \mathbf{0}_{N_e} \quad (6.20)$$

$$\dot{x}_\lambda = -\frac{F_{\text{out}}}{n_L} x_\lambda, \quad x_\lambda(0) = 1 \quad (6.21)$$

Notice the decoupling effect that the extent of reaction and inlet has on the system dynamics. Under this representation, the independent evolution of the reaction, the inlet, and outlet can be easily observed. Finally, the moles can be calculated using the inverse map \mathbf{T}_0^{-1} :

$$\mathbf{n} = \mathbf{T}_0^{-1} \begin{bmatrix} \mathbf{x}_r \\ \mathbf{x}_{\text{in}} \\ x_\lambda \end{bmatrix} \quad (6.22)$$

where $\mathbf{T}_0^{-1} = [\mathbf{N}^\top \quad \mathbf{X}_{\text{in}} \quad \mathbf{n}_0]$.

Remark 6.1: Both of the mole basis and extent basis representations exist individually as vector spaces. This implies that one can choose to work on either basis without any restriction. However, the existence of the linear diffeomorphism $\mathbf{T}_0 : \mathcal{M} \subseteq \mathbb{R}_{\geq 0}^S \mapsto \mathcal{X} = \mathbb{R}^{N_r} \oplus \mathbb{R}^{N_e} \oplus \mathbb{R}^{N_\varepsilon}$ is only guaranteed if the rank conditions 1–4 are satisfied. If the linear diffeomorphism \mathbf{T}_0 does not exist, then the spaces \mathcal{M} and \mathcal{X} are not homeomorphic.

6.4. The inlet composition uncertainty matrix $\Delta \mathbf{X}_{\text{in}}$

The blocks of \mathbf{T} and \mathbf{T}_0 require perfect knowledge of \mathbf{N} , \mathbf{X}_{in} , and \mathbf{n}_0 . However, in many practical situations these matrices are not known exactly, as the reaction stoichiometry might not be fully known, and inlet flows might be contaminated with other species. In this section, we address the second case, i.e. the stoichiometric matrix \mathbf{N} is completely known, while \mathbf{X}_{in} is uncertain. Furthermore, in order to give some structure to the results, we take the following assumption as valid:

Assumption 6.2: The inlet composition matrix is uncertain with respect to known

species in the process, i.e. the contamination cannot be a result of mixing the inlet with species not contained in the chemical reaction at hand.

6.4.1. Properties of \mathbf{X}_{in} and $\Delta\mathbf{X}_{\text{in}}$

Let us define the *assumed* inlet composition matrix as \mathbf{X}_{in}^o , and the *true* inlet composition matrix is $\mathbf{X}_{\text{in}} = \mathbf{X}_{\text{in}}^o + \Delta\mathbf{X}_{\text{in}}$. Due to some physical constraints, both the true \mathbf{X}_{in} , and the assumed \mathbf{X}_{in}^o inlet composition matrices satisfy the following properties:

1. \mathbf{X}_{in} is always a positive matrix.²
2. $\mathbf{1}_S^\top \mathbf{X}_{\text{in}} = \mathbf{1}_{1 \times N_\ell} \Rightarrow \|\mathbf{X}_{\text{in}}\|_1 = 1$
3. $0 \leq x_{i,j} \leq 1 \quad \forall i = 1, \dots, S. \quad \forall j = 1, \dots, \ell$, where $x_{i,j}$ is the i -th species composition in the j -th inlet stream.

As a consequence of the properties of the inlet composition matrix, it follows that

1. $\mathbf{1}_S^\top \Delta\mathbf{X}_{\text{in}} = \mathbf{0}_{1 \times N_\ell}$
2. $|\delta x_{i,j}| \leq 1 \quad \forall i = 1, \dots, S. \quad \forall j = 1, \dots, \ell$, where $\delta x_{i,j}$ is the perturbation to i -th species composition in the j -th inlet stream.

6.4.2. Equivalence between the system and model representations

The difference in the inlet composition matrices between the true and the model induces an error due to their influence on the real and modeled residence times. To show this effect, we assume that the true balance equation of a reaction process system in the mole basis is given by

$$\dot{\mathbf{n}} = \mathbf{N}^\top \mathbf{r} + \mathbf{X}_{\text{in}} \mathbf{F}_{\text{in}} - \varsigma \mathbf{n}, \quad \mathbf{n}(0) = \mathbf{n}_0 \quad (6.23)$$

and the model describing the process is

²A positive matrix is a matrix whose elements are all positive. Note that this is different from a Positive Definite Matrix, which only applies to symmetric matrices.

$$\dot{\mathbf{n}}^\circ = \mathbf{N}^\top \mathbf{r}^\circ + \mathbf{X}_{\text{in}}^\circ \mathbf{F}_{\text{in}} - \varsigma^\circ \mathbf{n}^\circ, \quad \mathbf{n}^\circ(0) = \mathbf{n}_0 \quad (6.24)$$

where $\varsigma = \frac{F_{\text{out}}}{n_L}$ and $\varsigma^\circ = \frac{F_{\text{out}}}{n_L^\circ}$ are the inverse of the residence time of the system and the model. Notice that ς is a time-varying function.

Likewise, the balance equation can be written in the extent basis for both the system and the model. In the case of the system, we have

$$\begin{aligned} \dot{\mathbf{x}}_r &= \mathbf{r}(\mathbf{x}_r, \mathbf{x}_{\text{in}}, x_\lambda) - \varsigma \mathbf{x}_r, & \mathbf{x}_r(0) &= \mathbf{0}_{N_r} \\ \dot{\mathbf{x}}_{\text{in}} &= \mathbf{F}_{\text{in}} - \varsigma \mathbf{x}_{\text{in}}, & \mathbf{x}_{\text{in}}(0) &= \mathbf{0}_{N_r} \\ \dot{\mathbf{x}}_{\text{inv}} &= -\varsigma \mathbf{x}_{\text{inv}}, & \mathbf{x}_{\text{inv}}(0) &= \mathbf{0}_{N_\varepsilon} \\ \dot{x}_\lambda &= -\varsigma x_\lambda, & x_\lambda(0) &= 1 \end{aligned} \quad (6.25)$$

Similarly, the extent representation is

6

$$\begin{aligned} \dot{\mathbf{x}}_r^\circ &= \mathbf{r}^\circ(\mathbf{x}_r^\circ, \mathbf{x}_{\text{in}}^\circ, x_\lambda^\circ) - \varsigma^\circ \mathbf{x}_r^\circ, & \mathbf{x}_r^\circ(0) &= \mathbf{0}_{N_r} \\ \dot{\mathbf{x}}_{\text{in}}^\circ &= \mathbf{F}_{\text{in}} - \varsigma^\circ \mathbf{x}_{\text{in}}^\circ, & \mathbf{x}_{\text{in}}^\circ(0) &= \mathbf{0}_{N_r} \\ \dot{\mathbf{x}}_{\text{inv}}^\circ &= -\varsigma^\circ \mathbf{x}_{\text{inv}}^\circ, & \mathbf{x}_{\text{inv}}^\circ(0) &= \mathbf{0}_{N_\varepsilon} \\ \dot{x}_\lambda^\circ &= -\varsigma^\circ x_\lambda^\circ, & x_\lambda^\circ(0) &= 1 \end{aligned} \quad (6.26)$$

Recall that in Remark 6.1, the mole and extent basis representations exist and they are independent from each other, and are related by a linear diffeomorphism \mathbf{T}_0 . The invertible linear map \mathbf{T}_0° relating (6.24) and (6.26) can be found if \mathbf{N} , $\mathbf{X}_{\text{in}}^\circ$, and \mathbf{n}_0 are known. However, the computation of the linear diffeomorphism between (6.23) and (6.25) cannot be performed directly because \mathbf{X}_{in} is not known. Nonetheless, since $\mathbf{X}_{\text{in}} = \mathbf{X}_{\text{in}}^\circ + \Delta \mathbf{X}_{\text{in}}$, the estimation of \mathbf{X}_{in} is addressed with the estimation of $\Delta \mathbf{X}_{\text{in}}$.

Additionally, it is clear to see from (6.25) and (6.26) that the equivalence of these representations depends on the values of ς and ς° . This is formalized in the following theorem:

Theorem 6.1: Let $\mathbf{F}_{\text{in}} > \mathbf{0}_{N_r}$ and $F_{\text{out}} > 0$ be known and equal for both the system and the model, then the extents \mathbf{x}_{in} , \mathbf{x}_{inv} , and x_λ in the representations (6.25) and (6.26) are equivalent if and only if $\varsigma = \varsigma^\circ \quad \forall t \in [0, \infty)$.

The proof of Theorem 6.1 can be found in Appendix A.

Theorem 6.1 holds trivially for $F_{\text{out}} = 0$ because $\varsigma = \varsigma^\circ = 0$ irrespective of the values of n_L and n_L° . Additionally, it is possible to delineate the conditions when $\varsigma = \varsigma^\circ \neq 0$. This is outlined in the following Lemma

Lemma 6.1 (Conservation of moles in the reaction dynamics): Let the stoichiometric $\mathbf{N} \in \mathbb{R}^{N_r \times S}$ be full row rank, i.e. $\text{rank}(\mathbf{N}) = N_r$. If the S -dimensional column vector of ones $\mathbf{1}_S$ is in the null space of \mathbf{N} , then the total number of moles is conserved by the chemical reaction, and the model and system inverse residence times ς° and ς are equal for all time.

Proof:

Consider the mole balance equations in (6.23) and (6.24), denote $n_L = \mathbf{1}_S^\top \mathbf{n}$ and $n_L^\circ = \mathbf{1}_S^\top \mathbf{n}^\circ$, and recall that $\varsigma = \frac{F_{\text{out}}}{n_L}$ and $\varsigma^\circ = \frac{F_{\text{out}}}{n_L^\circ}$

System:

$$\begin{aligned} \mathbf{1}_S^\top \dot{\mathbf{n}} &= \mathbf{1}_S^\top \mathbf{N}^\top \mathbf{r} + \mathbf{1}_S^\top \mathbf{X}_{\text{in}} \mathbf{F}_{\text{in}} - \frac{F_{\text{out}}}{n_L} \mathbf{1}_S^\top \mathbf{n}, & \mathbf{1}_S^\top \mathbf{n}(0) &= \mathbf{1}_S^\top \mathbf{n}_0 \\ \Rightarrow \quad \dot{n}_L &= \mathbf{1}_S^\top \mathbf{N}^\top \mathbf{r} + \underbrace{\mathbf{1}_{N_r}^\top \mathbf{F}_{\text{in}}}_{F_{\text{in}}} - F_{\text{out}}, & n_L(0) &= n_{L_0} \end{aligned} \quad (6.27)$$

Model

$$\begin{aligned} \mathbf{1}_S^\top \dot{\mathbf{n}}^\circ &= \mathbf{1}_S^\top \mathbf{N}^\top \mathbf{r}^\circ + \mathbf{1}_S^\top \mathbf{X}_{\text{in}}^\circ \mathbf{F}_{\text{in}} - \frac{F_{\text{out}}}{n_L^\circ} \mathbf{1}_S^\top \mathbf{n}^\circ, & \mathbf{1}_S^\top \mathbf{n}^\circ(0) &= \mathbf{1}_S^\top \mathbf{n}_0 \\ \Rightarrow \quad \dot{n}_L^\circ &= \mathbf{1}_S^\top \mathbf{N}^\top \mathbf{r}^\circ + \underbrace{\mathbf{1}_{N_r}^\top \mathbf{F}_{\text{in}}}_{F_{\text{in}}} - F_{\text{out}}, & n_L^\circ(0) &= n_{L_0} \end{aligned} \quad (6.28)$$

Notice that both (6.27) and (6.28) are equal for all time if $\mathbf{1}_S^\top \mathbf{N}^\top = \mathbf{0}_{N_r}^\top$, which is equivalent to requiring that $\mathbf{1}_S \in \ker(\mathbf{N}^\top)$ and the total number of moles is solely dominated by the total inlet and outlet flows. Since \mathbf{F}_{in} and F_{out} are known and equal for both model and system for all time, then $\mathbf{n}_L = \mathbf{n}_L^\circ \Rightarrow \varsigma = \varsigma^\circ \quad \forall t > 0$

It is worth noting that since \mathbf{N} is full row rank, \mathbf{N}^\top is full column rank, and thus $\ker(\mathbf{N}^\top) = \text{span}\{\mathbf{0}_{N_r}\}$. Therefore, the reaction vector $\mathbf{r} \notin \ker(\mathbf{N}^\top)$.

6.5. Estimating $\Delta\mathbf{X}_{\text{in}}$ from mole measurement in a semi-batch reactor

Let the mole balance in a semi-batch be given as in (6.8) and let $\varsigma = \varsigma^\circ = \frac{F_{\text{out}}}{n_L} = 0$. It follows by Theorem 6.1, the estimation can be done using the system's true extent representation or the model extent representation because both inverse residence times are equal. We assume again that the inlet composition matrix of the true system has inlet composition matrix $\mathbf{X}_{\text{in}} = \mathbf{X}_{\text{in}}^\circ + \Delta\mathbf{X}_{\text{in}}$. Suppose that we can perform noise-free measurements of the true moles \mathbf{n} of all the species in the reactor.

Let the representation of the system in terms of the *true* extents be given by

True extents

$$\dot{\mathbf{x}}_r = \mathbf{r}(\mathbf{x}_r, \mathbf{x}_{\text{in}}, x_\lambda), \quad \mathbf{x}_r(0) = \mathbf{0}_{N_r} \quad (6.29)$$

$$\dot{\mathbf{x}}_{\text{in}} = \mathbf{F}_{\text{in}}, \quad \mathbf{x}_{\text{in}}(0) = \mathbf{0}_{N_t} \quad (6.30)$$

$$\dot{\mathbf{x}}_{\text{inv}} = \mathbf{0}_{N_\varepsilon}, \quad \mathbf{x}_{\text{inv}}(0) = \mathbf{0}_{N_\varepsilon} \quad (6.31)$$

$$\dot{x}_\lambda = 0, \quad x_\lambda(0) = 1 \quad (6.32)$$

Integrating (6.30)–(6.32)

$$\mathbf{x}_{\text{in}} = \int_0^t \mathbf{F}_{\text{in}}(\tau) \, d\tau$$

$$\mathbf{x}_{\text{inv}} = \mathbf{0}_{N_\varepsilon}$$

$$x_\lambda = 1$$

Let the linear transformations \mathbf{T}_{01}° , \mathbf{T}_{02}° , \mathbf{T}_{03}° , and \mathbf{T}_{04}° be computed based on the model information, i.e. \mathbf{N} , $\mathbf{X}_{\text{in}}^\circ$, and \mathbf{n}_0 . We apply these transformations to the mole representation of the system in (6.23) to obtain the following set of equations:

Pseudo-extents

$$\dot{\mathbf{w}}_r = \mathbf{r}(\mathbf{w}_r, \mathbf{w}_{\text{in}}, w_\lambda) + \mathbf{T}_{10}^{\circ\top} \Delta\mathbf{X}_{\text{in}} \mathbf{F}_{\text{in}}, \quad \mathbf{w}_r(0) = 0 \quad (6.33)$$

$$\dot{\mathbf{w}}_{\text{in}} = \left(\mathbf{I}_{N_r} + \mathbf{T}_{20}^{\circ\top} \Delta\mathbf{X}_{\text{in}} \right) \mathbf{F}_{\text{in}}, \quad \mathbf{w}_{\text{in}}(0) = 0 \quad (6.34)$$

$$\dot{\mathbf{w}}_{\text{inv}} = \mathbf{T}_{30}^{\circ\top} \Delta\mathbf{X}_{\text{in}} \mathbf{F}_{\text{in}}, \quad \mathbf{w}_{\text{inv}}(0) = 0 \quad (6.35)$$

$$\dot{w}_\lambda = \mathbf{T}_{40}^{\circ\top} \Delta\mathbf{X}_{\text{in}} \mathbf{F}_{\text{in}}, \quad w_\lambda(0) = 1 \quad (6.36)$$

These variables \mathbf{w} do not represent the true extents \mathbf{x} of the system. The dynamics are not fully decoupled due to the presence of $\Delta\mathbf{X}_{\text{in}}$ in the representation. Nevertheless, the initial conditions of the transformed system are the same because these are known quantities.

Likewise, we integrate (6.34)–(6.36). Thus

6

$$\mathbf{w}_{\text{in}} = \mathbf{w}_{\text{in}}(0) + \int_0^t \mathbf{F}_{\text{in}}(\tau) \, d\tau + \mathbf{T}_{20}^{\circ\top} \Delta\mathbf{X}_{\text{in}} \int_0^t \mathbf{F}_{\text{in}}(\tau) \, d\tau = \mathbf{x}_{\text{in}} + \mathbf{T}_{20}^{\circ\top} \Delta\mathbf{X}_{\text{in}} \mathbf{x}_{\text{in}} \quad (6.37)$$

$$\mathbf{w}_{\text{inv}} = \mathbf{w}_{\text{inv}}(0) + \mathbf{T}_{30}^{\circ\top} \Delta\mathbf{X}_{\text{in}} \int_0^t \mathbf{F}_{\text{in}}(\tau) \, d\tau = \mathbf{T}_{30}^{\circ\top} \Delta\mathbf{X}_{\text{in}} \mathbf{x}_{\text{in}} \quad (6.38)$$

$$w_\lambda = w_\lambda(0) + \mathbf{T}_{40}^{\circ\top} \Delta\mathbf{X}_{\text{in}} \int_0^t \mathbf{F}_{\text{in}}(\tau) \, d\tau = 1 + \mathbf{T}_{40}^{\circ\top} \Delta\mathbf{X}_{\text{in}} \mathbf{x}_{\text{in}} \quad (6.39)$$

The equations (6.37)–(6.39) are equivalent to

$$\begin{bmatrix} \mathbf{w}_{\text{in}} - \mathbf{x}_{\text{in}} \\ \mathbf{w}_{\text{inv}} \\ w_\lambda - 1 \end{bmatrix} = \begin{bmatrix} \mathbf{T}_{20}^\top \\ \mathbf{T}_{30}^\top \\ \mathbf{T}_{40}^\top \end{bmatrix} \Delta\mathbf{X}_{\text{in}} \mathbf{x}_{\text{in}} \Leftrightarrow \text{vec} \left(\begin{bmatrix} \mathbf{w}_{\text{in}} - \mathbf{x}_{\text{in}} \\ \mathbf{w}_{\text{inv}} \\ w_\lambda - 1 \end{bmatrix} \right) = \left(\mathbf{x}_{\text{in}}^\top \otimes \begin{bmatrix} \mathbf{T}_{20}^{\circ\top} \\ \mathbf{T}_{30}^{\circ\top} \\ \mathbf{T}_{40}^{\circ\top} \end{bmatrix} \right) \text{vec} (\Delta\mathbf{X}_{\text{in}}) \quad (6.40)$$

We can set up constrained optimization based on (6.40)

$$\begin{aligned} \min_{\delta} \quad & \frac{1}{2} \|\mathbf{E} - \mathbf{D}\delta\|_2 \\ \text{s.t.} \quad & \begin{cases} \mathbf{1}_{SN_\ell}^\top \delta = 0 \\ \delta \geq -\text{vec}(\mathbf{X}_{\text{in}}^\circ) \\ \delta \leq \mathbf{1}_{SN_\ell} \end{cases} \end{aligned} \quad (6.41)$$

where $\delta = \text{vec}(\Delta\mathbf{X}_{\text{in}})$, $\mathbf{D} = \left(\mathbf{x}_{\text{in}}^\top \otimes \begin{bmatrix} \mathbf{T}_{20}^{\circ\top} \\ \mathbf{T}_{30}^{\circ\top} \\ \mathbf{T}_{40}^{\circ\top} \end{bmatrix} \right)$, and $\mathbf{E} = \begin{bmatrix} \mathbf{w}_{\text{in}} - \mathbf{x}_{\text{in}} \\ \mathbf{w}_{\text{inv}} \\ w_\lambda - 1 \end{bmatrix}$

The solution of the optimization (6.41), provides the estimate $\hat{\delta}$. This estimation allows us to retrieve $\Delta\mathbf{X}_{\text{in}}$.

$$\Delta\hat{\mathbf{X}}_{\text{in}} = \text{vec}_{S,N_\ell}^{-1}(\hat{\delta}) \quad (6.42)$$

6

6.6. Estimating $\Delta\mathbf{X}_{\text{in}}$ from mole measurement in a continuous stirred-tank reactor

In this section, we extend the previous result to a continuous stirred-tank reactor. Due to the presence of an outlet flow ($F_{\text{out}} > 0$), $\varsigma^\circ > 0$ and $\varsigma > 0$. Due to Theorem 6.1 and Lemma 6.1, both process and model inverse residence times $\varsigma \neq \varsigma^\circ \forall t \in (0, \infty)$; we assume that ς is can be measured. As in the previous case, the stoichiometric matrix \mathbf{N} and the inlet composition matrix $\mathbf{X}_{\text{in}}^\circ$ are known, except that the real system has a perturbed inlet composition matrix $\Delta\mathbf{X}_{\text{in}}$. Finally, we assume that the reacting mixture is homogeneous and well-stirred.

In general, the estimation of $\Delta\mathbf{X}_{\text{in}}$ can only be done using the system's true extent representation in (6.25) due to Theorem 6.1. With the exception of specific cases where Lemma 6.1 holds, inverse residence times of the system and the model are different, and the error convergence to zero cannot be guaranteed.

True extents

$$\dot{\mathbf{x}}_r = \mathbf{r}(\mathbf{x}_r, \mathbf{x}_{\text{in}}, x_\lambda) - \varsigma \mathbf{x}_r, \quad \mathbf{x}_r(0) = \mathbf{0}_{N_r} \quad (6.43)$$

$$\dot{\mathbf{x}}_{\text{in}} = \mathbf{F}_{\text{in}} - \varsigma \mathbf{x}_{\text{in}}, \quad \mathbf{x}_{\text{in}}(0) = \mathbf{0}_{N_t} \quad (6.44)$$

$$\dot{\mathbf{x}}_{\text{inv}} = -\varsigma \mathbf{x}_{\text{inv}}, \quad \mathbf{x}_{\text{inv}}(0) = \mathbf{0}_{N_\varepsilon} \quad (6.45)$$

$$\dot{x}_\lambda = -\varsigma x_\lambda, \quad x_\lambda(0) = 1 \quad (6.46)$$

Integrating (6.44)–(6.46)

$$\begin{aligned} \mathbf{x}_{\text{in}} &= \int_0^t \Phi_{N_t}(t, \tau) \mathbf{F}_{\text{in}}(\tau) \, d\tau \\ \mathbf{x}_{\text{inv}} &= \mathbf{0}_{N_\varepsilon} \\ x_\lambda &= \Phi(t, 0) \end{aligned}$$

6

where $\Phi_{N_t}(t, \tau) = \exp \left(- \int_\tau^t \varsigma(s) \mathbf{I}_{N_t} \, ds \right)$

As in the semi-batch case, the linear transformations \mathbf{T}_{01}° , \mathbf{T}_{02}° , \mathbf{T}_{03}° , and \mathbf{T}_{04}° are computed based on the model information, and applied to the mole representation of the system in (6.23) to obtain a pseudo-extent representation:

Pseudo-extents

$$\dot{\mathbf{w}}_r = \mathbf{r}(\mathbf{w}_r, \mathbf{w}_{\text{in}}, w_\lambda) + \mathbf{T}_{10}^{\circ\top} \Delta\mathbf{X}_{\text{in}} \mathbf{F}_{\text{in}} - \varsigma \mathbf{w}_r, \quad \mathbf{w}_r(0) = \mathbf{0}_{N_r} \quad (6.47)$$

$$\dot{\mathbf{w}}_{\text{in}} = \left(\mathbf{I}_{N_t} + \mathbf{T}_{20}^{\circ\top} \Delta\mathbf{X}_{\text{in}} \right) \mathbf{F}_{\text{in}} - \varsigma \mathbf{w}_{\text{in}}, \quad \mathbf{w}_{\text{in}}(0) = \mathbf{0}_{N_t} \quad (6.48)$$

$$\dot{\mathbf{w}}_{\text{inv}} = \mathbf{T}_{30}^{\circ\top} \Delta\mathbf{X}_{\text{in}} \mathbf{F}_{\text{in}} - \varsigma \mathbf{w}_{\text{inv}}, \quad \mathbf{w}_{\text{inv}}(0) = \mathbf{0}_{N_\varepsilon} \quad (6.49)$$

$$\dot{w}_\lambda = \mathbf{T}_{40}^{\circ\top} \Delta\mathbf{X}_{\text{in}} \mathbf{F}_{\text{in}} - \varsigma w_\lambda, \quad w_\lambda(0) = 1 \quad (6.50)$$

Integrate (6.48)–(6.50)

$$\mathbf{w}_{\text{in}} = \underbrace{\int_0^t \Phi_{N_\varepsilon}(t, \tau) \mathbf{F}_{\text{in}}(\tau) \, d\tau}_{\mathbf{x}_{\text{in}}} + \int_0^t \Phi_{N_\varepsilon}(t, \tau) \mathbf{T}_{2_0}^{\circ\top} \Delta \mathbf{X}_{\text{in}} \mathbf{F}_{\text{in}}(\tau) \, d\tau \quad (6.51)$$

$$\mathbf{w}_{\text{inv}} = \int_0^t \Phi_{N_\varepsilon}(t, \tau) \mathbf{T}_{3_0}^{\circ\top} \Delta \mathbf{X}_{\text{in}} \mathbf{F}_{\text{in}}(\tau) \, d\tau \quad (6.52)$$

$$w_\lambda = \Phi(t, 0) + \int_0^t \Phi(t, \tau) \mathbf{T}_{4_0}^{\circ\top} \Delta \mathbf{X}_{\text{in}} \mathbf{F}_{\text{in}}(\tau) \, d\tau \quad (6.53)$$

where $\Phi_{N_\varepsilon}(t, \tau) = \exp \left(- \int_\tau^t \varsigma(s) \mathbf{I}_{N_\varepsilon} \, ds \right)$ and $\Phi(t, \tau) = \exp \left(- \int_\tau^t \varsigma(s) \, ds \right)$.

Using the properties of the Kronecker product and the vectorization operator, the system of equations in (6.51)–(6.53) is equivalent to:

$$\begin{bmatrix} \mathbf{w}_{\text{in}} - \mathbf{x}_{\text{in}} \\ \mathbf{w}_{\text{inv}} \\ w_\lambda - x_\lambda \end{bmatrix} = \int_0^t F_{\text{in}}^\top(\tau) \otimes \Phi_{N_\varepsilon + N_\varepsilon + 1}(t, \tau) \, d\tau \begin{pmatrix} \mathbf{I}_{N_\varepsilon} \otimes \begin{bmatrix} \mathbf{T}_{2_0}^{\circ\top} \\ \mathbf{T}_{3_0}^{\circ\top} \\ \mathbf{T}_{4_0}^{\circ\top} \end{bmatrix} \end{pmatrix} \text{vec}(\Delta \mathbf{X}_{\text{in}}) \quad (6.54)$$

Equation (6.54) is linear in the vector $\boldsymbol{\delta} = \text{vec}(\Delta \mathbf{X}_{\text{in}})$. However, in order to estimate $\boldsymbol{\delta}$, it is necessary to calculate the value of the integral. This integral can be expressed in terms of \mathbf{x}_{in} as

$$\int_0^t F_{\text{in}}^\top(\tau) \otimes \Phi_{N_\varepsilon + N_\varepsilon + 1}(t, \tau) \, d\tau = (\mathbf{x}_{\text{in}}^\top \otimes \mathbf{I}_{N_\varepsilon + N_\varepsilon + 1}) \quad (6.55)$$

The details of the equality in (6.55) are provided in Appendix A.

Replacing (6.55) in (6.54), we arrive at the same expression obtained for the semi-batch case:

$$\begin{bmatrix} \mathbf{w}_{\text{in}} - \mathbf{x}_{\text{in}} \\ \mathbf{w}_{\text{inv}} \\ w_\lambda - x_\lambda \end{bmatrix} = \left(\mathbf{x}_{\text{in}}^\top \otimes \begin{bmatrix} \mathbf{T}_{2_0}^{\circ\top} \\ \mathbf{T}_{3_0}^{\circ\top} \\ \mathbf{T}_{4_0}^{\circ\top} \end{bmatrix} \right) \text{vec}(\Delta \mathbf{X}_{\text{in}}) \quad (6.56)$$

Analogous to the semi-batch case, a constrained optimization is set up based on (6.56)

$$\begin{aligned} \min_{\delta} \quad & \frac{1}{2} \|\mathbf{E} - \mathbf{D}\delta\|_2 \\ \text{s.t.} \quad & \begin{cases} \mathbf{1}_{SN_\ell}^\top \delta = 0 \\ \delta \geq -\text{vec}(\mathbf{X}_{\text{in}}^\circ) \\ \delta \leq \mathbf{1}_{SN_\ell} \end{cases} \end{aligned} \quad (6.57)$$

where $\delta = \text{vec}(\Delta \mathbf{X}_{\text{in}})$, $\mathbf{D} = \left(\mathbf{x}_{\text{in}}^\top \otimes \begin{bmatrix} \mathbf{T}_{20}^{\circ\top} \\ \mathbf{T}_{30}^{\circ\top} \\ \mathbf{T}_{40}^{\circ\top} \end{bmatrix} \right)$, and $\mathbf{E} = \begin{bmatrix} \mathbf{w}_{\text{in}} - \mathbf{x}_{\text{in}} \\ \mathbf{w}_{\text{inv}} \\ w_\lambda - x_\lambda \end{bmatrix}$

whose solution $\hat{\delta}$ allows us to retrieve the estimate $\Delta \hat{\mathbf{X}}_{\text{in}}$ in the same fashion as in the semi-batch case using (6.57).

The solutions to both optimization problems (6.41) and (6.57) are not unique because the matrix \mathbf{D} in the optimization problems is not full column rank. This is because we explicitly left out the extents of reaction from the calculation. The extent of reaction depends on the vector of chemical rates \mathbf{r} , which is a nonlinear function of unknown value, whose integral over time is finite but not zero based on Assumption 6.1. In general, the optimization will find the solution with the smallest norm, which is sufficient for the purposes of obtaining an estimate of the true inlet composition matrix.

6.7. Estimation of moles, reaction rate, and chemical kinetic parameters

One important aspect of reaction system is the estimation of the reaction rate \mathbf{r} and the chemical kinetic parameters. The estimation of chemical kinetic parameters have been addressed several times in literature using the extent representation due to its decoupling effect ([23],[169],[24],[146],[189]). All of these approaches have assumed perfect knowledge of the matrices required to construct the linear transformation \mathbf{T} . However, the estimation of these kinetic parameter is severely affected by the accuracy of the transformation. For example, if the inlet flows to the reactor come from another process or a recycle, then the composition matrix varies over time and will result in erroneous estimates of the internal states of the process. The

uncertainty in the inlet composition matrix is addressed in this section, where an approach to estimate the vector of moles \mathbf{n} , the chemical reaction rate \mathbf{r} , and the kinetic parameters is proposed.

In the previous sections, we have only considered the mass (mole) balance in the reactor, assuming that the process is isothermal. However, in this section, a more general setting can be assumed allowing temperature variations.

Consider the general enthalpy balance in the CSTR with a well-stirred mixture of S species, N_r independent reactions, N_t independent inlet flows and one outlet flow:

$$\dot{H} = \mathbf{h}_{\text{in}}^\top \mathbf{F}_{\text{in}} - F_{\text{out}} H + \dot{q}_{\text{ext}} + (P - P_0) \dot{V}_{\text{ol}} + V_{\text{ol}} \dot{P} \quad (6.58)$$

Hoang *et al.* [73] showed that if mixture is homogeneous, ideal, and incompressible then $h_i = h_{\text{ref}_i} + C_{p_i}(T - T_{\text{ref}})$, $P = P_0 = \text{constant} \Rightarrow \dot{P} = 0$, and thus (6.58) is equivalent to the heat balance:

$$\dot{Q} = \mathbf{q}_{\text{in}}^\top \mathbf{F}_{\text{in}} - F_{\text{out}} Q - \Delta \mathbf{H}^{\ominus^\top} \mathbf{r} - \dot{Q}_{\text{ext}} \quad (6.59)$$

where $q_{\text{in}_i} = C_{p_{\text{in}_i}}(T_{\text{in}} - T_{\text{ref}})$ is the molar heat of the inlet flows, $Q = C_{p_l}(T - T_{\text{ref}})$ is the total heat of the mixture, $\Delta \mathbf{H}^{\ominus} = \mathbf{N} \mathbf{h}_{\text{ref}}$ is the heat of reaction, and C_p is the molar heat capacity.

Rewriting (6.59) in terms of the temperature T , letting $T_{\text{ref}} = 0$, and adjoining the mole balance equation in (6.8), we get the full description of a non-isothermal CSTR

$$\dot{\mathbf{n}} = \mathbf{N}^\top \mathbf{r} + \mathbf{X}_{\text{in}} \mathbf{F}_{\text{in}} - \frac{F_{\text{out}}}{n_L} \mathbf{n}, \quad \mathbf{n}(0) = \mathbf{n}_0 \quad (6.60a)$$

$$\dot{T} = \frac{1}{n_L C_{p_l}} \left(\mathbf{C}_{p_{\text{in}}}^\top T_{\text{in}} \mathbf{F}_{\text{in}} - C_{p_l} F_{\text{out}} T - \Delta \mathbf{H}^{\ominus^\top} \mathbf{r} + \dot{Q}_{\text{ext}} \right), \quad T(0) = T_0 \quad (6.60b)$$

The balance equations in (6.60a) and (6.60b) can be written in matrix form as

$$\begin{bmatrix} \dot{\mathbf{n}} \\ \dot{T} \end{bmatrix} = -\varsigma \mathbf{I}_{S+1} \begin{bmatrix} \mathbf{n} \\ T \end{bmatrix} + \begin{bmatrix} \mathbf{X}_{\text{in}} & \mathbf{0}_{N_t} \\ \boldsymbol{\alpha} & \gamma \end{bmatrix} \begin{bmatrix} \mathbf{F}_{\text{in}} \\ \dot{Q}_{\text{ext}} \end{bmatrix} + \begin{bmatrix} \mathbf{N}^\top \\ \boldsymbol{\beta} \end{bmatrix} \mathbf{r} \quad (6.61)$$

where $\boldsymbol{\alpha}(t) = \frac{\mathbf{C}_{p_{\text{in}}}^\top T_{\text{in}}}{n_L C_{p_l}}$, $\boldsymbol{\beta}(t) = -\frac{\Delta \mathbf{H}^{\ominus^\top}}{n_L C_{p_l}}$, and $\gamma(t) = \frac{1}{n_L C_{p_l}}$.

Assumption 6.3: The time-varying parameters α , β , and γ vary very slowly and can be considered constant during a sufficiently long time window.

The equivalent extent representation of (6.61)

$$\begin{bmatrix} \dot{\mathbf{x}}_r \\ \dot{\mathbf{x}}_{\text{in}} \\ \dot{x}_\lambda \\ \dot{T} \end{bmatrix} = \underbrace{\begin{bmatrix} -\varsigma \mathbf{I}_{N_r} & & & \\ & -\varsigma \mathbf{I}_{N_\ell} & & \\ & & -\varsigma & \\ & & & -\varsigma \end{bmatrix}}_{\mathbf{A}(\varsigma)} \begin{bmatrix} \mathbf{x}_r \\ \mathbf{x}_{\text{in}} \\ x_\lambda \\ T \end{bmatrix} + \underbrace{\begin{bmatrix} \mathbf{0} & 0 \\ \mathbf{I}_{N_\ell} & 0 \\ \mathbf{0} & 0 \\ \alpha & \gamma \end{bmatrix}}_{\mathbf{B}} \begin{bmatrix} \mathbf{F}_{\text{in}} \\ \dot{Q}_{\text{ext}} \end{bmatrix} + \underbrace{\begin{bmatrix} \mathbf{I}_{N_r} \\ \mathbf{0} \\ \mathbf{0} \\ \beta \end{bmatrix}}_{\mathbf{B}_d} \mathbf{r} \quad (6.62)$$

$$\begin{bmatrix} \mathbf{n}_m \\ T \end{bmatrix} = \underbrace{\begin{bmatrix} \mathbf{N}_m^\top & \mathbf{X}_{\text{in},m} & \mathbf{n}_{0,m} & 0 \\ \mathbf{0} & \mathbf{0} & 0 & 1 \end{bmatrix}}_{\mathbf{C}_m} \begin{bmatrix} \mathbf{x}_r \\ \mathbf{x}_{\text{in}} \\ x_\lambda \\ T \end{bmatrix}$$

In order to perform the estimation of the vector of moles \mathbf{n} and the vector of chemical rates \mathbf{r} , we introduce a sequential state and disturbance estimation strategy ([116],[113]). The sequential strategy consists of an asymptotic observer (AO) to estimate the number of moles, and a parametric reaction rate estimator (RRE) to determine the reaction rate \mathbf{r} . The estimation scheme is shown in Figure 6.2

6

This scheme works under the following assumption:

Assumption 6.4: The inverse residence time ς , the mixture's temperature T , and the number of moles of S_m components $\mathbf{n}_m \in \mathbb{R}^m$ are measured, where $S_m < S$. This implies that the moles of $S - S_m$ components \mathbf{n}_{um} are not measured, mathematically the number of moles \mathbf{n} can be written as,

$$\mathbf{n} = \begin{bmatrix} \mathbf{n}_m \\ \mathbf{n}_{um} \end{bmatrix} = \begin{bmatrix} \mathbf{N}_m^\top \\ \mathbf{N}_{um}^\top \end{bmatrix} \mathbf{x}_r + \begin{bmatrix} \mathbf{X}_{\text{in},m} \\ \mathbf{X}_{\text{in},um} \end{bmatrix} \mathbf{x}_{\text{in}} + \begin{bmatrix} \mathbf{n}_{0,m} \\ \mathbf{n}_{0,um} \end{bmatrix} x_\lambda \quad (6.63)$$

where $\mathbf{N}_m \in \mathbb{R}^{N_r \times S_m}$, $\mathbf{N}_{um} \in \mathbb{R}^{N_r \times (S-S_m)}$, $\mathbf{X}_{\text{in},m}^\top \in \mathbb{R}^{N_\ell \times S_m}$, $\mathbf{X}_{\text{in},um}^\top \in \mathbb{R}^{N_\ell \times (S-S_m)}$, $\mathbf{n}_{0,m}^\top \in \mathbb{R}^{1 \times S_m}$, and $\mathbf{n}_{0,um}^\top \in \mathbb{R}^{1 \times (S-S_m)}$.

Therefore, the estimation of $\mathbf{n}_{um} \in \mathbb{R}^{S-S_m}$ is necessary to reconstruct the extent of reaction \mathbf{x}_r , the extents of inlet \mathbf{x}_{in} , the discounting factor x_λ , and the reaction rate r based on the knowledge of \mathbf{n}_m and \mathbf{T} . Finally, the conditions for the estimation of \mathbf{n}_{um} are given in the next theorem,

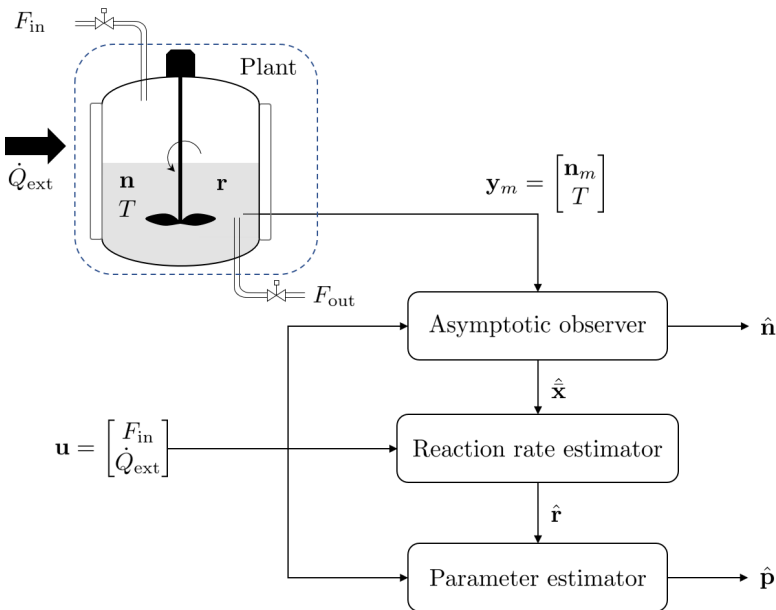


Figure 6.2: Sequential state and reaction rate estimation estimation strategy

6

Theorem 6.2: Consider the homogeneous reaction system given by the set of (6.62), where the reaction rate vector r is assumed as a bounded disturbance. If

$$\text{rank} \left(\begin{bmatrix} N_m^\top & X_{in_m} & n_{0m} & 0 \\ \mathbf{0} & \mathbf{0} & 0 & 1 \end{bmatrix} \right) = N_r + N_t + 2$$

and $\varsigma \neq 0$, the system (6.62) is always observable.

The proof of Theorem 6.2 can be found in Appendix A. A direct consequence of this theorem is the minimum number of measured species in the process:

Corollary 6.1: If $\text{rank}(C_m) = N_r + N_t + 2$ by Theorem 6.2 the system is observable and the number of measured species is $S_m \geq N_r + N_t + 1$.

6.7.1. Asymptotic observer

To construct the AO, let us introduce the change of variable $x_T = \beta x_r + T$. Differentiating the former expression with respect to time, and replacing in (6.62), the following equation is obtained:

$$\dot{x}_T = -\varsigma x_T + \alpha \mathbf{F}_{\text{in}} + \gamma \dot{Q}_{\text{ext}} \quad (6.64)$$

Notice that x_T has a physical meaning, and corresponds to the reaction-invariant heat space. The resulting overall dynamics become

$$\begin{aligned} \begin{bmatrix} \dot{\mathbf{x}}_{\text{in}} \\ \dot{x}_\lambda \\ \dot{x}_T \end{bmatrix} &= \begin{bmatrix} -\varsigma \mathbf{I}_{N_\ell} & & \\ & -\varsigma & \\ & & -\varsigma \end{bmatrix} \begin{bmatrix} \mathbf{x}_{\text{in}} \\ x_\lambda \\ x_T \end{bmatrix} + \begin{bmatrix} \mathbf{I}_{N_\ell} & 0 \\ \mathbf{0} & 0 \\ \alpha & \gamma \end{bmatrix} \begin{bmatrix} \mathbf{F}_{\text{in}} \\ \dot{Q}_{\text{ext}} \end{bmatrix} \\ \begin{bmatrix} \mathbf{n} \\ T \end{bmatrix} &= \left[\begin{array}{cc|c} \mathbf{X}_{\text{in}_m} & \mathbf{n}_{0_m} & \\ \mathbf{0} & 0 & \end{array} \right] \begin{bmatrix} \mathbf{x}_{\text{in}} \\ x_\lambda \\ x_T \end{bmatrix} + \mathbf{C}_T \mathbf{v}_\Upsilon \end{aligned} \quad (6.65)$$

where $\mathbf{C}_T = \begin{bmatrix} \mathbf{N}^\top & \mathbf{0} \\ \mathbf{0} & 1 \end{bmatrix}$, $\Upsilon = [\beta \ 1]$ and $\mathbf{v}_\Upsilon \in \ker(\Upsilon)$.

The model (6.65) is now suitable to develop the asymptotic observer, and it does not contain the nonlinearities arising from the reaction rate \mathbf{r} . Since the inverse residence time ς , and the inputs \mathbf{F}_{in} and \dot{Q}_{ext} are known, we can use (6.65) to obtain an online computation of $\hat{\mathbf{x}}_{\text{in}}$, \hat{x}_λ , and \hat{x}_T . Based on these estimation, the reconstruction of the extent of reaction $\hat{\mathbf{x}}_r$ is given by

$$\hat{\mathbf{x}}_r = \mathbf{N}^{\top+} (\mathbf{n}_m - \mathbf{X}_{\text{in}_m} \hat{\mathbf{x}}_{\text{in}} - \mathbf{n}_{0_m} \hat{x}_\lambda) \quad (6.66)$$

The advantage of using this representation is that no direct information of the reaction rate \mathbf{r} is necessary. The existence of the left-pseudoinverse of \mathbf{N}_m^\top is guaranteed if and only if $\text{rank}(\mathbf{N}_m) = N_r$. However, by Corollary 6.1, the number of measured species is $S_m \geq N_r + N_\ell + 1$, and therefore, $\mathbf{N}_m^{\top+}$ is defined. Moreover, the asymptotic estimator is stable and convergent if $\varsigma > 0$ [14]. This condition is equivalent to the detectability condition of the model (6.62) [113].

Likewise, the estimated vector moles $\hat{\mathbf{n}}$ is

$$\hat{\mathbf{n}} = \mathbf{N}^\top \hat{\mathbf{x}}_r + \mathbf{X}_{\text{in}} \hat{\mathbf{x}}_{\text{in}} + \mathbf{n}_0 \hat{x}_\lambda \quad (6.67)$$

Another advantage of the design presented here is that it uses temperature measurements rather than enthalpy measurement, exploiting the transformation variable Υ to reconstruct the states. In general, this facilitates implementation, since enthalpy measurement are generally not available during plant operation. This particular

feature differs from other similar AO structures in literature (see for example [21], [43]).

It is worth noting that to compute the vector $\hat{\mathbf{n}}$, it is necessary to have perfect knowledge of \mathbf{N} , \mathbf{X}_{in} , and \mathbf{n}_0 . However, in some instances, the inlet composition matrix \mathbf{X}_{in} can be uncertain. Therefore, it is important to estimate the inlet composition matrix.

6.7.2. Estimation of \mathbf{x}_r for uncertain \mathbf{X}_{in}

Let the true inlet composition matrix be $\mathbf{X}_{\text{in}} = \mathbf{X}_{\text{in}}^\circ + \Delta\mathbf{X}_{\text{in}}$, where $\mathbf{X}_{\text{in}}^\circ$ is an assumed inlet composition matrix, and $\Delta\mathbf{X}_{\text{in}}$ is the inlet composition uncertainty matrix. These matrices have the properties listed in Section 6.4 respectively.

The estimate $\hat{\mathbf{x}}_r$ in (6.66) can be written in terms of $\mathbf{X}_{\text{in}}^\circ$ and $\Delta\mathbf{X}_{\text{in}}$ as

$$\begin{aligned}\hat{\mathbf{x}}_r &= \mathbf{N}_m^{\top+} (\mathbf{n}_m - \mathbf{X}_{\text{in},m} \hat{\mathbf{x}}_{\text{in}} - \mathbf{n}_{0,m} \hat{x}_\lambda) \\ &= \underbrace{\mathbf{N}_m^{\top+} (\mathbf{n}_m - \mathbf{X}_{\text{in},m}^\circ \hat{\mathbf{x}}_{\text{in}} - \mathbf{n}_{0,m} \hat{x}_\lambda)}_{\hat{\mathbf{x}}_r} - \mathbf{N}_m^{\top+} \Delta\mathbf{X}_{\text{in},m} \hat{\mathbf{x}}_{\text{in}}\end{aligned}\quad (6.68)$$

where $\hat{\mathbf{x}}_r$ is the estimation of the extent of reaction based on the information of $\mathbf{X}_{\text{in}}^\circ$.

In order to estimate the measured part of the uncertainty matrix, we can use the measured vector of moles \mathbf{n}_m . Let us write the transformation matrices of the measured portions $\mathbf{T}_{0,m}^\circ$ as follows:

$$\mathbf{T}_{1_{0,m}}^\top = (\mathbf{Q}_{\text{in},m} \mathbf{N}_m^\top)^+ \mathbf{Q}_{\text{in},m} \quad (6.69)$$

$$\mathbf{T}_{2_{0,m}}^\top = (\mathbf{Q}_{r,m} \mathbf{X}_{\text{in},m})^+ \mathbf{Q}_{r,m} \quad (6.70)$$

$$\mathbf{T}_{3_{0,m}}^\top = \mathbf{Q}_{r,\text{in},m} \left(\mathbf{I}_{S_m} - [\mathbf{N}_m^\top \quad \mathbf{X}_{\text{in},m}] \begin{bmatrix} \mathbf{N}_m^{\top+} \\ \mathbf{X}_{\text{in},m}^{\top+} \end{bmatrix} \right) \quad (6.71)$$

$$\mathbf{T}_{4_{0,m}}^\top = \mathbf{e}_{S_m}^\top (S_m) [\mathbf{N}_m^\top \quad \mathbf{X}_{\text{in},m}^\circ \quad \mathbf{n}_{0,m}]^+ \quad (6.72)$$

where $\mathbf{e}_{S_m}(S_m)$ is the S_m -dimensional unit vector whose S_m -th entry is 1 and zero elsewhere, $\mathbf{Q}_{\text{in},m} \in \ker([\mathbf{X}_{\text{in},m}^\circ \quad \mathbf{n}_{0,m}]^\top)$, $\mathbf{Q}_{r,m} \in \ker([\mathbf{N}_m^\top \quad \mathbf{n}_{0,m}]^\top)$, and $\mathbf{Q}_{r,\text{in},m} \in \ker([\mathbf{N}_m^\top \quad \mathbf{X}_{\text{in},m}^\circ]^\top)$.

The matrices $\mathbf{T}_{1_{0_m}}^o$, $\mathbf{T}_{2_{0_m}}^o$, and $\mathbf{T}_{3_{0_m}}^o$ satisfy the conditions of the diffeomorphism for the reaction, inlet, and invariant spaces, respectively (see Table 6.1) but up to the matrices \mathbf{N}_m and $\mathbf{X}_{in_m}^o$. Once the linear transformation $\mathbf{T}_{0_m}^o$ based on S_m number of species is computed, the estimated extents $\hat{\mathbf{x}}_{in}$, $\hat{\mathbf{x}}_\lambda$ can be used set up the same optimization problem as in (6.57). In this case, the estimate $\Delta\hat{\mathbf{X}}_{in_m}$ can be estimated up to $S_m \times N_t$ elements. This is sufficient to appropriately reconstruct $\hat{\mathbf{x}}_r$ using (6.68).

The reconstruction of the vector of unmeasured moles $\hat{\mathbf{n}}_{um}$ will not converge to the true value of \mathbf{n}_{um} . As a matter of fact, if the matrices \mathbf{N} , \mathbf{X}_{in} , and \mathbf{n}_0 are not perfectly known, part of the information in the mole space will belong to the left null space of some of these matrices, and only an approximation can be obtained.

Computation of $\hat{\mathbf{n}}_{um}$

Since an estimate $\Delta\hat{\mathbf{X}}_{in_m}$ is available, an estimate of the real inlet composition matrix $\hat{\mathbf{X}}_{in_m} = \mathbf{X}_{in_m}^o + \Delta\hat{\mathbf{X}}_{in_m}$ can be computed. Therefore, with the information of \mathbf{N}_m , and $\hat{\mathbf{X}}_{in_m}$, the "true" transformation matrix $\mathbf{T}_{1_{0_m}}$ can also be calculated. We shall use these matrices to obtain an estimate $\hat{\mathbf{X}}_{in_{um}}$ provided that the conditions $S_{um} \leq N_r$ and $\text{rank}(\mathbf{N}_{um}) = S_{um}$ hold.

Using the matrix $\mathbf{T}_{1_{0_m}}$, we find a matrix \mathbf{T}_{1_0} such that conditions 1 and 3 of the diffeomorphism for the reaction space in Table 6.1 holds. This is achieved by

$$\mathbf{T}_{1_0} = \begin{bmatrix} \mathbf{N}^+ & \mathbf{n}_0^{\top+} \end{bmatrix} \begin{bmatrix} \mathbf{N}_m \\ \mathbf{n}_{0_m}^\top \end{bmatrix} \mathbf{T}_{1_{0_m}} \quad (6.73)$$

However, this matrix must also satisfy condition 2 of the diffeomorphism for the reaction space in Table 6.1. This condition can be exploited to find an estimate of $\hat{\mathbf{X}}_{in_{um}}$. Let $\mathbf{T}_{1_0}^\top = \begin{bmatrix} \mathbf{T}_{1_{0_1}}^\top & \mathbf{T}_{1_{0_2}}^\top \end{bmatrix}$, then

$$\mathbf{T}_{1_{0_1}}^\top \hat{\mathbf{X}}_{in_m} + \mathbf{T}_{1_{0_2}}^\top \hat{\mathbf{X}}_{in_{um}} = \mathbf{0}_{N_r \times N_t} \quad (6.74)$$

It is clear from (6.74) that if $\mathbf{T}_{1_{0_2}}^\top$ is full column rank, then an estimate $\hat{\mathbf{X}}_{in_{um}} = -\mathbf{T}_{1_{0_2}}^\top \mathbf{T}_{1_{0_1}}^\top \hat{\mathbf{X}}_{in_m}$. While this estimate precisely satisfies the equality, in general, it will not preserve the physical constraints of \mathbf{X}_{in} . Hence, to find the "best" matrix that satisfies the reaction-inlet space invariance respecting the physical constraints, the following optimization is formulated

$$\begin{aligned} \min_{\delta_{um}} \quad & \frac{1}{2} \|\mathbf{E} - \mathbf{D}\delta_{um}\|_2 \\ \text{s.t.} \quad & \begin{cases} (\mathbf{I}_{N_t} \otimes \mathbf{1}_{S_{um}}^\top) \delta_{um} \leq \mathbf{1}_{S_{um}N_t} - (\mathbf{I}_{N_t} \otimes \mathbf{1}_{S_{um}}^\top) \text{vec}(\hat{\mathbf{X}}_{in_m}) \\ \delta_{um} \geq \mathbf{0}_{S_{um}N_t} \\ \delta \leq \mathbf{1}_{S_{um}N_t} \end{cases} \end{aligned} \quad (6.75)$$

where $\delta_{um} = \text{vec}(\hat{\mathbf{X}}_{in_{um}})$, $\mathbf{D} = (\mathbf{I}_{N_t} \otimes \mathbf{T}_{102}^\top)$, and $\mathbf{E} = (\mathbf{I}_{N_t} \otimes \text{vec}(\hat{\mathbf{X}}_{in_m}))$. The estimated $\hat{\mathbf{X}}_{in_{um}}$ can be retrieved by

$$\hat{\mathbf{X}}_{in_{um}} = \text{vec}_{S_m, N_t}^{-1}(\hat{\delta}_{um}) \quad (6.76)$$

Concatenating $\hat{\mathbf{X}}_{in_m}$ and $\hat{\mathbf{X}}_{in_{um}}$ as $\hat{\mathbf{X}}_{in} = \begin{bmatrix} \hat{\mathbf{X}}_{in_m} \\ \hat{\mathbf{X}}_{in_{um}} \end{bmatrix}$, and along with \mathbf{N} , and \mathbf{n}_0 , the total number of moles can be recovered with (6.67).

6.7.3. Reaction rate estimator

The information of the AO can be utilized to estimate the vector of chemical reaction rates \mathbf{r} . Recall that the model structure (6.62) treats \mathbf{r} as a disturbance, which by 6.1, decays exponentially to zero as $t \rightarrow \infty$. Therefore, the following disturbance model is proposed

$$\begin{bmatrix} \dot{\bar{\mathbf{x}}} \\ \dot{\mathbf{r}} \end{bmatrix} = \begin{bmatrix} \mathbf{A}(\varsigma) & \mathbf{B}_d \\ \mathbf{0} & \mathbf{R}(\varsigma) \end{bmatrix} \begin{bmatrix} \bar{\mathbf{x}} \\ \mathbf{r} \end{bmatrix} + \begin{bmatrix} \mathbf{B} \\ \mathbf{0} \end{bmatrix} \mathbf{u} \quad (6.77)$$

$$\mathbf{y}_m = \begin{bmatrix} \mathbf{n}_m \\ T \end{bmatrix} = [\mathbf{C}_m \quad \mathbf{0}] \begin{bmatrix} \bar{\mathbf{x}} \\ \mathbf{0} \end{bmatrix}$$

where $\mathbf{R}(\varsigma) = -\varsigma \mathbf{I}_{N_r}$, $\bar{\mathbf{x}} = [\mathbf{x}_r^\top \quad \mathbf{x}_{in}^\top \quad x_\lambda \quad T]^\top$, $\mathbf{u} = [\mathbf{F}_{in}^\top \quad \dot{Q}_{in}]^\top$. Based on (6.77), the vector of chemical reaction rates \mathbf{r} can be estimated, and the RRE has the structure of a full-order Luenberger observer.

$$\begin{aligned} \begin{bmatrix} \hat{\dot{x}} \\ \hat{r} \end{bmatrix} &= \begin{bmatrix} \mathbf{A}(\varsigma) & \mathbf{B}_d \\ \mathbf{0} & \mathbf{R}(\varsigma) \end{bmatrix} \begin{bmatrix} \hat{x} \\ \hat{r} \end{bmatrix} + \begin{bmatrix} \mathbf{B} \\ \mathbf{0} \end{bmatrix} \mathbf{u} + \mathbf{L}(\varsigma) (\mathbf{y}_m - \hat{\mathbf{y}}) \\ \hat{\mathbf{y}} &= [\mathbf{C}_m \quad \mathbf{0}] \begin{bmatrix} \hat{\dot{x}} \\ \mathbf{0} \end{bmatrix} \end{aligned} \quad (6.78)$$

This estimator takes the state information from the estimates provided by the AO. Due to the sequential nature of the estimation, the convergence of the RRE must be faster than that of the AO. This can be ensured tuning the observer gain $\mathbf{L}(\varsigma)$. The ability to impose an arbitrary speed of convergence by modifying the structure of the RRE gain depends on the observability condition laid out in Theorem 6.2. Moreover, the RRE gain has a specific structure provided in the following theorem:

Theorem 6.3: Consider the estimation model given (6.78), and let the standing assumption on the measurement of ς hold. If the system is observable, then there exists a parametric observer gain $\mathbf{L}(\varsigma) = [\mathbf{L}_1^\top(\varsigma) \quad \mathbf{L}_2^\top(\varsigma)]^\top$ with $\mathbf{L}_1 = (\mu - \varsigma)\mathbf{C}_m^+$, and $\mathbf{L}_2 = \mu(\mu - \varsigma)\mathbf{B}_d^+\mathbf{C}_m^+$, where μ is the desired pole location such that $|\mu| > |\varsigma|$.

The proof of Theorem 6.3 can be found in appendix A.

6.7.4. Chemical kinetic parameter estimation

Parameter estimation can be performed imposing a particular structure to the vector of chemical reaction rates \mathbf{r} . These rates are typically modeled using the Law of Mass Action, in which the rate of chemical reaction is proportional to the concentrations of the reactants. Imposing this structure to the chemical reaction rate vector \mathbf{r} , each of its elements r_i is written as:

$$r_i = \sum_{\ell=1}^{S_e} \left(k_{i,\ell_0} \exp \left(-\frac{E_{a_i}}{RT} \right) \prod_{j=1}^{S_{r_i}} [C]_{i,j}^{\nu_{i,j}} \right) \quad (6.79)$$

where S_e is the number of equilibrium reactions, S_{r_i} is the number of reactants in the i -th reaction, k_{i,ℓ_0} is the pre-exponential factor, E_{a_i} is the normalized activation energy all of them in the i -th reaction, and R is the universal gas constant. $[C_{i,j}]$ and $\nu_{i,j}$ are the concentration and the stoichiometric coefficient of the j -th species in the i -th reaction, respectively.

With this structure the reaction rate vector can be expressed as

$$\hat{\mathbf{r}} = \mathbf{r}(\mathbf{p}) + \boldsymbol{\varepsilon} \quad (6.80)$$

The parameter vector \mathbf{p} can be calculated minimizing the standard least-squares criterion:

$$\min_{\mathbf{p}} \|\boldsymbol{\varepsilon}\|_2^2 = \min_{\mathbf{p}} \|\hat{\mathbf{r}} - \mathbf{r}(\mathbf{p})\|_2^2 \quad (6.81)$$

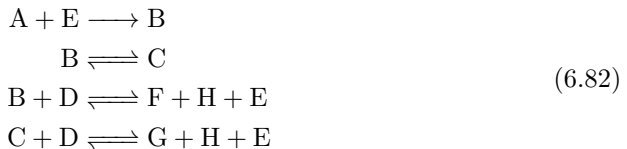
whose solution is given by $\hat{\mathbf{p}} = \arg(\min_{\mathbf{p}} \|\boldsymbol{\varepsilon}\|_2^2)$

6.8. Numerical example

In this section, we present an example to demonstrate the methodology introduced throughout this chapter.

6

Consider the reaction process system composed of a CSTR and a separation unit. In such a process, the following reactions take place:



The reactant D is fed in excess, while the desired products are F, G, and H. Since the reactant E is also a byproduct in the subsequent reactions, and D is fed in excess, these two are recycled to the feed of fresh D to ensure complete conversion of A and to promote the formation of the desired products. The recycled is cooled down to the same temperature T_{in} of the fresh feed. Additionally, the following variables are assumed to be measured: the composition of the fresh feed of D, the inlet flow to the reactor F_{in} , i.e. the sum of the fresh feed and the recycled streams, only a number $S_m = 6$ species are measured, namely A, B, C, D, E, and F, the inverse residence time ς , and the temperature in the process. The goal is to estimate the moles of the $S_{um} = 2$ unmeasured species (G and H), as well as the reaction kinetic parameters. A representation of the process is illustrated in Figure 6.3.

The stoichiometric matrix, the fresh feed composition matrix, and the initial conditions in the reactor are:

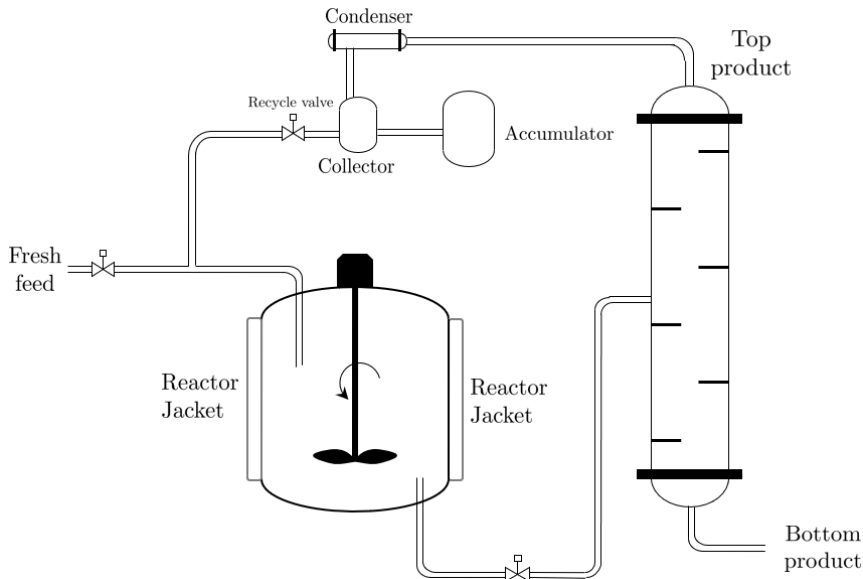


Figure 6.3: Reaction process system of a CSTR and a separation unit with a recycle stream.

6

$$\mathbf{N} = \begin{bmatrix} -1 & 1 & 0 & 0 & -1 & 0 & 0 & 0 \\ 0 & -1 & 1 & 0 & 0 & 0 & 0 & 0 \\ 0 & -1 & 0 & -1 & 1 & 1 & 0 & 1 \\ 0 & 0 & -1 & -1 & 1 & 0 & 1 & 1 \end{bmatrix}, \quad \mathbf{X}_{in}^o = \begin{bmatrix} 0 \\ 0 \\ 0 \\ 1 \\ 0 \\ 0 \\ 0 \\ 0 \end{bmatrix}, \quad \mathbf{n}_0 = \begin{bmatrix} 20 \\ 0 \\ 0 \\ 0 \\ 10 \\ 0 \\ 0 \\ 0 \end{bmatrix} \text{ kmol}$$

Define the matrices

$$\mathbf{N}_m = \begin{bmatrix} -1 & 1 & 0 & 0 & -1 & 0 \\ 0 & -1 & 1 & 0 & 0 & 0 \\ 0 & -1 & 0 & -1 & 1 & 1 \\ 0 & 0 & -1 & -1 & 1 & 1 \end{bmatrix}, \quad \mathbf{N}_{um} = \begin{bmatrix} 0 & 0 \\ 0 & 0 \\ 1 & 0 \\ 0 & 1 \end{bmatrix}$$

$$\mathbf{X}_{\text{in}_m}^{\circ} = \begin{bmatrix} 0 \\ 0 \\ 0 \\ 1 \\ 0 \\ 0 \end{bmatrix}, \quad \mathbf{n}_{0_m} = \begin{bmatrix} 20 \\ 0 \\ 0 \\ 0 \\ 10 \\ 0 \end{bmatrix} \text{ kmol}$$

From (6.65) the trajectories of \mathbf{x}_{in} , x_{λ} computed. Since ς and F_{in} are measured directly from the process, these values correspond to the true extents of inlets and discounting factor. We estimate the extent of reaction $\hat{\mathbf{x}}_r$ with (6.66) using the available information. Clearly this estimation will not be accurate because the fresh feed inlet composition matrix $\mathbf{X}_{\text{in}}^{\circ}$ is used for estimation instead of the real inlet composition matrix $\mathbf{X}_{\text{in}} = \mathbf{X}_{\text{in}}^{\circ} + \Delta \mathbf{X}_{\text{in}}$. In Figure 6.4 it can be observed that at the beginning the measured moles and the estimated moles are almost equal, but as the process progresses the composition of the inlet changes and the error between the two sets of trajectories start to diverge. The error is not the same for all the species; the error is more noticeable in the products n_G and n_H because they are sensitive to changes in the composition of the reagents. In Table 6.2 the root-mean-square error RMSE is shown.

6

Table 6.2: RMSE between the measured and the estimated moles using $\mathbf{X}_{\text{in}_m}^{\circ}$

Species	RMSE value (kmol)
n_A	0.2379
n_B	5.3118
n_C	4.6682
n_D	3.2182
n_E	4.1514
n_F	0
n_G	15.5537
n_H	17.2309

We estimate the uncertainty matrix $\Delta \hat{\mathbf{X}}_{\text{in}_m}$ to try to correct the discrepancies find at large process times. Based on \mathbf{N} , $\mathbf{X}_{\text{in}}^{\circ}$, and \mathbf{n}_0 , we can construct the transformation matrices \mathbf{T}_0° :

$$\mathbf{T}_{1_0}^{\circ} = \begin{bmatrix} \mathbf{T}_{1_{01}}^{\circ} \\ \mathbf{T}_{1_{02}}^{\circ} \end{bmatrix}, \quad \mathbf{T}_{2_0}^{\circ} = \begin{bmatrix} \mathbf{T}_{2_{01}}^{\circ} \\ \mathbf{T}_{2_{02}}^{\circ} \end{bmatrix}, \quad \mathbf{T}_{3_0}^{\circ} = \begin{bmatrix} \mathbf{T}_{3_{01}}^{\circ} \\ \mathbf{T}_{3_{02}}^{\circ} \end{bmatrix}, \quad \mathbf{T}_{4_0}^{\circ} = \begin{bmatrix} \mathbf{T}_{4_{01}}^{\circ} \\ \mathbf{T}_{4_{02}}^{\circ} \end{bmatrix}$$

However, recall that since only S_m number of moles are being measured, we find a transformation $\mathbf{T}_{0_m}^{\circ}$ using (6.69), (6.70), (6.71), and (6.72) such that conditions the conditions established in Table 6.1 hold for matrices \mathbf{N}_m , $\mathbf{X}_{\text{in}_m}^{\circ}$, and \mathbf{n}_{0_m} . Using

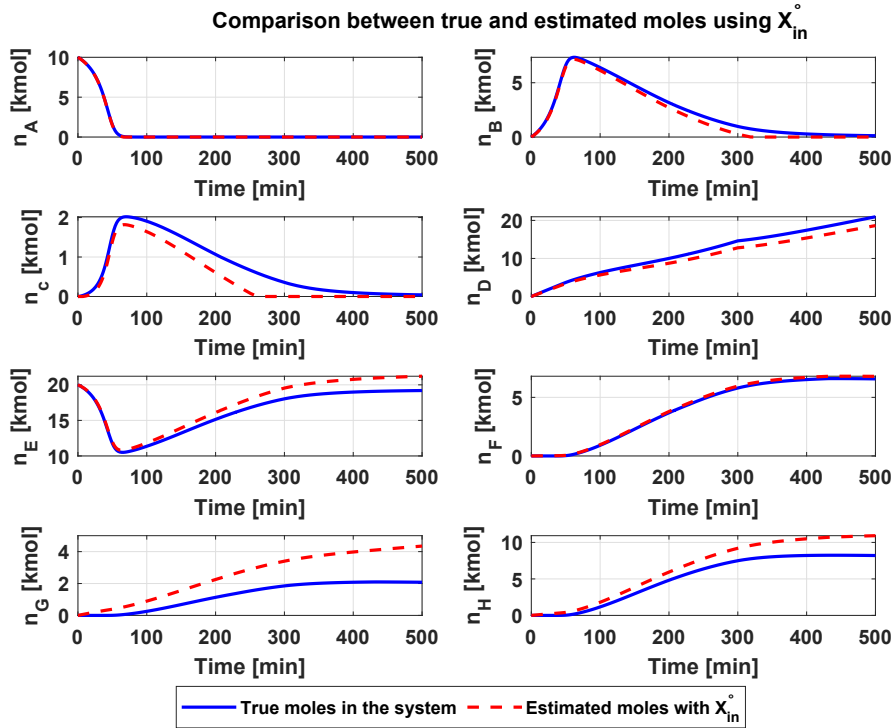


Figure 6.4: Comparison between true moles and moles estimated using $\mathbf{X}_{\text{in}}^\circ$

the matrices $\mathbf{T}_{2_{0m}}^\circ$, $\mathbf{T}_{3_{0m}}^\circ$, $\mathbf{T}_{4_{0m}}^\circ$, we set up an optimization similar to (6.57). Nevertheless, since $\mathbf{X}_{\text{in}_m}^\circ + \Delta \mathbf{X}_{\text{in}_m}$ might not need to sum up to 1, we introduce the slight modification by converting the equality constraint $\mathbf{1}_{S_m N_t}^\top \delta_m = \mathbf{0}_{S_m N_t}$ to an inequality $\mathbf{1}_{S_m N_t}^\top \delta_m \leq \mathbf{1}_{S_m N_t} - \mathbf{1}_{S_m N_t}^\top \text{vec}(\mathbf{X}_{\text{in}_m}^\circ)$. From the optimization, we find that

$$\Delta \hat{\mathbf{X}}_{\text{in}_m} = \begin{bmatrix} 0.0001505 \\ 0.0012055 \\ 0.0012055 \\ -0.0899629 \\ 0.0794682 \\ 0.0066291 \end{bmatrix} \Leftrightarrow \hat{\mathbf{X}}_{\text{in}_m} = \begin{bmatrix} 0.0001505 \\ 0.0012055 \\ 0.0012055 \\ 0.9100370 \\ 0.0794682 \\ 0.0066291 \end{bmatrix} \quad (6.83)$$

Observe that $\mathbf{1}_{S_m}^\top \mathbf{X}_{\text{in}_m} < 1$. We use $\hat{\mathbf{X}}_{\text{in}_m}$ to correct the estimate $\hat{\mathbf{x}}_r$ using (6.66). In Figure 6.5, both $\hat{\mathbf{x}}$ and $\hat{\mathbf{x}}_r$ are compared, where it can be seen that both sets of trajectories have the same trend but different magnitude. This is expected because

there is perfect knowledge of the inverse residence time ς , which is a critical variable for the correct determination of the extent of reaction in presence of inlet uncertainty as shown in Theorem 6.1.

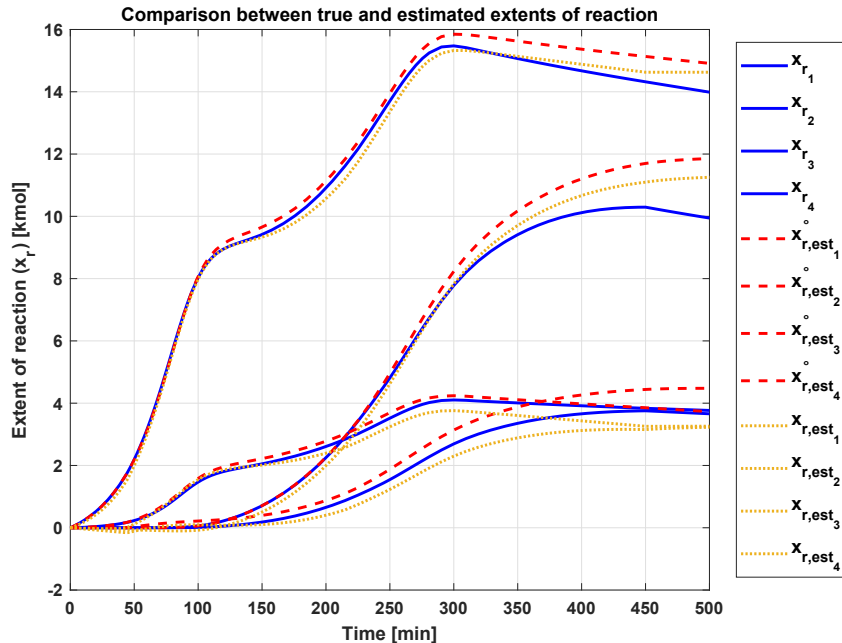


Figure 6.5: Comparison between true and estimated extents of reaction using $\mathbf{X}_{\text{in},m}^\circ$ and $\hat{\mathbf{X}}_{\text{in},m}$

We reconstruct the number of unmeasured moles proceeding as described in 6.7.2, by which we find that

$$\hat{\mathbf{X}}_{\text{in},um} = \begin{bmatrix} 0.000000028 \\ 0.001305436 \end{bmatrix} \text{ and thus } \hat{\mathbf{X}}_{\text{in}} = \begin{bmatrix} 0.000150503485191 \\ 0.001205525925511 \\ 0.001205525925511 \\ 0.910037050063140 \\ 0.079468237051390 \\ 0.006629144220325 \\ 0.000000028 \\ 0.001305436 \end{bmatrix}$$

Finally, with the information of $\hat{\mathbf{X}}_{\text{in}}$, and $\hat{\mathbf{x}}_r$, the estimate of the total number of moles $\hat{\mathbf{n}}$ is obtained from (6.67). A comparison between the true measured moles, the reconstructed moles using the fresh feed composition matrix $\mathbf{X}_{\text{in}}^\circ$, and $\hat{\mathbf{X}}_{\text{in}}$ is

shown in Figure 6.6. It can be observed that the estimation with the corrected inlet composition matrix matches better the measured moles and decreases the error. The RMSE for this case is show in Table 6.3.

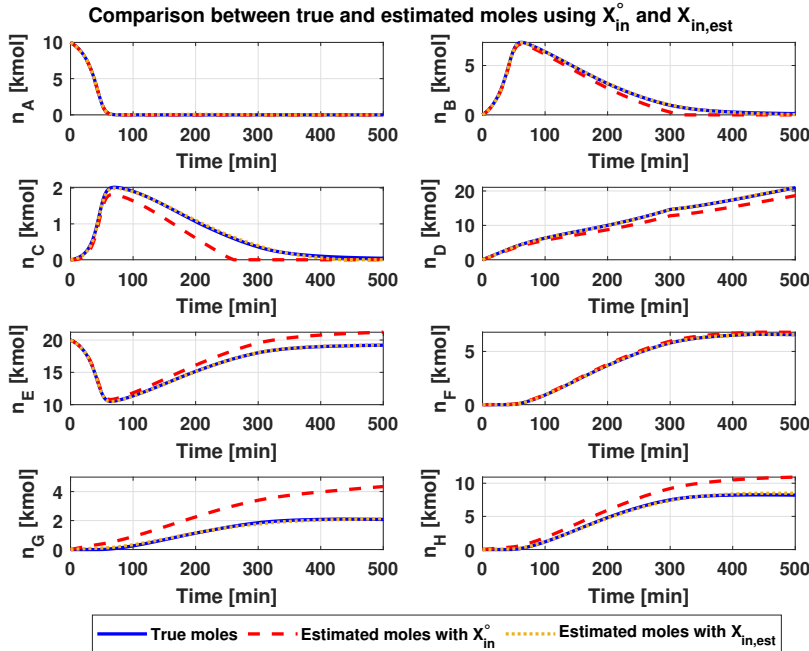


Figure 6.6: Comparison between true moles and estimated moles using \mathbf{X}_{in}^o and $\hat{\mathbf{X}}_{in}$.

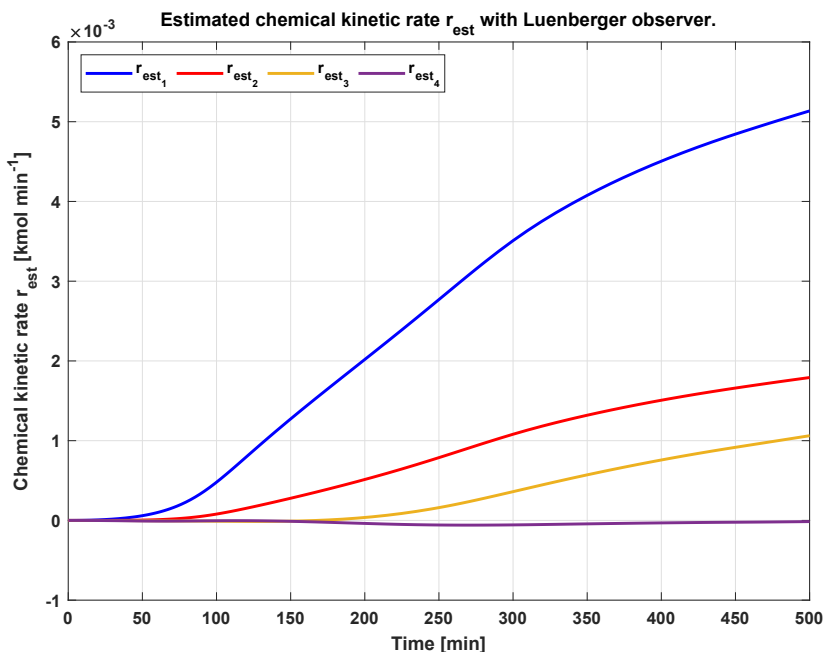
With this information, we proceed to estimate the reaction vector $\hat{\mathbf{r}}$ using the observer design of section 6.7.3, whose trajectories are shown in Figure 6.7. Finally, as a last step of the sequential design, the chemical kinetic parameters are estimated assuming that the chemical kinetic rates follow the Law of Mass Action as in (6.79). Therefore

$$\begin{aligned}
 r_1(\mathbf{p}) &= p_1 \exp\left(-\frac{p_8}{RT}\right) [C]_A [C]_E \\
 r_2(\mathbf{p}) &= p_2 \exp\left(-\frac{p_9}{RT}\right) [C]_B - p_3 \exp\left(-\frac{p_{10}}{RT}\right) [C]_C \\
 r_3(\mathbf{p}) &= p_4 \exp\left(-\frac{p_{11}}{T}\right) [C]_B [C]_D - p_5 \exp\left(-\frac{p_{12}}{RT}\right) [C]_E [C]_F [C]_H \\
 r_4(\mathbf{p}) &= p_6 \exp\left(-\frac{p_{13}}{RT}\right) [C]_C [C]_D - p_7 \exp\left(-\frac{p_{14}}{RT}\right) [C]_E [C]_G [C]_H
 \end{aligned} \tag{6.84}$$

Finally, we perform parameter estimation to obtain the vector of parameters \mathbf{p} . After performing sensitivity, parameters p_9 and p_{10} are not identifiable, and there-

Table 6.3: RMSE between the measured and the estimated moles using $\hat{\mathbf{X}}_{in}$

Species	RMSE value (kmol)
n_A	0.5188
n_B	0.4956
n_C	0.4403
n_D	0.7360
n_E	0.3630
n_F	0
n_G	0.6675
n_H	1.4609

Figure 6.7: Estimated chemical kinetic rates \hat{r} .

fore, are left out of the estimation procedure, and their initial values are fixed. The parameter estimation is done performing a Montecarlo simulation of a 100 runs with random variations of 10% over the initial guesses and solving the optimization problem. The results of the parameter estimation are shown in Table 6.4. The results are the variance-weighted mean of the trials and they are reported with a 95% confidence interval computed using the Student's t distribution.

Table 6.4: Chemical kinetic rate parameter estimates

Label (p)	Unit	Value $\times 10^7$	Confidence intervals $\times 10^7$
\hat{p}_1	$\text{kg}^2 \text{ kmol}^{-2} \text{ min}^{-1}$	1.000	[0.9978 1.003]
\hat{p}_2	kg kmol min^{-1}	0.1850	[0.1802 0.1898]
\hat{p}_3	kg kmol min^{-1}	0.006496	[0.002559 0.01043]
\hat{p}_4	$\text{kg}^2 \text{ kmol}^{-2} \text{ min}^{-1}$	2.002	[1.997 2.007]
\hat{p}_5	$\text{kg}^3 \text{ kmol}^{-3} \text{ min}^{-1}$	0.21161	[0.2111 0.2121]
\hat{p}_6	$\text{kg}^2 \text{ kmol}^{-2} \text{ min}^{-1}$	2.002	[1.998 2.006]
\hat{p}_7	$\text{kg}^3 \text{ kmol}^{-3} \text{ min}^{-1}$	0.2115	[0.2108 0.2121]
\hat{p}_8	kJ kmol^{-1}	0.09742	[0.07917 0.1157]
\hat{p}_{11}	kJ kmol^{-1}	0.1457	[0.1363 0.1551]
\hat{p}_{12}	kJ kmol^{-1}	0.003677	[0.003676 0.003678]
\hat{p}_{13}	kJ kmol^{-1}	0.08419	[0.08038 0.08799]
\hat{p}_{14}	kJ kmol^{-1}	0.00496	[0.004824 0.005096]

Chapter summary

Extents of reaction and inlets

- The extents of reaction and inlets describe independent dynamics that account for different effects in the process. As such, the extents of reaction depend solely on the reaction, whereas the extents of inlet on the inlet flow going into the process. They generate a set of fully decoupled dynamics that allow to perform model analysis, control and observer design, optimization, and/or parameter estimation.
- The process dynamics can be independently represented in the mole basis or in the extent basis. However, a linear diffeomorphism that relate both spaces exists under some specific rank conditions. If these conditions are not met, then the information obtained in one space cannot be translated into the other.
- The matrices related to the transformation must be well-known in order to obtain a reliable transformation.
- The extent representation can be obtained for batch, semi-batch and continuous processes discounting the effect of possible zero initial conditions. However, in the continuous process, a key variable is the inverse residence time, which acts as a time-varying pole of the system. The knowledge of this quantity is necessary to dynamically compute the extents, and to recover or estimate any information in the mole or extent spaces.

Uncertainty in the inlet composition matrix

- Uncertainty in the inlet composition matrix can occur when the process has a recycle stream or a process is fed with the outlet of another process upstream. In these cases, the inlet composition matrix has other components apart from the normal reactants. A different composition matrix will produce different results in term of computation of extents and also in the prediction of the number of moles in the reacting mixture.
- The estimation of the inlet composition uncertainty matrix can be addressed without information about the reaction, which is generally unknown in the process. On the one hand this lack of information will results in the non-uniqueness of the matrix. On the other hand, even when the uncertainty might not be unique, it still allows us to compute a good estimation of the number of moles.

Chapter summary

- The equivalence between an extent-based model represented by an incorrect inlet composition matrix and the true one depends on the inverse residence time. In general, the extents of inlet flow \mathbf{x}_{in} , initial condition discounting factor x_λ , and extent of invariant dynamics \mathbf{x}_{inv} will agree in both representations if and only if the inverse residence times are equal, which is guaranteed in the moles are conserved in the reaction dynamics. As a conclusion, the inverse residence time must be measured in case the moles are not conserved in the reaction.
- The inlet composition uncertainty matrix can be computed solving an optimization problem that minimizes the error between the true extents and those computed using the incorrect inlet composition matrix. This matrix can be used to obtain a corrected inlet composition matrix, which can be employed to estimate other variables in the reaction system.

Estimation of moles, chemical reaction rates, and chemical kinetic parameters

- The AO estimates the extent of reaction if \mathbf{N}_m is full column rank. However, it depends on the inlet composition matrix, and if it is not correct, the extent of reaction might converge to a different value.
- The estimation of a corrected value of the extent of reaction is achieved by estimating the uncertainty matrix in the inlet composition matrix. However, since only a specific number of species are being measured, this matrix can be estimated up to the number of measured components. This correction allows to also reconstruct correctly the unmeasured number of moles.
- The estimation of the unmeasured part of the inlet composition matrix is achieved exploiting the conditions that the linear transformation \mathbf{T} must satisfy. Nevertheless, an exact reconstruction of this matrix is not possible because this information is contained in the left null space of the inlet dynamics. We can still find a matrix that approximates the linear transformation conditions that also satisfy the physical properties of \mathbf{X}_{in} . This matrix also allows to compute an approximate vector of unmeasured moles, but this estimation will not converge to the true value.
- The reaction rate estimator models the reaction vector as an exponentially convergent function. This allows to include the unknown reaction dynamics in an observer structure to estimate the trajectories. Notice that since the reaction dynamics are unknown, the estimates might in practice differ from the actual trajectories. However, due to the assumption of uniform continuity of \mathbf{r} in a convex domain \mathbb{D}_r , the reaction eventually must decay to zero asymptotically.

Chapter summary

- The rate of convergence of the RRE can be arbitrarily chosen if the pair $(\mathbf{A}(\varsigma), \mathbf{C}_m)$ is observable. This is immediately satisfied if \mathbf{C}_m is full column rank. Additionally, due to the full column rank condition, the observer gain has a closed-form with a specific structure.
- Parameter estimation of chemical kinetic rates is performed using directly the information of the estimated reaction rate of the RRE. In general, this is a nonlinear optimization that can be efficiently implemented with optimization solvers. However, nonlinear optimization heavily depends on the initial conditions. As a consequence, a Monte-carlo simulation is performed choosing multiple random starting points. A mean weighted with the variance of each parameter is chosen as a metric to provide the parameter estimates.

7

Industrial Case Study: Resin production by reactive batch distillation

In this chapter, we present the approach for the dynamic model development of an industrial reactive distillation process for the production of a resin via condensation polymerization. First, a general description of the process is provided followed by the introduction of the chemical reaction characteristics and introduction of the proposed reaction mechanism. Furthermore, the general mass and energy balances as well as relevant hydraulic and thermodynamic aspects are revisited. In addition, specific simulation approaches used to simulate fast dynamics with smooth switching function, along with the assumptions made on the model are presented. The chapter also introduces an empirical modeling strategy to describe polymer viscosity, which serves as the critical variable to assess the product quality. The model prediction is compared to the real plant data to establish whether the model represents the process sufficiently well prior to model calibration.

Publications of this chapter:

Modeling of reactive batch distillation processes for control, Márquez-Ruiz, A. Méndez-Blanco, C., Özkan, L. Computers & Chemical Engineering 121, 86–98 (2019) ([114])

7.1. Introduction

The large-scale process industry is concerned with the conversion of raw materials to desired products. These products must comply with the quality requirements set by the market and customers. In order to attain such quality standards, and at the same time, produce sufficiently to satisfy the demand, two processes are essential: chemical reaction and distillation. Both processes are usually carried in a chemical reactor and a distillation column, separately. However, with the development of process intensification technologies, these two have been integrated into one unit operation known as reactive distillation (RD). Reactive distillation is an intensified process in which one or several chemical reactions and distillation occur simultaneously in a single device [152]. These processes can have two operation modes: continuous and batch operation. In particular, when the system is operated in batch mode, reactive distillation is then called reactive batch distillation (RBD). This type of operation is used in the process industry for the production of specialty products with high added value, as it allows for flexible adjustment and scaling of operating conditions more efficiently than continuous-time operations [168], [25]. RD and RBD present several advantages over the conventional unit operations, such as higher conversion rates, optimized energy management of the process and lower capital investments [152]. Despite the practical benefits of continuous and batch reactive distillation, these processes pose several challenges for control and optimization. The most important challenge could be the conflicting performance objectives in the process operation. Such unit operations are generally used for systems with equilibrium reactions, and thus, the role of distillation column is to remove one of the products to shift the equilibrium reaction towards the desired direction. In order to achieve the desired purity at the distillate stage, the reflux ratio needs to be increased to promote mass transfer between the phases in the column. This means that some part of the separated product returns back to the reaction zone to react again with other remaining components lowering the overall chemical conversion. As a consequence, to achieve both the purity at the distillate stage and the desired conversion at the reaction stage, excess raw material is loaded at the beginning of the production. The aforementioned conflicting operational objectives combined with nonlinear dynamics call for rigorous dynamic modeling able to describe a wider range of process operation.

As mentioned previously, reactive batch distillation is governed by complex dynamics. These complex phenomena are modelled rigorously to some degree in the form of nonlinear algebraic differential equations (DAE). However, most of the practical applications are based on the linearization of the nonlinear model [168], [134], [165], [3], [4], [2], or approximating the nonlinear behavior by a first-order transfer function with time delay [92] in order to design conventional control strategies, such as proportional-integral-derivative (PID) controllers. Nevertheless, these models are not suitable for monitoring, model-based control or handling of process constraints. Moreover, these models do not provide a good insight of the interactions in the

process when compared to rigorous physics-based models. Part of the recent research on RBD has focused on the development of rigorous models while studying alternative methods to simplify them without losing relevant information of their phenomenological description. One approach is to model RBD dynamics using travelling nonlinear waves [112], [65], [13]. This formulation captures process dynamics while reducing the number of components by clustering them in pseudo-components. A drawback of this approach is that the model still retains a distributed parameter structure, limiting its applicability to simple cases such as binary or ternary RBD. Another approach is the stage aggregation [98] [101], which provides a suitable modeling setting for distillation columns with a large number of stages, such as high purity distillation columns. However, RBD columns have generally fewer trays than a high purity column, and the assumption of steady-state stages cannot be imposed on RBD processes due to the batch nature of the operation. Márquez *et al.* [114] propose a modeling approach for control of a reactive batch distillation column based on a certain class of linear transformation based on the works of [7], [6] [5], [22]. Furthermore, Márquez *et al.* [116] employ a set of bounded smooth functions to simulate the fast dynamics of the reactive distillation column during the start-up, such as the sudden vapor formation. The process in [114] was assumed to be carried in one batch operational stage and at atmospheric pressure. These two aspects will be different in the industrial RBD process that will be presented here. In the actual industrial process, a polyesterification reaction is carried out in different operational steps based on the operating conditions, and the operating pressure is much higher than atmospheric pressure throughout the production campaign.

This chapter deals with the development of a simulation model of a real reactive batch distillation column. First, we explain the step-growth polyesterification reactions, their general mechanism, chemical kinetics, and the end-repeat segment modeling paradigm for polymers. We continue introducing a general description of reactive distillation processes to then focus on the fluid-dynamic and thermodynamic aspects to establish a mathematical model of the process. Details about numerical implementation are discussed to simulate fast changing dynamics such as phase transition. Moreover, concepts on polymer viscosity as well as a dynamic logistic growth model to predict viscosity are presented. Finally a simulation of the reactive batch distillation process is performed and compared to the real plant data.

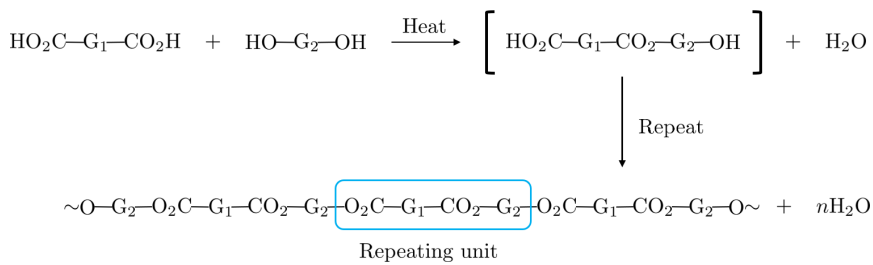
7.2. Polyesterification reaction

Polyesters form a category of polymers in which the main functional group in each of the repeating units is an ester [94]. In particular, polyester resins are synthetic resins formed by the reaction between dibasic organic acids and polyhydric alcohols [159]. These polyester resins have several industrial and domestic applications: creating molds, building boats, casting artificial ponds, swimming pools, and other outdoor

applications. Other application domains include:

- Construction materials.
- Aerospace, vehicle, and marine industries.
- Packaging material.
- Manufacturing of furniture, especially outdoor items.
- Composite materials, e.g. fiberglass resin.

Most polymer resins are produced through step-growth polymerization (polyesterification reaction). In this type of processes, polymers often grow through a condensation reaction, in which a small condensate molecule such as water or methanol is eliminated by the reaction between two functional groups [159]. A schematic representation of a condensation polymerization is shown in Figure 7.1



7

Figure 7.1: Simplified schematic representation of a condensation polymerization reaction. The functional group G₁ can be a radical group (R₁) or an aryl group (A_r). The functional group G₂ is typically another radical group (R₂).

As seen in Figure 7.1, one mole of alcohol reacts with one mole of acid to generate a mole of the repeating unit and a mole of water. However, in several cases, the anhydrous form of the dibasic acids are used instead of the aqueous form. The anhydrous form consumes one mole of water immediately; this change in the stoichiometry of the water needs to be taken into account in the modeling process of the reaction kinetics.

7.2.1. Polyesterification reaction mechanism

The chemical plant has several reactive batch distillation units that produce several grades and types of polyesters. In this thesis, the reaction mechanism is developed for only one of these products. This choice is motivated due to the small number of reactants involved, which simplifies the modeling and analysis tasks.

For the production of the chosen product, three reactants are used. Due to confidentiality reasons, they are named acid 1 (AC1), acid 2 (AC2), and alcohol 1 (AOH). Both acids are in their anhydrous form, i.e. they are crystalline powders. The reaction is also carried out using a small amount of water at the beginning to force the dissolution of the anhydrides into their aqueous form. Similarly, as shown in Figure 7.1, this reaction is also a polycondensation reaction. However, the existence of two acids in the reacting mixture produces a co-polymer, which is a polymer derived from more than one species of monomer [120].

In order to develop a mechanistic model describing the chemical kinetics of the system, we first need to define the chemical species considered in the reaction. Clearly, the reactants must be taken into account, however, since we are dealing with polymers, we shall approach the modeling task based on the fact that polymers are made up of several functional groups, and therefore, we assume that functional-group segments are connected in a linear chain by covalent bonds. Furthermore, we identify two types of functional-group segments: repeat segments and end segments. End segments are found only at the ends of polymer chains and are connected to other segments through one covalent bond. On the other hand, repeat segments occur in the interior of a polymer molecule and have two covalent bonds [159]. This idea is schematized in Figure 7.2. Therefore, for this particular case, we define additionally: the acid 1 end segment (AC1-end), the acid 2 end segment (AC2-end), the alcohol 1 end segment (AOH-end), the acid 1 repeat segment (AC1-rep), the acid 2 repeat segment (AC2-rep), and the alcohol 1 repeat segment (AOH-rep).

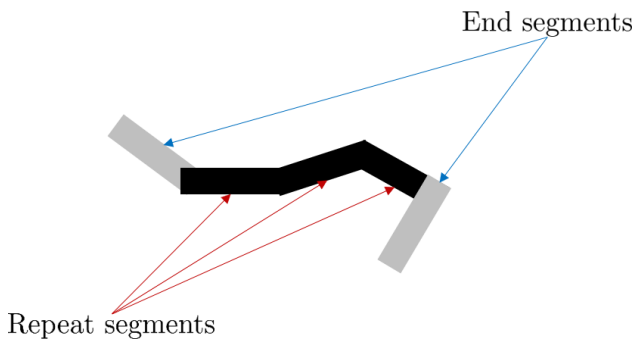


Figure 7.2: Repeat and end segment formalism to model polymer mixtures. Based on [159]

7.2.2. Chemical reactions

Based on this modeling formalism that allows us to split polymer depending of their location within the chain, the set of chemical reaction as well as the stoichiometry can be established. The standard condensation polymerization reactions can be summarized into the following categories

- Ring opening
- Forward condensation
- Backward condensation

Ring opening reaction: Hydration of anhydrides

Both AC1 and AC2 in anhydric form are solids, which at a molecular level are typically closed rings. These ring structures open after hydration to form the acids in solution. Once these acids are produced, they can react with the alcohol group starting the polymerization reaction. However, due to lack of data, this set of reactions is not considered. It is assumed that the acids in the reactor are already dissolved before reacting with the alcohol group.

Forward condensation reaction

With AC1-end:

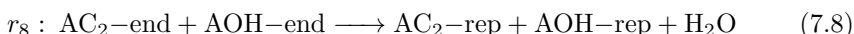
7

This forward condensation reaction is initiated with AC1 and AOH. These two species react to form the molecules AC1-end, AOH-end, and a molecule of water. The end groups react with the existing AC1 and AOH in the mixture to form acid and alcohol repetition segments. This is summarized in the following set of reactions:



With AC2-end:

Analogously, this forward condensation reaction is initiated with AC2 and AOH. Like in the previous case, these two species react to form the molecules AC2-end, AOH-end, and a molecule of water. The formed end groups react with the AC2 and AOH in the mixture to form also acid and alcohol repetition segments. This is summarized in the following set of reactions:



Backward condensation reaction

With AC1-rep:

This backward condensation reaction reverts the previous forward condensation reaction with AC1. In this case, the end groups hydrolyze to form the original species, namely AC1 and AOH. Additionally, the repetition groups interact with the end groups and water to form back more end groups. This is summarized in the following set of reactions:



7

With AC2-rep:

Likewise, this backward condensation reaction also reverts the previous forward condensation reaction with AC2. The end groups hydrolyze to form the original species, AC2 and AOH. Moreover, the repetition groups interact with the end groups and water to form back more end groups. This is summarized in the following set of reactions:



It is worth mentioning that these 16 reactions correspond to a set of equilibrium

reactions that are converted into a set of series reactions. This will help us express the reaction dynamics in a more convenient way later on.

7.2.3. Rate equations and stoichiometry

The equation describing the reaction dynamics are based on the mass-action principle

$$r_i^c = k_i \prod_{j=1}^{S_r} C_j^{\nu_j} \quad (7.17)$$

where r^c denotes a chemical reaction rate, k corresponds to the kinetic parameter of a particular reaction, $S_r < S$ is the number of reactants, C is the concentration, and ν is the stoichiometric coefficient.

The kinetic parameter is assumed to vary with the temperature following the Arrhenius law, thus

$$k_i = k_{i_0} \exp\left(-\frac{E_{a_i}}{RT}\right) \quad (7.18)$$

where k_0 is the pre-exponential factor, E_a is the activation energy, R is the universal gas constant, and T is the mixture's temperature.

Combining (7.17) and (7.18), the full rate equation for each reaction is given by

$$r_i^c = k_{i_0} \exp\left(-\frac{E_{a_i}}{RT}\right) \prod_{j=1}^{S_r} C_j^{\nu_j} \quad (7.19)$$

However, the reaction rate in (7.19) has units of concentration of moles per unit of mass of solution per unit of time. In order to convert from concentration per unit of time to a mole per unit of time, we multiply r_i^c with the total mass of the solution m_L in the reacting mixture. Thus

$$r_i = r_i^c m_L \quad (7.20)$$

On the other hand, the stoichiometry of the reaction dynamics is collected in the stoichiometric matrix. Let the S -dimensional vector of species be given by

$$\mathbf{n} = [n_1 \ n_2 \ n_3 \ n_4 \ n_5 \ n_6 \ n_7 \ n_8 \ n_9 \ n_{10}]^\top \quad (7.21)$$

where $n_1 = n_{\text{AC}_1}$, $n_2 = n_{\text{AC}_2}$, $n_3 = n_{\text{AOH}}$, $n_4 = n_{\text{H}_2\text{O}}$, $n_5 = n_{\text{AC}_1\text{-end}}$, $n_6 = n_{\text{AC}_2\text{-end}}$, $n_7 = n_{\text{AOH}\text{-end}}$, $n_8 = n_{\text{AC}_1\text{-rep}}$, $n_9 = n_{\text{AC}_2\text{-rep}}$, and $n_{10} = n_{\text{AOH}\text{-rep}}$.

Thus, stoichiometric matrix \mathbf{N} is

$$\mathbf{N} = \begin{bmatrix} -1 & 0 & -1 & 1 & 1 & 0 & 1 & 0 & 0 & 0 \\ 0 & 0 & -1 & 1 & -1 & 0 & 1 & 1 & 0 & 0 \\ -1 & 0 & 0 & 1 & 1 & 0 & -1 & 0 & 0 & 1 \\ 0 & 0 & 0 & 1 & -1 & 0 & -1 & 1 & 0 & 1 \\ 0 & 0 & 1 & -1 & 1 & 0 & -1 & -1 & 0 & 0 \\ 1 & 0 & 0 & -1 & -1 & 0 & 1 & 0 & 0 & -1 \\ 0 & 0 & 0 & -1 & 1 & 0 & 1 & -1 & 0 & -1 \\ 0 & -1 & -1 & 1 & 0 & 1 & 1 & 0 & 0 & 0 \\ 0 & 0 & -1 & 1 & 0 & -1 & 1 & 0 & 1 & 0 \\ 0 & -1 & 0 & 1 & 0 & 1 & -1 & 0 & 0 & 1 \\ 0 & 0 & 0 & 1 & 0 & -1 & -1 & 0 & 1 & 1 \\ 0 & 1 & 0 & -1 & 0 & -1 & 1 & 0 & 0 & -1 \\ 0 & 0 & 1 & -1 & 0 & 1 & -1 & 0 & -1 & 0 \\ 0 & 0 & 0 & -1 & 0 & 1 & 1 & 0 & -1 & -1 \end{bmatrix} \in \mathbb{R}^{N_r \times S} \quad (7.22)$$

7

The total reaction vector can be expressed in terms of the product of the stoichiometric matrix and the individual reactions. Denote the N_r -dimensional vector of individual reactions as

$$\mathbf{r} = [r_1 \ r_2 \ \cdots \ r_{16}]^\top \in \mathbb{R}^{N_r} \quad (7.23)$$

Then the total reaction vector \mathbf{r}_ν is

$$\mathbf{r}_\nu = \mathbf{N}^\top \mathbf{r} \quad (7.24)$$

The rate equations in (7.20) have parameters k_{o_i} , and E_{a_i} that depend on the specific species involved in the reaction. In order to use these reaction rate equations, we assume that reactants, their end, and repetition groups are chemically similar, i.e.

they exhibit the same dynamic behavior. Hence, we only find the specific kinetic parameters for the reaction between AC1 and AOH, and AC2 and AOH. For the rest of the components, the same parameters are assumed to be the same. For example, k_0 and E_a of the reaction between AC1 and AOH will be used to model the reactions between the end and repetition groups of the AC1 and AOH. In Tables 7.1 and 7.2 the values of each kinetic parameter used for the set of reactions are shown

Table 7.1: Kinetic parameters for the forward condensation polymerization reactions

Reaction set	k_o [kg kmol $^{-1}$ s $^{-1}$]	E_a [kJ kmol $^{-1}$]
AC1 forward cond.	4.56×10^5	4.64424×10^4
AC2 Forward cond.	5.73×10^8	8.45×10^4

Table 7.2: Kinetic parameters for the backward condensation polymerization reactions

Reaction set	k_o [kg 2 kmol $^{-2}$ s $^{-1}$]	E_a [kJ kmol $^{-1}$]
AC1 backward cond.	9.74167×10^5	4.64424×10^4
AC2 Backward cond.	1.169387×10^9	8.22×10^4

The values presented in Tables 7.1 and 7.2 are used as initial values to model the reaction dynamics. These parameters describe the chemical kinetics of species that are chemically similar to the species involved in the process. These values will be calibrated in Chapter 8 to reproduce the observed behavior in the process data.

7

Condensation reactions are typically equilibrium-controlled, thus requiring the removal of the byproducts to guarantee a high degree of conversion. This equilibrium shift towards the products is achieved by the distillation unit operation that continuously removes the condensates from the reaction mixture. Most reactive distillation processes are treated as complex distillation units where the reaction can be restricted to a specific part of the column or take place in the whole of it. The combination of two processes into one brings production benefits at the expense of inducing a more complex process behaviour. Therefore, we need rigorous models to describe its complex behavior that can be used to optimize it and make sound operational decisions.

7.3. Reactive distillation process

Reactive distillation is a complex process where many physical phenomena occur. Concentration rates evolve not only in time but also in space and they depend on mass transfer and reaction kinetics, which are described by nonlinear functions. A general and rigorous model that describes the dynamic behavior of this process can be in the following form:

$$\frac{\partial x_i}{\partial t} - \frac{\partial x_i}{\partial z} - D_x \frac{\partial^2 x_i}{\partial z^2} = -\mathcal{J}(x_i, y_i) + \mathbf{r}(x_i, T) \quad (7.25)$$

$$\varrho \frac{\partial y_i}{\partial t} - \vartheta \frac{1}{\vartheta} \frac{\partial y_i}{\partial z} - D_y \frac{\partial^2 y_i}{\partial z^2} = \mathcal{J}(x_i, y_i) \quad (7.26)$$

$$\alpha \frac{\partial^2 T}{\partial z^2} - \bar{v} \frac{\partial T}{\partial z} - \Delta H_r + \tilde{Q} = \rho C_{p_l} \frac{\partial T}{\partial t} \quad (7.27)$$

where, t is the time coordinate and z is the spatial coordinate; x and y are the liquid and vapor concentration of the mixture in the process, respectively; D_x and D_y diffusion coefficients; $\mathcal{J}(x, y)$ is the mass transfer rate, α is the thermal diffusivity, and \bar{v} the average velocity that the fluid is moving with; ΔH_r is the heat of reaction; \tilde{Q} is the heat flow; ρ and C_{p_l} are the mixture density and the mixture heat capacity, respectively.

With $\varrho = \frac{y}{x}$, the vapor-liquid distribution ratio, and $\vartheta = \frac{L}{V}$ is the vaporized fraction, where L and V are the liquid phase and vapor phase molar flows per stage, respectively. The liquid flow L can be calculated with the knowledge of the column internal design hydraulics. However, the vapor flow V is generally much more complicated to calculate. The terms accounting for reaction rates $r(x_i, T)$ and reaction heat ΔH_r , are set to zero in case of a non-reactive distillation process.

As seen in (7.25), (7.26) and (7.27), the rigorous model is described by a set of partial differential equations which are nonlinear and have a high computational cost. Thus, to simplify the model the spatial-coordinate in the model is discretized, allowing the reduction of an infinite-dimension system to one of finite-dimension. A scheme of the discretized model is shown in Figure 7.3.

7

The reactive distillation process considered in this thesis is a batch process that follows a tight recipe to produce a wide range of polymers as desired products. This process comprises a batch reactor at the bottom, which is loaded with material, and a distillation column on top of it with a packing inside. The reactor acts as both a chemical reactor and a reboiler of the distillation column, whereas the distillation column is mainly used to remove the excess of water formed and vaporized during the polymerization condensation reaction. Furthermore, the process operates in closed-loop, where both temperature and pressure of the reactor, as well as the column's top temperature are tightly controlled in order to conform to the production recipe. These variables are controlled by means of three inputs: the reactor temperature is controlled manipulating the inlet temperature of the jacket oil (heated up or down in an external process), the reactor pressure is controlled using the opening of the pressure valve at the top of the column (this valve is instead modeled at the juncture between the reactor and column), and the column's top temperature is controlled directly changing the reflux flow, or equivalently, the reflux ratio. The

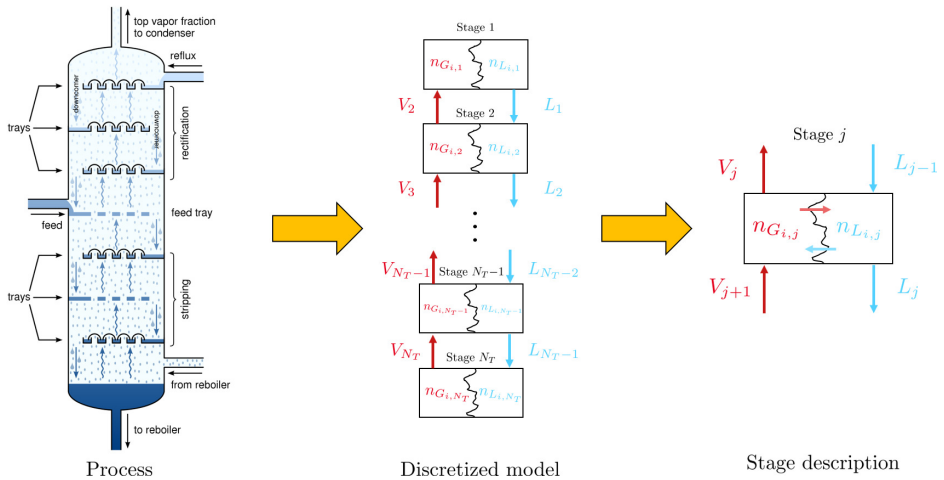


Figure 7.3: Lumped model representation of the reactive distillation column

key process variable to determine if the process has been completed is the viscosity of the polymer in the reactor. If it is within some prescribed range of values, then the process is deemed in specification or off specification. A scheme of the reactive batch distillation process is shown in Figure 7.4

7

Moreover, the production recipe contains different operational steps. These steps are mostly generated on the trajectories of both temperature and pressure within the reactor in closed loop. The steps are listed as follows:

1. Step 1: Filling
2. Step 2: Heat-up
3. Step 3: Heating on pressure
4. Step 4: Reaction
5. Step 5: Vacuum
6. Step 6: Cooling
7. Step 7: Discharging
8. Step 8: Cleaning

Due to the stage-wise nature of the process, the model structure will also change depending on the step where the process is operating. Thus, the model must take these changes into account. Moreover, the reactive batch distillation column has a

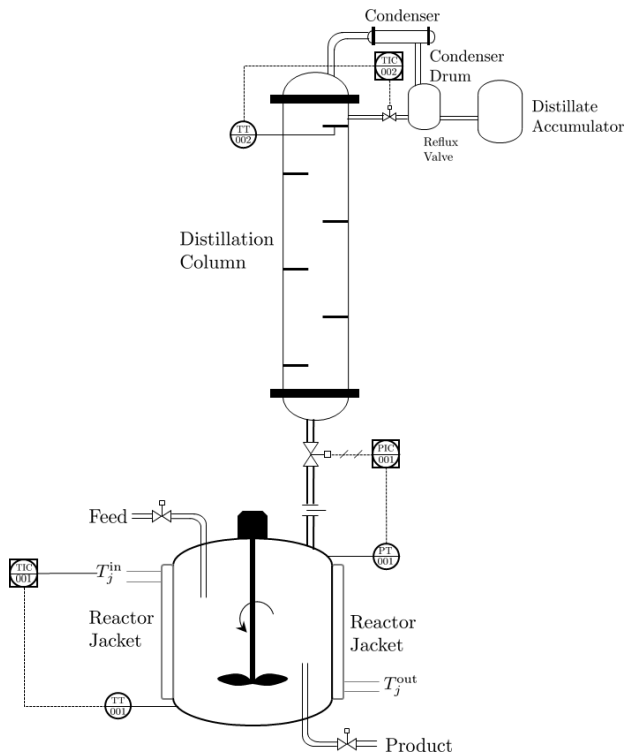


Figure 7.4: Reactive batch distillation process

7

packing to promote liquid-gas contact enhancing separation. However, for modeling purposes, the column will be assumed to be described by trays. Notice that this is not restrictive because calculations between trays and packed columns can be transformed using the height equivalent to a theoretical plate (HETP). This equivalence allows us to transform a tray-based representation of the model of the column into a packing-based one. Furthermore, the discretization allows us to generate a lumped model based on mass and energy balances. These balances are derived based on the following conditions and assumptions:

1. Phase equilibrium using the modified Raoult's law with liquid activity.
2. Liquid activity is modeled using poly-NRTL.
3. Vapor phase in the process follows the ideal gas law.
4. Thermal equilibrium, i.e. the phases have the same temperature distribution at each point.
5. Liquid phase accumulation is much larger than gas phase accumulation. Thus gas phase accumulation is negligible.

6. Total condenser.
7. The heat variation dQ of the system can be approximated by the heat capacity, i.e. changes of pressure in the liquid bulk are negligible¹. This allows to perform the approximation

$$dQ \approx d(n_L h_l) = h_l dn_L + n_L C_{pl} dT$$

where h_l is the liquid phase molar enthalpy, n_L the total number of moles in the liquid phase, and dT is the variation in temperature.

8. Computation of reflux \mathfrak{R} is based on the *internal reflux ratio* given by

$$\mathfrak{R} = \frac{L_{j-1}}{V_j} \in [0, 1] \quad (7.28)$$

where j is the stage number.

9. The number of internal trays $N_T = 8$ ($j = 1, \dots, NT$), and the number of species is $S = 10$ ($i = 1, \dots, S$)

Recall that the S -dimensional vector of moles \mathbf{n} is defined as in (7.21), and

$$n_{L_j} = \sum_i^S n_{l_{i,j}} = \mathbf{1}_S^\top \mathbf{n}_{l_j}$$

where $\mathbf{1}$ is a column vector of ones.

7

We use the aforementioned assumptions to model each step of the reactive batch distillation column. Furthermore, we introduce the following notation used throughout the RBD model:

F_{in} is the inlet molar liquid flow to the reactor, \mathbf{x}_{in} is the S -dimensional inlet composition vector of the inlet flow, \mathbf{n}_l is the S -dimensional vector of moles in the liquid phase, \mathbf{n}_g is S -dimensional vector of moles in the gas phase, n_L is the total number of moles in the liquid phase, $p_{i,j}$ is the partial pressure of i -th species in the j -th tray, h_{in} is the molar enthalpy of the inlet stream, h_l and C_{pl} are the molar enthalpy and the heat capacity of the liquid phase per stage, respectively; h_v is the molar enthalpy of the gas phase per stage, \mathbf{r} is the vector of chemical reactions, \mathbf{N} is the stoichiometric matrix; \mathbf{x} and \mathbf{y}^* are the S -dimensional vectors of liquid and vapor equilibrium compositions, respectively. ΔH_{vap} is the heat of vaporization, U_s is the overall heat transfer coefficient, A_s is the surface area of the reactor, M_{oil} is the total mass of oil in the reactor jacket, $C_{p_{\text{oil}}}$ is the heat capacity of the oil in the reactor jacket, F_{oil} is the inlet mass flow of oil to the reactor jacket, $T_{\text{jacket,in}}$ is the temperature of the oil at the inlet, and T_{jacket} is the oil temperature in the reactor jacket.

¹This assumption holds sufficiently well at each integration step of the model.

Step 1: Filling

This step accounts for loading the reactor with the necessary reactants. At the start of the process, the reactor contains only the acidic species (AC1 and AC2), then the alcohol (AOH) is added. In this particular step only the reactor is active in a semi-batch operation mode (the connection to the distillation column is closed).

Balance in the reactor: $j = N_T$

Component molar balance: Liquid phase

$$\frac{d\mathbf{n}_{l_j}}{dt} = F_{in}\mathbf{x}_{in} \quad (7.29)$$

Total molar balance (assumption 5)

$$\frac{dn_{L_j}}{dt} = F_{in} \quad (7.30)$$

Energy balance (assumptions 4 and 7)

7

$$\frac{dT_j}{dt} = \frac{1}{n_L C_{pl}} [F_{in}(h_{in} - h_{l_j})] \quad (7.31)$$

Step 2: Heat-up

After loading the reactor with the acidic species and the alcohol, the inlet flow is stopped, i.e. $F_{in} = 0$, and the reactor is closed. Similar to the filling stage, the connection to the distillation column is closed, and the process is driven in complete batch operation mode. However, in this step, the reactor is heated up to reach the activation temperature of the condensation reaction, but no vaporization occurs.

Balance in the reactor: $j = N_T$

Component molar balance: Liquid phase

$$\frac{d\mathbf{n}_{l_j}}{dt} = \mathbf{r}_\nu \quad (7.32)$$

Total molar balance (assumption 5)

$$\frac{dn_{L_j}}{dt} = \mathbf{0} \quad (7.33)$$

Energy balance (assumptions 4 and 7)

$$\frac{dT_j}{dt} = \frac{1}{n_L C_{p_L}} [\Delta H_r + U_s A_s (T_{\text{jacket}} - T_j)] \quad (7.34)$$

$$\frac{dT_{\text{jacket}}}{dt} = \frac{1}{M_{\text{oil}}} [F_{\text{oil}}(T_{\text{jacket,in}} - T_j) + \frac{U_s A_s}{C_{p_{\text{oil}}}} (T_j - T_{\text{jacket}})] \quad (7.35)$$

Step 3: Heat-up on pressure

7

Once the reactor has been heated up in the previous step, the process reaches a particular temperature value where the polymerization reactions start. This set of reactions generates water as a product, which vaporizes almost immediately due to the high temperatures in the reactor. The water vapor makes the pressure in the process to increase up to a pressure set-point defined by the process recipe. As in the previous two steps, only the reactor is active and the connection between the reactor and the distillation column remains closed.

Balance in the reactor: $j = N_T$

Component molar balance: Liquid phase

$$\frac{dn_{l_j}}{dt} = \mathbf{r}_\nu - V_j \mathbf{y}_j^* \quad (7.36)$$

Ideal gas law: Gas phase (assumption 3)

$$\mathbf{n}_{g_{i,j}} = \frac{p_{i,j} V_{\text{ol}}^g}{RT_j} \quad (7.37)$$

Total molar balance (assumption 5)

$$\frac{dn_{L_j}}{dt} = -V_j \quad (7.38)$$

Energy balance (assumptions 4 and 7)

$$\frac{dT_j}{dt} = \frac{1}{n_L C_{p_l}} \left[-V_j \Delta H_{\text{vap},j} - \Delta H_r + U_s A_s (T_{\text{jacket}} - T_j) \right] \quad (7.39)$$

$$\frac{dT_{\text{jacket}}}{dt} = \frac{1}{M_{\text{oil}}} \left[F_{\text{oil}} (T_{\text{jacket,in}} - T_j) + \frac{U_s A_s}{C_{p_{\text{oil}}}} (T_j - T_{\text{jacket}}) \right] \quad (7.40)$$

Step 4: Reaction

Once the internal pressure in the reactor reaches the pressure set-point, the valve connecting the reactor to the distillation column is opened, letting the gas accumulated in the reactor into the column. This causes a pressure drop in the process that is regulated by the pressure control loop to keep the pressure constant in the process. The vapor reaches the top of the column and it is then condensed back into liquid and returned back to the column using the reflux flow. The reflux flow is computed such that the top tray temperature remains close to the boiling temperature of the water at the operating pressure to ensure the continuous vaporization of water. Additionally, the temperature in the reactor is also kept constant at a temperature set-point defined by the production recipe. This is also done to guarantee a steady vapor flow from the reactor to the distillation column.

7

Balance in the reactor: $j = N_T$

Component molar balance: Liquid phase

$$\frac{d\mathbf{n}_{l_j}}{dt} = L_{j-1} \mathbf{x}_{j-1} - V_j \mathbf{y}_j^* + \mathbf{r}_\nu \quad (7.41)$$

Total molar balance (assumption 5)

$$\frac{dn_{L_j}}{dt} = L_{j-1} - V_j \quad (7.42)$$

Energy balance (assumptions 4 and 7)

$$\frac{dT_j}{dt} = \frac{1}{n_L C_{pl}} \left[L_{j-1}(h_{l_{j-1}} - h_{l_j}) - V_j \Delta H_{\text{vap},j} - \Delta H_r + U_s A_s (T_{\text{jacket}} - T_j) \right] \quad (7.43)$$

$$\frac{dT_{\text{jacket}}}{dt} = \frac{1}{M_{\text{oil}}} \left[F_{\text{oil}}(T_{\text{jacket,in}} - T_j) + \frac{U_s A_s}{C_{p_{\text{oil}}}} (T_j - T_{\text{jacket}}) \right] \quad (7.44)$$

Balance in the distillation column: $\forall j = 3, \dots, N_T - 1$

Component molar balance: Liquid phase

$$\frac{d\mathbf{n}_{l_j}}{dt} = L_{j-1} \mathbf{x}_{j-1} + V_{j+1} \mathbf{y}_{j+1}^* - L_j \mathbf{x}_j - V_j \mathbf{y}_{i,j}^* \quad (7.45)$$

Total molar balance (assumption 5)

$$\frac{dn_{L_j}}{dt} = L_{j-1} + V_{j+1} - L_j - V_j \quad (7.46)$$

7

Energy balance (assumptions 4 and 7)

$$\frac{dT_j}{dt} = \frac{1}{n_L C_{pl}} \left[L_{j-1}(h_{l_{j-1}} - h_{l_j}) + V_{j+1}(h_{v_{j+1}} - h_{l_j}) - V_j(h_{v_j} - h_{l_j}) \right] \quad (7.47)$$

Balance in the reflux and distillate drums: $\forall j = 1, 2$

Component molar balance: Liquid phase

$$\frac{d\mathbf{n}_{l_1}}{dt} = (1 - \mathfrak{R}) V_{j-2} \mathbf{x}_{j-1} \quad (7.48)$$

$$\frac{d\mathbf{n}_{l_2}}{dt} = \mathbf{0} \quad (7.49)$$

Energy balance (assumptions 6)

$$\frac{dT_j}{dt} = \mathbf{0} \quad (7.50)$$

$$\forall i = 1, \dots, S, \quad \forall j = 1, \dots, N_T$$

Ideal gas law: Gas phase (assumption 3)

$$\mathbf{n}_{g_{i,j}} = \frac{p_{i,j} V_{\text{ol}}^g}{RT_j} \quad (7.51)$$

Step 5: Vacuum

After some time, the pressure of the process is driven back to atmospheric pressure. At this point, a sample of the polymer in the reactor is taken to assess its physico-chemical properties. This off-line analysis will determine the point when vacuum is activated; this is done in order to extract all the residual water vapor, while initiating the gelation of the polymer, and making the viscosity of the polymer increase exponentially. In this particular step, the connection between the reactor and the column is closed again, while the vapor is bypassed directly to the condenser and distillate drum (stage 1). Thus, the constitutive equations remain the same as in the reaction step except:

Balance in the reflux and distillate drums: $\forall j = 1, 2$

Component molar balance: Liquid phase

$$\frac{d\mathbf{n}_{l_1}}{dt} = (1 - \mathfrak{R})V_{j-2}\mathbf{y}_{j-2}^* + V_{N_T}\mathbf{y}_{N_T}^* \quad (7.52)$$

$$\frac{d\mathbf{n}_{l_2}}{dt} = \mathbf{0} \quad (7.53)$$

Total molar balance (assumption 5)

$$\frac{dn_{L_1}}{dt} = (1 - \mathfrak{R})V_{j-2} + V_{N_T} \quad (7.54)$$

The steps 6 and 7 corresponding to cooling and discharge are not presented because these can be described by a combination of the previous steps, while being less critical for the production and the product quality.

So far, we have presented the model representing the dynamics of the RBD. Additionally, we need to include the constitutive relations, such as thermodynamic and fluid dynamic relationships. The former allows us to compute properties of the species involved in the process, while the latter allow us to calculate the different liquid and vapor flows interacting in the process. These relationships are explained in detail in the next sections.

7.3.1. Thermodynamic relationships

Thermodynamic relationships are the set of algebraic equations (constitutive relations) that allow the calculation of extensive and intensive properties of each of the species. These equations are important because they express the relationships necessary to be able to simulate the process model. Most of these relationships are related to the well-understood concept of phase equilibrium. Assuming that the whole process is in instantaneous equilibrium, the process pressure can be explicitly computed using vapor-liquid equilibrium (VLE) equations:

7

Equilibrium pressure

The two phases in the reactive batch distillation process are assumed to reach instantaneous equilibrium. This implies that the composition in the liquid of a particular species is related to the composition in the gas phase. The gas phase generates a pressure over the bulk of the liquid phase, which is given by the modified Raoult's law

$$\forall j = 1, \dots, N_T - 1$$

$$P_j = \sum_{i=1}^S x_{i,j} \gamma_{i,j} P_{i,j}^{\text{sat}} \quad (7.55)$$

Notice that the equilibrium pressure P in each stage is a function of the stage liquid composition x , the activity coefficient γ per component per stage, and P^{sat} . The activity coefficient is calculated using the poly-NRTL activity model, which is based on the standard non-random two liquids (NRTL), and also contains the so-called

Flory-Huggins (FH) correction to account for the behavior of polymers. The model is given by

$$\ln(\gamma_i) = \ln(\gamma_i)^{\text{NRTL}} + \ln(\gamma_i)^{\text{FH}} \quad (7.56)$$

with

$$\ln(\gamma_i)_{i=s}^{\text{NRTL}} = \frac{\sum_J x_J G_{Js} \tau_{Js}}{\sum_K x_K G_{Ks}} + \sum_J \frac{x_J G_{Js}}{\sum_K x_K G_{KJ}} \left(\tau_{sJ} - \frac{\sum_K x_K G_{KJ} \tau_{KJ}}{\sum_K x_K G_{KJ}} \right) \quad (7.57)$$

$$\ln(\gamma_i)_{i=p}^{\text{NRTL}} = \sum_I \mu_{I,p} \left[\frac{\sum_J x_J G_{JI} \tau_{JI}}{\sum_K x_K G_{KI}} + \sum_J \frac{x_J G_{JI}}{\sum_K x_K G_{KJ}} \left(\tau_{IJ} - \frac{\sum_K x_K G_{KJ} \tau_{KJ}}{\sum_K x_K G_{KJ}} \right) \right] \quad (7.58)$$

$$\ln(\gamma_i)^{\text{FH}} = \ln \left(\frac{\phi_i}{x_i} \right) + 1 - \theta_i \sum_k \left(\frac{\phi_k}{\theta_k} \right) \quad (7.59)$$

and

$$x_I = \frac{x_i \mu_{I,i}}{\sum_j x_j \mu_{J,j}}$$

$$G_{JI} = \exp(-\beta_{JI} \tau_{JI})$$

$$\tau_{JI} = \frac{g_{JI} - g_{II}}{RT}$$

$$\phi_i = \frac{n_i \theta_i}{\sum_j n_j \theta_j}$$

where g_{JI} is the energy of interaction between $J-I$ pairs of species, g_{II} is the energy of interaction between $J-I$ pairs of species, x is the liquid molar composition, μ is the degree of polymerization, n is the number of moles, θ is the ratio of polymer molar volume to segment molar volume, ϕ is the volume fraction (approximated as segment molar fraction), τ is the interaction parameter, β is the NRTL non-randomness factor. The indexes s and p stand for solvent and polymer, respectively. The sub and superscripts i and j are component-based indexes, and I and J are segment-based indexes.

The equilibrium pressure given in (7.55), also depends on the saturation pressure of each component. Saturation pressures are usually computed using some form of

the Antoine's equation, which is an exponential relationship between temperature and saturation pressure. The modified Antoine's equation used for this specific polymerization process is the Design Institute for Physical Properties (DIPPR) equation 101:

$$\ln(P_{i,j}) = a_{1,i} + \frac{a_{2,i}}{T_j} + a_{3,i} \ln(T_j) + a_{4,i} T_j^{a_{5,i}} \quad (7.60)$$

where $a_{1,i} - a_{5,i}$ are parameters that are specific for each of the i -th species and for the corresponding equation.

Heat capacity

The calculation of heat capacities in the model is crucial to calculate the temperatures in the process using the energy balance. By definition, an infinitesimal change in the system's internal energy is given by

$$\begin{aligned} dU &= dQ - dW \\ dU &= dQ - PdV_{\text{ol}} \\ dU + d(PV_{\text{ol}}) &= dQ - PdV_{\text{ol}} + d(PV_{\text{ol}}) \\ d(U + PV_{\text{ol}}) &= dQ + V_{\text{ol}}dP \end{aligned} \quad (7.61)$$

$dH = dQ + V_{\text{ol}}dP$ (By assumption 7, we have that)
 $dQ \approx dH = d(n_L h_l)$

7

where U is the internal energy in the system, Q is the heat content in the system, W is the work performed or received in the system, P is the system's pressure, V_{ol} is the geometric volume, and H is the total enthalpy of the process.

Since (7.61) does not depend on variations of pressure P (assumed to be negligible), it only depends on the temperature T . Thus we can define the heat capacity as

$$C_{p_l} \equiv \left(\frac{\partial h_l}{\partial T} \right)_P \quad (7.62)$$

Therefore

$$dh_l = \left(\frac{\partial h_l}{\partial T} \right)_P dT = C_{p_l} dT \quad (7.63)$$

Hence

$$dQ \approx dH = d(n_L h_l) = h_l dn_L + n_L C_{p_l} dT \quad (7.64)$$

The total change in enthalpy can be found solving (7.63) integrating from an initial (reference) state to an arbitrary final state.

$$\Delta h_l = \int_{T_{\text{ref}}}^{T_f} C_{p_l} \, dT \quad (7.65)$$

where the heat capacity C_{p_l} is computed using DIPPR equation 100. For the i -th component in the j -th stage, we have

$$C_{p_{l_{i,j}}} = a_{1,i} + a_{2,i}T_j + a_{3,i}T_j^2 + a_{4,i}T_j^3 + a_{5,i}T_j^4 + a_{6,i}T_j^5 + a_{7,i}T_j^6 \quad (7.66)$$

7

where $a_{1,i} - a_{7,i}$ are parameters that are specific for each of the i -th species and for the corresponding equation.

The total heat capacity of each stage $C_{p_{l_j}}$ is given by the arithmetic mixing rule:

$$C_{p_{l_j}} = \sum_{i=1}^S x_{i,j} C_{p_{l_{i,j}}} \quad (7.67)$$

Heat of vaporization

The heat of vaporization is the energy required to produce a change from the liquid phase to the gas phase. In the reactive batch distillation process, the liquid mixture is heated up to vaporize the water produced in the polymerization reaction. Therefore, it is necessary to account for the change in total energy caused by the vaporization of the liquid phase. The heat of vaporization of a pure substance is a function solely of the temperature given by the Clapeyron equation

$$\Delta h_{\text{vap}} = T \Delta v_{lg} \frac{dP^{\text{sat}}}{dT} \quad (7.68)$$

where Δv_{lg} is the change in specific volume due to phase change between liquid and gas phases.

If the phase transition between the liquid phase and the gas phase occurs at temperatures much lower than the critical temperature, the specific volume of the gas phase v_g largely exceeds that of the liquid phase v_l , we have that

$$\Delta v_{lg} \approx v_g \quad (7.69)$$

By assumption 3, during the vaporization the gas phase behaves as an ideal gas

$$v_g = \frac{\bar{R}T}{P^{\text{sat}}} \quad (7.70)$$

with \bar{R} is the specific gas constant.

Replacing (7.70) in (7.68), and integrating from an initial (reference) state to an arbitrary final state, we obtain the Clausius-Clapeyron equation

$$\Delta h_{\text{vap}} = \frac{T_f T_{\text{ref}}}{T_f - T_{\text{ref}}} \bar{R} \ln \left(\frac{P_f^{\text{sat}}}{P_{\text{ref}}^{\text{sat}}} \right) \quad (7.71)$$

Despite the usefulness of the Clausius-Clapeyron equation, it approximates the total change in the specific volume Δv_{lg} to the specific volume of the gas phase v_g at temperatures much lower than the critical temperature. Thus, to avoid this approximation, we use DIPPR equation 106 that takes into account information of the critical temperature of the substance. For the i -th component in the j -th stage, the DIPPR equation 106 is given by

$$\Delta h_{\text{vap}_{i,j}} = a_{1,i} (1 - T_{r_{i,j}})^{a_{2,i} + a_{3,i} T_{r_{i,j}} + a_{4,i} T_{r_{i,j}}^2 + a_{5,i} T_{r_{i,j}}^3} \quad (7.72)$$

with $T_{r_{i,j}} = \frac{T_j}{T_{c_i}}$, where T_r is the reduced temperature, and T_c is the critical temperature. $a_{1,i} - a_{5,i}$ are parameters that are specific for each of the i -th species and

for the corresponding equation.

The total heat of vaporization of each stage ΔH_{vap} is given by the arithmetic mixing rule:

$$\Delta H_{\text{vap}_j} = \sum_{i=1}^S x_{i,j} \Delta h_{\text{vap}_{i,j}} \quad (7.73)$$

Finally, the enthalpy of the gas phase in the model is computed as

$$h_{v_j} = h_{l_j} + \Delta H_{\text{vap}_j} \quad (7.74)$$

Calculation of mixture's boiling point

A relevant quantity that will be used extensively in modeling of the reactive batch distillation column is the boiling points of the mixtures at each tray. These boiling points can be computed using the modified Raoult's law for non-ideal mixtures in (7.55). However, notice that both the activity coefficient γ and the saturation pressure P^{sat} are nonlinear functions of the temperature of the mixture. Thus, the equilibrium pressure relation cannot be analytically solved for the boiling temperature, and therefore, we must resort to a numerical method to calculate it. Since the equilibrium pressure relation is a continuous function of the temperature, any root-finding algorithm can be employed such that

$$P_j - \sum_{i=1}^S x_{i,j} \gamma_{i,j}(T_{\text{boil}_j}) P_{i,j}^{\text{sat}}(T_{\text{boil}_j}) = 0, \quad P_j \geq 0 \text{ bar}_a \quad (7.75)$$

Notice that the quantity $\sum_{i=1}^S x_{i,j} \gamma_{i,j}(T_{\text{boil}_j}) P_{i,j}^{\text{sat}}(T_{\text{boil}_j})$ must be greater than zero. If it is zero, it means that there is no material on the tray and it would not make sense to define a boiling point.

Heat of reaction

The heat released or absorbed by the reaction is calculated using the heat of reaction. In the case of the reactive batch distillation process, the polymerization reaction

induces a change in the total energy content of the liquid mixture, and thus, it is necessary to account for these changes in the energy balance. The heat of reaction is typically modeled from enthalpies of formation of the involved species applying Hess' law as follows:

$$\Delta\mathbf{H}^\ominus = \sum_{i=1}^{S_p} \nu_i \Delta H_{f_i}^\ominus + \sum_{i=1}^{S_r} \nu_i \Delta H_{f_i}^\ominus \quad (7.76)$$

where $\Delta\mathbf{H}^\ominus \in \mathbb{R}^{1 \times N_r}$ is the vector of heat of reaction, $\Delta H_{f_i}^\ominus$ is the standard heat of formation of the i -th species, S_r is the number of reactants, and S_p .

In vector form, the heat of reaction can be written as:

$$\Delta\mathbf{H}^{\ominus\top} = \Delta\mathbf{H}_f^{\ominus\top} \mathbf{N}^\top \quad (7.77)$$

with $\Delta\mathbf{H}_f^\ominus = [\Delta H_{f_1}^\ominus \quad \cdots \quad \Delta H_{f_S}^\ominus]^\top$.

Finally, since the enthalpy is an extensive property that changes with the amount of moles present in the mixture, the enthalpy of the reaction scales proportionally to the moles used in the reaction. Therefore, the total heat of reaction at a given moment of the process is

$$\Delta H_r = \Delta\mathbf{H}^{\ominus\top} \mathbf{r} = \Delta\mathbf{H}_f^{\ominus\top} \mathbf{r}_\nu \quad (7.78)$$

If the heat of reaction $\Delta H_r > 0$ the reaction is said to be endothermic, i.e. the reaction requires energy to take place. On the other hand, if $\Delta H_r < 0$, the reaction is said to be exothermic, or in other words, the reaction releases energy while it progresses.

7.3.2. Fluid dynamic relationships

One of the most challenging aspects of the modeling is the computation of the liquid and vapor flows going through the reactor and column. These flows determine how fast the accumulation of matter in each stage occurs, as well as the transfer of matter between the phases. Ultimately, how these flows propagate in the process determine how long it takes to achieve an appropriate separation. Another aspect about these

liquid and vapor flows is that they are only present when certain operating conditions are met. The calculation of the liquid and vapor flow rates in the distillation column is addressed independently for each type of flow.

Computation of liquid flows

The computation of liquid flows running down a distillation column has been subject to extensive study in the literature due its importance in modeling the distillation process. Despite the large number of equations and correlations to calculate liquid flows (see e.g. [201], [108]), the Francis' weir equation will be used because of its simplicity and effectiveness in providing reasonable magnitudes for the liquid flows.

The Francis' weir equation provides the height H_{ow} (in meters) required by a liquid to flow over the weir [201] according to

$$H_{ow} = 1.43 \sqrt[3]{\frac{1}{g} \left(\frac{Q_L}{L_w} \right)^2} \quad (7.79)$$

where Q_L is the volumetric liquid flow over the weir, ℓ_w is the weir length, and g is the gravity acceleration.

7

However, we are interested in an explicit expression to calculate the volumetric flow Q_L . Rearranging (7.79), we obtain the expression to compute the volumetric liquid flow per stage in the column.

$$Q_L = \ell_w \sqrt{\left(\frac{H_{ow}}{1.43} \right)^3 g} \quad (7.80)$$

The design dimensions of the distillation column are used to compute the weir length ℓ_w .

$$\ell_w = \sqrt{\frac{4A_t}{\pi}} \quad (7.81)$$

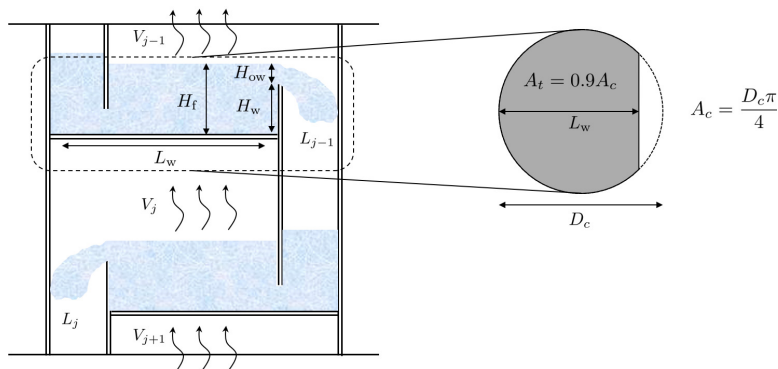
with $A_t = 0.9A_c$, and $A_c = \frac{D_c \pi}{4}$. Where A_t is the tray cross-section area, which is typically 90% of the total available cross-section area, A_c is the cross-section area

of the column, and D_c is the diameter of the distillation column. Furthermore, the height of liquid over weir H_{ow} can be computed from the total liquid height H_f in the tray and the actual height of the weir H_w .

$$H_{ow} = \max(0, H_f - H_w) \quad (7.82)$$

with $H_f = \frac{m_L}{\rho_L A_t}$, where m_L is the total mass of liquid in the tray, and ρ_L is the density of the liquid in the tray.

Notice that the form of (7.82) is nonzero positive when the liquid height in the tray H_f exceeds that of the weir H_w . The former is guaranteed to vary as it explicitly depends on both the total liquid mass in the tray and its corresponding density. In Figure 7.5 a schematic representation of the internal configuration of a typical tray distillation column is shown.



7

Figure 7.5: Longitudinal and cross sections of the distillation column

Finally, since the molar and energy balances require liquid molar flows L , we use the following expression to convert the flow calculation basis from volumetric flow rate to molar flow rate.

$$L = Q_L \rho_n \quad (7.83)$$

where ρ_n is the liquid molar density of the mixture.

Computation of vapor flows

The vapor flows in the distillation column are strongly dependent on the temperature profile in the process, and by extension, they also depend on the energy balance. They also exhibit a fast switching behavior, as these flows suddenly appear when the mixture's temperature exceeds the boiling point. In view of this, we use the approach proposed in [114], where the general mass and energy balances are used to compute steady state vapor flows. The true vapor flows are later computed as a fraction of these steady state vapor flows based on the difference between the mixture's boiling point and the temperature of the liquid in each tray.

Recall that the total mass and energy balances in an arbitrary j -th stage of a reaction system with phase transition (vaporization or condensation), negligible gas phase accumulation, and exogenous heat input are given by

$$\frac{dn_{Lj}}{dt} = L_{j-1} + V_{j+1} - L_j - V_j \quad (7.84)$$

$$\frac{d(n_L h_l)}{dt} = L_{j-1} h_{l_{j-1}} + V_{j+1} h_{v_{j+1}} - L_j h_{l_j} - V_j h_{v_j} - \Delta H_r + \bar{Q} \quad (7.85)$$

Replacing (7.84) in (7.85), making use of (7.74), and assuming that the net accumulation of energy in the j -th stage is zero (energy is at steady state), we obtain

$$\begin{aligned} \frac{d(n_L h_l)}{dt} &= L_{j-1} h_{l_{j-1}} + V_{j+1} h_{v_{j+1}} - L_j h_{l_j} - V_j h_{v_j} - \Delta H_r + \bar{Q} \\ h_{l_j} \frac{dn_L}{dt} + n_{Lj} \underbrace{\frac{dh_{l_j}}{dt}}_{\equiv 0} &= L_{j-1} h_{l_{j-1}} + V_{j+1} h_{v_{j+1}} - L_j h_{l_j} - V_j h_{v_j} - \Delta H_r + \bar{Q} \end{aligned} \quad (7.86)$$

$$0 = L_{j-1}(h_{l_{j-1}} - h_{l_j}) + V_{j+1}(h_{v_{j+1}} - h_{l_j}) - V_j^{\text{ss}} \Delta H_{\text{vap}_j} - \Delta H_r + \bar{Q}$$

$$V_j^{\text{ss}} = \frac{L_{j-1}(h_{l_{j-1}} - h_{l_j}) + V_{j+1}(h_{v_{j+1}} - h_{l_j}) - \Delta H_r + \bar{Q}}{\Delta H_{\text{vap}_j}}$$

The vapor flow calculation in steady state in (7.86) might take negative values for some values of the enthalpies or heat of reaction. To enforce positiveness of the solution, we apply the max function. Hence

$$V_j^{\text{ss}} = \max \left(0, \frac{L_{j-1}(h_{l_{j-1}} - h_{l_j}) + V_{j+1}(h_{v_{j+1}} - h_{l_j}) - \Delta H_r + \bar{Q}}{\Delta H_{\text{vap}_j}} \right) \quad (7.87)$$

Since the process is not actually at steady state in terms of energy, we make use of a smooth activation function such that the temperature-dependent switching behavior can be captured in the model. To this end, we introduce the switching function ω in the j -th stage of the form

$$\omega_j = \frac{1}{2} [1 + \tanh k_t(T_j - T_{\text{boil}_j})] \quad (7.88)$$

where k_t is a user-defined constant to control the switching speed in terms of the temperature, and T_{boil} is the mixture's boiling point.

Furthermore, in order to take into account the average pressure drop ΔP along the distillation column, a modification is performed to the switching function ω as follows

$$\omega_j = \frac{1}{4} [1 + \tanh k_t(T_j - T_{\text{boil}_j})] [1 + \tanh k_p(P_j - P_{j-1} - \Delta P)] \quad (7.89)$$

7

where k_p is a user-defined constant to control the switching speed in terms of the pressure, and ΔP is the average pressure drop in the column.

Finally, true vapor flow V_j is computed based on the steady state vapor flow V_j^{ss} and the modified switching function

$$V_j = \omega_j V_j^{\text{ss}} \quad (7.90)$$

Notice that the switching function $\omega_j : \mathbb{R}_{\geq 0} \times \mathbb{R}_{\geq 0} \mapsto [0, 1]$, and thus the true vapor flow V_j will always have V_j^{ss} as an upper bound.

7.4. Polymer viscosity

One of the key variables in the process to assess the product quality is the (dynamic) viscosity of the polymer mixture in the reactor. A high value of viscosity correlates

with higher degrees of conversion, and thus higher concentrations of polymer in the reactor. However, modeling viscosity, and especially for liquid mixtures is a difficult task due to the complex nonlinear behavior of the interacting phenomena that govern the viscosity behavior. Prediction of the dynamic viscosity of liquid mixtures has been addressed extensively in literature, ranging from theoretical approaches based on statistical mechanics to more empirical ones for diverse industrial applications (see [206],[207]). However, most of the theoretical approaches require a large number of experimental parameters that are not readily available to perform an explicit calculation of the mixture's viscosity. Practical approaches, circumvent this issue by computing each pure component viscosity and applying a simplified mixing rule, at the expense of losing generality. Nevertheless, they might provide a satisfactory approximate answer that can be good enough to make informed decisions. In this section, we develop a dynamic model that describes the viscosity of the polymer produced in the RBD.

7.4.1. Modeling of viscosity

According to Kim *et al.* [93], the viscosity of polymeric mixture depends on the temperature, the polymer concentration (monomer conversion), the weight-average molar mass of the polymer, and the shear rate. However, at high temperatures the shear thinning effects are negligible, and thus the shear rate can be assumed to be zero [93]. A suitable candidate model to describe the polymer viscosity in the RBD should contain these aforementioned variables.

7

In order to develop an empirical model for the viscosity, let us first take the following considerations into account:

- Polymerization is a step-growth polymerization. Condensation polymerization (polymerization reactions that produce smaller molecules as byproduct, such as water) is a type of step-growth polymerization.
- The product is a high-molecular weight linear polymer.

Degree of polymerization (\bar{X})

The average number degree of polymerization is a measure of the number of repeating units in a polymer molecule [148]. Polymer molecules come in different sizes (chain lengths, for linear polymers), so the average molecular mass will depend on the method of averaging. Among the several ways to average the polymer molecule distribution, there are two that are typically used in polymer analysis. These are the average-number degree of polymerization \bar{X}_n , and the weight-average degree of

polymerization \bar{X}_w . Likewise, the same distinction can be made to quantify the mass distribution in a polymer chain with the number-average \bar{M}_n and the weight-average \bar{M}_w molar masses of a polymer. The relation between the degree of polymerization and the molar mass of the same macromolecule is given by:

$$\bar{X}_n = \frac{\bar{M}_n}{M_0} \quad (7.91)$$

$$\bar{X}_w = \frac{\bar{M}_w}{M_0} \quad (7.92)$$

where M_0 is the molecular weight of the repeating unit.

Fractional monomer conversion ξ

The fractional monomer conversion ξ is the fraction of functional groups in deficient concentration that have reacted [148]. This quantity is bounded by $0 \leq \xi \leq 1$, and it is defined as

$$\xi = \frac{\text{no. functional groups used}}{\text{no. functional groups initially}} \quad (7.93)$$

Relationships between polymer molar mass, conversion and degree of polymerization

The relationship between the monomer fractional conversion ξ and the both number-average and weight-average degrees of polymerization in the case of a high-molecular weight linear polymer is given by [148]

$$\bar{X}_n = \frac{1}{1 - \xi} \quad (7.94)$$

$$\bar{X}_w = \frac{1 + \xi}{1 - \xi} \quad (7.95)$$

Additionally, again under the assumption of a high-molecular weight linear polymer, the average-number degree of polymerization can be computed as [159]:

$$\bar{X}_n = \frac{\sum C_{\text{rep}} + \sum C_{\text{end}}}{\frac{1}{2} \sum C_{\text{end}}} \quad (7.96)$$

where C_{rep} and C_{end} are the concentrations of the repeating and end segments, respectively.

Substituting (7.96) in (7.94), we can compute the fractional monomer conversion ξ

$$\xi = 1 - \frac{1}{\bar{X}_n} = 1 - \frac{1}{2} \frac{\sum C_{\text{end}}}{\sum C_{\text{rep}} + \sum C_{\text{end}}} \quad (7.97)$$

Replacing (7.97) in (7.95), the value of \bar{X}_w can be computed. Finally, the polymer weight-average molar mass \bar{M}_w can be computed replacing the value of \bar{X}_w in (7.92). Thus

$$\bar{M}_w = M_0 \bar{X}_w = M_0 \left(\frac{1 + \xi}{1 - \xi} \right) \quad (7.98)$$

A high weight-average molar mass means that larger chains of polymer are being formed in the process, leading to a reacting mixture with a higher viscosity. It is also worth noting that the polymer is not the only present species in the mixture because the reactants, as well as other unreacted end segments, make part of the reacting mixture. Therefore, the contribution of the weight-average molar mass \bar{M}_w of the polymer is weighted by its true weight fraction w_{poly} . Finally, the weight average molar mass and viscosity should exhibit a direct proportionality relationship.

7

$$\eta \propto w_{\text{poly}} \bar{M}_w \quad (7.99)$$

$$\text{where } w_{\text{poly}} = \frac{\sum m_{\text{rep}}}{\sum_{i=1}^S m_i}.$$

Another important variable in the prediction of the viscosity of polymers is the temperature. The viscosity of a substance decreases with the temperature due to an increase in the kinetic energy of molecules, which reduces the internal friction [30]. Therefore, we can establish an inverse proportionality relation between the viscosity and temperature.

$$\eta \propto \frac{1}{T} \quad (7.100)$$

7.4.2. The logistic equation: population growth dynamics

A more difficult task is to establish a particular structure to the function that explicitly describes the relationship between the viscosity, molar mass, polymer concentration, and temperature. Mendelson [122],[123] reported that the viscosity follows an exponential growth with respect to the polymer concentration and weight average molar mass, as well as an exponential decay with respect to the temperature. Thus, we shall impose this type of behavior in the empirical model.

A relevant aspect to consider is that the polymer viscosity cannot grow unbounded. In general, it will stop when the conversion of the reactants or monomers reach the unity. Therefore, the viscosity should behave in such a way that it increases exponentially when the molar mass and fractions of polymer are high, while reaching a settling point whenever a complete conversion has been achieved. We propose a population growth-like dynamics to model the viscosity dynamics. We can model this behavior using a logistic differential equation

7

$$\frac{d\eta}{dt} = \frac{\varphi}{K}\eta(K - \eta), \quad K > 0, \quad \eta(0) = \eta_0 > 0, \quad \forall t \geq 0 \quad (7.101)$$

where K is a parameter akin to the carrying capacity, i.e. the maximum attainable value by the viscosity under the given the reaction conditions, and φ is the growth rate.

If both K and φ are constant, the differential equation (7.101) has the logistic equation as a solution

$$\eta(t) = \frac{K}{1 + \left(\frac{K - \eta_0}{\eta_0}\right)e^{-\varphi t}} \quad (7.102)$$

This equation generates an "S-shaped" curve whose maximum value is provided by K , and φ defines the steepness of the curve. The inflection point where the curve starts to decrease its growth is given by the point $(t, \eta) = \left(\frac{1}{\varphi} \ln \left(\frac{K - \eta_0}{\eta_0}\right), \frac{K}{2}\right)$

However, considering the physical meaning of the carrying capacity $K(t)$, the maximum value attained by the viscosity will be a result of the trade-off between the

direct proportional effect of polymer concentration and molar mass, and the inverse proportional effect of the temperature. This implies that the carrying capacity will vary in time as well. Thus, the carrying capacity is modeled according to the following empirical relationship

$$K(t) = \frac{c_1 w_{\text{poly}} \bar{M}_w}{c_2 T} \quad (7.103)$$

where c_1 and c_2 are empirical scaling parameters to ensure dimensional soundness.

On the other hand, the growth rate φ usually increases exponentially fast whenever the copolymer reaches the gelation point, where the degree of polymerization becomes *infinite* [148]. This gelation point naturally depends on the fraction of formed polymer and reactive groups in the mixture. In the case of condensation polymerization, since the main byproduct is water, we approximate the aforementioned fraction as $1 - w_{\text{H}_2\text{O}}$. Therefore, we model the growth rate φ as

$$\varphi = c_3(1 - w_{\text{H}_2\text{O}}) \quad (7.104)$$

Since both the carrying capacity K and φ are time-varying, the analytic solution of (7.101) cannot be expressed explicitly as in (7.102).

7.5. Simulation of the reactive batch distillation column model

To simulate the RBD model presented 7.3, a ratio of 15:40:45 (AC1:AC2:AOH) in mass base is assumed. Moreover, recall that the RBD process operates in closed-loop, hence, in the following we also provide the modeling of the control inputs to properly represent the plant. The control inputs in the plant are the inlet temperature of the jacket oil, the opening of the pressure control valve, and the opening of the reflux valve.

7.5.1. Loading flow

Since there is no information about the total quantities used in the real process, we compute the necessary molar proportions in terms of an arbitrary mass base $m_{\text{total}}^{\text{base}}$

$$w_{\ell_*} = \frac{n_{\ell_*} M_*}{m_{\text{base}}^{\text{base}}} \Rightarrow n_{\ell_*} = m_{\text{total}}^{\text{base}} \frac{w_{\ell_*}}{M_*} \quad (7.105)$$

where w_{ℓ_*} and M_* are the loading mass fraction and molar mass of the reactants, respectively, of an arbitrary substance in a solution of $m_{\text{total}}^{\text{base}}$ total loading mass units. The use of an arbitrary base is beneficial because it allows to scale the quantities if necessary.

The amount of loading moles for each of the species in the process (acid 1, acid 2, and alcohol 1), assuming $m_{\text{total}}^{\text{base}} = 2000$ kg, is

$$n_{\ell_{\text{AC1}}} = 2000 \text{ kg} \times \frac{w_{\ell,\text{AC1}}}{M_{\text{AC1}} \text{ kg kmol}^{-1}} = 2.1255 \text{ kmol}$$

$$n_{\ell_{\text{AC2}}} = 2000 \text{ kg} \times \frac{w_{\ell,\text{AC2}}}{M_{\text{AC2}} \text{ kg kmol}^{-1}} = 4.8155 \text{ kmol}$$

$$n_{\ell_{\text{AOH}}} = 2000 \text{ kg} \times \frac{w_{\ell,\text{AOH}}}{M_{\text{AOH}} \text{ kg kmol}^{-1}} = 7.6155 \text{ kmol}$$

7

However, in the real process, only AC1 and AC2 are present in the reactor at the start of the production. The alcohol AOH is loaded into the reactor during the loading phase. Hence, the initial condition $n_{0_{\text{AOH}}} = 0$. Nevertheless, the loading condition $n_{\ell_{\text{AOH}}} = 7.6155$ kmol will be used as the target amount for the filling of the reactor.

Based on the plant data, the reactor is loaded with an inlet flow with composition $x_{\text{AOH},N_T} = 1$. However, since it is not known what the inlet flow profile is, we propose multiple profiles that achieve the same loading composition. We here show two profiles:

Constant profile

This profile can be achieved assuming that the inlet flow F_{in} remains constant during the loading time interval $[t_{0_\ell}, t_{f_\ell}]$.

Consider the component mole balance during the filling step shown in (7.29), and integrate it

$$\int dn_{l_{AOH,N_T}} = \int_{t_{0_\ell}=0}^{t_{f_\ell}} F_{in} x_{in,AOH} dt \quad (7.106)$$

$$n_{l_{AOH,N_T}}(t_{f_\ell}) - n_{l_{AOH,N_T}}(t_{0_\ell}) = F_{in} x_{in,AOH}(t_{f_\ell})$$

We are interested only in the moles of AOH, so the initial number of moles in the reactor is $n_{l_{AOH,N_T}}(t_{0_\ell}) = 0$ at $t_{0_\ell} = 0$. The filling final time is free and depends on specific operating conditions in the real plant. Nonetheless, it is known that at t_{f_ℓ} the total number of moles of alcohol must be $n_{l_{AOH,N_T}}(t_{f_\ell}) = 7.6155$ kmol. Finally, the inlet flow is given by:

$$F_{in} = \frac{7.6155 \text{ kmol}}{t_{f_\ell}} \quad (7.107)$$

whose actual value will not be shown for confidentiality reasons

In order to stop the filling once the mass fraction is attained, we use the following switch

$$\omega_w = \frac{1}{2} \left[1 + \tanh \left(10^4 \frac{w_{\ell,AOH}^{\text{ref}} - w_{\ell,AOH}}{2} \right) \right]$$

7

Thus

$$\bar{F}_{in} = F_{in} \omega_w \quad (7.108)$$

Rate-limited profile

In this particular approach, we do not assume the inlet flow to be constant but its rate of change, i.e. $dF_{in}/dt = c_{in}$. By imposing constancy on the rate of the inlet flow we obtain an explicit relationship

$$\frac{dF_{in}}{dt} = c_{in} \Rightarrow F_{in}(t) = c_{in} t \quad (7.109)$$

We solve once more (7.29)

$$\begin{aligned} \int dn_{l_{AOH,N_T}} &= \int_{t_0}^{t_{f_\ell}} F_{in} x_{in,AOH} dt \\ \int dn_{l_{AOH,N_T}} &= c_{in} x_{in,AOH} \int_{t_0}^{t_{f_\ell}} t dt \\ n_{l_{AOH,N_T}}(t_{f_\ell}) - n_{l_{AOH,N_T}}(t_0) &= \frac{1}{2} c_{in} x_{in,AOH} (t_{f_\ell}^2 - t_0^2) \end{aligned} \quad (7.110)$$

Again, $t_0 = 0$ and $n_{l_{AOH,N_T}}(t_0) = 0$, and $n_{l_{AOH,N_T}}(t_{f_\ell}) = 7.6155$ kmol. Solving for c_{in}

$$c_{in} = \frac{2n_{l_{AOH,N_T}}(t_{f_\ell})}{t_{f_\ell}^2} \Rightarrow F_{in} = \frac{2n_{l_{AOH,N_T}}(t_{f_\ell})}{t_{f_\ell}^2} t \quad (7.111)$$

Likewise, we also introduce the same switching function ω_w as before to ensure that the flow reaches zero once the mass fraction reaches the desired value, i.e. $\bar{F}_{in} = F_{in}\omega_w$.

7

Notice that the choice of functions to model the inlet flow is not limited to these two approaches. However, these are the simplest ways to model and implement in simulation.

7.5.2. Jacket oil inlet temperature

The jacket oil inlet temperature $T_{jacket,in}$ is changed by an upstream heat exchanger whose information was not available to us so its dynamics is not specified in the model. Furthermore, as mentioned in Section 7.3, this process follows a tight recipe that is divided into several stages. The criteria to transition from one stage to another is largely based on knowledge obtained over the years of operation. This results in loosely defined values to enable these transitions, with many of the stage changes relying on time progression.

Given the available information, we model the jacket oil inlet temperature as a piece-wise function of time using the provided plant data of the reactor and jacket temperature profiles. The modeled $T_{jacket,in}$ is of the form

$$T_{\text{jacket,in}} = \begin{cases} f_1(t), & t_0 \leq t \leq t_1 \\ f_2(t), & t_1 < t \leq t_2 \\ f_3(t), & t_2 < t \leq t_3 \\ f_4(t), & t_3 < t \leq t_4 \\ f_5(t), & t_4 < t \leq t_5 \\ f_6(t), & t_5 < t \end{cases} \quad \begin{array}{l} \text{Filling step} \\ \text{Heat-up step} \\ \text{Heat on pres. step} \\ \text{Reaction step} \\ \text{Vacuum step} \\ \text{Cooling step} \end{array} \quad (7.112)$$

However, to avoid hard switching between these functions, which could potentially create some numerical problems, we transform (7.112) into a sum using smooth activation functions

$$\omega_{T_i}(t, t_{s_i}, t_{s_{i+1}}) = \frac{1}{4} \left[1 + \tanh \left(10 \frac{t - t_{s_i}}{2} \right) \right] \left[1 + \tanh \left(10 \frac{t_{s_{i+1}} - t}{2} \right) \right]$$

Thus

$$T_{\text{jacket,in}} = \sum_{i=1}^{N_s} f_i \omega_{T_i}(t) \quad (7.113)$$

where N_s is the number of stages included in the model.

7.5.3. Pressure control valve and reflux flow

Both the process pressure and the reflux flow are tightly controlled during the production to ensure the quality of the polymer being produced, so these two variables must also be included in the model of the process. While mass and energy balances are conserved throughout the discretization, the momentum is not, and an algebraic relationship (eq. (7.55)) is used to compute the pressure at each tray. As a consequence, the pressure does not propagate in the model as it does in the real process². However, since the pressure in the RBD is generated by the vaporization of water in the reactor, the pressure control valve is placed close to the reactor to ensure fast response to changes in the controlled variable.

In terms of computation, the pressure control valve κ_{valve} is a variable that is bounded in the $[0, 1]$ interval. A value of 1 represents a fully open valve, while

²The pressure could be computed from momentum balance equations, e.g. Bernoulli momentum conservation equation. However, these equations require solving implicit ordinary or partial differential equations, which might render the model impractical.

a value of 0 means that the valve is completely closed. The valve κ_{valve} is modeled as

$$\kappa_{\text{valve}} = \frac{1}{2} \left[1 + \tanh \left(10 \frac{P_8 - P_8^{\text{ref}}}{2} \right) \right] \in [0, 1] \quad (7.114)$$

where P_8^{ref} is the pressure reference to be followed by the production recipe.

Conversely, the reflux flow is used to increase and improve the overall separation in the process. As mentioned in assumption 8 in Section 7.3, the reflux being used in the model is the internal reflux flow. This quantity is defined as the ratio between the vapor flow leaving the column at the top and the returning liquid as shown in (7.28). Notice that the maximum amount of liquid that can be returned to the column is exactly all of the vapor flow. Hence, the internal reflux ratio $\mathfrak{R} \in [0, 1]$. The reflux ratio may be viewed as a valve that is fully open ($\mathfrak{R} = 1$) when all vapor converted into liquid is returned to the column, and fully closed ($\mathfrak{R} = 0$) when no liquid is returned, sending all the condensed liquid to the distillate drum. Additionally, the goal of the distillation column is to remove the excess of water formed during the polyesterification reaction as a byproduct, then it is desired that the temperature at the top of the column is as close as possible to the boiling point of the water at the process pressure. In order to achieve this, the reflux ratio \mathfrak{R} is modeled as follows

7

$$\mathfrak{R} = \frac{1}{2} \left[1 + \tanh \left(\frac{T_3 - T_3^{\text{ref}}}{2} \right) \right] \in [0, 1] \quad (7.115)$$

where T_3 is the temperature of the top tray of the column, and T_3^{ref} is the value of the reference.

It is worth noting that this reference is dynamic, and depends upon the pressure and the liquid molar composition in the tray. Moreover, it can be assumed that water is present at the top of the column in excess because it is the lightest component of the mixture. Thus, we take $\mathbf{x}_3^{\text{ref}}$ as the S -dimensional zero vector except at position 4 (position corresponding to the water) whose value equals 1, and make use of (7.75) to compute T_3^{ref} .

Finally, the RBD model is simulated using the kinetic parameters shown in Tables 7.1 and 7.2. Other important parameters such as the the overall heat transfer coefficient U_s , the surface area of the reactor A_s , the total mass of oil in the reactor jacket M_{oil} , the heat capacity of the oil in the reactor jacket $C_{p_{\text{oil}}}$, F_{oil} inlet mass flow of oil to the reactor jacket, and the vector of standard heat of formation $\Delta\mathbf{H}_f^\ominus$

are given initial guesses based on available literature and process heuristics. These parameters along with the reaction kinetic parameters are estimated in Section 8.2 of Chapter 8 to calibrate the process to the existing plant data. The thermodynamic parameters used for the DIPPR equations are assumed to be exact, and thus will not be subject to calibration.

In Figures 7.6, 7.7, a comparison between the reactor temperature and pressure trajectories corresponding to the simulated model and the real plant data. As seen in Figure 7.6, most discrepancies are present during the transient steps of the process, specifically during the filling and heating steps. During the filling step, the controller is not active and the temperature evolution depends solely on thermodynamic parameters such as heat capacities of the mixture and the alcohol, as well as the actual number of moles in the reactor. The peak in the pressure trajectory during the heating on pressure of the model is due to an overproduction of water, which vaporizes creating an excessive pressure build-up in the reactor. The overproduction is a direct consequence of incorrect values of the chemical kinetic parameters in the model. Another step where discrepancies are observed is in the vacuum step. Here, the mismatch between the process and the model is due to two main factors: the difference in the amount of water present in the real process and the model, and the difference between real and simulated vapor flows (that allow for the removal of water). These aforementioned differences arise from the uncertainty in the kinetic parameters, the proposed reaction mechanism, and the fluid dynamic assumptions.

Most of these discrepancies can be explained by the uncalibrated parameters in the model. These discrepancies will be minimized performing parameter estimation in Chapter 8.

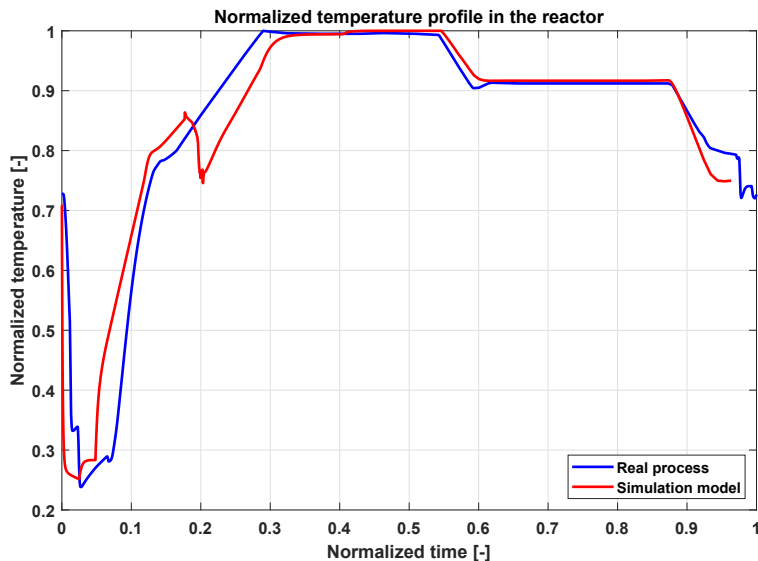


Figure 7.6: Temperature profile in the reactor (real process vs. simulation).

7

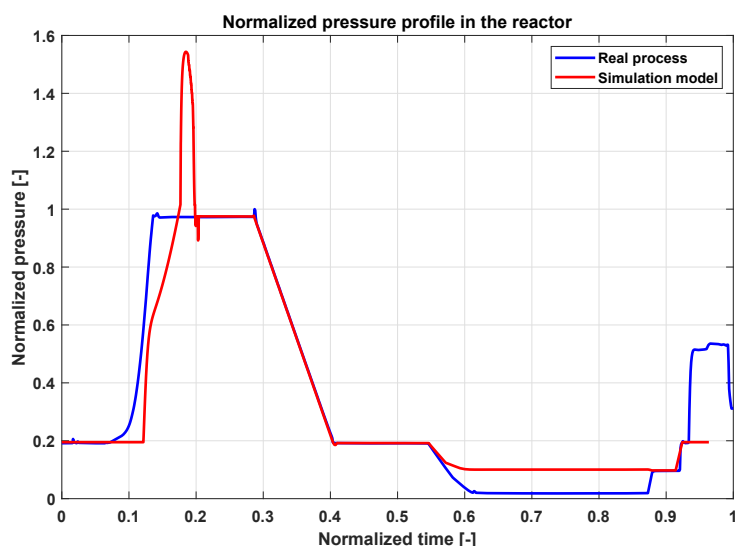


Figure 7.7: Pressure profile in the reactor (real process vs. simulation).

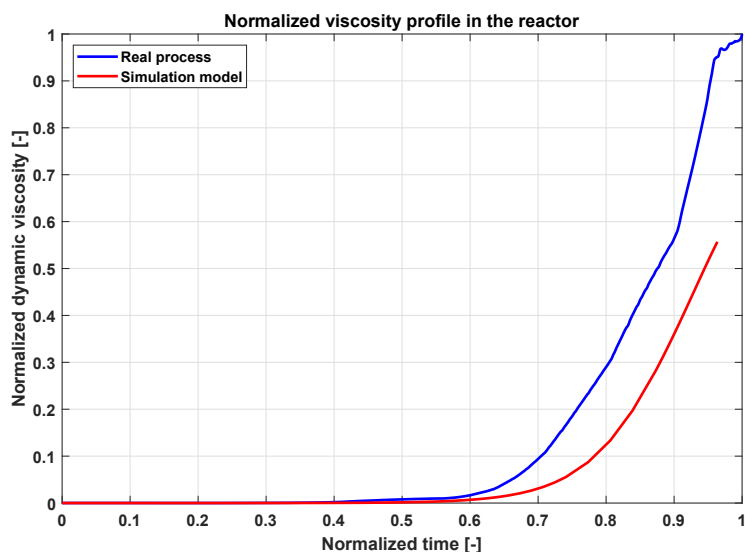


Figure 7.8: Viscosity profile in the reactor (real process vs. simulation).

Chapter summary

Polyesterification reaction

- The polyesterification reaction is a condensation reaction in which a polymer is formed and a molecule of water is generated as a by-product. The polymer produced in the industrial case study is a co-polymer, which is the result of the combination of two different functional polymer chain in the mixture.
- The condensation reaction corresponding to the RBD model uses three reactants: acid 1, acid 2, and alcohol 1 in excess to ensure complete conversion of the acids.
- The condensation reaction is subdivided into a series of equilibrium reactions based on the repeat and end segment formalism. This modeling approach of the polymer molecules allows to represent them based on groups of molecules rather than individually, which simplifies the reaction modeling task. Moreover, the set of equilibrium reactions are computed assuming the mass-action principle and the Arrhenius' law.
- There are in total 10 species and 16 chemical reactions modeled in the reaction mechanism of the process.

Reactive batch distillation model

7

- Reactive batch distillation is an intensified process that combines both chemical reaction and separation in one unit, bringing together the advantages of these two phenomena at the expense of introducing more dynamic coupling and making it more difficult to model and control.
- Reactive batch distillation is attractive for condensation polymerization because it is able to shift the chemical equilibrium by continuous removal of water in the process, while producing more polymer.
- The reactive batch distillation process is modeled discretizing the spatial domain with transfer stages as shown Figure 7.3. The RBD model has in total eight stages numbered in ascending order from top to bottom. The bottom stage serves as a batch reactor, and the topmost stage is the distillate drum where the by-product (water) is collected.
- The RBD model is developed based on certain assumptions to simplify it. It contains 90 states, more than 450 thermodynamic and fluid dynamic algebraic relationships, and approximately 130 parameters.
- The computation of the process vapor flows is performed using a heuristic approach assuming that the tray vapor flow reaches instantaneously a fraction of the stage theoretical steady-state vapor flow value.

Chapter summary

Modeling of polymer viscosity

- Polymer viscosity is a quantity that depends on temperature, shear rate, concentration of polymer, and degree of polymerization (conversion of the polymer). This variable is used in the process to assess quality of the product.
- Polymer viscosity tends to follow an exponential growth, which marks the start of the so-called gelation point. This is the moment when the degree of polymerization tends to infinity.
- The polymer viscosity is modeled using a time-varying population growth dynamics, choosing a small number of explanatory variables available. In the RBD model, the temperature, the weight-average molar mass of the polymer, and the weight fractions of polymer and water are used to describe the behavior of the viscosity. Scaling parameters are also introduced to shape the model's prediction to represent the data, as well as to ensure dimension compatibility in the viscosity model.

Input signals in the RBD model

- Limited information is provided on the loading inlet flow F_{in} of the process. This is modeled assuming an arbitrary mass of material in the reactor, and approximating from the data the time it takes to load the reactor. The loading inlet flow is computed using two approaches: a constant profile and a rate-limited profile. Both approaches generate the required mass fraction of reactants in the reactor.
- The inlet temperature of the reactor jacket oil $T_{jacket,in}$ is changed by an unknown external process based on the production recipe. The process relies heavily on operator experience and human intervention, and there are not well-defined conditions in the recipe. Therefore, the inlet temperature of the oil was modeled using a time-switching piecewise function approximated from the plant data.
- The valve opening κ_{valve} controls the passage of vapor flow in the process, regulating the process pressure. Since the valve opening is a number between 0 and 1, it is modeled using a hyperbolic tangent based on the error between the process pressure and the corresponding pressure set point. This set point varies depending on the batch step at which the process is operated.

Chapter summary

- The internal reflux ratio \mathfrak{R} controls the amount of liquid returned to the column. Hence, it regulates the separation in the process by increasing or decreasing the contact between the species. The internal reflux ratio is also a variable that varies between 0 and 1, and it is modeled using a hyperbolic tangent function. In this case, the hyperbolic tangent is a function of the error between the top temperature and the top temperature set point, which is usually the boiling point of water at the operating pressure to guarantee the constant vaporization of water.
- The reactor temperature control loop and the reflux control loop have conflicting effects. On the one hand, the reactor temperature control tries to keep the temperature high to promote the chemical reaction as condensation polymerization is an endothermic reaction. On the other hand, the reflux ratio tries to keep the separation degree high to obtain as pure water as possible. This comes at the expense of returning more liquid to the process, lowering the temperature in the reactor.
- The RBD model output trajectories show a good agreement with the trends of the real process output data trajectories. The discrepancies can be minimized by optimizing the model parameters.

8

Model Calibration and Optimization of Reactive Batch Distillation Column

In this chapter, the calibration of the RBD model of the industrial case study is presented. Output parametric sensitivity analysis as well as parametric ranking based on successive orthogonalization are implemented. A normalization is applied to the cost function to circumvent the scale dependency of the sensitivity matrix. Furthermore, the ranked-interval multiple shooting parameter estimation is employed to address the large number of parameters and states of the RBD model while exploiting the step-wise nature of batch processes. Additionally, optimal process trajectories are calculated considering separate optimization problems corresponding to the different batch steps. The optimization uses piece-wise constant inputs to ensure minimal time of each sub-problem while optimizing other relevant process variables.

8.1. Introduction

The use of first-principle models to make decisions, monitor, optimize, and/or control a process encompasses the so-called digital twin paradigm [63] or master model paradigm [12]. This particular setting requires constant communication between the plant and the model to perform periodic alignment of the model outputs and plant measurements if needed. In general, the plant-model alignment is carried out adjusting the model parameters until there is a good level of agreement between the plant and model outputs. As a consequence, parameter operational identifiability tools are employed to assess parameter identifiability following two main focuses: gradient-based (local) and gradient-free (global) approaches. Each of these approaches serves to analyze the operational identifiability of simulation first principle models (see e.g. [106], [107], [130], [153] [143], [144]). Global approaches tend to provide a more concrete picture of the effect of parameters over the model's operation space than the local ones. However, these global methods need to finely grid the parameter space to run the model for every possible combination of parameters. This makes these approaches impractical for large-scale models with a large number of parameters because the computations become intractable. Due to this limitation, gradient-based approaches are applied to assess identifiability around an operating trajectory of the process..

Additionally, trajectory optimization of reactive distillation processes has also been addressed extensively in the literature to improve the operating process regimes. For instance, Mujtaba and Macchietto [135] proposed two sequential optimization schemes: the first one to maximize conversion with operational bounds on the reflux ratio under fixed batch time as optimization variable using robust DAE integration algorithm combined with sequential quadratic programming (SQP). The second optimization is the maximization of the profit, which is solved using a polynomial fitting employing the solution of the previous optimization. Analogously, Fernholz *et al.* [49] worked on the optimization of a semibatch reactive distillation process with a heterogeneously catalyzed esterification reaction of methanol and acetic acid. The authors found that the productivity-optimal problem led to higher conversions under the same batch time when the reflux ratio, the heat duty, the feed rate, and the initial amount of methanol are optimized. They found these solutions solving two optimization problems: time-optimal and productivity-optimal problems using control vector parametrization (CVP) and nonlinear programming (NLP). However, none of the applications has dealt with a pressure-varying step-wise operation. The pressure control introduces another input that interacts with the reflux ratio and heat duty, while step-wise operation strategy makes the process behave as an event-triggered system, whose trajectories are not smooth functions of time.

This chapter deals with the calibration and optimization of the reactive batch distillation simulation model. First, a sensitivity analysis along with a parameter ranking procedure are performed to select the identifiable parameters in the simula-

tion model. Subsequently, the model parameters are estimated using ranked-interval multiple shooting parameter estimation to align the simulation model outputs to the plant data. Finally, the input trajectories are optimized per operating step using the calibrated model. The optimization is performed to minimize the batch time while maximizing the polymer viscosity, which is equivalent to maximizing the polymer yield.

8.2. Model calibration

The RBD simulation model will be calibrated using the real plant output data. The scope of the calibration will be limited to perform parameter estimation assuming that the simulation model belongs to the chosen model set. This is motivated by the results obtained in Chapter 7, where it is observed that the model is able to reproduce the trends of the process output trajectories. Additionally, the RBD model has over 250 parameters that can be categorized in four groups:

- Thermodynamic parameters: These parameters correspond to those used in the DIPPR equations to compute thermodynamic properties of the chemical species, such as equations (7.66), (7.60), or (7.72). The thermodynamic parameters are assumed to be at the correct value, and they are not considered in the parameter estimation, i.e. they will remain fixed during the model calibration.
- Kinetic parameters: These parameters are those necessary to compute the vector of reactions \mathbf{r} in (7.17) and (7.18), namely the pre-exponential factors $k_{i,o}$ and activation energies $E_{a,i}$. These parameters are uncertain, and therefore will be included in the parameter vector \mathbf{p} . The presence of uncertainty is due to the fact that the values provided in Tables 7.1 and 7.2 do not correspond to the reactants used in the actual process but to chemically similar species¹.

Moreover, the standard heats of formation $\Delta\mathbf{H}_f^\ominus$ of the end and repetition segments are also included because the standard heat of formation for the species in the model are not reported in the literature. The universal gas constant R and the stoichiometric matrix \mathbf{N} are assumed to be correct, and will not be estimated during the model calibration.

- Operational parameters: These are parameters related to the operating conditions of the process. These parameters correspond to the ones used to model the reactor jacket such as M_{oil} , $C_{p,oil}$, F_{oil} , U_s , and A_s . The aforementioned parameters have an influence on the process trajectories. Therefore, all of these will be included in the parameter vector \mathbf{p} .

¹Due to limited availability of data in literature.

- Viscosity parameters: These parameter pertain to the empirical population growth-based equation (7.101), (7.103), and (7.104) to model the evolution of the viscosity in the RBD. These parameters will be used to capture some of the unmodeled dynamics of the polymer viscosity. Parameters c_1 , c_2 , and c_3 will be therefore included in the parameter estimation for the calibration of the RBD model.

The parameter vector \mathbf{p} contains 23 parameters out of the almost 250 based on the distinction made previously. In Table 8.1, the nominal values \mathbf{p}_{nom} of \mathbf{p} are provided, and will serve as initial values for the model calibration.

Table 8.1: Nominal parameters of the model subject to calibration

Label	Parameter	Name	Value	Note
p_1	$\Delta H_{f_{AC1-\text{end}}}^\ominus$	Std. heat of formation (AC1 end segment)	327.22 kJ kg ⁻¹	Computed from [147]
p_2	$\Delta H_{f_{AC2-\text{end}}}^\ominus$	Std. heat of formation (AC2 end segment)	398.39 kJ kg ⁻¹	Computed from [147]
p_3	$\Delta H_{f_{AOH-\text{end}}}^\ominus$	Std. heat of formation (AOH end segment)	781.58 kJ kg ⁻¹	Computed from [147]
p_4	$\Delta H_{f_{AC1-\text{rep}}}^\ominus$	Std. heat of formation (AC1 repeat segment)	82.08 kJ kg ⁻¹	Computed from [147]
p_5	$\Delta H_{f_{AC2-\text{rep}}}^\ominus$	Std. heat of formation (AC2 repeat segment)	199.49 kJ kg ⁻¹	Computed from [147]
p_6	$\Delta H_{f_{AOH-\text{rep}}}^\ominus$	Std. heat of formation (AOH repeat segment)	546.76 kJ kg ⁻¹	Computed from [147]
p_7	E_{a_1}	Activation energy (AC1 forward cond.)	4.64424×10^4 kJ kmol ⁻¹	Kuo and Chen [95]
p_8	E_{a_2}	Activation energy (AC1 backward cond.)	4.64424×10^4 kJ kmol ⁻¹	Kuo and Chen [95]
p_9	E_{a_3}	Activation energy (AC2 forward cond.)	8.45×10^4 kJ kmol ⁻¹	Darda <i>et al.</i> [38]
p_{10}	E_{a_4}	Activation energy (AC2 backward cond.)	8.22×10^4 kJ kmol ⁻¹	Hu <i>et al.</i> [78]
p_{11}	k_{0_1}	Pre-exp. factor (AC1 forward cond.)	4.56×10^5 kg kmol ⁻¹ s ⁻¹	Kuo and Chen [95]
p_{12}	k_{0_2}	Pre-exp. factor (AC1 backward cond.)	9.74167×10^5 kg ² kmol ⁻² s ⁻¹	Kuo and Chen [95]
p_{13}	k_{0_3}	Pre-exp. factor (AC2 forward cond.)	5.73×10^8 kg kmol ⁻¹ s ⁻¹	Darda <i>et al.</i> [38]
p_{14}	k_{0_4}	Pre-exp. factor (AC2 backward cond.)	1.169387×10^9 kg ² kmol ⁻² s ⁻¹	Hu <i>et al.</i> [78]
p_{15}	U_s	Overall heat transf. coef.	1.8 kW m ⁻² K ⁻¹	Sinnot [162]
p_{16}	A_s	Reactor's surface area	25 m ²	Assuming cylindrical vessel
p_{17}	$C_{p_{\text{oil}}}$	Oil heat capacity	2.3 kJ kg ⁻¹ K ⁻¹	Sinnot [162]
p_{18}	F_{oil}	Inlet mass flow of oil	10 kg s ⁻¹	Assumed
p_{19}	M_{oil}	Total mass of oil	50 kg	Assumed

Table 8.1 (Cont.): Nominal parameters of the model subject to calibration

Label	Parameter	Name	Value	Note
p_{20}	F_{in}	Loading inlet molar flow	$4.47971 \times 10^{-3} \text{ kmol s}^{-1}$	Computed based on calculation basis (see sec. 7.5.1)
p_{21}	c_1	Viscosity scaling factor 1	$0.01 \text{ kmol m}^{-1} \text{ s}^{-1}$	Initial guess
p_{22}	c_2	Viscosity scaling factor 2	$2 \times 10^{-5} \text{ K}^{-1}$	Initial guess
p_{23}	c_3	Viscosity scaling factor 3	$2 \times 10^{-4} \text{ s}^{-1}$	Initial guess

In the actual process, there are only three continuously measured outputs, namely the reactor temperature T_r , the reactor pressure P_r , and the polymer viscosity η , thus $\mathbf{y} = [T_r \ P_r \ \eta]^\top$. However, since there are 23 parameters to be estimated, it is necessary to assess if all these parameters can be identified from the measured outputs.

8.2.1. Sensitivity analysis

To assess the identifiability of parameters, the absolute output parametric sensitivities $\partial_{p_j} y_i(t_k)$ are computed for each of the outputs T_r , P_r , and η with respect to the parameters shown in Table 8.1. The sensitivities are collected in the absolute sensitivity matrix \mathbf{S}

$$\mathbf{S} = \begin{bmatrix} s_{T_r, \Delta H_{f_{AC1-\text{end}}}^\ominus(t_0)} & s_{T_r, \Delta H_{f_{AC2-\text{end}}}^\ominus(t_0)} & \cdots & s_{T_r, c_3}(t_0) \\ s_{P_r, \Delta H_{f_{AC1-\text{end}}}^\ominus(t_0)} & s_{P_r, \Delta H_{f_{AC2-\text{end}}}^\ominus(t_0)} & \cdots & s_{P_r, c_3}(t_0) \\ s_{\eta, \Delta H_{f_{AC1-\text{end}}}^\ominus(t_0)} & s_{\eta, \Delta H_{f_{AC2-\text{end}}}^\ominus(t_0)} & \cdots & s_{\eta, c_3}(t_0) \\ \vdots & \vdots & \ddots & \vdots \\ s_{T_r, \Delta H_{f_{AC1-\text{end}}}^\ominus(t_N)} & s_{T_r, \Delta H_{f_{AC2-\text{end}}}^\ominus(t_N)} & \cdots & s_{T_r, c_3}(t_N) \\ s_{P_r, \Delta H_{f_{AC1-\text{end}}}^\ominus(t_N)} & s_{P_r, \Delta H_{f_{AC2-\text{end}}}^\ominus(t_N)} & \cdots & s_{P_r, c_3}(t_N) \\ s_{\eta, \Delta H_{f_{AC1-\text{end}}}^\ominus(t_N)} & s_{\eta, \Delta H_{f_{AC2-\text{end}}}^\ominus(t_N)} & \cdots & s_{\eta, c_3}(t_N) \end{bmatrix} \quad (8.1)$$

However, the model structure and state space dimension of the RBD is too complex to derive analytic expressions for each of the elements of \mathbf{S} . Thus, the true absolute output parametric sensitivities $s_{i,j}$ can be approximated using (4.24) via symmetric differences (central differences). The quality of the approximation $s_{i,j}$ strongly depends on the step size h_{p_j} . In the case of the RBD model, the step size in each parameter h_{p_j} is varied for every parameter based on $h_{p_j} = p_j \times \delta_{p_j}$. Moreover, the

parameter variation is set to $\delta_{p_j} = \sqrt[3]{\epsilon}$ as it is optimal for central differences [156], where ϵ is the machine epsilon.

The approximate AOPS depend on the order of magnitude of the outputs and parameters under analysis. Due to this explicit dependence, the absolute sensitivities are not dimensionless quantities, where the AOPS $s_{i,j}$ has dimensions [unit y_i]/[unit p_j]. Therefore, we can use (4.25) to compute the approximate relative output parametric sensitivities $\bar{s}_{i,j}$, which allows to perform a reasonable comparison between each sensitivity per parameter. Likewise, we collect the approximate ROPS in the matrix $\bar{\mathbf{S}}$

$$\bar{\mathbf{S}} = \begin{bmatrix} \bar{s}_{T_r, \Delta H_{f_{AC1-end}}^\ominus}(t_0) & \bar{s}_{T_r, \Delta H_{f_{AC2-end}}^\ominus}(t_0) & \cdots & \bar{s}_{T_r, c_3}(t_0) \\ \bar{s}_{P_r, \Delta H_{f_{AC1-end}}^\ominus}(t_0) & \bar{s}_{P_r, \Delta H_{f_{AC2-end}}^\ominus}(t_0) & \cdots & \bar{s}_{P_r, c_3}(t_0) \\ \bar{s}_{\eta, \Delta H_{f_{AC1-end}}^\ominus}(t_0) & \bar{s}_{\eta, \Delta H_{f_{AC2-end}}^\ominus}(t_0) & \cdots & \bar{s}_{\eta, c_3}(t_0) \\ \vdots & \vdots & \ddots & \vdots \\ \bar{s}_{T_r, \Delta H_{f_{AC1-end}}^\ominus}(t_N) & \bar{s}_{T_r, \Delta H_{f_{AC2-end}}^\ominus}(t_N) & \cdots & \bar{s}_{T_r, c_3}(t_N) \\ \bar{s}_{P_r, \Delta H_{f_{AC1-end}}^\ominus}(t_N) & \bar{s}_{P_r, \Delta H_{f_{AC2-end}}^\ominus}(t_N) & \cdots & \bar{s}_{P_r, c_3}(t_N) \\ \bar{s}_{\eta, \Delta H_{f_{AC1-end}}^\ominus}(t_N) & \bar{s}_{\eta, \Delta H_{f_{AC2-end}}^\ominus}(t_N) & \cdots & \bar{s}_{\eta, c_3}(t_N) \end{bmatrix} \quad (8.2)$$

8.2.2. Ranking of parameters based on output parametric sensitivity per operational step

8

Once the approximate relative output parametric sensitivity matrix $\bar{\mathbf{S}}$ is computed from (8.2), parameter identifiability can be assessed based on the overall contribution of each parameter to all of the outputs. This overall contribution is contained in the vectors spanning the columns of $\bar{\mathbf{S}}$, which can be extracted using the SOM. The SOM generates the following matrix decomposition

$$\bar{\mathbf{S}}\Pi = \mathbf{Q}\mathbf{R} = \mathbf{Q}\Sigma\tilde{\mathbf{R}} \quad (8.3)$$

where Π is a permutation matrix, \mathbf{Q} is an orthogonal matrix, Σ is a diagonal matrix that contains the orthogonal fractions of $\bar{s}_{i,j}$, and $\tilde{\mathbf{R}}$ is a upper triangular matrix with ones on the main diagonal.

The magnitudes of the SOM decomposition orthogonal fractions and collinearity indexes are shown in Figures 8.1 and 8.2. In these figures it can be seen that the parameter c_3 generates the largest variation among all the parameters. This is

due to the fact that it generates a sensitivity trajectory that is almost orthogonal to all the other parameters. On the other hand, the heat transfer surface area A_s is ranked the lowest due to having the smallest orthogonal fraction magnitude. Nonetheless, the SOM decomposition will naturally vary depending on the scaling of the sensitivities, but also on the portion of the trajectory being analyzed. Notice that the method assumes that each column of the matrix $\bar{\mathbf{S}}$ is composed of $N \cdot n_y$ -dimensional blocks that contain the approximate relative sensitivity of all the outputs combined. The implication of this is that the SOM provides an average ranking over the entire trajectory. However, for applications with clearly defined operational steps, taking the full trajectory might vanish more noticeable effects of parameters in some portions of the output trajectories.

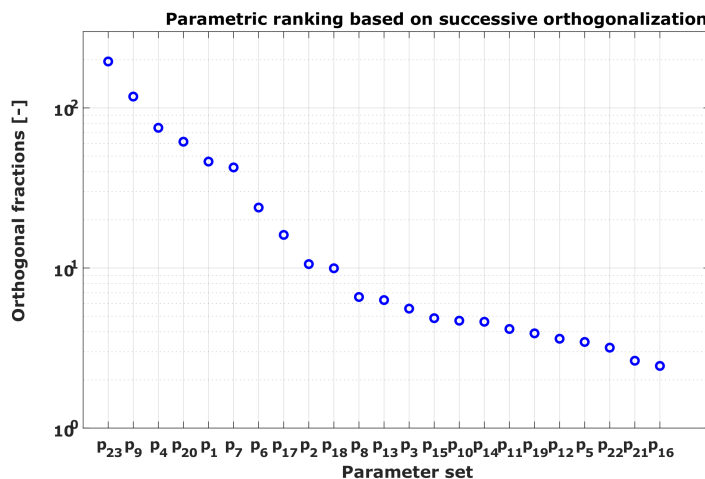


Figure 8.1: Magnitudes of the orthogonal fractions of approximate relative output parametric sensitivity matrix $\bar{\mathbf{S}}$.

In the RBD model, the process is divided in different batch steps as shown in Chapter 7. In each of these steps, the outputs exhibit a specific behavior, and the parametric sensitivities will differ depending on the specific operating portion of the trajectory. Therefore, the output trajectories are divided into the different batch steps, and parametric rankings are performed only considering the corresponding portion of the output trajectories. In Table 8.2 the comparison between a full-trajectory ranking and step-wise ranking is presented. We only consider steps 1 through 6 because steps 7 and 8 mark the conclusion of the process, and the output parametric sensitivities will be zero.

The ranking varies greatly in each step of the process, and parameters that have a low rank in the full-trajectory ranking have a higher rank in the step-wise analysis. Thus, focusing on each batch step could potentially improve the estimation of certain parameters whose sensitivities go to zero or are shadowed by other parameters in regions of the trajectory. The different parameter selections in each of the process

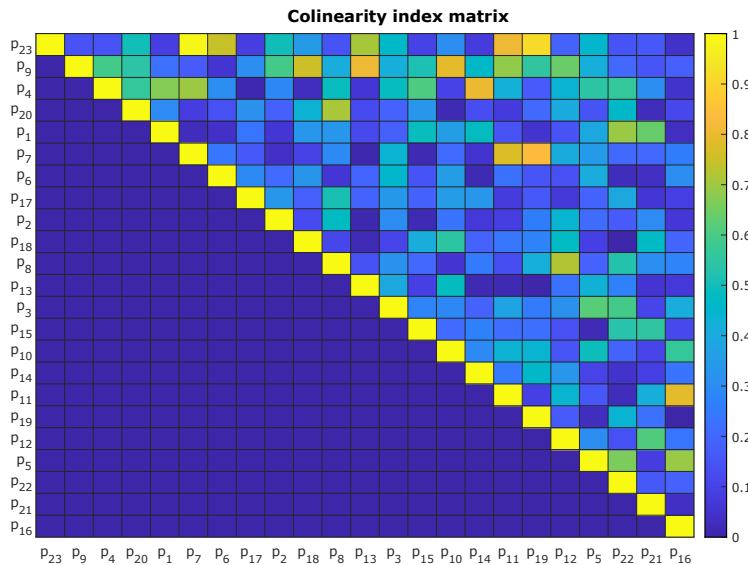


Figure 8.2: Magnitudes of the collinear indexes of approximate relative output parametric sensitivity matrix $\bar{\mathbf{S}}$.

operating steps are performed setting the cut-off value to $\delta_s = n_p \times \delta_\epsilon(\|\bar{\mathbf{S}}\|_2)$, where δ_s is the sensitivity cut-off value, n_p is the number of parameter is the original parameter set, and $\delta_\epsilon(\|\bar{\mathbf{S}}\|_2)$ is the distance from $\|\bar{\mathbf{S}}\|_2$ to the next larger floating-point number of the same precision as $\|\bar{\mathbf{S}}\|_2$.

8

The cut-off value δ_s takes into account the smallest number the computer can represent before the matrix $\bar{\mathbf{S}}$ drops in rank due to floating-point errors. A parameter is considered not identifiable if an element σ_i of Σ is smaller than δ_s . We apply this cut-off value to each of the step-wise parametric ranking presented in Table 8.2 to obtain reduced parameter vector per batch step. The reduced parameter vector \mathbf{p}^{red} for each step is provided in Table 8.3

Notice that from steps 2 to 6 the whole of the parameter set is identifiable. However, as previously mentioned, the ranking in each step changes indicating that the parameters also change their effect on all the outputs depending on the operating point. The step 1 (filling step) has a strict reduced parameter set, where the parameters related with the inputs (loading inlet flows, and reactor jacket-related parameters) dominate the step. Therefore, in this step it is much easier to identify these parameters. After the filling, the chemical reaction takes places and the outputs start to also exhibit sensitivity to chemical kinetic and viscosity-related parameters. The step-wise parameter ranking provides insight on how the identifiability of each parameter changes as the process progresses. Additionally, it serves as groundwork to implement the ranked interval multiple shooting parameter estimation RIMSPE

Table 8.2: Parametric ranking comparison: full-trajectory vs. step-wise

Ranking	Full trajectory	step 1	step 2	step 3	step 4	step 5	step 6
1	c_3	F_{in}	E_{a_3}	E_{a_3}	k_{0_3}	k_{0_4}	E_{a_3}
2	E_{a_3}	F_{oil}	E_{a_1}	$C_{p_{oil}}$	E_{a_3}	c_3	E_{a_1}
3	$\Delta H_{f_{AC1\text{-rep}}}^\ominus$	M_{oil}	F_{in}	F_{in}	$\Delta H_{f_{AC2\text{-rep}}}^\ominus$	E_{a_3}	$\Delta H_{f_{AC2\text{-rep}}}^\ominus$
4	F_{in}	$C_{p_{oil}}$	F_{oil}	F_{oil}	$C_{p_{oil}}$	F_{oil}	$\Delta H_{f_{AC2\text{-end}}}^\ominus$
5	$\Delta H_{f_{AC1\text{-end}}}^\ominus$	A_s	k_{0_3}	E_{a_4}	E_{a_4}	U_s	F_{oil}
6	E_{a_1}	E_{a_1}	M_{oil}	E_{a_2}	E_{a_2}	k_{0_2}	$C_{p_{oil}}$
7	$\Delta H_{f_{AOH\text{-rep}}}^\ominus$	U_s	U_s	E_{a_1}	F_{oil}	E_{a_4}	$\Delta H_{f_{AC1\text{-rep}}}^\ominus$
8	$C_{p_{oil}}$	$\Delta H_{f_{AC2\text{-end}}}^\ominus$	$C_{p_{oil}}$	A_s	M_{oil}	$\Delta H_{f_{AOH\text{-rep}}}^\ominus$	E_{a_2}
9	$\Delta H_{f_{AC2\text{-end}}}^\ominus$	$\Delta H_{f_{AOH\text{-end}}}^\ominus$	k_{0_1}	k_{0_3}	E_{a_1}	F_{in}	c_3
10	F_{oil}	$\Delta H_{f_{AC1\text{-end}}}^\ominus$	$\Delta H_{f_{AOH\text{-end}}}^\ominus$	c_3	U_s	$\Delta H_{f_{AC2\text{-end}}}^\ominus$	U_s
11	E_{a_2}	k_{0_1}	E_{a_4}	U_s	F_{in}	c_2	$\Delta H_{f_{AOH\text{-end}}}^\ominus$
12	k_{0_3}	E_{a_3}	$\Delta H_{f_{AC1\text{-end}}}^\ominus$	M_{oil}	k_{0_2}	M_{oil}	$\Delta H_{f_{AOH\text{-rep}}}^\ominus$
13	$\Delta H_{f_{AOH\text{-end}}}^\ominus$	k_{0_3}	A_s	k_{0_2}	$\Delta H_{f_{AC2\text{-end}}}^\ominus$	c_1	M_{oil}
14	U_s	c_2	k_{0_2}	$\Delta H_{f_{AC1\text{-end}}}^\ominus$	c_3	$\Delta H_{f_{AC1\text{-end}}}^\ominus$	k_{0_2}
15	E_{a_4}	c_1	$\Delta H_{f_{AC2\text{-rep}}}^\ominus$	$\Delta H_{f_{AC2\text{-end}}}^\ominus$	$\Delta H_{f_{AC1\text{-end}}}^\ominus$	E_{a_2}	F_{in}
16	k_{0_4}	$\Delta H_{f_{AC2\text{-rep}}}^\ominus$	E_{a_2}	$\Delta H_{f_{AOH\text{-rep}}}^\ominus$	$\Delta H_{f_{AOH\text{-end}}}^\ominus$	$\Delta H_{f_{AOH\text{-end}}}^\ominus$	k_{0_4}
17	k_{0_1}	$\Delta H_{f_{AC1\text{-rep}}}^\ominus$	$\Delta H_{f_{AC2\text{-end}}}^\ominus$	c_2	$\Delta H_{f_{AC1\text{-rep}}}^\ominus$	A_s	$\Delta H_{f_{AC1\text{-end}}}^\ominus$
18	M_{oil}	E_{a_2}	$\Delta H_{f_{AOH\text{-rep}}}^\ominus$	k_{0_4}	k_{0_1}	$C_{p_{oil}}$	k_{0_1}
19	k_{0_2}	k_{0_2}	c_2	$\Delta H_{f_{AC2\text{-rep}}}^\ominus$	c_2	k_{0_1}	c_2
20	$\Delta H_{f_{AC2\text{-rep}}}^\ominus$	E_{a_4}	c_1	$\Delta H_{f_{AOH\text{-end}}}^\ominus$	A_s	$\Delta H_{f_{AC2\text{-rep}}}^\ominus$	E_{a_4}
21	c_2	$\Delta H_{f_{AOH\text{-rep}}}^\ominus$	c_3	c_1	$\Delta H_{f_{AOH\text{-end}}}^\ominus$	k_{0_3}	c_1
22	c_1	k_{0_4}	$\Delta H_{f_{AC1\text{-rep}}}^\ominus$	$\Delta H_{f_{AC1\text{-rep}}}^\ominus$	k_{0_4}	$\Delta H_{f_{AC1\text{-rep}}}^\ominus$	A_s
23	A_s	c_3	k_{0_4}	k_{0_1}	c_1	E_{a_1}	k_{0_3}

approach described in Chapter 4, which can be useful to avoid local minima in gradient-based optimization. The specific application of this approach to the RBD model will be explained in the next section.

8.2.3. Ranked interval multiple shooting parameter estimation

The parameters are estimated using the RIMSPE dividing the output trajectories into rank interval and shooting intervals. The rank interval are given by the six operating steps, and the shooting intervals are arbitrary. Notice that in this particular setting ofRIMSPE, we solve as many optimization problems as batch steps there are.

Let $I_\varrho \quad \forall \varrho = 1, \dots, 6$ be the set of RI, $I_\lambda \quad \forall \lambda = 0, \dots, \ell$ be the set of ShI in each RI, and \mathbf{x}_l and $\mathbf{x}(\tau_l)$ be the l -th optimized and simulated vectors of states in the ϱ -th ranked interval, respectively. The parameter estimation problems in the RIMSPE are

Table 8.3: Reduced parameter sets per batch step

step 1	step 2	step 3	step 4	step 5	step 6
F_{in}	E_{a_3}	E_{a_3}	k_{0_3}	k_{0_4}	E_{a_3}
F_{oil}	E_{a_1}	$C_{p_{oil}}$	E_{a_3}	c_3	E_{a_1}
M_{oil}	F_{in}	F_{in}	$\Delta H_{f_{AC2\text{-rep}}}^\ominus$	E_{a_3}	$\Delta H_{f_{AC2\text{-rep}}}^\ominus$
$C_{p_{oil}}$	F_{oil}	F_{oil}	$C_{p_{oil}}$	F_{oil}	$\Delta H_{f_{AC2\text{-end}}}^\ominus$
A_s	k_{0_3}	E_{a_4}	E_{a_4}	U_s	F_{oil}
E_{a_1}	M_{oil}	E_{a_2}	E_{a_2}	k_{0_2}	$C_{p_{oil}}$
U_s	U_s	E_{a_1}	F_{oil}	E_{a_4}	$\Delta H_{f_{AC1\text{-rep}}}^\ominus$
$\Delta H_{f_{AC2\text{-end}}}^\ominus$	$C_{p_{oil}}$	A_s	M_{oil}	$\Delta H_{f_{AOH\text{-rep}}}^\ominus$	E_{a_2}
$\Delta H_{f_{AOH\text{-end}}}^\ominus$	k_{0_1}	k_{0_3}	E_{a_1}	F_{in}	c_3
$\Delta H_{f_{AC1\text{-end}}}^\ominus$	$\Delta H_{f_{AOH\text{-end}}}^\ominus$	c_3	U_s	$\Delta H_{f_{AC2\text{-end}}}^\ominus$	U_s
k_{0_1}	E_{a_4}	U_s	F_{in}	c_2	$\Delta H_{f_{AOH\text{-end}}}^\ominus$
E_{a_3}	$\Delta H_{f_{AC1\text{-end}}}^\ominus$	M_{oil}	k_{0_2}	M_{oil}	$\Delta H_{f_{AOH\text{-rep}}}^\ominus$
k_{0_3}	A_s	k_{0_2}	$\Delta H_{f_{AC2\text{-end}}}^\ominus$	c_1	M_{oil}
c_2	k_{0_2}	$\Delta H_{f_{AC1\text{-end}}}^\ominus$	c_3	$\Delta H_{f_{AC1\text{-end}}}^\ominus$	k_{0_2}
	$\Delta H_{f_{AC2\text{-rep}}}^\ominus$	$\Delta H_{f_{AC2\text{-end}}}^\ominus$	$\Delta H_{f_{AC1\text{-end}}}^\ominus$	E_{a_2}	F_{in}
	E_{a_2}	$\Delta H_{f_{AOH\text{-rep}}}^\ominus$	$\Delta H_{f_{AOH\text{-end}}}^\ominus$	$\Delta H_{f_{AOH\text{-end}}}^\ominus$	k_{0_4}
	$\Delta H_{f_{AC2\text{-end}}}^\ominus$	c_2	$\Delta H_{f_{AC1\text{-rep}}}^\ominus$	A_s	$\Delta H_{f_{AC1\text{-end}}}^\ominus$
	$\Delta H_{f_{AOH\text{-rep}}}^\ominus$	k_{0_4}	k_{0_1}	$C_{p_{oil}}$	k_{0_1}
	c_2	$\Delta H_{f_{AC2\text{-rep}}}^\ominus$	c_2	k_{0_1}	c_2
	c_1	$\Delta H_{f_{AOH\text{-end}}}^\ominus$	A_s	$\Delta H_{f_{AC2\text{-rep}}}^\ominus$	E_{a_4}
	c_3	c_1	$\Delta H_{f_{AOH\text{-end}}}^\ominus$	k_{0_3}	c_1
	$\Delta H_{f_{AC1\text{-rep}}}^\ominus$	$\Delta H_{f_{AC1\text{-rep}}}^\ominus$	k_{0_4}	$\Delta H_{f_{AC1\text{-rep}}}^\ominus$	A_s
	k_{0_4}	k_{0_1}	c_1	E_{a_1}	k_{0_3}

8

$$\begin{aligned} \min_{\mathbf{z}_1} \quad & J(\mathbf{z}_1) \\ \text{s.t.} \quad & G_{1,l}(\mathbf{z}_1) = 0 \end{aligned} \quad \dots \quad \begin{aligned} \min_{\mathbf{z}_6} \quad & J(\mathbf{z}_6) \\ \text{s.t.} \quad & G_{6,l}(\mathbf{z}_6) = 0 \end{aligned} \quad (8.4)$$

and

$$\begin{aligned} \dot{\mathbf{x}}_{l+1}(t, \mathbf{z}_\varrho^{\text{red}}) &= \mathbf{f}(\mathbf{u}_{l+1}(t), \mathbf{z}_\varrho^{\text{red}}), \quad \mathbf{x}_l = \mathbf{x}(\tau_l), \quad t \in [\tau_l, \tau_{l+1}] \\ \dot{\mathbf{y}}_{l+1}(t, \mathbf{z}_\varrho^{\text{red}}) &= \mathbf{g}(\mathbf{z}_\varrho^{\text{red}}) \end{aligned} \quad (8.5)$$

where the cost functions $J(\mathbf{z}_\varrho) = \|\mathbf{y}_\varrho - \hat{\mathbf{y}}(\mathbf{z}_\varrho)\|_2^2$, with \mathbf{y} and $\hat{\mathbf{y}}(\mathbf{z}_\varrho)$ are the actual process output and the simulated model output of the ϱ -th operational step.

Since the RIMSPE enlarge the parameter space with the state of each RI, choosing the number of subdivision ℓ will control the trade-off between flexibility to avoid local minima and the computation power that the algorithm might take. This is due to the fact that at the ϱ -th rank interval, the size of the enlarged parameter vector \mathbf{z}_ϱ will be $n_z = n_x \times \ell + n_p^{\text{red}}$. The state space dimension n_x of the RBD model is 90, therefore, choosing a relative large number of ShI ℓ makes the size n_z grow quickly. In order to make the estimation procedure tractable, the number of shooting interval is limited to $\ell = 5$ in every rank interval. Furthermore, each cost function is normalized following the procedure detailed in Chapter 4 Section 4.5.1 to ensure that the optimization algorithm uses the relative sensitivity matrix.

The parameter estimation results for each batch operating step is shown in Figure 8.3. The parameters are also presented with the uncertainty regions for a 95% confidence. Likewise, the corresponding simulation of the output trajectories are presented in Figure 8.4.

8.3. Optimization of the RBD process

The RBD process is run for a fixed amount of time to produce a copolymer. The quality of the product is assessed measuring the viscosity of the copolymer in the reactor at the end of the process. The process has also very distinct batch steps in which different operating conditions are employed. Nevertheless, the industrial RBD process has been optimized through time based on experience and heuristics, but since a rigorous calibrated mathematical model is now available, the process operation can be optimized using model-based computational routines. The optimization of this process has two objectives: maximize the yield of polymer at the end of the batch (equivalent to maximizing the mixture's viscosity), and minimize the batch time.

The approach followed is the optimization of the individual batch steps, such that each one generates the maximum yield in the minimum time. Additionally, two assumptions are made:

1. The simulation model uses the same recipe and initial operating conditions as the plant. This is done to fix the many degrees of freedom that the process simulation model has.
2. The input trajectories are finely discretized assuming piece-wise constant functions over time to approximate a smooth function.

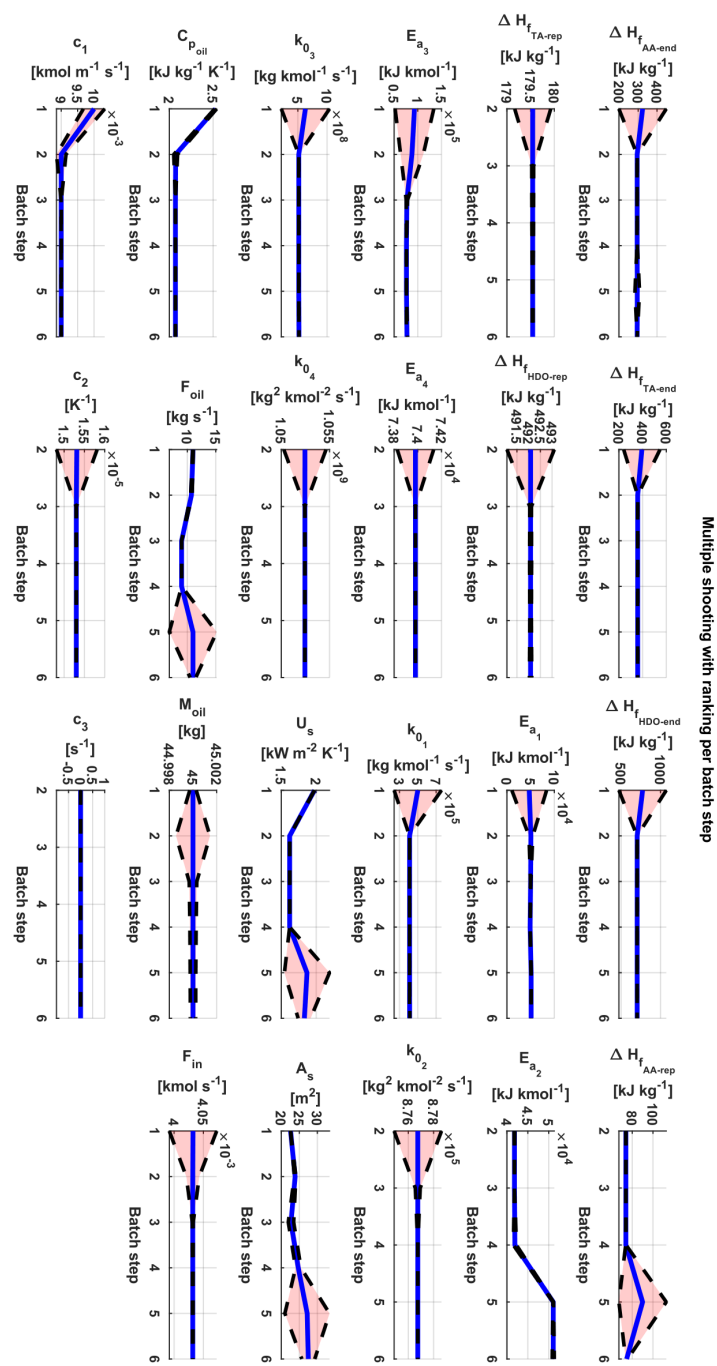


Figure 8.3: Estimated parameters using multiple-shooting method (RIMsPE) per batch step (blue) with 95% confidence interval (light red).

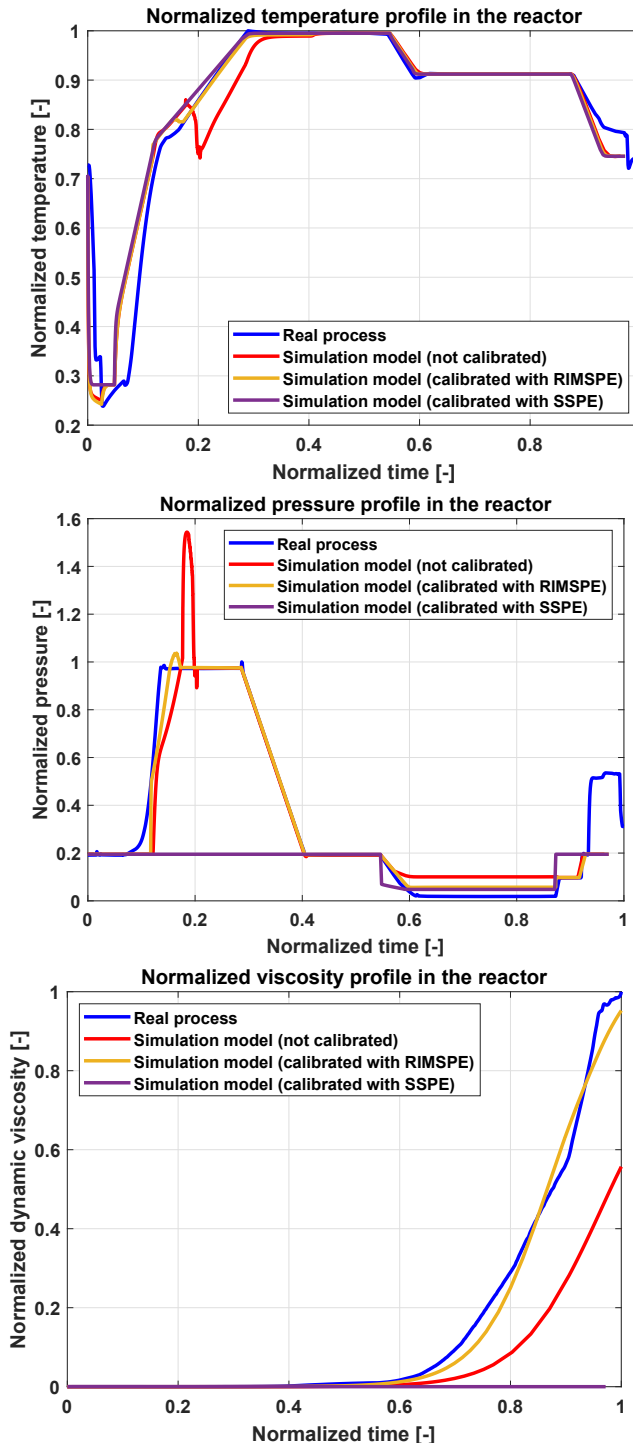


Figure 8.4: Calibrated temperature, pressure, and viscosity profiles in the reactor.

Optimization of the filling step

In this step, the reactor is active and pre-heated at a temperature T_{r_0} . It is also loaded with AOH to reach the specified recipe composition. The distillation column is inactive, and the temperature of the process is not high enough to promote chemical reaction or vaporization. The AOH is loaded at a lower temperature, which greatly reduces the temperature of the reactor. This temperature drop has to be compensated for in the heating step, increasing the batch time. Thus, in the filling step, the following operational constraint is imposed: the temperature of the reacting mixture T_r cannot be lower than the initial pre-heating temperature T_{r_0} and not greater than the reaction activation temperature T_{r_a} . Furthermore, in this step the maximum filling time t_{f_1} is the variable to be minimized. The inputs to optimize over are the loading inlet flow F_{in} and the jacket oil inlet temperature $T_{\text{jacket,in}}$. The minimization problem is

$$\begin{aligned}
 & \min_{F_{\text{in}}, T_{\text{jacket,in}}} \quad \int_0^{t_{f_1}} dt \\
 & \text{s.t.} \quad \dot{\mathbf{x}} = f(\mathbf{x}, \mathbf{u}, \mathbf{p}), \quad \mathbf{x}(0) = \mathbf{x}_0 \\
 & \quad \hat{\mathbf{y}} = [T_r \quad P_r \quad \eta]^T \\
 & \quad w_{\text{AOH}}(t_{f_\ell}) = 0.45 \\
 & \quad T_{r_0} \leq T_r \leq T_{r_a} \\
 & \quad 0 \leq V_{\text{ol}} \leq V_{\text{ol}}^{\max} \\
 & \quad 0 \leq F_{\text{in}} \leq F_{\text{in}}^{\max} \\
 & \quad t_{f_1}^{\min} \leq t_{f_1} \leq t_{f_1}^{\max}
 \end{aligned} \tag{8.6}$$

Optimization of heating and heating on pressure steps

In the heating step, the reactor is active and the temperature is $T_r \in [T_{r_0}, T_{r_a}]$. This step is used to increase the temperature sufficiently high so that $T_r = T_{r_a}$, and to initiate the condensation reaction. The reaction produces the polymer as products, as well as water as by product. At the operating conditions, the formed water vaporizes and increases the internal pressure of the reactor, starting the heating on pressure step. The operational constraints for these two combined steps are the maximum allowed pressure and the maximum allowed temperature in the reactor. Moreover, the goal of the optimization is to maximize the composition of water in the mixture along the whole duration of the step. This implies that the conversion is pushed towards the direction of the products, and vaporizing the water. The optimization variable is the jacket oil inlet temperature $T_{\text{jacket,in}}$. The minimization problem is

$$\begin{aligned}
& \min_{T_{\text{jacket,in}}} && t_{f_2} - \lambda_2 \|x_{\text{H}_2\text{O}}(t_{f_2})\|_2^2 \\
\text{s.t.} & && \dot{\mathbf{x}} = f(\mathbf{x}, \mathbf{u}, \mathbf{p}), \quad \mathbf{x}(t_{f_1}^*) = \mathbf{x}_{f_1} \\
& && \hat{\mathbf{y}} = [T_r \quad P_r \quad \eta]^\top \\
& && T_{r_0} \leq T_r \leq T_r^{\max} \\
& && 1 \leq P_r \leq P_r^{\max} \\
& && t_{f_1}^{\max} \leq t_{f_2} \leq t_{f_2}^{\max}
\end{aligned} \tag{8.7}$$

Optimization of reaction step

In the reaction step, both the reactor and column are active. This step is used to remove the water vapor from the reactor as fast as possible by opening the connection between the reactor and the distillation column. The removal of water shifts the equilibrium reactions to the product side, promoting the formation of more polymer and water as byproduct. In this optimization step, the goal is to minimize the partial pressure of water in the reactor. The input to optimize over is the jacket oil inlet temperature $T_{\text{jacket,in}}$, the internal reflux ratio \mathfrak{R} , and the valve opening κ_{valve} . The minimization problem is

$$\begin{aligned}
& \min_{T_{\text{jacket,in}}, \mathfrak{R}, \kappa_{\text{valve}}} && t_{f_3} + \lambda_3 \|p_{\text{H}_2\text{O}}(t_{f_3})\|_2^2 \\
\text{s.t.} & && \dot{\mathbf{x}} = f(\mathbf{x}, \mathbf{u}, \mathbf{p}), \quad \mathbf{x}(t_{f_2}^*) = \mathbf{x}_{f_2} \\
& && \hat{\mathbf{y}} = [T_r \quad P_r \quad \eta]^\top \\
& && T_{r_0} \leq T_r \leq T_r^{\max} \\
& && 1 \leq P_r \leq P_r^{\max} \\
& && 0 \leq \mathfrak{R} \leq 1 \\
& && 0 \leq \kappa_{\text{valve}} \leq 1 \\
& && t_{f_2}^{\max} \leq t_{f_3} \leq t_{f_3}^{\max}
\end{aligned} \tag{8.8}$$

Optimization of the production step

In this step, both the reactor and column are active producing and distilling as much water as possible. After steering the process to an operating condition where the water concentration is minimal with respect to (8.8), this step is used to increase the viscosity in the mixture. This increase is caused by the complete removal of the water in the process, which causes an exponential growth in the viscosity. The goal in this optimization step is to maximize the polymer viscosity in the reactor

along the whole duration of the step while keeping the molar composition of water in the distillate high (at least 95%). The input to optimize over is the jacket oil inlet temperature $T_{\text{jacket,in}}$, the internal reflux ratio \mathfrak{R} , and the valve opening κ_{valve} . The minimization problem is

$$\begin{aligned}
 & \min_{T_{\text{jacket,in}}, \mathfrak{R}, \kappa_{\text{valve}}} && t_{f_4} - \lambda_4 \|\eta(t_{f_4})\|_2^2 \\
 & \text{s.t.} && \dot{\mathbf{x}} = f(\mathbf{x}, \mathbf{u}, \mathbf{p}), \quad \mathbf{x}(t_{f_3}^*) = \mathbf{x}_{f_31} \\
 & && \hat{\mathbf{y}} = [T_r \quad P_r \quad \eta]^T \\
 & && T_{r0} \leq T_r \leq T_r^{\max} \\
 & && 1 \leq P_r \leq P_r^{\max} \\
 & && 0.95 \leq x_{\text{H}_2\text{O}}^{\text{D}} \leq 1 \\
 & && 0 \leq \mathfrak{R} \leq 1 \\
 & && 0 \leq \kappa_{\text{valve}} \leq 1 \\
 & && t_{f_3}^{\max} \leq t_{f_4} \leq t_{f_4}^{\max}
 \end{aligned} \tag{8.9}$$

The weighting factor λ_i used in each of the optimization serves to three purposes: first, it provides a relative importance to one of the variables in the cost function. Secondly, it makes the cost function dimensionally consistent. Lastly, it makes both quantities in the cost function to be comparable in magnitude as the time variable outweighs the other quantities in the cost function due to its monotonic growth. It is computed as follows:

$$\lambda_j = \bar{\lambda} \times 10^{\lceil \log_{10}(t_{f_j}) - 1 \rceil - \lceil \log_{10}(\|g(\mathbf{x})_j\|_2^2) - 1 \rceil} \tag{8.10}$$

where $\bar{\lambda}$ is a user-defined weighting factor, $g(\mathbf{x})_j$ is any function of the states that is to be optimized in the j -th optimization step, $\log_{10}(\cdot)$ is the base 10 logarithm, and $\lceil \cdot \rceil$ is the ceiling function.

The optimized inputs and outputs of the process are shown in Figures 8.5 and 8.6, respectively. It can be observed that the total batch time of the process was greatly reduced by almost 25%. This was achieved by increasing the heat jacket inlet oil temperature during the filling step to keep the temperature T at the initial pre-heating temperature T_0 . In the original operation, the reactor is filled with an alcohol, which has a temperature much lower than that of the reactor. By allowing the jacket to operate during the filling, there is less time spent to reach the reaction temperature. The operating pressure is reached at around 2.3% of the total batch time, whereas in the original operation it is reached at 15% of the total batch time. This results in reaching the desired value of the polymer viscosity 1.32 times quicker. However, there is an increase in the energy employed at the beginning of

the process, where the $T_{jacket,in}$ is constantly manipulated to keep the temperature in the set point. The chattering-like behavior is the result of the discretization used in the optimization. Additionally, the process is allowed to reach a higher pressure to explore other points of the operational space that could be beneficial for the production of the polymer. Moreover, the optimization does not impose any set point on the pressure, and allows it to vary as long as it improves the objective of each optimization step. Reducing the time batch comes at the expense of having a larger energy demand in the process, especially during the filling step. During the feeding of alcohol to the process, maintaining a constant temperature obviously requires supplying a great amount of thermal energy. Therefore, if the energy demand is also to be decreased, it is recommended that the AOH at the inlet is preheated to a value closer to the initial temperature of the reactor. If this is not possible, the temperature set point can be lowered to allow some flexibility in the temperature profile and energy input.

The profiles of the molar compositions in both the distillate and reactor steps are displayed in Figure 8.7. As expected, the water in the reaction zone is completely removed, and collected at the distillate step, where the composition of water is kept at roughly 100%. Furthermore, the species AC1-rep, AC2-rep, and AOH-rep are segments that form the copolymer produced. The total polymer composition, which accounts the contribution of these three species, is shown in Figure 8.8. It is observed that the molar composition of the polymer reaches 91%, the unconverted end groups account for a 7% of the composition, and a 2% corresponds to unreacted excess AOH. It is also recommended to decrease the amount of alcohol used or increase the proportions of AC1 and AC2 in the recipe to reduce the percentage of unreacted end groups in the mixture.

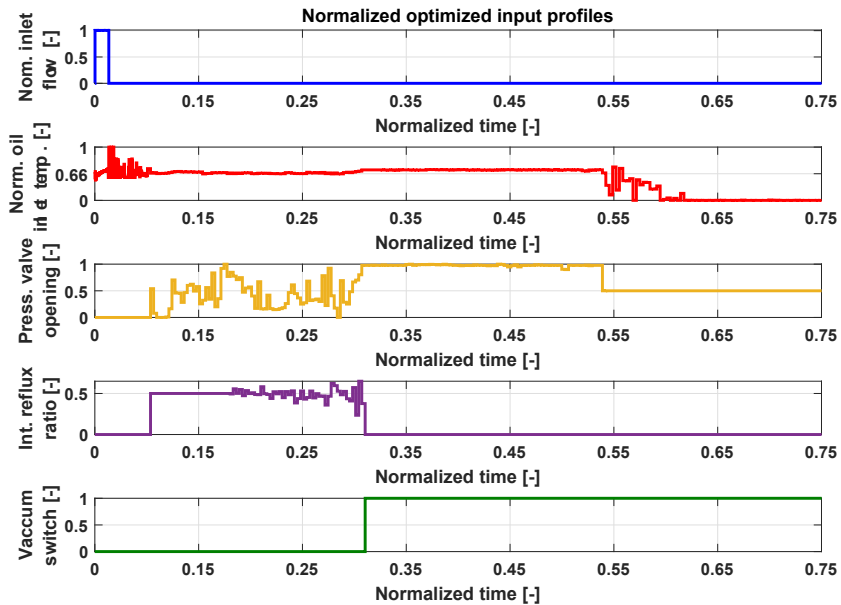


Figure 8.5: Optimized input profiles for the RBD process (time normalized with respect to the unoptimized model)

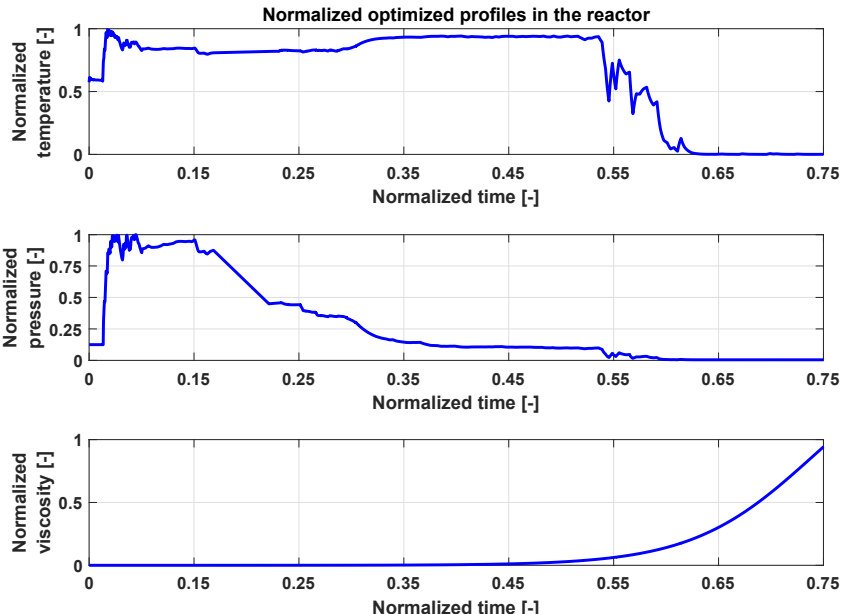


Figure 8.6: Optimized output profiles for the RBD process (time normalized with respect to the unoptimized model).

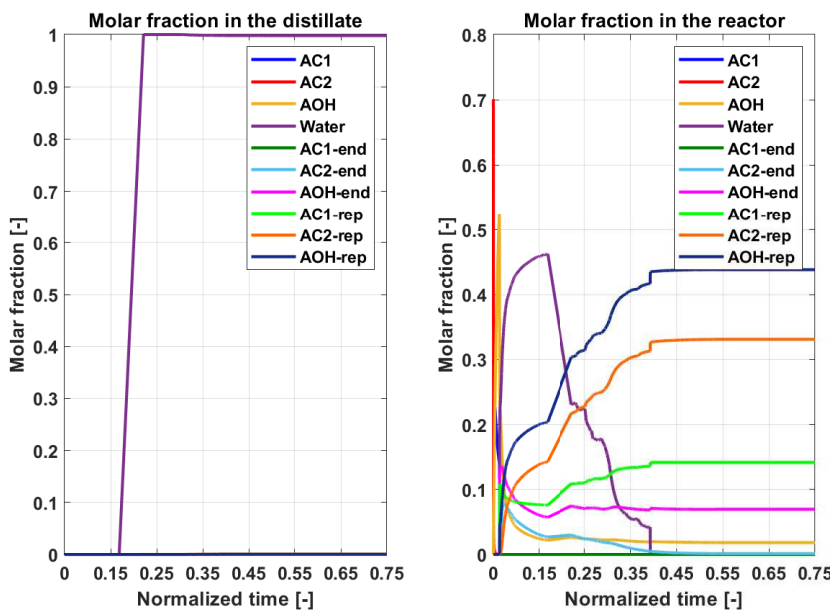


Figure 8.7: Optimized composition profiles for the RBD process at the reactor (right) and distillate (left) steps (time normalized with respect to the unoptimized model).

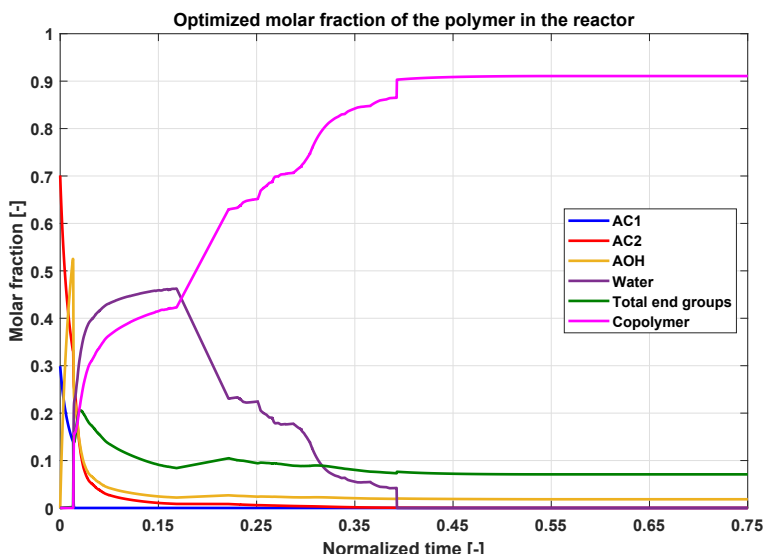


Figure 8.8: Optimized polymer composition profile for the RBD process (time normalized with respect to the unoptimized model).

Chapter summary

Parameter estimation

- Parameter estimation is performed on the RBD model to match the behavior of the model to the real plant behavior. Sensitivity analysis is also implemented along with parameter ranking using a successive orthogonalization method (SOM) to pinpoint the most identifiable parameters of the model. Sensitivity analysis is unit-dependent, so the sensitivity measures are made relative to the trajectories and parameters to eliminate the dependency on physical units.
- The sensitivity analysis and parameter ranking are performed over the whole model trajectory. However, due to the nature of the batch process at hand, the ranking is divided per batch step because the output parametric sensitivities change dynamically in each of these steps over time. As a consequence, depending on the batch step, the number of identifiable parameters also changes due to the presence or lack of excitation in that specific operating region.
- The output trajectory used for parameter estimation is subdivided into rank and shooting intervals to apply the ranked-interval multiple-shooting parameter estimation (RIMSPE). This method allows more flexibility in the optimization problem, helping to avoid local minima in the search space. The number of shooting intervals is a critical parameter because the larger it is, the more degrees of freedom the optimization algorithm has over a specific region to find optimal parameter. This comes at the expense of increasing rapidly the number of degrees of freedom of the entire optimization and requiring more computation power.
- The objective of parameter estimation is to minimize the total output error. The optimization problem is modified accordingly to ensure that the optimization gradient-based algorithm computed a relative sensitivity matrix during the parameter update step via a trajectory normalization.
- The ranked-interval multiple-shooting based parameter estimation helped to calibrate effectively the RBD model and obtain a lower total error between the process data and the model prediction. A weighted mean was used to find single parameter values based on their respective variances.

Chapter summary

Process trajectory optimization

- The optimization of trajectories is divided into different steps to simplify the optimization problem as the RBD model is simulated over a long period of time.
- Each optimization step minimizes the time of the step and optimizes a specific process variable that steers the process in the right direction. Given the step-wise nature of the RBD model, the input variables to optimize over, as well as the optimization constraints, change in each optimization step.
- The computation of the optimal input trajectories is performed discretizing the inputs into piece-wise constant functions. The number of discretization points is a critical parameter in the optimization as a large number generates trajectories that tightly steers the output trajectories to the optimal points.
- The optimization achieves a polymer viscosity similar to that of the real process. Furthermore, the optimized batch time corresponds to a 25% reduction compared to the original one.
- The optimization achieves shorter batch times while minimizing and maximizing the composition in the reactor of water and polymer, respectively. Furthermore, the composition of water at the distillate step is kept close to 98%, well above the 95% imposed in the constraint.
- The reduction of batch time comes at the expense of a higher energy consumption. The filling step is the portion where time is lost due to the decrease of the temperature, which makes a reheating process necessary to reach the reaction activation temperature.

9

Conclusions and recommendations

The interest in opportunities to improve operation of industrial process is in high demand due to the current technological, environmental, and societal challenges. Digital twins (3D representation + simulation model) have emerged as a very valuable solution due to the flexibility and potential uses they have. Specifically, the simulation model of a digital twin is its main attribute, which allows for multiple model-based technologies, e.g. control, parameter estimation, process optimization, etc. However, these models tend to lose their fidelity over time due to operating changes in the process, so they need to be calibrated in order to obtain a good description of the process. Under the assumption of no undermodeling, the calibration can be understood as re-estimating the model parameter to minimize the model-plant error. In the case of batch processes, model parameters are generally more difficult to estimate because parameter identifiability will change over time due to the constant dynamic evolution of the system's trajectory at each batch step. Motivated by the challenges present in model calibration for batch processes, we focus our attention to the global objective

Global objective

Develop effective tools for the online maintenance of first principles models of batch reaction processes

In order to address this objective, we split the problem into three main parts

- a. What to update: Selection of parameters to be updated within the set of all model parameters.
- b. How to update: Methodologies to update parameters offline and online to ensure good performance of the simulation model.

These two aspects are explored in detail in the chapters of this thesis, where different related research questions are answered.

9.1. Conclusions

9.1.1. Structural identifiability

1 Research question on parameter sensitivity and structural identifiability

How is state and output parametric sensitivity controllability related to identifiability?

This is answered in Chapter 3 by developing a mathematical setting where an open-loop linearized model around a fixed point or dynamic trajectory is adjoined with its parameter sensitivity representation. Parameter structural identifiability of the model is assessed from an output controllability point of view, verifying that the input-to-output-sensitivity map is full rank. Output controllability-based identifiability is first studied for SISO models, where the rank of the controllability matrix coincided with the number of identifiable parameter. However, the extension to MIMO is not trivial due to the ordering of the elements in the controllability matrix. Through the analysis of this question, we bridge the connection between state controllability and observability with parameter identifiability; and how identifiability analysis can be addressed using system theoretic tools.

9

2. Research subquestion

What is the effect of feedback and controllers on the structural identifiability?

A natural extension to the open-loop case is to explore the implications of having a controller interconnected with the model in a closed loop. In this particular context, we prove that a controller cannot improve structural identifiability of the model because it does not change the parametric information in the loop. This is demonstrated showing that the null space of the open-loop model structure is contained in the null space of the closed-loop model structure. Moreover, it is also shown that the controller can impact the model parameter identifiability if this property is not taken into account in the controller design. The closed-loop analysis provides insight on the limits of what can be achieved with the controller. Additionally, it paves the way to establishing the conditions for the design of identifiability-aware controller. For this research subquestion, it is determined that the null space of the Jacobian matrix of the controller coefficients cannot have a common vector with the null space of the Jacobian vector of the open-loop model structure. The value of this analysis resides in that it can be ascertained whether a specific control design will impact the structural identifiability of the original model. This is especially important if the model needs to be constantly updated for calibration.

9.1.2. Operational identifiability and offline gradient-based parameter estimation

3. Research subquestion

How can parameters be estimated accurately in models exploiting the variations of the parametric sensitivities along the output trajectories?

Operational identifiability is the main focus of Chapter 4. In this setting a full data set is used to extract the average parameter sensitivity information of the process outputs. However, since parameter sensitivities are time-varying functions that depend on the internal states of the system, the average sensitivity might provide an incomplete analysis. A segmented operational identifiability analysis is developed, where the output trajectory is divided in several interval to analyze the parameter sensitivity of each segment. This allows to obtain a more precise selection of the data where each parameter is maximally identifiable, i.e. the output parameter sensitivity is maximal. The subset selection is done using user-defined cut-off values based on sensitivity measures.

Given how parametric sensitivity dynamically affects the parameter selection to perform estimation, various methods are developed to address this issue. A first approach is the modified greedy algorithm, where a number of parameter realizations are generated using Latin Hypercube Sampling to finally perform parameter

selection based on the sensitivity analysis. The parameter subset that generates the smallest nonlinear least-square error is labeled as the optimal parameter set.

A second approach named cascade identifiable adaptive optimization assumes a preliminary parameter selection, and solves a nonlinear least-squares problem to find the optimal parameters. At the optimum point, the sensitivity-based parameter selection is applied again to obtain a new parameter subset selection, and the parameter estimation is performed once more. The iterative process ends when the elements of the new subset are equal to those of the previous run.

It is also possible that at certain points of the parameter space, the optimization is not well-defined, or very close to become ill-conditioned. To circumvent this, the multiple shooting method has gained popularity, as it segments the trajectory in equidistant shooting nodes, solving one parameter optimization per segment. We improved this existing approach by proposing a different parameter subset selection in each of the shooting segments. This provides the method with extra flexibility that enhances the estimation capabilities under ill-conditioned cost functions. This particular approach is implemented in Chapter 8 to calibrate the model of the reactive batch distillation case study. Nonetheless, since the model dimension is already large, a low number of shooting nodes is chosen to be able to solve the optimization problem.

9.1.3. Online parameter estimation

4. Research subquestion

How to design a parameter estimation methodology in an online setting to address potential parameter variations in a first-principle model?

9

This research question is addressed in Chapter 5, where parameter estimation is approached as a control design problem. Online parameter estimation has been classically done assuming that the time derivative of the parameter vector is zero. The values of the parameters are corrected to their true values designing an observer that makes the estimation error zero. However, we focus on exploring the dual of this design problem, viewing the parameter in the system as extra control actions whose dynamics can be calculated such that the model output tracks the system measurement. We utilize a Lyapunov function of the system-model error as a starting point to propose different control laws that guarantee negative definiteness of the time derivative of this function. The control laws depends on gain matrices that need to be computed solving optimization problems. Analogous to the observer-based

parameter estimation, the control-based parameter estimation will converge to the true parameter values if the (subset of) parameters are at least uniquely identifiable in the neighborhood of the point or trajectory at which the system is operated. Moreover, the effect of noise is also studied, where it is concluded that in the presence of measurement noise, the estimation is severely impacted, and measurement filters must be implemented before enabling the online parameter estimation loop.

9.1.4. Extent-based sequential estimation for process systems with unknown reaction dynamics

5. Research subquestion

What is the effect of uncertainty on the extent transformation and parameter estimation in reaction systems models?

In Chapter 6, this question is answered assuming that the variability in the inlet composition can be captured by a static matrix that acts on the system in an additive way. It is concluded that the extent transformation cannot fully decouple the mole dynamics as some effects of the inlet dynamics are still present in the reaction and invariant dynamics. This leads to a representation that is not based on the true extents. The presence of uncertainty in the inlet composition has important consequences for the extent-based control or parameter estimation. Hence, the (approximate) knowledge of this matrix is relevant if other model-based tasks are required.

Given that the knowledge of the uncertainty matrix is necessary, a method to estimate this uncertainty matrix for semi-batch and CSTR cases with unknown reaction dynamics and partial mole measurement is developed. In the semi-batch case, the procedure is simpler due to the lack of an outlet flow. In the CSTR case, the analysis and problem set-up are more involved because the mixture's residence time is affected by the inlet uncertainty. Nevertheless, in both cases, the estimation of the uncertainty matrix reduces to solving a constrained linear optimization. Using the uncertainty matrix, the unmeasured moles, the unknown extent of reaction as well as the reaction kinetic parameters can be calculated. Although, the uncertainty can be estimated, uniqueness cannot be guaranteed due to the lack of information on the true reaction dynamics. Nonetheless, if the changes in the inlet composition are not too abrupt, the estimated uncertainty recovers the behavior of the process sufficiently well.

9.1.5. Reactive batch distillation column: modeling and calibration

6. Research subquestion

How to develop both rigorous and accurate models of a reactive batch distillation process?

Chapters 7 and 8 provide a detailed model of a reactive batch distillation column for the production of a resin. Standard mass and energy balances as well as extensive thermodynamic and hydraulic relationships are used to model the process. Furthermore, a dynamic grey-box model is developed to predict the polymer viscosity, which is a key product quality indicator. The viscosity model is based on the logistic differential equation given the exponential growth the polymer viscosity exhibits for conversions of reactants close to 1. Additionally, the reactive batch distillation model is calibrated estimating selected model parameters based on sensitivity analysis. This is performed using the modified multiple shooting method described in Chapter 4 to exploit the different operation stages in the process. Finally, the process is optimized based on the available model to minimize batch time while maximizing the polymer viscosity. The optimization is performed stage-wise, i.e. the outcome of the previous optimization serves as the initial condition for the next operating step. The optimization provides an operating trajectory that reduces the batch time by 25% at the expense of an increased energy input to counteract the loss of thermal energy during the loading of the reactor.

9.2. Recommendations

In this thesis, structural and operational identifiability as well as offline and online parameter estimation are studied with special emphasis on process systems models. However, there are some limitations to the developments presented in this work, which should be addressed in future research.

9.2.1. Identifiability and control design

Most controllers are designed to comply with plant performance specifications. However, controller usually induce a linearizing effect on the process outputs, thereby impacting parameter identifiability, whether by reducing the actual sensitivity magnitude or increasing the null space dimension of the sensitivity matrix. Hence, it is important to include identifiability criteria (when possible) in the controller design

phase to make online (or offline) model update a simpler task.

9.2.2. Closed-loop identifiability in the nonlinear case

Although, we have presented a closed-loop structural identifiability analysis setting for linear models, most of the models in science and engineering are nonlinear and have several algebraic relationships. Hence, a natural extension to this analysis is to develop tools that allow the analysis of nonlinear models in closed-loop directly, i.e. without linearizing them around a particular operating point or trajectory. This could circumvent the local nature of the analysis in the case of linear systems.

9.2.3. Process model update: Input-output pairing and measurement selection

Input-output pairing in a system (resp. model) is usually done taking into account the control effort required from a particular input to a determined output. Likewise, sensor arrangement is chosen in such a way that the system is at least detectable. However, parameter identifiability is also a function of the input-output map of the model. Therefore, it is also crucial to include in the analysis how parameter identifiability changes with respect to different input-output pairings and sensor arrangements. Some key parameters in the model may affect noticeably certain unmeasured outputs, while their effect on the measured ones is subtle, making the overall parameter estimation impractical. A good example of this issue is the chemical kinetic parameters in the reactive batch distillation column model. The measured outputs are temperature, pressure, and polymer viscosity. Although the influence of the kinetic parameters can be detected in these measured outputs, their effect is masked by other latent dynamics, making their estimation difficult. In this example, a good option is to have some form of measurement of the concentration in the reactor to improve the identifiability of these parameters.

9.2.4. Inlet composition uncertainty

The inlet composition uncertainty can be estimated using a static matrix that allows to recover information on number of moles and reaction dynamic, provided the changes in the inlet composition are not too abrupt. Nevertheless, the assumption of a unique static uncertainty matrix that on average approximates the true behavior of the system can be limited. To this end, a possible extension is to express the uncertain system using a linear parameter-varying approach (LPV), which encodes

all possible time-varying changes of the inlet composition. The LPV approach could lead to a more precise estimation of the uncertainty and of the unknown dynamics in the process.

Glossary

List of Acronyms

AC1	Acid 1
AC1-end	Acid 1 end segment
AC1rep	Acid 1 repeat segment
AC2	Acid 2
AC2-end	Acid 2 end segment
AC2rep	Acid 2 repeat segment
AO	Asymptotic observer
AOH	Alcohol 1
AOH-end	Alcohol 1 end segment
AOHrep	Alcohol 1 repeat segment
AOPS	Absolute output parametric sensitivity
CIAO	Cascaded identifiable adaptive optimization
CSP	Constraint satisfaction problem
CSTR	Continuous stirred-tank reactor
CVP	Control vector parametrization
DAE	Differential algebraic equation
DIPPR	Design Institute for Physical Properties
DT	Digital twin
EKF	Extended Kalman filter
FH	Flory-Huggins

FIM	Fisher Information Matrix
GRASP	Greedy random adaptive search procedure
HETP	Height equivalent to a theoretical plate
ILC	Iterative learning control
IMA	Internal modifier adaptation
IoT	Internet of Things
LHS	Latin hypercube sampling
LMI	Linear matrix inequality
LPV	Linear parameter-varying
LTI	Linear time-invariant
MA	Modifier adaptation
mGRASP	Modified greedy random adaptive search procedure
MIMO	Multiple-input multiple output
MAy	Output modifier adaptation
ML	Machine learning
MLE	Maximum likelihood estimator
MSPE	Multiple shooting parameter estimation
NLP	Nonlinear programming
NRTL	Non-random two liquids
ODE	Ordinary differential equation
P	Proportional
PCA	Principal component analysis
PDE	Partial differential equation
PDF	Probability density function
PI	Proportional-Integral
PID	Proportional-Integral-Derivative
PLSs	Projection to latent spaces
RIMSPE	Ranked interval multiple shooting parameter estimation

RD	Reactive distillation
RBD	Reactive batch distillation
RGA	Relative gain array
RI	Rank interval
RMSE	Root-mean-square error
ROPS	Relative output parametric sensitivity
RRE	Reaction rate estimator
RTO	Real-time optimization
SGI	Structurally globally identifiable
ShI	Shooting interval
SISO	Single-input single-output
SLI	Structurally locally identifiable
SOM	Successive orthogonalization method
SQP	Sequential quadratic programming
SSPE	Single shooting parameter estimation
SVD	Singular value decomposition
TI	Tuning importance
VLE	Vapor-liquid equilibrium

A

Mathematical proofs and derivations

A

A.1. Mathematical proofs

A.1.1. Proof Theorem 3.4

Proof:

Let model output \mathbf{y} be a smooth functions of the state \mathbf{x} and the input \mathbf{u} . Consider the function V

$$V(\mathbf{p}) := \frac{1}{2}\boldsymbol{\varepsilon}(\mathbf{p})^\top \boldsymbol{\varepsilon}(\mathbf{p}) \quad (\text{A.1})$$

where $\boldsymbol{\varepsilon}(\mathbf{p}) = \mathbf{y}_m - \delta\mathbf{y} = \mathbf{y}_m(t) - \mathbf{C}(\mathbf{p})\delta\mathbf{x}$. Furthermore, consider its approximation about a point \mathbf{p}_0 .

$$\begin{aligned} V(\mathbf{p}) \approx & V(\mathbf{p}_0) + \mathbf{J}^\top(\mathbf{p})|_{\mathbf{p}_0} (\mathbf{p} - \mathbf{p}_0) \\ & + \frac{1}{2}(\mathbf{p} - \mathbf{p}_0)^\top \mathbf{H}(\mathbf{p})|_{\mathbf{p}_0} (\mathbf{p} - \mathbf{p}_0) \end{aligned} \quad (\text{A.2})$$

where

$$\mathbf{J}(\mathbf{p}) = \frac{\partial V(\mathbf{p})}{\partial \mathbf{p}} = -\mathbf{S}^\top(\mathbf{p}) \left(\mathbf{y}_m - \delta\mathbf{y}(\mathbf{p}) \right)$$

and

$$\mathbf{H}(\mathbf{p}) = \frac{\partial^2 V(\mathbf{p})}{\partial \mathbf{p}^\top \partial \mathbf{p}} = \frac{\partial \mathbf{S}^\top(\mathbf{p})}{\partial \mathbf{p}^\top} (\mathbf{I}_{n_p} \otimes \boldsymbol{\varepsilon}(\mathbf{p})) + \mathbf{S}^\top(\mathbf{p}) \mathbf{S}(\mathbf{p})$$

with $\mathbf{S}(\mathbf{p}) = \frac{\partial \delta\mathbf{y}(t, \mathbf{p})}{\partial \mathbf{p}^\top}$ the Jacobian of the output with respect to the parameter vector or the sensitivity matrix of the model.

The necessary condition to minimize the approximation of $V(\mathbf{p})$ is

$$\begin{aligned} \mathbf{J}(\mathbf{p})|_{\mathbf{p}_0} + \mathbf{H}(\mathbf{p})|_{\mathbf{p}_0} (\mathbf{p} - \mathbf{p}_0) &= 0 \\ \Rightarrow \mathbf{p} &= \mathbf{p}_0 - \mathbf{H}^{-1}(\mathbf{p})|_{\mathbf{p}_0} \mathbf{J}(\mathbf{p})|_{\mathbf{p}_0} \end{aligned} \quad (\text{A.3})$$

The Hessian of the cost function can be approximated near the optimum neglecting the first term. Thus

$$\mathbf{H}(\mathbf{p}) \approx \mathbf{S}^\top(\mathbf{p})\mathbf{S}(\mathbf{p}) = \left(\frac{\partial \delta \mathbf{y}(t, \mathbf{p})}{\partial \mathbf{p}^\top} \right)^\top \left(\frac{\partial \delta \mathbf{y}(t, \mathbf{p})}{\partial \mathbf{p}^\top} \right) \quad (\text{A.4})$$

Such an approximation of the Hessian holds in the neighborhood of the optimum, where both the error and its second derivative are weakly correlated [187]. Moreover, uniqueness of the parameter vector \mathbf{p} requires that the approximated Hessian is invertible at \mathbf{p}_0 . The approximation of the Hessian is invertible if and only if the Jacobian \mathbf{S} is full column rank at \mathbf{p}_0 , i.e. $\text{rank}(\mathbf{S}|_{\mathbf{p}_0}) = n_p$. Moreover, recall that \mathbf{y} is continuous in \mathbf{u} , hence, the Jacobian $\mathbf{S}(\mathbf{p})$ is a linear map from \mathbf{u} to the parametric sensitivities of the output \mathbf{y} .

We now show that each block $\bar{\mathbf{W}}_{i,j}^{x_p}$ of \mathfrak{W} contains the same information of the Jacobian of the output \mathbf{S} with respect to the parameter vector. The Jacobian matrix \mathbf{S} has the form

$$\mathbf{S}(\mathbf{p}) = \begin{bmatrix} \mathbf{S}_1(\mathbf{p}) \\ \vdots \\ \mathbf{S}_{n_p}(\mathbf{p}) \end{bmatrix} = \begin{bmatrix} \partial_{\mathbf{p}_1} \delta \mathbf{y}_1(t, \mathbf{p}) & \cdots & \partial_{\mathbf{p}_{n_p}} \delta \mathbf{y}_1(t, \mathbf{p}) \\ \vdots & \ddots & \vdots \\ \partial_{\mathbf{p}_1} \delta \mathbf{y}_{n_y}(t, \mathbf{p}) & \cdots & \partial_{\mathbf{p}_{n_p}} \delta \mathbf{y}_{n_y}(t, \mathbf{p}) \end{bmatrix}$$

We differentiate with respect to \mathbf{p} the output of (3.3)

$$\delta \mathbf{y}_p = \mathcal{C} \delta \bar{\mathbf{x}} + \mathfrak{C} \delta \bar{\mathbf{x}}_p \quad (\text{A.5})$$

The solution of (3.3) for $\delta \bar{\mathbf{x}}_0 \neq \mathbf{0}$ is

$$\begin{aligned} \delta \bar{\mathbf{x}} &= e^{\mathbf{A}(\mathbf{p})(t-t_0)} \delta \bar{\mathbf{x}}_0 + \int_{t_0}^t e^{\mathbf{A}(\mathbf{p})(t-\tau)} \mathbf{B}(\mathbf{p}) \delta \mathbf{u}(\tau) \, d\tau \\ &= \sum_{k=0}^{\infty} \frac{(t-t_0)^k \mathbf{A}^k(\mathbf{p})}{k!} \delta \bar{\mathbf{x}}_0 + \int_{t_0}^t \sum_{k=0}^{\infty} \frac{(t-\tau)^k \mathbf{A}^k(\mathbf{p})}{k!} \mathbf{B}(\mathbf{p}) \delta \mathbf{u}(\tau) \, d\tau \end{aligned} \quad (\text{A.6})$$

Differentiate (A.6) with respect to \mathbf{p}

A

$$\begin{aligned}\delta\bar{\mathbf{x}}_{\mathbf{p}} &= \frac{\partial}{\partial \mathbf{p}} \left(e^{\mathbf{A}(\mathbf{p})(t-t_0)} \delta\bar{\mathbf{x}}_0 + \int_{t_0}^t e^{\mathbf{A}(\mathbf{p})(t-\tau)} \mathbf{B}(\mathbf{p}) \delta\mathbf{u}(\tau) d\tau \right) \\ &= \frac{\partial}{\partial \mathbf{p}} \left(\sum_{k=0}^{\infty} \frac{(t-t_0)^k \mathbf{A}^k(\mathbf{p})}{k!} \delta\bar{\mathbf{x}}_0 + \int_{t_0}^t \sum_{k=0}^{\infty} \frac{(t-\tau)^k \mathbf{A}^k(\mathbf{p})}{k!} \mathbf{B}(\mathbf{p}) \delta\mathbf{u}(\tau) d\tau \right)\end{aligned}\quad (\text{A.7})$$

Stacking (A.6) and (A.7), and applying the Cayley-Hamilton Theorem, we have

$$\begin{bmatrix} \delta\bar{\mathbf{x}} \\ \delta\bar{\mathbf{x}}_{\mathbf{p}} \end{bmatrix} = \Lambda_e \gamma_0 + \mathbf{K}_e \gamma = \begin{bmatrix} \Lambda^x \\ \Lambda^{x_{\mathbf{p}}} \end{bmatrix} \gamma_0 + \begin{bmatrix} \mathbf{K}^x \\ \mathbf{K}^{x_{\mathbf{p}}} \end{bmatrix} \gamma \quad (\text{A.8})$$

with $\Lambda_e = [(\Lambda_e)_0 \quad (\Lambda_e)_1 \quad \cdots \quad (\Lambda_e)_{n_x(n_p+1)-1}]$

where

$$(\Lambda_e)_0 = \begin{bmatrix} \mathbf{I}_{n_x} & \\ & \mathbf{I}_{n_x n_p} \end{bmatrix} \text{ and } (\Lambda_e)_i = \begin{bmatrix} \mathbf{A}^i & \mathbf{0} \\ \sum_{j=0}^{i-1} \mathfrak{A}^j \mathcal{A} \mathbf{A}^{i-j-1} & \mathfrak{A}^i \end{bmatrix}$$

and

$$\gamma_0 = \begin{bmatrix} v_0(t-t_0) \delta\bar{\mathbf{x}}_0 \\ v_0(t-t_0) \delta\bar{\mathbf{x}}_{\mathbf{p}_0} \\ v_1(t-t_0) \delta\bar{\mathbf{x}}_0 \\ v_1(t-t_0) \delta\bar{\mathbf{x}}_{\mathbf{p}_0} \\ \vdots \\ v_{n_x(n_p+1)-1}(t-t_0) \delta\bar{\mathbf{x}}_0 \\ v_{n_x(n_p+1)-1}(t-t_0) \delta\bar{\mathbf{x}}_{\mathbf{p}_0} \end{bmatrix}, \quad \gamma = \begin{bmatrix} \int v_0(\tau) \mathbf{u}(\tau) d\tau \\ \int v_1(\tau) \mathbf{u}(\tau) d\tau \\ \vdots \\ \int v_{n_x(n_p+1)-1}(\tau) \mathbf{u}(\tau) d\tau \end{bmatrix}, \quad v_k(\cdot) = \frac{(\cdot)^k}{k!}$$

Substituting (A.8) in (A.5)

$$\delta\mathbf{y}_{\mathbf{p}} = (\mathcal{C}\Lambda^x + \mathfrak{C}\Lambda^{x_{\mathbf{p}}})\gamma_0 + (\mathcal{C}\mathbf{K}^x + \mathfrak{C}\mathbf{K}^{x_{\mathbf{p}}})\gamma \quad (\text{A.9})$$

Thus

$$\begin{aligned} \Pi^y \delta \mathbf{y}_p &= \Pi^y \begin{bmatrix} \partial_{\mathbf{p}_1} y_1 \\ \vdots \\ \partial_{\mathbf{p}_1} y_{n_y} \\ \vdots \\ \partial_{\mathbf{p}_{n_p}} y_1 \\ \vdots \\ \partial_{\mathbf{p}_{n_p}} y_{n_y} \end{bmatrix} = \begin{bmatrix} \partial_{p_1} y_1 \\ \vdots \\ \partial_{\mathbf{p}_{n_p}} y_1 \\ \vdots \\ \partial_{\mathbf{p}_1} y_{n_y} \\ \vdots \\ \partial_{\mathbf{p}_{n_p}} y_{n_y} \end{bmatrix} \\ &= \text{vec}(\mathbf{S}^\top) = \Pi^y \mathbf{O}^{x_p} \Pi^{u^\top} \Pi \gamma_0 + \Pi^y \mathbf{W}^{x_p} \Pi^{u^\top} \Pi^u \gamma \\ &= \bar{\mathbf{O}}^{x_p} \bar{\gamma}_0 + \bar{\mathbf{W}}^{x_p} \bar{\gamma} \end{aligned} \quad (\text{A.10})$$

with $\mathbf{O}^{x_p} = \mathcal{C}\Lambda^x + \mathcal{C}\Lambda^{x_p}$

Applying the inverse vectorization operator on both sides of (A.10)

$$\mathbf{S}^\top = [\mathfrak{O} \quad \mathfrak{W}] \begin{bmatrix} \mathbf{G}_0 \\ \mathbf{G} \end{bmatrix} \quad (\text{A.11})$$

where $\mathfrak{O} = (\text{vec}^\top(\mathbf{I}_{n_y}) \otimes \mathbf{I}_{n_p}) (\mathbf{I}_{n_y} \otimes \bar{\mathbf{O}}^{x_p})$, $\mathfrak{W} = (\text{vec}^\top(\mathbf{I}_{n_y}) \otimes \mathbf{I}_{n_p}) (\mathbf{I}_{n_y} \otimes \bar{\mathbf{W}}^{x_p})$, $\mathbf{G}_0 = \mathbf{I}_{n_y} \otimes \bar{\gamma}_0$, and $\mathbf{G} = \mathbf{I}_{n_y} \otimes \bar{\gamma}$

It follows that

$$\mathcal{R}(\mathbf{S}^\top) = \mathcal{R} \left([\mathfrak{O} \quad \mathfrak{W}] \begin{bmatrix} \mathbf{G}_0 \\ \mathbf{G} \end{bmatrix} \right) \subseteq \mathcal{R}([\mathfrak{O} \quad \mathfrak{W}]) \quad (\text{A.12})$$

Recalling that the structural identifiability setting assumed persistence of excitation, and assuming that $\bar{\mathbf{x}}_0 \neq \mathbf{0}$, the matrix \mathbf{G}_0 and \mathbf{G} have independent block rows. Thus

$$\begin{aligned} \mathcal{R}(\mathbf{S}^\top) &= \mathcal{R}([\mathfrak{O} \quad \mathfrak{W}]) \\ \Rightarrow \dim(\mathcal{R}(\mathbf{S}^\top)) &= \dim(\mathcal{R}([\mathfrak{O} \quad \mathfrak{W}])) \leq n_p \end{aligned} \quad (\text{A.13})$$

Finally, it follows from the previous equality that $\text{rank}(\mathbf{S}^\top) = n_p \Leftrightarrow \text{rank}([\mathfrak{O} \quad \mathfrak{W}]) = n_p$

A

■

A.1.2. Proof Theorem 6.1*Proof:*

Let the error between the system and the model extents of inlet, invariant and initial condition discounting factor be $\boldsymbol{\varepsilon}_{\text{in}} := \mathbf{x}_{\text{in}} - \mathbf{x}_{\text{in}}^{\circ}$, $\boldsymbol{\varepsilon}_{\text{inv}} := \mathbf{x}_{\text{inv}} - \mathbf{x}_{\text{inv}}^{\circ}$, and $\boldsymbol{\varepsilon}_{\lambda} := \mathbf{x}_{\lambda} - \mathbf{x}_{\lambda}^{\circ}$, and suppose that $\varsigma = \varsigma^{\circ} = \varsigma$. Differentiating the error terms and substituting (6.25) and (6.26)

$$\begin{aligned}\dot{\boldsymbol{\varepsilon}}_{\text{in}} &= -\varsigma(\mathbf{x}_{\text{in}} - \mathbf{x}_{\text{in}}^{\circ}) = -\varsigma\boldsymbol{\varepsilon}_{\text{in}}, & \boldsymbol{\varepsilon}_{\text{in}}(0) &= \mathbf{0}_{N_{\varepsilon}} \\ \dot{\boldsymbol{\varepsilon}}_{\text{inv}} &= -\varsigma(\mathbf{x}_{\text{inv}} - \mathbf{x}_{\text{inv}}^{\circ}) = -\varsigma\boldsymbol{\varepsilon}_{\text{inv}}, & \boldsymbol{\varepsilon}_{\text{inv}}(0) &= \mathbf{0}_{N_{\varepsilon}} \\ \dot{\boldsymbol{\varepsilon}}_{\lambda} &= -\varsigma(x_{\lambda} - x_{\lambda}^{\circ}) = -\varsigma\boldsymbol{\varepsilon}_{\lambda}, & \boldsymbol{\varepsilon}_{\lambda}(0) &= 0\end{aligned}\tag{A.14}$$

The previous equation can be written in matrix form:

$$\dot{\boldsymbol{\varepsilon}} = -\varsigma\boldsymbol{\varepsilon}, \quad \boldsymbol{\varepsilon}(0) = \mathbf{0}_{N_{\varepsilon}+N_{\varepsilon}+1}\tag{A.15}$$

$$\text{where } \boldsymbol{\varepsilon} = \begin{bmatrix} \boldsymbol{\varepsilon}_{\text{in}} \\ \boldsymbol{\varepsilon}_{\text{inv}} \\ \boldsymbol{\varepsilon}_{\lambda} \end{bmatrix}$$

The equation (A.15) describes a linear time-varying system whose only time-varying pole is always negative for all time. Its solution is given in terms of the state transition matrix $\Phi(t, \tau)$.

$$\boldsymbol{\varepsilon}(t) = \Phi(t, 0)\boldsymbol{\varepsilon}(0)\tag{A.16}$$

Since the initial conditions are zero, (A.16) holds trivially and it is always zero for all $t \in [0, \infty)$. We shall also show that $\boldsymbol{\varepsilon} \rightarrow \mathbf{0}$ as $t \rightarrow \infty$ irrespective of the initial conditions.

To show that (A.16) converges to zero as $t \rightarrow \infty$, let $\mathbf{A}(t) = -\varsigma\mathbf{I}_{N_{\varepsilon}+N_{\varepsilon}+1}$ be the state time-varying matrix. Since $\mathbf{A}(t)$ is diagonal, by linearity of the integral operator, $\int_{\tau}^t \mathbf{A}(s) \, ds$ is also diagonal, and commutes with $\mathbf{A}(t)$. As noted in [88], if the time-

varying matrix $\mathbf{A}(t)$ commutes with $\int_{\tau}^t \mathbf{A}(s) \ ds$, then $\Phi(t, \tau) = \exp\left(\int_{\tau}^t \mathbf{A}(s) \ ds\right)$. Hence (A.16) can be rewritten as

$$\boldsymbol{\varepsilon} = \exp\left(\int_0^t \mathbf{A}(s) \ ds\right) \boldsymbol{\varepsilon}(0) \quad (\text{A.17})$$

Applying limit as $t \rightarrow \infty$

$$\lim_{t \rightarrow \infty} \boldsymbol{\varepsilon} = \lim_{t \rightarrow \infty} \exp\left(\int_0^t \mathbf{A}(s) \ ds\right) \boldsymbol{\varepsilon}(0) = \exp\left(\lim_{t \rightarrow \infty} \int_0^t \mathbf{A}(s) \ ds\right) \boldsymbol{\varepsilon}(0) \quad (\text{A.18})$$

Recall that the integral $\int_0^t \mathbf{A}(s) \ ds = -\int_0^t \varsigma(s) \mathbf{I}_{N_t + N_\varepsilon + 1} \ ds$. Since $\varsigma > 0 \quad \forall t \in [0, \infty)$, it is not absolutely integrable, and its integral is not bounded as $t \rightarrow \infty$. Therefore

$$\begin{aligned} \lim_{t \rightarrow \infty} \int_0^t \mathbf{A}(s) \ ds &= -\int_0^t \varsigma(s) \mathbf{I}_{N_t + N_\varepsilon + 1} \ ds \rightarrow -\infty \\ \Rightarrow \exp\left(\lim_{t \rightarrow \infty} \int_0^t \mathbf{A}(s) \ ds\right) &\rightarrow \mathbf{0} \\ \Rightarrow \boldsymbol{\varepsilon} &\rightarrow \mathbf{0} \end{aligned} \quad (\text{A.19})$$

Now suppose that $\varsigma \neq \varsigma^\circ \quad \forall t \in [0, \infty)$, and that $\boldsymbol{\varepsilon} \rightarrow \mathbf{0}$ as $t \rightarrow \infty$. The error dynamics are given by

$$\begin{aligned} \dot{\boldsymbol{\varepsilon}}_{\text{in}} &= -\varsigma \mathbf{x}_{\text{in}} + \varsigma^\circ \mathbf{x}_{\text{in}}^\circ, & \boldsymbol{\varepsilon}_{\text{in}}(0) &= \mathbf{0}_{N_t} \\ \dot{\boldsymbol{\varepsilon}}_{\text{inv}} &= -\varsigma \mathbf{x}_{\text{inv}} + \varsigma^\circ \mathbf{x}_{\text{inv}}^\circ, & \boldsymbol{\varepsilon}_{\text{inv}}(0) &= \mathbf{0}_{N_\varepsilon} \\ \dot{\varepsilon}_\lambda &= -\varsigma x_\lambda + \varsigma^\circ x_\lambda^\circ, & \varepsilon_\lambda(0) &= 0 \end{aligned} \quad (\text{A.20})$$

Rewriting $\mathbf{x}_{\text{in}}^\circ$, $\mathbf{x}_{\text{inv}}^\circ$, and x_λ° in terms of $\boldsymbol{\varepsilon}_{\text{in}}$, $\boldsymbol{\varepsilon}_{\text{inv}}$, and ε_λ

$$\dot{\boldsymbol{\varepsilon}} = -\varsigma \boldsymbol{\varepsilon} + (\varsigma^\circ - \varsigma) \mathbf{x}_{\text{in} - \lambda}, \quad \boldsymbol{\varepsilon}(0) = \mathbf{0}_{N_t + N_\varepsilon + 1 \times 1} \quad (\text{A.21})$$

where $\mathbf{x}_{\text{in} - \lambda} = \begin{bmatrix} \mathbf{x}_{\text{in}} \\ \mathbf{x}_{\text{inv}} \\ x_\lambda \end{bmatrix}$

A

Likewise, denote the state matrix $\mathbf{A}(t) = -\varsigma \mathbf{I}_{N_\ell + N_\varepsilon + 1}$. The state transition matrix can be written as $\Phi(t, \tau) = \exp\left(\int_\tau^t \mathbf{A}(s) \, ds\right)$

The solution of (A.21) is

$$\lim_{t \rightarrow \infty} \boldsymbol{\varepsilon} = \lim_{t \rightarrow \infty} \Phi(t, 0)\boldsymbol{\varepsilon}(0) + \lim_{t \rightarrow \infty} \int_0^t \Phi(t, \tau)(\varsigma^\circ - \varsigma)\mathbf{x}_{\text{in}-\lambda}(\tau) \, d\tau \quad (\text{A.22})$$

The first term $\lim_{t \rightarrow \infty} \Phi(t, 0)\boldsymbol{\varepsilon}(0) \rightarrow \mathbf{0}$ as shown previously. We now show that second term does not decay to zero.

By the Rogers-Hölder inequality, we have that if $\Phi(t, \tau)(\varsigma^\circ - \varsigma)\mathbf{x}_{\text{in}-\lambda} \in L^1(0, \infty)$ (space of absolutely integrable functions) then

$$\begin{aligned} \|\Phi(t, \tau)(\varsigma^\circ - \varsigma)\mathbf{x}_{\text{in}-\lambda}(\tau)\|_{L^1} &\leq \|\Phi(t, \tau)\|_{L^1} \|(\varsigma^\circ - \varsigma)\mathbf{x}_{\text{in}-\lambda}\|_{L^1} \\ &\leq \|\Phi(t, \tau)\|_{L^1} \|(\varsigma^\circ - \varsigma)\|_{L^1} \|\mathbf{x}_{\text{in}-\lambda}\|_{L^1} \end{aligned} \quad (\text{A.23})$$

Let \mathbf{c} be a vector of constants. Since $\lim_{t \rightarrow \infty} \Phi(t, \tau) \rightarrow \mathbf{0} \Rightarrow \lim_{t \rightarrow \infty} \|\Phi(t, \tau)\|_{L^1} \rightarrow \mathbf{c}$. However, for $\lim_{t \rightarrow \infty} \|\varsigma^\circ - \varsigma\|_{L^1} \rightarrow \mathbf{0}$, $|\varsigma^\circ - \varsigma| = 0$ in the limit, and this would imply that $\varsigma = \varsigma^\circ$ as $t \rightarrow \infty$. But since our assumption is such that for all time, $\varsigma \neq \varsigma^\circ$, then $\lim_{t \rightarrow \infty} \|\varsigma^\circ - \varsigma\|_{L^1} \not\rightarrow \mathbf{0}$. Moreover, $\mathbf{x}_{\text{in}-\lambda}$ does not decay to zero due to effect of \mathbf{F}_{in} on \mathbf{x}_{in} . Therefore, $\Phi(t, \tau)(\varsigma^\circ - \varsigma)\mathbf{x}_{\text{in}-\lambda} \in L^1(0, \infty)$, implying that $\lim_{t \rightarrow \infty} \boldsymbol{\varepsilon} \not\rightarrow \mathbf{0}$ is a contradiction from our assumption on convergence to zero of the error.

■

A.1.3. Proof Theorem 6.2

Proof:

Let $\mathbf{C}_m = \begin{bmatrix} \mathbf{N}_m^\top & \mathbf{X}_{\text{in}m} & \mathbf{n}_{0m} & 0 \\ 0 & 0 & 0 & 1 \end{bmatrix} \mathbb{R}^{(S_m+1) \times (N_r+N_\ell+2)}$, and $\mathbf{A} \in \mathbb{R}^{N_r+N_\ell+2}$ be the diagonal state matrix.

Let $\text{rank}(\mathbf{C}_m) = N_r + N_\ell + 2$, and assume that the pair $(\mathbf{A}, \mathbf{C}_m)$ is not observable. Due to lack of observability, by the Popov-Belevich-Hautus theorem, there exists a vector $\mathbf{v} \neq 0$ such that

$$\mathbf{A}\mathbf{v} = -\varsigma \mathbf{v}, \quad \mathbf{C}_m \mathbf{v} = 0$$

A

However, $\mathbf{A} = -\varsigma \mathbf{I}_{S+1}$ with $\varsigma > 0 \ \forall t \geq 0$. Hence, the eigenvectors of \mathbf{A} are the standard bases of \mathbb{R}^{S+1} . Since \mathbf{C}_m is full-column rank, $\text{im}(\mathbf{C}_m) \subseteq \mathbb{R}^{S+1} \Leftrightarrow \ker(\mathbf{C}_m) = \emptyset$. Hence, only $\mathbf{v} = \mathbf{0}$ is contained in $\ker(\mathbf{C}_m)$. This contradicts the PBH theorem and the assumption of unobservability of the pair $(\mathbf{A}, \mathbf{C}_m)$.

■

A.1.4. Proof Theorem 6.3

Proof:

The system is observable provided that $\text{rank}(\mathbf{C}_m) = N_r + N_t + 2$, i.e. \mathbf{C}_m is full-column rank. Let us define the error dynamics as $\dot{\tilde{\mathbf{x}}}_e = \mathbf{x}_e - \hat{\mathbf{x}}_e$, therefore

$$\dot{\tilde{\mathbf{x}}}_e = (\mathbf{A}_e - \mathbf{L}\mathbf{C}_e)\mathbf{x}_e$$

The error dynamics converge asymptotically arbitrarily fast by placing the poles of \mathbf{A}_e using \mathbf{L} . The state error matrix $\mathbf{A}_e - \mathbf{L}\mathbf{C}_e$ can be made equal to a matrix whose eigenvalues are at desired values. Let $\mathcal{A} = \mathbf{A} - \mathbf{L}_1\mathbf{C}_m$, and \mathbf{M}_1 and \mathbf{M}_2 be matrices whose eigenvalues are the observer desired pole locations. Hence, for some \mathbf{L}_1 and \mathbf{L}_2 , the closed-loop matrix can be made equal to:

$$\begin{bmatrix} \mathcal{A} & \mathbf{B}_d \\ -\mathbf{L}_2\mathbf{C}_m & \mathbf{R} \end{bmatrix} = \begin{bmatrix} \mathbf{M}_1 & \mathbf{B}_d \\ -(\mathbf{M}_2 - \mathbf{R})\mathbf{B}_d^+\mathbf{M}_1 & \mathbf{R} \end{bmatrix}$$

Performing block LDU decomposition on the left-hand side matrix, we get

$$\begin{bmatrix} \mathbf{I} & \mathbf{0} \\ -\mathbf{L}_2\mathbf{C}_m\mathcal{A}^{-1} & \mathbf{I} \end{bmatrix} \begin{bmatrix} \mathcal{A} & \mathbf{0} \\ \mathbf{0} & \mathbf{R} + \mathbf{L}_2\mathbf{C}_m\mathcal{A}^{-1}\mathbf{B}_d \end{bmatrix} \begin{bmatrix} \mathbf{I} & \mathcal{A}^{-1}\mathbf{B}_d \\ \mathbf{0} & \mathbf{I} \end{bmatrix} = \begin{bmatrix} \mathbf{M}_1 & \mathbf{B}_d \\ \mathbf{Z} & \mathbf{R} \end{bmatrix}$$

where $\mathbf{Z} = -(\mathbf{M}_2 - \mathbf{R})\mathbf{B}_d^+\mathbf{M}_1$

Multiplying both sides with the inverse of the block upper triangular matrix on the right-hand side gives us

A

$$\begin{bmatrix} \mathcal{A} & \mathbf{0} \\ -\mathbf{L}_2 \mathbf{C}_m & \mathbf{R} + \mathbf{L}_2 \mathbf{C}_m \mathcal{A}^{-1} \mathbf{B}_d \end{bmatrix} = \begin{bmatrix} \mathbf{M}_1 & \mathbf{B}_d \\ \mathbf{Z} & \mathbf{R} \end{bmatrix} \begin{bmatrix} \mathbf{I} & -\mathcal{A}^{-1} \mathbf{B}_d \\ \mathbf{0} & \mathbf{I} \end{bmatrix} \quad (\text{A.24})$$

$$\begin{bmatrix} \mathcal{A} & \mathbf{0} \\ -\mathbf{L}_2 \mathbf{C}_m & \mathbf{R} + \mathbf{L}_2 \mathbf{C}_m \mathcal{A}^{-1} \mathbf{B}_d \end{bmatrix} = \begin{bmatrix} \mathbf{M}_1 & -\mathbf{M}_1 \mathcal{A}^{-1} \mathbf{B}_d + \mathbf{B}_d \\ \mathbf{Z} & \mathbf{Z} \mathcal{A}^{-1} \mathbf{B}_d + \mathbf{R} \end{bmatrix}$$

The matrix on the right-hand side of the equation can be made block triangular if we choose $\mathbf{L}_1 = (\mathbf{A} - \mathbf{M}_1) \mathbf{C}_m^+$. Replacing \mathbf{L}_1 in $\mathcal{A} = \mathbf{A} - \mathbf{L}_1 \mathbf{C}_m$, it follows that $\mathcal{A} = \mathbf{A} - (\mathbf{A} - \mathbf{M}_1) \mathbf{C}_m^+ \mathbf{C}_m = \mathbf{M}_1$, and $-\mathbf{M}_1 \mathcal{A}^{-1} \mathbf{B}_d + \mathbf{B}_d = -\mathbf{M}_1 \mathbf{M}_1^{-1} \mathbf{B}_d + \mathbf{B}_d = \mathbf{0}$. Thus (A.24) results in

$$\begin{bmatrix} \mathbf{M}_1 & \mathbf{0} \\ -\mathbf{L}_2 \mathbf{C}_m & \mathbf{R} + \mathbf{L}_2 \mathbf{C}_m \mathbf{M}_1^{-1} \mathbf{B}_d \end{bmatrix} = \begin{bmatrix} \mathbf{M}_1 & \mathbf{0} \\ \mathbf{Z} & \mathbf{Z} \mathbf{M}_1^{-1} \mathbf{B}_d + \mathbf{R} \end{bmatrix} \quad (\text{A.25})$$

Furthermore, notice that $\mathbf{L}_2 = (\mathbf{M}_2 - \mathbf{R}) \mathbf{B}_d^+ \mathbf{M}_1 \mathbf{C}_m^+$ ensures that $-\mathbf{L}_2 \mathbf{C}_m = -(\mathbf{M}_2 - \mathbf{R}) \mathbf{B}_d^+ \mathbf{M}_1$, and that $\mathbf{R} + \mathbf{L}_2 \mathbf{C}_m \mathcal{A}^{-1} \mathbf{B}_d = \mathbf{R} + (\mathbf{M}_2 - \mathbf{R}) \mathbf{B}_d^+ \mathbf{M}_1 \mathbf{C}_m^+ \mathbf{C}_m \mathcal{A}^{-1} \mathbf{B}_d = \mathbf{M}_2$. Finally, the closed-loop observer dynamics in (A.25) are given by

$$\begin{bmatrix} \mathbf{M}_1 & \mathbf{0} \\ -(\mathbf{M}_2 - \mathbf{R}) \mathbf{B}_d^+ \mathbf{M}_1 & \mathbf{M}_2 \end{bmatrix} \quad (\text{A.26})$$

Because the matrix is block lower triangular, its eigenvalues are

$$\text{eig} \left(\begin{bmatrix} \mathbf{M}_1 & \mathbf{0} \\ -(\mathbf{M}_2 - \mathbf{R}) \mathbf{B}_d^+ \mathbf{M}_1 & \mathbf{M}_2 \end{bmatrix} \right) = \text{eig}(\mathbf{M}_1) \cup \text{eig}(\mathbf{M}_2) \quad (\text{A.27})$$

In particular, let us establish $\mathbf{M}_1 = -\mu \mathbf{I}_{N_r+N_\ell+2}$ and $\mathbf{M}_2 = -\mu \mathbf{I}_{N_r}$. Since $\mathbf{A} = -\varsigma \mathbf{I}_{N_r+N_\ell+2}$, and $\mathbf{R} = -\varsigma \mathbf{I}_{N_r}$, it is desired that $|\mu| > |\varsigma|$. Hence the observer is given by $\mathbf{L}_1 = (\mu - \varsigma) \mathbf{C}_m^+$, and $\mathbf{L}_2 = \mu(\mu - \varsigma) \mathbf{B}_d^+ \mathbf{C}_m^+$

■

A.2. Mathematical derivations

A.2.1. Successive orthogonalization method matrix decomposition

Let the sensitivity matrix be given by $\mathbf{S} = [\mathbf{s}_1 \ \mathbf{s}_2 \ \cdots \ \mathbf{s}_{n_p}]$, and assume that $\|\mathbf{s}_1\|_2 > \|\mathbf{s}_2\|_2 > \cdots > \|\mathbf{s}_{n_p}\|_2$. The sensitivity matrix \mathbf{S} have the following QR decomposition

$$\mathbf{S}\Pi = \mathbf{Q}\mathbf{R} \quad (\text{A.28})$$

with

$$\mathbf{Q} = [\mathbf{v}_1 \ \mathbf{v}_2 \ \cdots \ \mathbf{v}_{n_p}], \quad \mathbf{R} = \begin{bmatrix} \mathbf{v}_1^\top \mathbf{s}_1 & \mathbf{v}_1^\top \mathbf{s}_2 & \cdots & \mathbf{v}_1^\top \mathbf{s}_{n_p} \\ 0 & \mathbf{v}_2^\top \mathbf{s}_2 & \cdots & \mathbf{v}_2^\top \mathbf{s}_{n_p} \\ \vdots & \vdots & \ddots & \vdots \\ 0 & 0 & \cdots & \mathbf{v}_{n_p}^\top \mathbf{s}_{n_p} \end{bmatrix}$$

and the matrix $\mathbf{Q}^\top \mathbf{Q} = \mathbf{I}_{n_p}$

The matrix \mathbf{R} can be further decomposed into

$$\mathbf{R} = \Sigma \tilde{\mathbf{R}} \quad (\text{A.29})$$

with

$$\Sigma = \begin{bmatrix} \mathbf{v}_1^\top \mathbf{s}_1 & 0 & \cdots & 0 \\ 0 & \mathbf{v}_2^\top \mathbf{s}_2 & \cdots & 0 \\ \vdots & \vdots & \ddots & \vdots \\ 0 & 0 & \cdots & \mathbf{v}_{n_p}^\top \mathbf{s}_{n_p} \end{bmatrix}, \quad \tilde{\mathbf{R}} = \begin{bmatrix} 1 & \frac{\mathbf{v}_1^\top \mathbf{s}_2}{\mathbf{v}_1^\top \mathbf{s}_1} & \cdots & \frac{\mathbf{v}_1^\top \mathbf{s}_{n_p}}{\mathbf{v}_1^\top \mathbf{s}_1} \\ 0 & 1 & \cdots & \frac{\mathbf{v}_2^\top \mathbf{s}_{n_p}}{\mathbf{v}_2^\top \mathbf{s}_2} \\ \vdots & \vdots & \ddots & \vdots \\ 0 & 0 & \cdots & 1 \end{bmatrix}$$

We now analyze the terms of $\tilde{\mathbf{R}}$. Define θ as the angle between any two vectors \mathbf{s}_i and \mathbf{s}_j , with $\|\mathbf{s}_i\|_2 > \|\mathbf{s}_j\|_2$. The inner product of these two vectors is defined as

$$\langle \mathbf{s}_i, \mathbf{s}_j \rangle = \mathbf{s}_i^\top \mathbf{s}_j = \|\mathbf{s}_i\|_2 \|\mathbf{s}_j\|_2 \cos(\theta) \quad (\text{A.30})$$

Let $\mathbf{v}_i = \frac{\mathbf{s}_i}{\|\mathbf{s}_i\|_2}$. Thus, the elements of $\tilde{\mathbf{R}}$ are equal to

A

$$\frac{\mathbf{v}_i^\top \mathbf{s}_j}{\mathbf{v}_i^\top \mathbf{s}_i} = \frac{\mathbf{s}_i^\top \mathbf{s}_j}{\mathbf{s}_i^\top \mathbf{s}_i} = \frac{\|\mathbf{s}_j\|_2}{\|\mathbf{s}_i\|_2} \cos(\theta) \quad (\text{A.31})$$

Notice that $\|\mathbf{s}_j\|_2 \cos(\theta)$ is the magnitude of the projection of \mathbf{s}_j onto \mathbf{s}_i as illustrated on Figure A.1. Since $\|\mathbf{s}_j\|_2 < \|\mathbf{s}_i\|_2$ and $\cos(\theta) \in [-1, 1]$, we have that

$$0 \leq \frac{\|\mathbf{s}_j\|_2}{\|\mathbf{s}_i\|_2} \cos(\theta) \leq 1 \quad (\text{A.32})$$

Therefore, based off of (A.32), the elements of $\tilde{\mathbf{R}}$ characterize the collinear portion between \mathbf{s}_j and \mathbf{s}_i that has to be removed from \mathbf{s}_j to make it orthogonal to \mathbf{s}_i . This quantity is controlled by the cosine of θ , and attains its maximum magnitude at $\theta = 0$ or $\theta = \pi$, which implies that the vectors are collinear, and the sensitivities generate the same response in the parameter space.

On the other hand, for the elements of Σ , we have that since \mathbf{s}_i is the vector with the largest norm, it is selected first. Hence

$$\mathbf{v}_i^\top \mathbf{s}_i = \frac{\mathbf{s}_i^\top}{\|\mathbf{s}_i\|_2} \mathbf{s}_i = \frac{\|\mathbf{s}_i\|_2^2}{\|\mathbf{s}_i\|_2} = \|\mathbf{s}_i\|_2 \quad (\text{A.33})$$

For the rest of elements, let $\tilde{\mathbf{s}}_j = \mathbf{s}_j - \mathbf{v}_i(\mathbf{v}_i^\top \mathbf{s}_j)$, by the Gram-Schmidt orthogonalization procedure, we have that $\mathbf{v}_j = \frac{\tilde{\mathbf{s}}_j}{\|\tilde{\mathbf{s}}_j\|_2}$. Therefore,

$$\begin{aligned} \mathbf{v}_j^\top \mathbf{s}_j &= \frac{\tilde{\mathbf{s}}_j^\top}{\|\tilde{\mathbf{s}}_j\|_2} \mathbf{s}_j \\ &= \frac{1}{\|\tilde{\mathbf{s}}_j\|_2} (\mathbf{s}_j^\top \mathbf{s}_j - \mathbf{v}_i^\top \mathbf{s}_j \mathbf{v}_i^\top \mathbf{s}_j) \\ &= \frac{1}{\|\tilde{\mathbf{s}}_j\|_2} \left(\mathbf{s}_j^\top \mathbf{s}_j - \frac{\mathbf{s}_i^\top \mathbf{s}_j}{\|\mathbf{s}_i\|_2} \frac{\mathbf{s}_i^\top \mathbf{s}_j}{\|\mathbf{s}_i\|_2} \right) \\ &= \frac{1}{\|\tilde{\mathbf{s}}_j\|_2} (\|\mathbf{s}_j\|_2^2 - \|\mathbf{s}_j\|_2^2 \cos^2(\theta)) \\ &= \frac{1}{\|\tilde{\mathbf{s}}_j\|_2} \|\mathbf{s}_j\|_2^2 \sin^2(\theta) \end{aligned} \quad (\text{A.34})$$

Notice again that $\|\mathbf{s}_j\|_2^2 \sin^2(\theta)$ is the magnitude of the projection of \mathbf{s}_j onto the axis orthogonal to \mathbf{s}_i , and thus, $\|\mathbf{s}_j\|_2 \sin(\theta) = \|\tilde{\mathbf{s}}_j\|_2$ as shown on Figure A.1. Finally,

(A.34) is equivalent to $\mathbf{v}_j^\top \mathbf{s}_j = \|\tilde{\mathbf{s}}_j\|_2$. Inspecting this equality, it can be seen that the elements of Σ correspond to the magnitude of the orthogonal fractions of the sensitivities. In other words, they correspond to the magnitude of the fully decoupled sensitivity directions. Naturally, the smaller these magnitudes are, the smaller the contributions of the corresponding parameters in these fully decoupled directions.

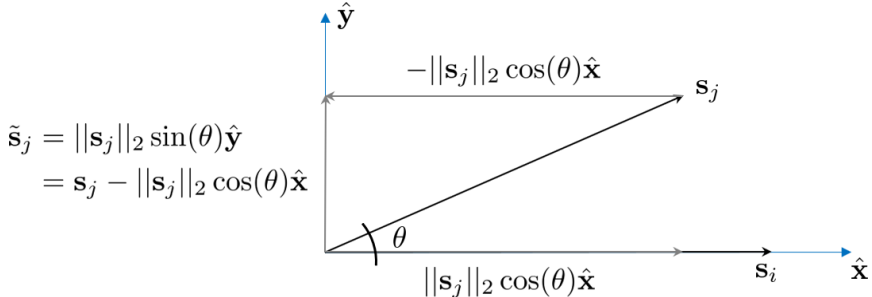


Figure A.1: Vector orthogonalization

A

A.2.2. Relationship between convolution integral and the extents of inlet

The equality in (6.55) can be obtained noting that due to the fact that $\Phi(t, \tau)$ is a diagonal matrix, the extent of inlet \mathbf{x}_{in} is

$$\begin{aligned}
\mathbf{x}_{\text{in}} &= \int_0^t \Phi_{N_\ell}(t, \tau) F_{\text{in}}(\tau) d\tau \\
&= \int_0^t \begin{bmatrix} e^{-\int_\tau^t \varsigma(s) ds} & & \\ & \ddots & \\ & & e^{-\int_\tau^t \varsigma(s) ds} \end{bmatrix} \begin{bmatrix} F_{\text{in}_1}(\tau) \\ \vdots \\ F_{\text{in}_{N_\ell}}(\tau) \end{bmatrix} d\tau \\
&= \int_0^t \left(\begin{bmatrix} F_{\text{in}_1}(\tau) \\ \vdots \\ F_{\text{in}_{N_\ell}}(\tau) \end{bmatrix}^\top \otimes \begin{bmatrix} e^{-\int_\tau^t \varsigma(s) ds} & & \\ & \ddots & \\ & & e^{-\int_\tau^t \varsigma(s) ds} \end{bmatrix} \right) \text{vec}(\mathbf{I}_{N_\ell}) d\tau \\
&= \begin{bmatrix} \left(\mathbf{I}_{N_\ell} \otimes \int_0^t F_{\text{in}_1}(\tau) e^{-\int_\tau^t \varsigma(s) ds} d\tau \right)^\top \\ \vdots \\ \left(\mathbf{I}_{N_\ell} \otimes \int_0^t F_{\text{in}_{N_\ell}}(\tau) e^{-\int_\tau^t \varsigma(s) ds} d\tau \right)^\top \end{bmatrix} \text{vec}(\mathbf{I}_{N_\ell})
\end{aligned} \tag{A.35}$$

Inspecting each individual extent of inlet x_{in_i} , one obtains

$$\begin{bmatrix} x_{\text{in}_1} \\ x_{\text{in}_2} \\ \vdots \\ x_{\text{in}_{N_\ell}} \end{bmatrix} = \int_0^t \begin{bmatrix} F_{\text{in}_1} e^{\int_\tau^t \varsigma(s) ds} \\ F_{\text{in}_2} e^{\int_\tau^t \varsigma(s) ds} \\ \vdots \\ F_{\text{in}_{N_\ell}} e^{\int_\tau^t \varsigma(s) ds} \end{bmatrix} d\tau \tag{A.36}$$

Observe that each $\int_0^t F_{\text{in}_i}(\tau) e^{-\int_\tau^t \varsigma(s) ds} d\tau = x_{\text{in}_i}$. Hence

$$\begin{aligned}
& \left[\left(\mathbf{I}_{N_\varepsilon} \otimes \int_0^t F_{\text{in}_1}(\tau) e^{- \int_\tau^t \varsigma(s) \, ds} \right) \cdots \left(\mathbf{I}_{N_\varepsilon} \otimes \int_0^t F_{\text{in}_{N_\varepsilon}}(\tau) e^{- \int_\tau^t \varsigma(s) \, ds} \right) \right] \text{vec}(\mathbf{I}_{N_\varepsilon}) \, d\tau \\
&= \left[(\mathbf{I}_{N_\varepsilon} \otimes x_{\text{in}_1}) \cdots (\mathbf{I}_{N_\varepsilon} \otimes x_{\text{in}_{N_\varepsilon}}) \right] \text{vec}(\mathbf{I}_{N_\varepsilon}) \, d\tau \\
&= (\mathbf{x}_{\text{in}}^\top \otimes \mathbf{I}_{N_\varepsilon}) \text{vec}(\mathbf{I}_{N_\varepsilon})
\end{aligned} \tag{A.37}$$

Comparing (A.37) with (A.35) we have that

$$\mathbf{F}_{\text{in}}(\tau) \otimes \Phi_{N_\varepsilon} \, d\tau = (\mathbf{x}_{\text{in}}^\top \otimes \mathbf{I}_{N_\varepsilon}) \tag{A.38}$$

Therefore, since $\Phi(t, \tau)$ is diagonal, by induction

$$\int_0^t \mathbf{F}_{\text{in}}(\tau) \otimes \Phi_{N_\varepsilon + N_\varepsilon + 1} \, d\tau = (\mathbf{x}_{\text{in}}^\top \otimes \mathbf{I}_{N_\varepsilon + N_\varepsilon + 1}) \tag{A.39}$$

Bibliography

- [1] P. de Aguiar et al. “D-optimal designs”. In: *Chemometrics and intelligent laboratory systems* 30.2 (1995), pp. 199–210.
- [2] M. Al-Arfaj and W. Luyben. “Comparative control study of ideal and methyl acetate reactive distillation”. In: *Chemical Engineering Science* 57.24 (2002b), pp. 5039–5050.
- [3] M. Al-Arfaj and W. Luyben. “Comparison of Alternative Control Structures for an Ideal Two-Product Reactive Distillation Column”. In: *Industrial and Engineering Chemistry Research* 39 (2000), pp. 3298–3307.
- [4] M. Al-Arfaj and W. Luyben. “Control of ethylene glycol reactive distillation column”. In: *AICHE journal* 48.4 (2002a), pp. 905–908.
- [5] M. Amrhein et al. “Extents of reaction and flow for homogeneous reaction systems with inlet and outlet streams”. In: *AICHE journal* 56.11 (2010), pp. 2873–2886.
- [6] O. A. Asbjørnsen. “Reaction Invariants in the Control of Chemical Reactors”. In: *Chemical Engineering Science* 27.4 (1972), pp. 709–717.
- [7] O. A. Asbjørnsen and M. Fjeld. “Response Modes of Continuous Stirred Tank Reactors”. In: *Chemical Engineering Science* 25 (1970), pp. 1627–1636.
- [8] K. Åström and B. Wittenmark. *Adaptive control*. Courier Corporation, 2008.
- [9] S. Aumi et al. “Data-based modeling and control of nylon-6, 6 batch polymerization”. In: *IEEE Transactions on Control Systems Technology* 21.1 (2012), pp. 94–106.
- [10] O. Aydogmus and A.H. Tor. “A Modified Multiple Shooting Algorithm for Parameter Estimation in ODEs Using Adjoint Sensitivity Analysis”. In: *Applied Mathematics and Computation* 390 (2021), p. 125644.
- [11] T. Backx, O. Bosgra, and W. Marquardt. “Industrial challenges in modeling of processes and model reduction”. In: *Proc. ADCHEM 2006, Int. Symp. Advanced Control of Chemical Processes Gramado*. 2006, pp. 143–151.
- [12] T. Backx, O. Bosgra, and W. Marquardt. “Integration of model predictive control and optimization of processes: enabling technology for market driven process operation”. In: *IFAC Proceedings Volumes* 33.10 (2000), pp. 249–260.
- [13] L. Balasubramhanya and F.J. Doyle III. “Nonlinear Model-Based Control of a Batch Reactive Distillation Column”. In: *Journal of Process Control* 10.2–3 (2000), pp. 209–218.

- [14] G. Bastin and D. Dochain. "CHAPTER 3 - State and parameter estimation with known yield coefficients". In: *On-line Estimation and Adaptive Control of Bioreactors*. Ed. by G. Bastin and D. Dochain. Process Measurement and Control. Amsterdam: Elsevier, 1990, pp. 101–200.
- [15] A. Bazanella, M. Gevers, and L. Miškovic. "Closed-loop identification of MIMO systems: a new look at identifiability and experiment design". In: *European Journal of Control* 16.3 (2010), pp. 228–239.
- [16] R. Bellman and K.J. Åström. "On structural identifiability". In: *Mathematical biosciences* 7.3-4 (1970), pp. 329–339.
- [17] B. Bequette. "Nonlinear control of chemical processes: A review". In: *Industrial & Engineering Chemistry Research* 30.7 (1991), pp. 1391–1413.
- [18] R. Berber. "Control of batch reactors: a review". In: *Methods of model based process control* (1995), pp. 459–494.
- [19] R. Berk. *Regression analysis: A constructive critique*. Vol. 11. Sage, 2004.
- [20] M. Bevilacqua et al. "Digital twin reference model development to prevent operators' risk in process plants". In: *Sustainability* 12.3 (2020), p. 1088.
- [21] N. Bhatt. "Extents of reaction and mass transfer in the analysis of chemical reaction systems". PhD thesis. EPFL, 2011.
- [22] N. Bhatt, M. Amrhein, and D. Bonvin. "Extents of Reaction, Mass Transfer and Flow for Gas–Liquid Reaction Systems". In: *Industrial & Engineering Chemistry Research* 49.17 (2010), pp. 7704–7717.
- [23] N. Bhatt, M. Amrhein, and D. Bonvin. "Incremental identification of reaction and mass–transfer kinetics using the concept of extents". In: *Industrial & engineering chemistry research* 50.23 (2011), pp. 12960–12974.
- [24] J. Billeter, S. Srinivasan, and D. Bonvin. "Extent-based kinetic identification using spectroscopic measurements and multivariate calibration". In: *Analytica Chimica Acta* 767 (2013), pp. 21–34.
- [25] D. Bonvin, B. Srinivasan, and D. Hunkeler. "Control and optimization of batch processes". In: *IEEE Control Systems Magazine* 26.6 (2006), pp. 34–45.
- [26] R. Boudjemaa et al. *Automatic differentiation techniques and their application in metrology*. Tech. rep. National Physical Laboratory, 2003.
- [27] G. Box and H.L. Lucas. "Design of experiments in non-linear situations". In: *Biometrika* 46.1/2 (1959), pp. 77–90.
- [28] S. Boyd and L. Vandenberghe. *Convex optimization*. Cambridge university press, 2004.
- [29] J. Brewer. "Kronecker products and matrix calculus in system theory". In: *IEEE Transactions on circuits and systems* 25.9 (1978), pp. 772–781.
- [30] The Editors of Encyclopaedia. Britannica. "Viscosity". 2021. URL: www.britannica.com/science/viscosity.

- [31] R. Burritt and K. Christ. "Industry 4.0 and environmental accounting: a new revolution?" In: *Asian Journal of Sustainability and Social Responsibility* 1.1 (2016), pp. 23–38.
- [32] E.A. Catchpole, J.T. Morgan, and S.N. Freeman. "Estimation in parameter-redundant models". In: *Biometrika* 85.2 (1998), pp. 462–468.
- [33] M. Chappell and K. Godfrey. "Structural identifiability of the parameters of a nonlinear batch reactor model". In: *Mathematical biosciences* 108.2 (1992), pp. 241–251.
- [34] L. Cheng, Z. Lu, and L. Zhang. "New spearman correlation based sensitivity index and its unscented transformation solutions". In: *Journal of Engineering Mechanics* 142.2 (2016), p. 04015076.
- [35] D. Cole and R. McCrea. "Parameter redundancy in discrete state-space and integrated models". In: *Biometrical Journal* 58.5 (2016), pp. 1071–1090.
- [36] D. Cole, B. Morgan, and D. Titterington. "Determining the parametric structure of models". In: *Mathematical biosciences* 228.1 (2010), pp. 16–30.
- [37] B. Corbett, B. Macdonald, and P. Mhaskar. "Model predictive quality control of polymethyl methacrylate". In: *IEEE Transactions on Control Systems Technology* 23.2 (2014), pp. 687–692.
- [38] P. Darda et al. "Reaction kinetics of polybutylene terephthalate polycondensation reaction". In: *AICHe journal* 51.2 (2005), pp. 622–630.
- [39] D. Degenerin et al. "Sensitivity analysis for the reduction of complex metabolism models". In: *Journal of Process Control* 14.7 (2004), pp. 729–745.
- [40] P. Del Moral. "Nonlinear filtering: Interacting particle resolution". In: *Comptes Rendus de l'Académie des Sciences-Series I-Mathematics* 325.6 (1997), pp. 653–658.
- [41] L. Denis-Vidal and G. Joly-Blanchard. "An easy to check criterion for (un)identifiability of uncontrolled systems and its applications". In: *IEEE Transactions on Automatic Control* 45.4 (2000), pp. 768–771.
- [42] D. Dochain. "State and parameter estimation in chemical and biochemical processes: a tutorial". In: *Journal of process control* 13.8 (2003), pp. 801–818.
- [43] D. Dochain, F. Couenne, and C. Jallut. "Enthalpy based modelling and design of asymptotic observers for chemical reactors". In: *International Journal of Control* 82.8 (2009), pp. 1389–1403.
- [44] H. Dötsch and P. Van den Hof. "Test for local structural identifiability of high-order non-linearly parametrized state space models". In: *Automatica* 32.6 (1996), pp. 875–883.
- [45] F. Encinas and A. De Herde. "Sensitivity analysis in building performance simulation for summer comfort assessment of apartments from the real estate market". In: *Energy and Buildings* 65 (2013), pp. 55–65.

- [46] N. Evans and M. Chappell. “Extensions to a procedure for generating locally identifiable reparameterisations of unidentifiable systems”. In: *Mathematical biosciences* 168.2 (2000), pp. 137–159.
- [47] P. Ekhoff. *System identification*. Vol. 14. Wiley London, 1974.
- [48] T. A Feo and M. Resende. “Greedy randomized adaptive search procedures”. In: *Journal of global optimization* 6.2 (1995), pp. 109–133.
- [49] G. Fernholz et al. “Optimal operation of a semi-batch reactive distillation column”. In: *Computers and Chemical Engineering* 24.2–7 (2000), pp. 1569–1575.
- [50] M. Fjeld, O. A. Asbjørnsen, and K. Åström. “Reaction invariants and their importance in the analysis of eigenvectors, state observability and controllability of the continuous stirred tank reactor”. In: *Chemical Engineering Science* 29.9 (1974), pp. 1917–1926.
- [51] J. Flores-Cerrillo and J. MacGregor. “Control of batch product quality by trajectory manipulation using latent variable models”. In: *Journal of Process Control* 14.5 (2004), pp. 539–553.
- [52] J. Flores-Cerrillo and J. MacGregor. “Control of particle size distributions in emulsion semibatch polymerization using mid-course correction policies”. In: *Industrial & engineering chemistry research* 41.7 (2002), pp. 1805–1814.
- [53] M. Forgione et al. “Batch-to-batch model improvement for cooling crystallization”. In: *Control Engineering Practice* 41 (2015), pp. 72–82.
- [54] U. Forssell and L. Ljung. “Closed-loop identification revisited”. In: *Automatica* 35.7 (1999), pp. 1215–1241.
- [55] P.M. Frank. *Introduction to system sensitivity theory*. Academic Press, 1978.
- [56] A. Gábor and J. Banga. “Robust and efficient parameter estimation in dynamic models of biological systems”. In: *BMC systems biology* 9.1 (2015), p. 74.
- [57] R. Ganguli and S. Adhikari. “The digital twin of discrete dynamic systems: Initial approaches and future challenges”. In: *Applied Mathematical Modelling* 77 (2020), pp. 1110–1128.
- [58] Y. Gao et al. “Real-time modeling and simulation method of digital twin production line”. In: *2019 IEEE 8th joint international information technology and artificial intelligence conference (ITAIC)*. IEEE. 2019, pp. 1639–1642.
- [59] G. A Gericke et al. “Design of digital twins for optimization of a Water Bottling plant”. In: *IECON 2019-45th Annual Conference of the IEEE Industrial Electronics Society*. Vol. 1. IEEE. 2019, pp. 5204–5210.
- [60] S. Glad. “Solvability of differential algebraic equations and inequalities: an algorithm”. In: *Control Conference (ECC), 1997 European*. IEEE. 1997, pp. 1195–1200.
- [61] G. Golub and C. Van Loan. *Matrix computations*. Vol. 3. John Hopkins University press, 2013.

- [62] J.E. Graciano, D.F. Mendoza, and G.A.C Le Roux. “Performance comparison of parameter estimation techniques for unidentifiable models”. In: *Computers & Chemical Engineering* 64 (2014), pp. 24–40.
- [63] M. Grieves and J. Vickers. “Digital twin: Mitigating unpredictable, undesirable emergent behavior in complex systems”. In: *Transdisciplinary perspectives on complex systems*. Springer, 2017, pp. 85–113.
- [64] Engineering Group. “Digital Twin”. 2021. URL: www.eng.it/resources/whitepaper/doc/digital-twin/digital-twin_whitepaper_en.pdf.
- [65] S. Grüner and A. Kienle. “Equilibrium theory and nonlinear waves for reactive distillation columns and chromatographic reactors”. In: *Chemical Engineering Science* 59.4 (2004), pp. 901–918.
- [66] B. He and K.-J. Bai. “Digital twin-based sustainable intelligent manufacturing: A review”. In: *Advances in Manufacturing* 9.1 (2021), pp. 1–21.
- [67] J. Helton and F.J. Davis. “Latin hypercube sampling and the propagation of uncertainty in analyses of complex systems”. In: *Reliability Engineering & System Safety* 81.1 (2003), pp. 23–69.
- [68] R. Hille and H. Budman. “Experimental Design for Batch-to-Batch Optimization under Model-Plant Mismatch”. In: *Industrial & Engineering Chemistry Research* 58.30 (2019), pp. 13599–13610.
- [69] R. Hille and H. Budman. “Simultaneous identification and optimization of biochemical processes under model-plant mismatch using output uncertainty bounds”. In: *Computers & Chemical Engineering* 113 (2018), pp. 125–138.
- [70] C. Himpe. “emgr—The Empirical Gramian Framework”. In: *Algorithms* 11.7 (2018), p. 91.
- [71] C. Himpe and M. Ohlberger. “A unified software framework for empirical Gramians”. In: *Journal of Mathematics* 2013 (2013).
- [72] H. Hjalmarsson. “From experiment design to closed-loop control”. In: *Automatica* 41.3 (2005), pp. 393–438.
- [73] N.H. Hoang, D. Rodrigues, and D. Bonvin. “Revisiting the concept of extents for chemical reaction systems using an enthalpy balance”. In: *Computers & Chemical Engineering* 136 (2020), p. 106652.
- [74] P. Van den Hof. “Closed-loop issues in system identification”. In: *IFAC Proceedings Volumes* 30.11 (1997), pp. 1547–1560.
- [75] P. Van den Hof, J. Van Doren, and S. Douma. “Identification of parameters in large scale physical model structures, for the purpose of model-based operations”. In: *Model-Based Control*. Springer, 2009, pp. 125–143.
- [76] C. J Hopfe and J. Hensen. “Uncertainty analysis in building performance simulation for design support”. In: *Energy and Buildings* 43.10 (2011), pp. 2798–2805.

- [77] C. Hu, W. Shi, and L. Jiang. "Application case of digital twin technology in electric power system". In: *IOP Conference Series: Materials Science and Engineering*. Vol. 788. 1. IOP Publishing. 2020, p. 012083.
- [78] L. Hu et al. "Kinetics and Modeling of Melt Polycondensation for Synthesis of Poly [(butylene succinate)-co-(butylene terephthalate)], 1-Esterification". In: *Macromolecular Reaction Engineering* 4.9-10 (2010), pp. 621–632.
- [79] I. Ipsen. *Numerical matrix analysis: Linear systems and least squares*. SIAM, 2009.
- [80] M. Jansen. "Analysis of variance designs for model output". In: *Computer Physics Communications* 117.1-2 (1999), pp. 35–43.
- [81] A.M. Jeffrey, X. Xia, and I. Craig. "Identifiability of HIV/AIDS models". In: *Deterministic and Stochastic Models of AIDS Epidemics and HIV Infections with Intervention* (2005), pp. 255–286.
- [82] A.M. Jeffrey, X. Xia, and I.K. Craig. "Identifiability of an extended HIV model". In: *IFAC Proceedings Volumes* 36.15 (2003), pp. 507–512.
- [83] J. Jeong and P. Qiu. "Quantifying the relative importance of experimental data points in parameter estimation". In: *BMC systems biology* 12.6 (2018), pp. 1–14.
- [84] I.T. Jolliffe. "Discarding variables in a principal component analysis. I: Artificial data". In: *Applied statistics* (1972), pp. 160–173.
- [85] S. Julier and J. Uhlmann. "New extension of the Kalman filter to nonlinear systems". In: *Signal processing, sensor fusion, and target recognition VI*. Vol. 3068. International Society for Optics and Photonics. 1997, pp. 182–193.
- [86] R. Kalman. "A new approach to linear filtering and prediction problems". In: *Journal of Basic Engineering* 82.1 (1960), pp. 35–45.
- [87] R. Kalman and R. Bucy. "New results in linear filtering and prediction theory". In: *J. Basic Engrg. ASME, Ser. D* 83 (1961), pp. 95–108.
- [88] E. Kamen. "The Control Systems Handbook: Control System Advanced Methods". In: CRC press, 2018. Chap. Fundamentals of Linear Time-Varying Systems.
- [89] A. Kampker et al. "Business models for industrial smart services—the example of a digital twin for a product-service-system for potato harvesting". In: *Procedia Cirp* 83 (2019), pp. 534–540.
- [90] X. Kan, H. Shu, and Y. Che. "Asymptotic parameter estimation for a class of linear stochastic systems using Kalman-Bucy filtering". In: *Mathematical Problems in Engineering* 2012 (2012).
- [91] S. Khajavi et al. "Digital twin: vision, benefits, boundaries, and creation for buildings". In: *IEEE access* 7 (2019), pp. 147406–147419.
- [92] R. Khaledi and B. Young. "Modeling and model predictive control of composition and conversion in an ETBE reactive distillation column". In: *Industrial & engineering chemistry research* 44.9 (2005), pp. 3134–3145.

- [93] K-J. Kim, K-Y. Choi, and J.C. Alexander. “Dynamics of a continuous stirred tank reactor for styrene polymerization initiated by a binary initiator mixture. II: Effect of viscosity dependent heat transfer coefficient”. In: *Polymer Engineering & Science* 32.7 (1992), pp. 494–505.
- [94] H. Köpnick et al. “Polyesters”. In: *Ullmann's encyclopedia of industrial chemistry* (2000).
- [95] C.T. Kuo and S.A. Chen. “Kinetics of polyesterification: Adipic acid with ethylene glycol, 1, 4-butanediol, and 1, 6-hexanediol”. In: *Journal of Polymer Science Part A: Polymer Chemistry* 27.8 (1989), pp. 2793–2803.
- [96] Y. Lecourtier, F. Lamnabhi-Lagarrigue, and E. Walter. “Volterra and generating power series approaches to identifiability testing”. In: *Identifiability of parametric models* (1987), pp. 50–66.
- [97] J. Lee and K. Lee. “Iterative learning control applied to batch processes: An overview”. In: *IFAC Proceedings Volumes* 39.2 (2006), pp. 1037–1046.
- [98] J. Lévine and P. Rouchon. “Quality control of binary distillation columns via nonlinear aggregated models”. In: *Automatica* 27.3 (1991), pp. 463–480.
- [99] R. Li, M.A. Henson, and M.J. Kurtz. “Selection of model parameters for off-line parameter estimation”. In: *IEEE Transactions on control systems technology* 12.3 (2004), pp. 402–412.
- [100] Y. Liao et al. “Past, present and future of Industry 4.0—a systematic literature review and research agenda proposal”. In: *International journal of production research* 55.12 (2017), pp. 3609–3629.
- [101] A. Linhart and S. Skogestad. “Reduced distillation models via stage aggregation”. In: *Chemical Engineering Science* 65.11 (2010), pp. 3439–3456.
- [102] P. van Lith et al. “Multiple nonlinear parameter estimation using pi feedback control”. In: *Control Engineering Practice* 9.5 (2001), pp. 517–531.
- [103] Z. Liu, N. Meyendorf, and N. Mrad. “The role of data fusion in predictive maintenance using digital twin”. In: *AIP Conference Proceedings*. Vol. 1949. 1. AIP Publishing LLC. 2018, p. 020023.
- [104] L. Ljung and T. Glad. “On global identifiability for arbitrary model parametrizations”. In: *Automatica* 30.2 (1994), pp. 265–276.
- [105] Z. Lu, E. Martin, and J. Morris. “Parameter Estimation for Batch Processes Using a Bayesian Approach”. In: *IFAC Proceedings Volumes* 37.9 (2004), pp. 703–708.
- [106] B.F. Lund, H.E. Berntsen, and B.A. Foss. “Methods for parameter ranking in nonlinear, mechanistic models”. In: *IFAC Proceedings Volumes* 38.1 (2005), pp. 578–583.
- [107] B.F. Lund and B.A. Foss. “Parameter ranking by orthogonalization—Applied to nonlinear mechanistic models”. In: *Automatica* 44.1 (2008), pp. 278–281.

- [108] H. Mahdipoor. "Effect of liquid flow regimes on dynamic simulation of tray columns". In: *Industrial & engineering chemistry research* 45.14 (2006), pp. 5172–5178.
- [109] A. Marchetti, B. Chachuat, and D. Bonvin. "Modifier-adaptation methodology for real-time optimization". In: *Industrial & engineering chemistry research* 48.13 (2009), pp. 6022–6033.
- [110] A. Marchetti et al. "Modifier adaptation as a feedback control scheme". In: *Industrial & Engineering Chemistry Research* 59.6 (2020), pp. 2261–2274.
- [111] A. Marchetti et al. "Modifier adaptation for real-time optimization—methods and applications". In: *Processes* 4.4 (2016), p. 55.
- [112] W. Marquardt. "Traveling waves in chemical processes". In: *International Chemical Engineering* 30.4 (1990), pp. 585–606.
- [113] A. Márquez-Ruiz, C. Méndez-Blanco, and L. Özkan. "Constrained Control and Estimation of Homogeneous Reaction Systems Using Extent-Based Linear Parameter Varying Models". In: *Industrial & Engineering Chemistry Research* 59.6 (2020), pp. 2242–2251.
- [114] A. Márquez-Ruiz, C. Méndez-Blanco, and L. Özkan. "Modeling of reactive batch distillation processes for control". In: *Computers & Chemical Engineering* 121 (2019), pp. 86–98.
- [115] A. Marquez-Ruiz et al. "Model learning predictive control for batch processes: A reactive batch distillation column case study". In: *Industrial & Engineering Chemistry Research* 58.30 (2019), pp. 13737–13749.
- [116] A. Márquez-Ruiz et al. "State and parameter estimation based on extent transformations". In: *Computer Aided Chemical Engineering*. Vol. 44. Elsevier, 2018, pp. 583–588.
- [117] R. Martí. "Multi-start methods". In: *Handbook of metaheuristics*. Springer, 2003, pp. 355–368.
- [118] J. Matias and J. Jäschke. "Online model maintenance via output modifier adaptation". In: *Industrial & Engineering Chemistry Research* 58.30 (2019), pp. 13750–13766.
- [119] J. Matias and J. Jäschke. "Using a neural network for estimating plant gradients in real-time optimization with modifier adaptation". In: *IFAC-PapersOnLine* 52.1 (2019), pp. 808–813.
- [120] A. McNaught, A. Wilkinson, et al. *Compendium of chemical terminology*. Vol. 1669. Blackwell Science Oxford, 1997.
- [121] T.Y. Melesse, V. Di Pasquale, and S. Riemma. "Digital Twin models in industrial operations: State-of-the-art and future research directions". In: *IET Collaborative Intelligent Manufacturing* 3.1 (2021), pp. 37–47.
- [122] R. Mendelson. "A method for viscosity measurements of concentrated polymer solutions in volatile solvents at elevated temperatures". In: *Journal of Rheology* 23.5 (1979), pp. 545–556.

- [123] R. Mendelson. "Concentrated solution viscosity behavior at elevated temperatures—Polystyrene in ethylbenzene". In: *Journal of Rheology* 24.6 (1980), pp. 765–781.
- [124] C. Méndez-Blanco and L. Özkan. "A State and Output Sensitivity Controllability Approach for Structural Identifiability of Linear State Space Models". In: *59th IEEE Conference on Decision and Control (CDC)*. IEEE. 2020, pp. 294–299.
- [125] C. Méndez-Blanco and L. Özkan. "Extent based reconstruction of the inlet composition matrix in process systems with feed variability and unknown reaction dynamics". In: *13th IFAC Symposium on Dynamics and Control of Process Systems including Biosystems*. 2022.
- [126] C. Méndez-Blanco and L. Özkan. "Local parameter identifiability of large-scale nonlinear models based on the output sensitivity covariance matrix". In: *16th IFAC Symposium on Advanced Control of Chemical Processes (AD-CHEM)*. Vol. 54. 3. Elsevier, 2021, pp. 415–420.
- [127] C. Méndez-Blanco and L. Özkan. "Parameter Estimation for Multi-Stage Processes: A multiple shooting approach integrated with sensitivity analysis (in preparation)". In: *To be submitted to Industrial & Engineering Chemistry Research* 1 (2023).
- [128] D. Merlini, R. Sprugnoli, and M.C. Verri. "Lagrange inversion: when and how". In: *Acta applicandae mathematica* 94.3 (2006), pp. 233–249.
- [129] P. Mhaskar, A. Garg, and B. Corbett. *Modeling and Control of Batch Processes: Theory and Applications*. Springer, 2019.
- [130] H. Miao et al. "On identifiability of nonlinear ODE models and applications in viral dynamics". In: *SIAM review* 53.1 (2011), pp. 3–39.
- [131] C. Michalik, R. Hannemann, and W. Marquardt. "Incremental single shooting—a robust method for the estimation of parameters in dynamical systems". In: *Computers & Chemical Engineering* 33.7 (2009), pp. 1298–1305.
- [132] Q. Min et al. "Machine learning based digital twin framework for production optimization in petrochemical industry". In: *International Journal of Information Management* 49 (2019), pp. 502–519.
- [133] T. Moi, A. Cibicik, and T. Rølvåg. "Digital twin based condition monitoring of a knuckle boom crane: An experimental study". In: *Engineering Failure Analysis* 112 (2020), p. 104517.
- [134] M. Sneesby et al. "ETBE synthesis via Reactive Distillation. 2. Dynamic Simulation and Control Aspects". In: *Industrial and Engineering Chemistry Research* 36 (1997), pp. 1870–1881.
- [135] I. Mujtaba and S. Macchietto. "Efficient Optimization of Batch Distillation with Chemical Reaction Using Polynomial Curve Fitting Techniques". In: *Industrial and Engineering Chemistry Research* 36.6 (1997), pp. 2287–2295.
- [136] I. Niven. "Formal power series". In: *The American Mathematical Monthly* 76.8 (1969), pp. 871–889.

- [137] K. Ogata. *Modern control engineering*. Prentice Hall Upper Saddle River, NJ, 2009.
- [138] Y. Okura and K. Fujimoto. “A study on robust nonlinear optimal control for parameter variation”. In: *2016 IEEE 55th Conference on Decision and Control (CDC)*. IEEE. 2016, pp. 4469–4473.
- [139] A. Papasavvas and G. François. “Internal modifier adaptation for the optimization of large-scale plants with inaccurate models”. In: *Industrial & Engineering Chemistry Research* 58.30 (2019), pp. 13568–13582.
- [140] T. Perez and G.C. Goodwin. “Constrained predictive control of ship fin stabilizers to prevent dynamic stall”. In: *Control Engineering Practice* 16.4 (2008), pp. 482–494.
- [141] P. Pichlík. “Comparison of Different Kalman Filters Types Performance for a Locomotive Slip Control Purposes”. In: *Czech Technical University, Prague* (2017).
- [142] H. Pohjanpalo. “System identifiability based on the power series expansion of the solution”. In: *Mathematical biosciences* 41.1-2 (1978), pp. 21–33.
- [143] T. Quaiser, W. Marquardt, and M. Mönnigmann. “Local identifiability analysis of large signaling pathway models”. In: *2nd Conference Foundation of Systems Biology in Engineering, Proceedings Plenary and Contributed Papers*. 2007, pp. 465–470.
- [144] T. Quaiser and M. Mönnigmann. “Systematic identifiability testing for unambiguous mechanistic modeling—application to JAK-STAT, MAP kinase, and NF- κ B signaling pathway models”. In: *BMC systems biology* 3.1 (2009), p. 50.
- [145] A. Ribeiro et al. “On the smoothness of nonlinear system identification”. In: *Automatica* 121 (2020), p. 109158.
- [146] D. Rodrigues, J. Billeter, and D. Bonvin. “Global identification of kinetic parameters via the extent-based incremental approach”. In: *Computer Aided Chemical Engineering*. Vol. 40. Elsevier, 2017, pp. 2119–2124.
- [147] S. Roy. “Calculation of heat of polymerisation: group-contribution method”. In: *Polymer Bulletin* 42.2 (1999), pp. 229–236.
- [148] A. Rudin. *Elements of Polymer Science & Engineering: An Introductory Text and Reference for Engineers and Chemists*. Elsevier, 1998.
- [149] M.P. Saccomani. “Some results on parameter identification of nonlinear systems”. In: *Cardiovascular Engineering: An International Journal* 4.1 (2004), pp. 95–102.
- [150] M.P. Saccomani. “Structural vs. Practical Identifiability in System Biology”. In: *IWBBIQ*. 2013, pp. 305–313.
- [151] M.P. Saccomani et al. “A new differential algebra algorithm to test identifiability of nonlinear systems with given initial conditions”. In: *Decision and Control, 2001. Proceedings of the 40th IEEE Conference on*. Vol. 4. IEEE. 2001, pp. 3108–3113.

- [152] M. Sakuth, D. Reusch, and R. Janowsky. “Reactive Distillation”. In: *Ullmann's Encyclopedia of Industrial Chemistry*. Vol. 31. Wiley-VCH, 2008.
- [153] A. Saltelli et al. *Global sensitivity analysis: the primer*. John Wiley & Sons, 2008.
- [154] A. Saltelli et al. “Variance based sensitivity analysis of model output. Design and estimator for the total sensitivity index”. In: *Computer physics communications* 181.2 (2010), pp. 259–270.
- [155] B. Saltik et al. “Sensor configuration problem: application to a membrane separation unit”. In: *IFAC-PapersOnLine* 49.7 (2016), pp. 189–194.
- [156] T. Sauer. *Numerical Analysis*. 3rd. Pearson, 2018.
- [157] K. Schittkowski. “Experimental design tools for ordinary and algebraic differential equations”. In: *Industrial & Engineering Chemistry Research* 46.26 (2007), pp. 9137–9147.
- [158] M. Schönlein. “Asymptotic stability and smooth Lyapunov functions for a class of abstract dynamical systems”. In: *Discrete & Continuous Dynamical Systems* 37.7 (2017), pp. 4053–4069.
- [159] K. Seavey and Y.A. Liu. *Step-growth polymerization process modeling and product design*. John Wiley & Sons, 2009.
- [160] C. Seigneur, G. Stephanopoulos, and R.W. Carr Jr. “Dynamic sensitivity analysis of chemical reaction systems: a variational method”. In: *Chemical Engineering Science* 37.6 (1982), pp. 845–853.
- [161] R. Shi and J. MacGregor. “Modeling of dynamic systems using latent variable and subspace methods”. In: *Journal of Chemometrics: A Journal of the Chemometrics Society* 14.5-6 (2000), pp. 423–439.
- [162] R. Sinnot. *Chemical Engineering Design (Coulson & Richardson's Volume 6)*. 4th. Elsevier Butterworth-Heinemann, 2005.
- [163] S. Skogestad. *Chemical and energy process engineering*. CRC press, 2008.
- [164] K. Smith. “On the standard deviations of adjusted and interpolated values of an observed polynomial function and its constants and the guidance they give towards a proper choice of the distribution of observations”. In: *Biometrika* 12.1/2 (1918), pp. 1–85.
- [165] M. Sneesby, M. Tadé, and T. Smith. “Two-point Control of a Reactive Distillation Column for Composition and Conversion”. In: *Journal of Process Control* 9.1 (1999), pp. 19–31.
- [166] I. Sobol. “Global sensitivity indices for nonlinear mathematical models and their Monte Carlo estimates”. In: *Mathematics and computers in simulation* 55.1-3 (2001), pp. 271–280.
- [167] S. Somjai and K. Jermsittiparsert. “The trade-off between cost and environmental performance in the presence of sustainable supply chain”. In: *International Journal of Supply Chain Management* 8.4 (2019), pp. 237–247.

- [168] E. Sørensen and S. Skogestad. "Batch Processing Systems Engineering". In: Springer Berlin Heidelberg, 1996. Chap. Control Strategies for a Combined Batch Reactor/Batch Distillation Process, pp. 274–294.
- [169] S. Srinivasan, J. Billeter, and D. Bonvin. "Extent-based incremental identification of reaction systems using concentration and calorimetric measurements". In: *Chemical engineering journal* 207 (2012), pp. 785–793.
- [170] R. Stark, C. Fresemann, and K. Lindow. "Development and operation of Digital Twins for technical systems and services". In: *CIRP Annals* 68.1 (2019), pp. 129–132.
- [171] J. Stigter and R. Peeters. "On a geometric approach to the structural identifiability problem and its application in a water quality case study". In: *2007 European Control Conference (ECC)*. IEEE. 2007, pp. 3450–3456.
- [172] C. Sun and J. Hahn. "Parameter reduction for stable dynamical systems based on Hankel singular values and sensitivity analysis". In: *Chemical engineering science* 61.16 (2006), pp. 5393–5403.
- [173] X. Sun et al. "A digital twin-driven approach for the assembly-commissioning of high precision products". In: *Robotics and Computer-Integrated Manufacturing* 61 (2020), p. 101839.
- [174] T. Sutton and J. Macgregor. "The analysis and design of binary vapour-liquid equilibrium experiments. Part II: The design of experiments". In: *The Canadian Journal of Chemical Engineering* 55.5 (1977), pp. 609–613.
- [175] A. Tammaro et al. "Extending Industrial Digital Twins with Optical Object Tracking." In: *CEIG*. 2017, pp. 23–26.
- [176] F. Tao et al. "Digital twin-driven product design framework". In: *International Journal of Production Research* 57.12 (2019), pp. 3935–3953.
- [177] M. Thompson and M. Kramer. "Modeling chemical processes using prior knowledge and neural networks". In: *AIChe Journal* 40.8 (1994), pp. 1328–1340.
- [178] A. Tsen et al. "Predictive control of quality in batch polymerization using hybrid ANN models". In: *AIChe Journal* 42.2 (1996), pp. 455–465.
- [179] E. Tunali and T.J. Tarn. "New results for identifiability of nonlinear systems". In: *IEEE Transactions on Automatic Control* 32.2 (1987), pp. 146–154.
- [180] T. Turányi. "Sensitivity analysis of complex kinetic systems. Tools and applications". In: *Journal of mathematical chemistry* 5.3 (1990), pp. 203–248.
- [181] S. Vajda. "Structural equivalence of linear systems and compartmental models". In: *Mathematical Biosciences* 55.1-2 (1981), pp. 39–64.
- [182] S. Vajda et al. "Qualitative and quantitative identifiability analysis of non-linear chemical kinetic models". In: *Chemical Engineering Communications* 83.1 (1989b), pp. 191–219.

- [183] Sandor Vajda, Keith R Godfrey, and Herschel Rabitz. “Similarity transformation approach to identifiability analysis of nonlinear compartmental models”. In: *Mathematical biosciences* 93.2 (1989a), pp. 217–248.
- [184] J. Van Doren et al. “Determining identifiable parameterizations for large-scale physical models in reservoir engineering”. In: *IFAC Proceedings Volumes* 41.2 (2008), pp. 11421–11426.
- [185] J. Van Doren et al. “Determining identifiable parametrizations for large-scale physical models in reservoir engineering”. In: *IFAC Proceedings Volumes* 41.2 (2008), pp. 11421–11426.
- [186] J.E. Vandezande, D.A. Vander Griend, and R.L. DeKock. “Reaction Extrema: Extent of Reaction in General Chemistry”. In: *Journal of Chemical Education* 90.9 (2013), pp. 1177–1179.
- [187] M. Verhaegen and V. Verdult. *Filtering and system identification: a least squares approach*. Cambridge university press, 2007.
- [188] A. Villaverde, A. Barreiro, and A. Papachristodoulou. “Structural Identifiability Analysis via Extended Observability and Decomposition”. In: *IFAC-PapersOnLine* 49.26 (2016), pp. 171–177.
- [189] Kris Villez, Julien Billeter, and Dominique Bonvin. “Incremental parameter estimation under rank-deficient measurement conditions”. In: *Processes* 7.2 (2019), p. 75.
- [190] E. Walter. *Identifiability of state space models: with applications to transformation systems*. Vol. 46. Springer Science & Business Media, 1982.
- [191] E. Walter and Y. Lecourtier. “Unidentifiable compartmental models: What to do?” In: *Mathematical biosciences* 56.1-2 (1981), pp. 1–25.
- [192] E. Walter, Y. Lecourtier, and J. Happel. “On the structural output distinguishability of parametric models, and its relations with structural identifiability”. In: *IEEE Transactions on Automatic Control* 29.1 (1984), pp. 56–57.
- [193] E. Walter and L. Pronzato. “Identifiabilities and nonlinearities”. In: *Nonlinear Systems: Modeling and Estimation*. Ed. by A.J. Fossard and D. Normand-Cyrot. Vol. 1. Springer, 1995. Chap. 3.
- [194] E. Walter and L. Pronzato. *Identification of Parametric Models from Experimental Data*. Springer, 1997.
- [195] E. Walter and L. Pronzato. “Qualitative and quantitative experiment design for phenomenological models—a survey”. In: *Automatica* 26.2 (1990), pp. 195–213.
- [196] J. Wan, O. Marjanovic, and B. Lennox. “Disturbance rejection for the control of batch end-product quality using latent variable models”. In: *Journal of Process Control* 22.3 (2012), pp. 643–652.
- [197] T. Wanasinghe et al. “Digital twin for the oil and gas industry: Overview, research trends, opportunities, and challenges”. In: *IEEE Access* 8 (2020), pp. 104175–104197.

- [198] Y. Wang, F. Gao, and F. Doyle III. “Survey on iterative learning control, repetitive control, and run-to-run control”. In: *Journal of Process Control* 19.10 (2009), pp. 1589–1600.
- [199] Climate Watch. *Historical GHG Emissions*. 2021. URL: www.climatewatchdata.org/ghg-emissions.
- [200] S.R. Weijers and P.A. Vanrolleghem. “A procedure for selecting best identifiable parameters in calibrating activated sludge model no. 1 to full-scale plant data”. In: *Water science and technology* 36.5 (1997), pp. 69–79.
- [201] E.F. Wijn. “Weir flow and liquid height on sieve and valve trays”. In: *Chemical Engineering Journal* 73.3 (1999), pp. 191–204.
- [202] H. Wu et al. “Parameter identifiability and estimation of HIV/AIDS dynamic models”. In: *Bulletin of mathematical biology* 70.3 (2008), pp. 785–799.
- [203] X. Xia and C.H. Moog. “Identifiability of nonlinear systems with application to HIV/AIDS models”. In: *IEEE transactions on automatic control* 48.2 (2003), pp. 330–336.
- [204] K.Z. Yao et al. “Modeling ethylene/butene copolymerization with multi-site catalysts: parameter estimability and experimental design”. In: *Polymer Reaction Engineering* 11.3 (2003), pp. 563–588.
- [205] H.J. Zander, R. Dittmeyer, and J. Wagenhuber. “Dynamic modeling of chemical reaction systems with neural networks and hybrid models”. In: *Chemical Engineering & Technology: Industrial Chemistry-Plant Equipment-Process Engineering-Biotechnology* 22.7 (1999), pp. 571–574.
- [206] C.K. Zéberg-Mikkelsen. “Viscosity Study of Hydrocarbon Fluids at Reservoir Conditions: Modeling and Measurements”. PhD thesis. Technical University of Denmark Lyngby, 2001.
- [207] B. Zhmud. “Viscosity blending equations”. In: *Lube Mag* 121 (2014), pp. 24–9.
- [208] X. Zhu et al. “Parameter estimation for nonlinear dynamic systems from a feedback control viewpoint”. In: *2005 International Conference on Control and Automation*. Vol. 1. IEEE. 2005, pp. 119–124.

Acknowledgements

Firt and foremost, I would like to thank my supervisor and promotor dr. Leyla Özkan, who trusted in my capabilities and gave me the chance to work in this project. All the discussions we had helped me navigate the meandering path of a PhD. Your support in each step of the project gave me the courage to continue. I also would like to thank you for giving me a lot of teaching exposure, which is something I enjoyed greatly during my years as a PhD candidate. I would also like to express my gratitude to my other promotor prof. dr. ir. Paul van den Hof. Your input and suggestions guided me to ask new question and understand ideas from different perspective otherwise difficult to see. Your support in the final instances of the PhD helped me to push through. Thank you to both of you for the time you devoted to proofread the manuscript and all the feedback you gave me to improve.

To all my colleagues and staff at the Control Systems Group: Tom, Zuan, Paul, Clarisse, Chris, Stefanie, Birgit, Feye, Mannes, Ming, Francis, Patrick, Víctor, Yorick, Yanin, Ioannis, Carlos González, Tolga, Diana, Hiltje, Wim, Will, and so many others who were part of it, thank you for contributing to an inspiring work environment. Many thanks to Carlos Robles for all nice moments at CS, your technical insights and knowledge, specially in parameter estimation and bioprocesses were instrumental in portions of the thesis. Likewise, thanks for the good Mexican dinner parties; they were a lot of fun. Special thanks to Alejandro, without whom I would not have even thought of pursuing a PhD. Our technical discussions were very enriching to address the problems from a innovative perspective; the ideas we discussed were of great help in several aspects of my thesis. Your enthusiasm and advice helped me enormously in remaining positive through this journey. I am extremely grateful for your support since day one back when I was a master student. I also extend my gratitude to all the committee members for also having taken the time to read and provide valuable feedback to enhance the quality of the thesis.

Huge thanks to Yoel, Camila, and Brian, who for years have supported and listened to me, sticking with me during the PhD journey. Yoel, thank you for your endless and unconditional patience and care through thick and thin; Camila, thank you for your mature advice that helped me seeing things under a different light; Brian, thank you for being that one true open-minded Dutch friend (and for the free Dutch lessons) who is always ready to help. Last but not least, I thank my parents and my sister for always being there, helping me staying focused on the bright side even when things did not go my way. To my aunts, uncles, and cousins in Spain, thank you for being my safe haven where I can always run back to, and to all my family who has always kept me in their good wishes and prayers.

Curriculum Vitæ

Carlos S. Méndez Blanco was born on October 20th, 1990 in Puerto Ordaz, Venezuela. He received his B.Sc. degree in Chemical Engineering from Simón Bolívar University in Venezuela in 2015. From 2015 to 2017, he followed the M.Sc. program in Systems and Control at Delft University of Technology in Delft, The Netherlands. He completed his M.Sc. thesis titled "Control of reactive batch distillation columns via the extents transformation". The graduation project was performed in the Control System (CS) Group at Eindhoven University of Technology (TU/e) and in collaboration with DSM. In September 2017, he started his Ph.D. project in the Control System Group at TU/e under the supervision of dr. Leyla Özkan in the IN-SPEC project to research on *parameter estimation and automatic model update*. This project was funded by the Institute for Sustainable Process Technology (ISPT) and TKI Energie en Industrie. Since May 2022, he works as a Thermal Control Engineer at ASML in Veldhoven, the Netherlands.



List of Publications

8. C. Méndez-Blanco, L. Özkan, *Parameter Estimation for Multi-Stage Processes: A multiple shooting approach integrated with sensitivity analysis* Submitted to Industrial & Engineering Chemistry Research.
7. C. Méndez-Blanco, L. Özkan, *Extent-based reconstruction of the inlet composition matrix in process systems with feed variability*, 13th IFAC Symposium on Dynamics and Control of Process Systems (DYCOPS), 2022.
6. C. Méndez-Blanco, L. Özkan, *Local parameter identifiability of large-scale non-linear models based on the output sensitivity covariance matrix*, 16th IFAC Symposium on Advanced Control of Chemical Processes (ADCHEM), 415–420, 2021.
5. C. Méndez-Blanco, L. Özkan, *A State and output sensitivity controllability approach for structural identifiability of linear state space models*, 59th IEEE Conference on Decision and Control (CDC), 294–299, 2020.
4. A. Márquez-Ruiz, C. Méndez-Blanco, L. Özkan, *Constrained control and estimation of homogeneous reaction systems using extent-based linear parameter varying models*, Industrial and Engineering Chemistry Research 59, 2242–2251, 2020.
3. A. Márquez-Ruiz, C. Méndez-Blanco, L. Özkan, *Modeling of reactive batch distillation processes for control*, Computers & Chemical Engineering 121, 86–98, 2019.
2. A. Márquez-Ruiz, C. Méndez-Blanco, L. Özkan, *Control of homogeneous reaction systems using extent-based LPV models*, 10th IFAC Symposium on Advanced Control of Chemical Processes (ADCHEM) 51, 548–553, 2018.
1. A. Márquez-Ruiz, C. Méndez-Blanco, M. Porru, L. Özkan, *State and parameter estimation based on extent transformations*, Computer Aided Chemical Engineering 44, 583–588, 2018.